

**A Study on the Homogeneous and Surface Initiated Atom  
Transfer Radical Polymerization of Thermoresponsive Polymers  
from Regioselectively and Non-Regioselectively Substituted  
Cellulose Derivatives**

by

Ana Filipa de Assunção Xavier

Licentiate, New University of Lisbon, 2001

M.Sc., University of Aveiro, 2005

A THESIS SUBMITTED IN PARTIAL FULFILLMENT OF  
THE REQUIREMENTS FOR THE DEGREE OF

DOCTOR OF PHILOSOPHY

in

THE FACULTY OF GRADUATE AND POSTDOCTORAL STUDIES

(Forestry)

THE UNIVERSITY OF BRITISH COLUMBIA  
(Vancouver)

February 2014

© Ana Filipa de Assunção Xavier, 2014

## ABSTRACT

The demand for environmentally friendly innovative materials and chemicals is driving research focused on utilizing renewable biopolymers. Cellulose is an abundant biopolymer, and is of particular interest due to its versatility and aptitude for chemical modification.

Novel cellulosic materials were prepared by grafting thermoresponsive polymers, poly(*N*-isopropylacrylamide) (PNIPAM) and poly(2-(2-methoxyethoxy)ethyl methacrylate-co-oligo(ethyleneglycol) methacrylate) (P(DEGMA<sub>95</sub>-co-OEGMA<sub>5</sub>), from regioselectively substituted cellulose and corresponding cellulosic honeycomb films using homogeneous and surface initiated atom transfer radical polymerization (ATRP/SI-ATRP).

First, regioselective 6-*O*-(2-bromoisobutyryl)-TMS-*O*-cellulose was synthesized and used to produce a homogeneous honeycomb film. PNIPAM was then grafted from its surface via SI-ATRP, and the successful modification was confirmed by attenuated total reflectance-Fourier transform-infra-red spectroscopy, atomic force microscopy-quantitative nanomechanical mapping and contact angle.

Next, the role of regioselective substitution of cellulose on the formation of homogeneous honeycomb films was investigated using 3-*O*-substituted cellulose. 3-*O*-(2-bromoisobutyryl)-2,6-TDMS-*O*-cellulose and 2,3-*O*-(2-bromoisobutyryl)-2,6-TDMS-*O*-cellulose were synthesized and their ability to form homogeneous honeycomb films tested. Unfortunately, the poor reactivity of the 2,6-*O*-TDMS-cellulose resulted in very low 3-*O*- modification. Regardless, both 3-*O*-(2-bromoisobutyryl)-2,6-TDMS-*O*-cellulose and 2,3-*O*-(2-bromoisobutyryl)-2,6-*O*-TDMS-cellulose formed honeycomb films, however, the latter produced more homogeneous films with smaller pore diameters. PNIPAM was then successfully grafted from the surface of the 2,3-*O*-(2-bromoisobutyryl)-2,6-*O*-TDMS-cellulose honeycomb films, dramatically changing their surface properties.

Finally, an alternative synthetic protocol was developed to increase the initiator density of the regioselective 3-*O*-cellulose. A new macroinitiator, 3-*O*-(3-*O*-(2-bromoisobutyryl)-hydroxypropyl)-2,6-*O*-TDMS-cellulose was synthesized and the effect of regiochemistry on the ATRP reaction, specifically termination reactions between growing chains was studied. PNIPAM and P(DEGMA<sub>95</sub>-co-OEGMA<sub>5</sub>) were grafted from 3-*O*-(3-*O*-(2-bromoisobutyryl)-hydroxypropyl)-2,6-*O*-TDMS-cellulose and the effects of temperature, Cu(II), ligand, dilution, monomer concentration and initiator density were assessed through kinetic plots. The grafting of PNIPAM gave promising results; linear kinetic plots and copolymers with low polydispersity index. However, the linear kinetic regime was short and the conversions were low. On the other hand, the grafting of P(DEGMA<sub>95</sub>-co-OEGMA<sub>5</sub>) was very challenging mainly due to the low solubility and, in some cases, insolubility of the copolymers. Nevertheless when a macroinitiator with a lower initiator density was used, a soluble copolymer with a lower PDI was obtained.

## PREFACE

A version of section 3.2 (Synthesis of 3-O-(2-Bromoisobutyryl)-2,6-O-TDMS-cellulose and 2,3-O-(2-Bromoisobutyryl)-2,6-O-TDMS-cellulose for the Preparation of Thermoresponsive Honeycomb Patterned Films via ATRP) was published in: Xavier, A. F.; Kadla, J. F. In *ACS Symposium Series-Functional Materials from Renewable Sources*; ACS, Ed.; 2012; Vol. 1107, pp. 37–55.

I conducted all the testing and wrote the manuscript.

# TABLE OF CONTENTS

ABSTRACT .....	ii
PREFACE .....	iii
TABLE OF CONTENTS .....	iv
LIST OF TABLES .....	viii
LIST OF FIGURES .....	x
LIST OF SCHEMES .....	xvi
LIST OF EQUATIONS .....	xvii
LIST OF ABBREVIATIONS .....	xviii
ACKNOWLEDGEMENTS .....	xxii
DEDICATION .....	xxiii
1 INTRODUCTION .....	1
1.1 Cellulose .....	2
1.2 Cellulose Derivatives .....	4
1.2.1 Cellulose ethers .....	6
1.2.2 Cellulose esters .....	7
1.3 Regioselective Substitution of Cellulose .....	8
1.4 Graft Copolymers .....	14
1.4.1 Controlled/"living" radical polymerization .....	18



1.4.1.1	Atom Transfer Radical Polymerization (ATRP).....	20
1.4.1.2	Cellulose graft copolymers via ATRP .....	24
1.5	Thermoresponsive Polymers .....	27
1.6	Honeycomb Films .....	34
1.7	Hypothesis/Goals .....	41
1.7.1	Synthesis of 6-O-(2-bromoisobutyryl) TMS-O-cellulose for the preparation of thermoresponsive honeycomb patterned films via surface initiated ATRP .....	41
1.7.2	Synthesis of 3-O-(2-bromoisobutyryl) 2,6-O-TDMS cellulose and 2,3-O-(2-bromoisobutyryl) 2,6-O-TDMS cellulose for the preparation of thermoresponsive honeycomb patterned films via ATRP .....	42
1.7.3	Homogeneous ATRP of thermoresponsive copolymers from 3-O-(3-O-(2-bromoisobutyryl)-hydroxypropyl)-2,6-O-TDMS cellulose .....	42
2	EXPERIMENTAL .....	44
2.1	Materials .....	44
2.2	Methods.....	44
2.3	Synthesis .....	46
2.3.1	Regenerated cellulose .....	46
2.3.2	Synthesis of 6-O-(2-bromoisobutyryl) cellulose .....	46
2.3.3	Synthesis of 6-O-(2-bromoisobutyryl)-acetyl-O-cellulose .....	47
2.3.4	Synthesis of 6-O-(2-bromoisobutyryl)-trimethylsilyl-O-cellulose .....	48
2.3.5	Preparation of honeycomb films .....	48
2.3.6	Surface initiated ATRP of NIPAM from honeycomb films made from 6-O-(2-bromoisobutyryl)-trimethylsilyl-O-cellulose.....	49
2.3.7	Synthesis of 2,6-O-(hexyldimethylsilyl) cellulose .....	49
2.3.8	Synthesis of 3-O-(propanoyl)-2,6-O-TDMS cellulose .....	50
2.3.9	Synthesis of 3-O-(2-bromoisobutyryl)-2,6-O-TDMS cellulose .....	50
2.3.10	Synthesis of 3-O-octyl-2,6-O-TDMS cellulose .....	51
2.3.11	Synthesis of 3-O-acetyl-2,6-O-TDMS cellulose .....	52
2.3.12	Synthesis of 3-O-(2-bromo-2-methylpropyl)-2,6-O-TDMS cellulose .....	52
2.3.13	Synthesis of 2,3-O-(2-bromoisobutyryl)-2,6-O-(hexyldimethylsilyl) cellulose .....	53
2.3.14	Synthesis of 3-O-allyl-2,6-O-TDMS cellulose .....	53
2.3.15	Synthesis of 3-O-(3-O-hydroxypropyl)-2,6-O-TDMS cellulose .....	54
2.3.16	Synthesis of 3-O-(3-O-(2-bromoisobutyryl)-hydroxypropyl)-2,6-O-TDMS cellulose .....	55

2.3.17	Homogeneous polymerization of NIPAM from 3-O-(3-O-(2-bromoisobutyryl)-hydroxypropyl)-2,6-O-TDMS cellulose through ATRP .....	55
2.3.18	Homogeneous copolymerization of DEGMA and OEGMA from 3-O-(3-O-(2-bromoisobutyryl)-hydroxypropyl)-2,6-O-TDMS cellulose .....	56
<b>3</b>	<b>RESULTS AND DISCUSSION.....</b>	<b>57</b>
3.1	Synthesis of 6-O-(2-Bromoisobutyryl)-TMS-O-Cellulose for Preparation of Thermoresponsive Honeycomb Patterned Films via Surface Initiated ATRP .....	57
3.1.1	Synthesis and characterization of 6-O-(2-bromoisobutyryl)-2,3-O-TMS cellulose ..	57
3.1.2	Preparation of honeycomb films from 6-O-(2-bromoisobutyryl) TMS-O-cellulose derivatives with different DS .....	66
3.1.3	Surface modification of honeycomb films made from regioselectively substituted cellulose derivative via surface initiated ATRP .....	76
3.1.4	Conclusions .....	81
3.2	Synthesis of 3-O-(2-Bromoisobutyryl)-2,6-O-TDMS-Cellulose and 2,3-O-(2-Bromoisobutyryl)-2,6-O-TDMS-Cellulose for the Preparation of Thermoresponsive Honeycomb Patterned Films via ATRP .....	83
3.2.1	Synthesis of 3-O-(2-bromoisobutyryl)-2,6-O-TDMS cellulose .....	83
3.2.2	Synthesis of 2,3-O-(2-bromoisobutyryl)-2,6-O-TDMS-cellulose .....	91
3.2.3	Honeycomb Film Formation.....	97
3.2.4	Surface initiated ATRP.....	99
3.2.5	Conclusions .....	101
3.3	Homogeneous ATRP of Thermoresponsive Copolymers from Regioselectively Substituted 3-O-(3-O-(2-Bromoisobutyryl)-Hydroxypropyl)-2,6-O-TDMS Cellulose.....	103
3.3.1	Synthesis of 3-O-(3-O-(2-bromoisobutyryl)-hydroxypropyl)-2,6-O-TDMS cellulose .....	103
3.3.2	Homogeneous polymerization of NIPAM from 3-O-(3-O-(2-bromoisobutyryl)-hydroxypropyl)-2,6-O-TDMS cellulose .....	108
3.3.3	Homogeneous copolymerization of DEGMA and OEGMA from 3-O-(3-O-(2-bromoisobutyryl)-hydroxypropyl)-2,6-O-TDMS cellulose .....	117

3.3.4	Effect of the degree of substitution on the homogeneous ATRP of DEGMA and OEGMA from 3-O-(3-O-(2-bromoisobutyryl)-hydroxypropyl)-2,6-O-TDMS cellulose .....	144
3.3.5	Conclusions .....	153
4	CONCLUSIONS.....	155
5	FUTURE WORK .....	157
	REFERENCES.....	159
	APPENDIX.....	175

## LIST OF TABLES

<b>Table 1.2.1.</b> Commercially relevant cellulose ethers and their primary applications. <sup>32</sup> .....	6
<b>Table 1.2.2.</b> Commercially relevant cellulose esters and their primary applications. <sup>50</sup> .....	8
<b>Table 1.5.1.</b> LCST of poly(OEGMA-co-DEGMA] prepared by ATRP. ....	32
<b>Table 3.1.1.</b> Effect of molar equivalents of 2-bromoisobutyryl bromide (BribuBr) on the degree of substitution (DS), Mn and PDI of 6-O-(2-bromoisobutyryl)-TMS-O-cellulose derivatives. ....	58
<b>Table 3.1.2.</b> Experimental conditions used in the production of honeycomb films from 6-O-(2-bromoisobutyryl) TMS-O-cellulose with low and medium DS and different flow/humidity. ....	67
<b>Table 3.1.3.</b> Experimental conditions used in the production of honeycomb films from 6-O-(2-bromoisobutyryl) TMS-O-cellulose with different DS and concentration. ....	70
<b>Table 3.1.4.</b> Experimental conditions used in the production of honeycomb films from 6-O-(2-bromoisobutyryl) TMS-O-cellulose with different DS. ....	74
<b>Table 3.1.5.</b> Experimental conditions used in surface initiated ATRP of NIPAM from the surface of honeycomb film. ....	76
<b>Table 3.2.1.</b> Experimental conditions used in the synthesis of 3-O-(2-bromoisobutyryl) 2,6-O-TDMS cellulose. ....	87
<b>Table 3.2.2.</b> Functional groups used to synthesize 3-O-2,6-O-TDMS cellulose derivatives. ....	89
<b>Table 3.2.3.</b> Effect of base on the synthesis of 2,3-O-(2-bromoisobutyryl)-2,6-O-TDMS cellulose. ....	92
<b>Table 3.2.4.</b> Effect of time and temperature on the synthesis of 2,3-O-(2-bromoisobutyryl) 2,6-O-TDMS cellulose. ....	93
<b>Table 3.2.5.</b> Effect of changing the mole equivalents of 2-bromoisobutyryl bromide and anhydrous pyridine in the synthesis of 2,3-O-(2-bromoisobutyryl) 2,6-O-TDMS cellulose. ....	94
<b>Table 3.2.6.</b> Effect of 2 <sup>nd</sup> reaction cycle in the synthesis of 2,3-O-(2-bromoisobutyryl) 2,6-O-TDMS cellulose. ....	94
<b>Table 3.2.7.</b> Experimental conditions used in the surface initiated ATRP. ....	99
<b>Table 3.3.1.</b> Molar equivalents of allyl chloride used in the synthesis of macroinitiator 3-O-propyl-(2-bromoisobutyryl)-2,6-O-TDMS cellulose (Scheme 3.3.1, step b) with different DS. ....	107

<b>Table 3.3.2.</b> Experimental conditions used in the ATRP of NIPAM from 3-O-(3-O-(2-bromoisobutyryl)-hydroxypropyl)-2,6-O-TDMS cellulose and respective conversions. ....	109
<b>Table 3.3.3.</b> $Mn_{(th)}$ , $Mn_{(GPC-MALS)}$ , PDI, conversion and DP of macroinitiators and respective cellulose-based graft copolymers after 3 hours of reaction.....	115
<b>Table 3.3.4.</b> Experimental conditions used in the ATRP of P(DEGMA <sub>95</sub> -co-OEGMA <sub>5</sub> ) from 3-O-(3-O-(2-bromoisobutyryl)-hydroxypropyl)-2,6-O-TDMS cellulose and the resulting conversions....	119
<b>Table 3.3.5.</b> Experimental conditions used in the ATRP of P(DEGMA <sub>95</sub> -co-OEGMA <sub>5</sub> ) from 3-O-(3-O-(2-bromoisobutyryl)-hydroxypropyl)-2,6-O-TDMS cellulose and respective conversions. ....	120
<b>Table 3.3.6.</b> Set of selected experiments and respective time of reaction, conversion, DP and solubility in THF, CHCl <sub>3</sub> and H <sub>2</sub> O at 30 wt% copolymer.....	126
<b>Table 3.3.7.</b> Decomposition temperature of macroinitiator, P(DEGMA <sub>90</sub> -co-OEGMA <sub>10</sub> ) and cellulose-based graft copolymers and complementing information concerning DP.....	131
<b>Table 3.3.8.</b> Glass transition temperature of macroinitiator, P(DEGMA <sub>90</sub> -co-OEGMA <sub>10</sub> ) and cellulose-based graft copolymers and complementing information concerning DP and solubility. ....	133
<b>Table 3.3.9.</b> DP, $Mn_{(th)}$ , $Mn_{(GPC-MALS)}$ and PDI of macroinitiator and respective cellulose-based graft copolymers. ....	135
<b>Table 3.3.10.</b> dn/dc values of the different cellulose-based graft copolymers.....	137
<b>Table 3.3.11.</b> Characterization of cellulose-based graft copolymers at different reaction times.	142
<b>Table 3.3.12.</b> Experimental conditions used in the ATRP of P(DEGMA <sub>95</sub> -co-OEGMA <sub>5</sub> ) from 3-O-(3-O-(2-bromoisobutyryl)-hydroxypropyl)-2,6-O-TDMS cellulose with different DS of 2-bromoisobutyryl and respective conversions. ....	144
<b>Table 3.3.13.</b> Cellulose-based graft copolymers with high and low initiator density and respective conversion, DP and solubility in THF, CHCl <sub>3</sub> and H <sub>2</sub> O.....	146
<b>Table 3.3.14.</b> DP, $Mn_{(th)}$ , $Mn_{(GPC-MALS)}$ , PDI of macroinitiator and respective cellulose-based graft copolymers. ....	151

# LIST OF FIGURES

<b>Figure 1.1.1.</b> Structural representation of cellulose .....	2
<b>Figure 1.1.2.</b> Intra- (red wavy lines) and intermolecular (black dashed lines) hydrogen bonds between adjacent AGU molecules of cellulose I (a) and cellulose II (b). <sup>25–28</sup> .....	3
<b>Figure 1.2.1.</b> Representative structures of some of the commercially relevant cellulose ethers. ..	6
<b>Figure 1.2.2.</b> Representative structures of some of the commercially relevant cellulose esters. ..	7
<b>Figure 1.3.1.</b> Inter- and intramolecular hydrogen bonding established in 2,3-O-methylcellulose (top) and 6-O-methylcellulose (bottom). <sup>55</sup> .....	9
<b>Figure 1.4.1.</b> Examples of nitrogen based ligands used in ATRP in conjunction with copper. ....	22
<b>Figure 1.5.1. a)</b> Molecular structure of PNIPAM and identification of the hydrophilic and hydrophobic groups; <b>b)</b> Thermoresponsive behaviour of PNIPAM below and above the LCST <sup>260</sup> . .....	29
<b>Figure 1.6.1.</b> Simplified mechanism for the formation of honeycomb films through “breath-figure” method; <b>a)</b> nucleation of water droplets; <b>b)</b> water droplets in close packed array; <b>c)</b> water droplets in close packed array sink into solution; <b>d)</b> nucleation of new water droplets; <b>e)</b> formation of a close packed array of water droplets; <b>f)</b> solvent and water evaporation with simultaneous precipitation of polymer around water droplets and formation of honeycomb film. <sup>300</sup> .....	36
<b>Figure 1.6.2.</b> SEM images of hepatocytes 72 h after culture on <b>(a)</b> flat film and <b>(b)</b> honeycomb film. <sup>328</sup> .....	40
<b>Figure 3.1.1.</b> Comparison of FTIR spectra of 6-O-(2-bromoisobutyryl) TMS-O-cellulose with different DS; a) low DS (0.24); b) medium DS (0.50); c) high DS (0.80).....	59
<b>Figure 3.1.2.</b> <sup>1</sup> H/ <sup>13</sup> H heteronuclear single-quantum correlation spectroscopy (HSQC) of 6-O-(2-bromoisobutyryl)-2,3,6-O-acetyl cellulose. ....	60
<b>Figure 3.1.3.</b> <sup>1</sup> H/ <sup>1</sup> H homonuclear correlation spectroscopy (COSY) of 6-O-(2-bromoisobutyryl)-2,3,6-O-acetyl cellulose. ....	61
<b>Figure 3.1.4.</b> <sup>1</sup> H/ <sup>13</sup> H heteronuclear multiple-bond correlation spectroscopy (HMBC) of 6-O-(2-bromoisobutyryl)-2,3,6-O-acetyl cellulose. ....	62
<b>Figure 3.1.5.</b> Comparison of <sup>1</sup> H-NMR spectrum of 6-O-(2-bromoisobutyryl)-TMS-O-cellulose; a) low DS, b) medium DS, c) high DS, d) non-regioselectively substituted 2,3,6-O-(2-bromoisobutyryl)-TMS-O-cellulose. ....	63

<b>Figure 3.1.6. 1:</b> Comparison of $^{13}\text{C}$ -NMR spectrum of 6-O-(2-bromoisobutryl)-TMS-O-cellulose; a) low DS, b) medium DS, c) high DS, d) non-regioselectively substituted with high DS; <b>2:</b> Zoom-in of respective carbonyl region.....	65
<b>Figure 3.1.7.</b> Experimental setup for formation of honeycomb films. ....	66
<b>Figure 3.1.8.</b> SEM images of honeycomb films from 6-O-(2-bromoisobutryl) TMS-O-cellulose with low (0.26) DS at different flow/humidity: 1) 0.5 L/min and 2) 0.9 L/min. ....	68
<b>Figure 3.1.9.</b> SEM images of honeycomb films from 6-O-(2-bromoisobutryl) TMS-O-cellulose with medium DS (0.52) at different flow/humidity; 3) 0.7 L/min; 4) 0.9 L/min.....	69
<b>Figure 3.1.10.</b> SEM images of honeycomb films from 6-O-(2-bromoisobutryl) TMS-O-cellulose with low (0.26) DS at different concentrations: 5) 3mg/mL; 6) 4 mg/mL and ;7) 8 mg/mL.....	71
<b>Figure 3.1.11.</b> SEM images of honeycomb films from 6-O-(2-bromoisobutryl) TMS-O-cellulose with medium (0.52) DS at different concentrations; 8) 2 mg/mL; 9) 3 mg/mL; 10) 4 mg/mL; 11) 5 mg/mL.....	72
<b>Figure 3.1.12.</b> SEM images of honeycomb films from 6-O-(2-bromoisobutryl) TMS-O-cellulose with high (0.80) DS at different concentrations. 12) 2 mg/mL; 13) 3 mg/mL; 14) 4 mg/mL. ....	73
<b>Figure 3.1.13.</b> SEM images of honeycomb films from 6-O-(2-bromoisobutryl) TMS-O-cellulose with different DS at a concentration of 3mg/mL. 5) DS = 0.26; 9) DS = 0.52; 13) DS = 0.8; 15) DS=2.2.....	75
<b>Figure 3.1.14.</b> Comparison of ATR-FTIR spectra of PNIPAM (bottom), 6-O-(2-bromoisobutryl) TMS-O-cellulose (middle) and honeycomb film from 6-O-(2-bromoisobutryl)-TMS-O-cellulose medium DS (top) after surface initiated ATRP. ....	77
<b>Figure 3.1.15.</b> Optical micrographs of honeycomb films from 6-O-(2-bromoisobutryl) TMS-O-cellulose with medium DS before (left) and after (right) surface initiated ATRP. ....	78
<b>Figure 3.1.16.</b> AFM 3D height images of the honeycomb film from 6-O-(2-bromoisobutryl) TMS-O-cellulose with medium DS before (left) and after (right) surface initiated ATRP. Pore depth and width measurements, n = 4. ....	78
<b>Figure 3.1.17.</b> AFM 2D modulus images of the honeycomb film from 6-O-(2-bromoisobutryl) TMS-O-cellulose with medium DS before (left) and after (right) surface initiated ATRP. Modulus measurements, n = 5.....	79
<b>Figure 3.1.18.</b> AFM 3D image of elastic modulus overlaid on top of height, before (left) and after (right) ATRP.....	80

<b>Figure 3.1.19.</b> Contact angle analysis of honeycomb film surface from 6-O-(2-bromoisobutyryl) TMS-O-cellulose with medium DS before (left) and after (right) surface initiated ATRP. Measurements were done in triplicate. ....	80
<b>Figure 3.2.1.</b> Quantitative $^{13}\text{C}$ -NMR of 2,6-O-TDMS cellulose with DS ~ 2.1. ....	84
<b>Figure 3.2.2.</b> Comparison of $^1\text{H}$ -NMR of 3-O-propanoyl-2,6-O-TDMS cellulose (bottom) and 2,3-O-propanoyl-2,6-O-TDMS cellulose (top). ....	85
<b>Figure 3.2.3.</b> Comparison of $^{13}\text{C}$ -NMR of 3-O-propanoyl-2,6-O-TDMS cellulose (bottom) and 2,3-O-propanoyl-2,6-O-TDMS cellulose (top). ....	86
<b>Figure 3.2.4.</b> $^1\text{H}$ -NMR spectrum of 3-O-(2-bromoisobutyryl)-2,6-O-TDMS cellulose. ....	88
<b>Figure 3.2.5.</b> Comparison of $^1\text{H}$ -NMR spectra of a) 3-O-octyl-2,6-O-TDMS cellulose, b) 3-O-acetyl-2,6-O-TDMS cellulose, c) 3-O-(2-bromoisobutyryl)-2,6-O-TDMS cellulose and d) 3-O-(2-bromo-2-methylpropyl)-2,6-O-TDMS cellulose. ....	89
<b>Figure 3.2.6.</b> Quantitative $^{13}\text{C}$ -NMR of 2,6-O-TDMS cellulose with DS = 1.3. ....	91
<b>Figure 3.2.7.</b> $^1\text{H}$ -NMR spectrum of 2,3-O-(2-bromoisobutyryl)-2,6-O-TDMS cellulose in $\text{CHCl}_3$ . .	95
<b>Figure 3.2.8.</b> Quantitative $^{13}\text{C}$ -NMR spectrum of 2,3-O-(2-bromoisobutyryl)-2,6-O-TDMS-cellulose in benzene. ....	96
<b>Figure 3.2.9.</b> Optical microscope images of honeycomb films formed from 3-O-(2-bromoisobutyryl)-2,6-O-TDMS-cellulose (left) and 2,3-O-(2-bromoisobutyryl)-2,6-O-TDMS cellulose (right). ....	97
<b>Figure 3.2.10.</b> SEM images of the 2,3-O-(2-bromoisobutyryl)-2,6-O-TDMS-cellulose honeycomb films. ....	98
<b>Figure 3.2.11.</b> SEM images of honeycomb films from 2,3-O-(2-bromoisobutyryl)-2,6-O-TDMS cellulose before (left) and after surface initiated ATRP (right) with 1 wt% (top) and 10wt% (bottom) NIPAM/ $\text{H}_2\text{O}$ solutions. ....	100
<b>Figure 3.2.12.</b> Contact angle measurements of honeycomb films from 2,3-O-(2-bromoisobutyryl)-2,6-O-TDMS-cellulose before (left) and after SI ATRP (right) with 1wt% (top) and 10wt% (bottom) of NIPAM/ $\text{H}_2\text{O}$ (see Table 3.2.7 for details). Measurements were done in triplicate. ....	101
<b>Figure 3.3.1.</b> Comparison of $^1\text{H}$ -NMR spectra of a) 3-O-allyl-2,6-O-TDMS cellulose, b) 3-hydroxy-propyl 2,6-O-TDMS cellulose and c) 3-O-(3-O-(2-bromoisobutyryl)-hydroxypropyl)-2,6-O-TDMS cellulose, see Scheme 3.3.1. ....	105
<b>Figure 3.3.2.</b> Comparison of quantitative $^{13}\text{C}$ -NMR spectra of a) 3-O-allyl-2,6-O-TDMS cellulose, b) 3-O-hydroxy-propyl-2,6-O-TDMS cellulose and c) 3-O-(3-O-(2-bromoisobutyryl)-hydroxypropyl)-2,6-O-TDMS cellulose see Figure 3.3.1 for peak identification. ....	106



**Figure 3.3.3.**  $^1\text{H}$ -NMR spectrum of 30 min aliquot obtained from homogeneous polymerization of NIPAM from the macroinitiator with high DS, see **Scheme 3.3.2** for identification of the peaks. 110

**Figure 3.3.4.** Semi-logarithmic plots of NIPAM polymerization under different experimental conditions, using the cellulose-based macroinitiator with high DS. MI:NIPA:Me<sub>6</sub>TREN:Cu(I)Cl:Cu(II)Cl<sub>2</sub> - 1:100:x:y;z; solvent: THF/MeOH; [MeOH] = 5 wt%; MI – macroinitiator with high DS. (a) concentration of MI wt%, I – 0.1; II – 0.05.; (b) Temperature, II – RT; III – 55 °C. (c) Molar equivalents of Cu(II), II – 0.05 ; IV – 0.2. (d) Effect of ARGET, II – ATRP; V – ATRP-ARGET, tin<sup>II</sup> 2-ethylhexanoate (Sn(EH)<sub>2</sub>) = 0.1 molar equivalents and Cu(II) = 0.1 molar equivalents; (e) MI with low DS, IV – MI DS = 1; VI – MI DS = 0.2..... 111

**Figure 3.3.5.** Comparison of FTIR spectra of PNIPAM (bottom), cellulose-based macroinitiator with high DS (middle) and the synthesized 3-O-(3-O-(2-bromoisobutyryl)-hydroxypropyl)-2,6-O-TDMS cellulose-g-PNIPAM (top)..... 113

**Figure 3.3.6.** Comparison of  $^1\text{H}$ -NMR spectra of cellulose-based macroinitiator with high DS (bottom) and the synthesized 3-O-(3-O-(2-bromoisobutyryl)-hydroxypropyl)-2,6-O-TDMS cellulose-g-PNIPAM (top). ..... 114

**Figure 3.3.7.**  $^1\text{H}$ -NMR spectra of different aliquots collected at 0, 10, 30 and 60 min, obtained from experiment 5. See Scheme 3.3.3 for the identification of the peaks..... 121

**Figure 3.3.8.** Semi-logarithmic plots of copolymerization of DEGMA and OEGMA, under different experimental conditions, from cellulose-based macroinitiator with high DS. (MI:(DEGMA+OEGMA):Ligand:CuX - 1:100:1.2:1, DEGMA:OEGMA=95:5; solvent: THF) a) Effect of Solvent: Exp # 1: THF/MeOH, Exp # 2: THF; b) Molar equivalents of Cu(II) at RT: Exp # 2: Cu(II)=0.2; Exp # 3: 0.1; c) Effect of Temperature using 0.1 molar equivalents of Cu(II): Exp # 3: RT, Exp # 4: 55 °C; d) Effect of Molar equivalents of Cu(II) at 55 °C: Exp # 4: Cu(II) = 0.1, Exp # 5: Cu(II) = 0..... 122

**Figure 3.3.9.** Semi-logarithmic plot of copolymerization of DEGMA and OEGMA, under different experimental conditions, from cellulose-based macroinitiator with high DS. (MI:(DEGMA:OEGMA):Lig:CuX - 1:100:1.2:1; DEGMA:OEGMA=95:5; solvent: THF). a) Effect of Temperature: Exp # 5: 55°C, Exp # 6: RT; b) Effect of Ligand: Exp # 5: Me<sub>6</sub>TREN; Exp # 7: PMDETA; c) Effect of Halogen: Exp # 5: CuCl, Exp # 8: CuBr; d) [MI] wt%: Exp # 5: 0.5, Exp # 9: 0.25, Exp # 10: 0.125. .... 123

**Figure 3.3.10.** Semi-logarithmic plot of copolymerization of DEGMA and OEGMA from cellulose-based macroinitiator with high DS and with different monomer concentrations. MI:(DEGMA+OEGMA):Lig:CuX: Exp # 5 – 1:100:1.2:1; Exp # 11 - 1:50:1.2:1; Exp # 12 - 1:25:1.2:1; Exp # 13 - 1:10:1.2:1. Ratios were given in molar equivalents with respect to molar

equivalents of MI. DEGMA:OEGMA = 95:5; solvent - THF. Exp # 5 was done in duplicate (error bars correspond to n = 2) .....	125
<b>Figure 3.3.11.</b> Comparison of ATR-FTIR spectra of cellulose-based macroinitiator with high (DS=1) DS (bottom), P(DEGMA <sub>90</sub> -co-OEGMA <sub>10</sub> ) (middle) and the synthesized 3-O-(3-O-(2-bromoisobutyryl)-hydroxypropyl)-2,6-O-TDMS cellulose-g-P(DEGMA <sub>95</sub> -co-OEGMA <sub>5</sub> ) (top).....	127
<b>Figure 3.3.12.</b> Comparison of <sup>1</sup> H-NMR spectra of cellulose-based macroinitiator with high DS (bottom) and the synthesized 3-O-(3-O-(2-bromoisobutyryl)-hydroxypropyl)-2,6-O-TDMS cellulose-g-(P(DEGMA <sub>95</sub> -co-OEGMA <sub>5</sub> ) with lower (middle) and higher (top)DP of P(DEGMA <sub>95</sub> -co-OEGMA <sub>5</sub> ), see Scheme 3.3.3.....	128
<b>Figure 3.3.13.</b> Comparison of <sup>13</sup> C-NMR spectra of cellulose-based macroinitiator with high DS (bottom) and the synthesized 3-O-(3-O-(2-bromoisobutyryl)-hydroxypropyl)-2,6-O-TDMS cellulose-g-(P(DEGMA <sub>95</sub> -co-OEGMA <sub>5</sub> ) with a lower (middle) and higher (top) DP of P(DEGMA <sub>95</sub> -co-OEGMA <sub>5</sub> ). See Scheme 3.3.3 and Figure 3.3.12 for the identification of the peaks.....	129
<b>Figure 3.3.14.</b> Comparison of TGA thermograms of P(DEGMA <sub>90</sub> -co-OEGMA <sub>10</sub> ), MI (macroinitiator) and copolymers # 5, 7 and 9. ....	130
<b>Figure 3.3.15.</b> Comparison of DSC thermograms of P(DEGMA <sub>90</sub> -co-OEGMA <sub>10</sub> ), MI (macroinitiator) and copolymers # 5, 7 and 9. ....	132
<b>Figure 3.3.16.</b> Chart illustrating relation between T <sub>g</sub> (°C) and DP of P(DEGMA <sub>90</sub> -co-OEGMA <sub>10</sub> ), macroinitiator and cellulose-based graft copolymers .....	134
<b>Figure 3.3.17.</b> MALS (left) and RID (right) chromatograms of cellulose-based graft copolymers. ....	136
<b>Figure 3.3.18.</b> Absorbance vs. temperature plot illustrating the LCST of cellulose-based graft copolymers # 7 (left) and 9 (right) at a wavelength of 670 nm. ....	138
<b>Figure 3.3.19.</b> Thermoresponsive behaviour of cellulose-based graft copolymers. From left to right, copolymers # 4, 5, 6, at RT (top) and at 60 °C (bottom). ....	139
<b>Figure 3.3.20.</b> Thermoresponsive behaviour of cellulose-based graft copolymers. From left to right, copolymers # 8, 10 and 13 at RT (top) and at 60 °C (bottom). ....	140
<b>Figure 3.3.21.</b> Semi-logarithmic plot of copolymerization of DEGMA and OEGMA from cellulose-based macroinitiator (Exp # 9) and respective data collected at different reaction times. MI:(DEGMA:OEGMA):Lig:CuX - 1:100:1.2:1; DEGMA:OEGMA = 95:5; solvent: THF, room temperature. Experiment # 9 (diamond) was done in duplicate. ....	141
<b>Figure 3.3.22.</b> Comparison of ATR-FTIR spectra of copolymers # 9 at 5min (green), 15min (red) and 60min (black). ....	143

<b>Figure 3.3.23.</b> Semi-logarithmic plot of copolymerization of DEGMA and OEGMA from cellulose-based macroinitiator with different DS. Experiment # 5 (square) was done in duplicate. ....	145
<b>Figure 3.3.24.</b> Comparison of ATR-FTIR spectra of cellulose-based macroinitiator with low DS (bottom) and the synthesized 3-O-(3-O-(2-bromoisobutyryl)-hydroxypropyl)-2,6-O-TDMS cellulose- <i>g</i> -(P(DEGMA <sub>95</sub> -co-OEGMA <sub>5</sub> )) (top). ....	146
<b>Figure 3.3.25.</b> Comparison of <sup>1</sup> H-NMR spectra of cellulose-based macroinitiator with low DS (bottom) and the synthesized 3-O-(3-O-(2-bromoisobutyryl)-hydroxypropyl)-2,6-O-TDMS cellulose- <i>g</i> -(P(DEGMA <sub>95</sub> -co-OEGMA <sub>5</sub> )) (top). ....	147
<b>Figure 3.3.26.</b> Comparison of <sup>13</sup> C-NMR spectra of cellulose-based macroinitiator with low DS (bottom) and the synthesized 3-O-(3-O-(2-bromoisobutyryl)-hydroxypropyl)-2,6-O-TDMS cellulose- <i>g</i> -(P(DEGMA <sub>95</sub> -co-OEGMA <sub>5</sub> )) (top). See Figure 3.3.25 for peak number assignments. ....	148
<b>Figure 3.3.27.</b> Comparison of TGA thermograms of P(DEGMA <sub>90</sub> -co-OEGMA <sub>10</sub> ), MI (macroinitiator) and copolymers 5, and 15. ....	149
<b>Figure 3.3.28.</b> Comparison of DSC thermograms of P(DEGMA <sub>90</sub> -co-OEGMA <sub>10</sub> ), MI (macroinitiator) and copolymers 5, and 15. ....	150
<b>Figure 3.3.29.</b> MALS and RID chromatograms of copolymer # 15. ....	152

## LIST OF SCHEMES

<b>Scheme 1.4.1.</b> General reaction scheme of ATRP and contributing reactions. $K_{ET}$ - equilibrium constant for electron transfer; $K_X$ - equilibrium constant for the heterolytic cleavage of the $Mt^{n+1}-X$ bond; $K_{EA}$ - equilibrium constant for electron affinity of the halogen; $K_{BD}$ - equilibrium constant for bond dissociation of the alkyl halide. ....	20
<b>Scheme 3.1.1.</b> Proposed synthetic scheme to synthesize 6-O-(2-bromoisobutyryl)-TMS-O-cellulose: a. DMA-LiCl, TDMS-Cl, imidazole; b. 2-bromoisobutyryl bromide, anhydrous pyridine; c. DMA, anhydrous pyridine, HMDS-Cl. ....	57
<b>Scheme 3.2.1.</b> Synthetic scheme for the synthesis of 3-O-(2-bromoisobutyryl)-2,6-O-TDMS cellulose; a) DMA/LiCl, TDMS-Cl, imidazole b) anhydrous pyridine, 2-bromoisobutyryl bromide, THF. ....	83
<b>Scheme 3.3.1.</b> Synthetic scheme to synthesize 3-O-(3-O-(2-bromoisobutyryl)-hydroxypropyl)-2,6-O-TDMS cellulose: a. DMA-LiCl, TDMS-Cl, imidazole; b. Allyl-Cl; NaH; c. i) 9-BBN; ii) NaOH, $H_2O_2$ ; d. 2-bromoisobutyryl bromide, anhydrous pyridine. ....	104
<b>Scheme 3.3.2.</b> Schematic illustration of the polymerization of NIPAM from 3-O-(3-O-(2-bromoisobutyryl)-hydroxypropyl)-2,6-O-TDMS cellulose .....	108
<b>Scheme 3.3.3.</b> Schematic illustration of the copolymerization of P(DEGMA <sub>95</sub> -co-OEGMA <sub>5</sub> ) from 3-O-(3-O-(2-bromoisobutyryl)-hydroxypropyl)-2,6-O-TDMS cellulose. ....	118

**LIST OF EQUATIONS**

**Equation 3.1.1** .....58

**Equation 3.3.1** .....124

**Equation 3.3.2** .....136

## LIST OF ABBREVIATIONS

2D-NMR	Two dimensional nuclear magnetic resonance spectroscopy
AFM	Atomic force microscopy
AGET	Activators generated by electron transfer
ARGET	Activators regenerated by electron transfer
AGU	Anhydroglucose units
[Amim]Cl	1-allyl-3-methylimidazolium
ATR	Attenuated total reflectance
ATRP	Atom transfer radical polymerization
- <i>b</i> -	Block
9-BBN	9-Borabicyclo (3.3.1) nonane
Bipy	Bipyridine
[Bmim]Cl	1-buty-3-methylimidazolium chloride
BribuBr	2-Bromoisobutyryl bromide
C	Concentration
<sup>13</sup> C	Carbon 13
°C	Degree Celsius
CDA	Cellulose diacetate
CH <sub>3</sub> /CH <sub>2</sub> /CH	Methyl/Methylene/Methine
CHCl <sub>3</sub> /CDCl <sub>3</sub>	Chloroform/Deuterated chloroform
- <i>co</i> -	Copolymer
Conv	Conversion
Cr(III)acac	Chromium(III) acetylacetonate
CRP	Controlled radical polymerization
CYCLAM	Tetraazacyclotetradecane
DEGMA	2-(2-Methoxyethoxy)ethyl methacrylate
DMA	Dimethylacetamide
DMAEMA	2-(dimethylamino)ethyl methacrylate
DMF	Dimethylformamide
DMSO	Dimethyl sulfoxide
dn/dc	Differential index of refraction

DP	Degree of polymerization
DS	Degree of substitution
DSC	Differential scanning calorimetry
EC	Ethyl cellulose
Exp	Experiment
F	Flow
FTIR	Fourier transform infra-red
-g-	Graft
g/mg	Gram/milligram
GPa/MPa	Gigapascal/Megapascal
GPC	Gel permeation chromatography
H	Humidity, percentage
$^1\text{H}$	Proton
h	Hour
HEMA	2-Hydroxyethyl methacrylate
HMDS	1,1,1,3,3,3-Hexamethyldisilazane
HPC	Hydroxypropyl cellulose
ICAR	Initiators for continuous activator regeneration
$\text{KH}_2\text{PO}_4$	Potassium phosphate monobasic
$\text{K}_2\text{HPO}_4$	Potassium phosphate dibasic
L/mL/ $\mu\text{L}$	Liter/Milliliter/ $\mu\text{L}$
LCST	Lower critical solution temperature
LiCl	Lithium chloride
M	Molar
MA	Methyl acrylate
MALS	Multi angle light scattering
$\text{Me}_4\text{Cyclam}$	1,4,8,11-Tetraaza-1,4,8,11-tetramethylcyclotetradecane
MeOH	Methanol
$\text{Me}_6\text{TREN}$	Tris[2-dimethylamino)ethyl]amine
MI	Macroinitiator
Min	Minute
$M_n$	Number average molecular weight
$M_{n(\text{th})}$	Theoretical number average molecular weight
Mol/mmol/ $\mu\text{Mol}$	mole/millimole/micromole

Mw	Weight average molecular weight
NaH	Sodium hydride
NMP	N-Methyl-2-pyrrolidone
NMP	Nitroxide mediated polymerization
NMR	Nuclear magnetic resonance
NH <sub>3</sub>	Ammonia
OEGMA	Oligo(ethyleneglycol) methacrylate
P4VP	Poly(4-vinylpyridine)
PDI	Polydispersity index
PEO	Polyethylene oxide
PEG	Polyethylene glycol
PMDETA	N,N,N,N,N'-
	Pentamethyldiethylenetriamine
PMMA	Polymethyl methacrylate
PNIPAM	Poly(N-isopropylacrylamide)
PSt	Polystyrene
PVME	Poly(vinyl methylether)
QNM	Quantitative nanomechanical mapping
RAFT	Reversible addition-fragmentation chain transfer
Refl	Reflux
RID	Refractive index detector
ROMP	Ring-opening metathesis polymerization
RT	Room temperature
SEM	Scanning electron microscopy
SFRP	Stable free radical polymerization
S <sub>N</sub> 1 and S <sub>N</sub> 2	Nucleophilic substitution
T	Temperature
t	Time
TBAF	Tetrabutylammonium fluoride
Td	Decomposition temperature
TDMS	Hexyldimethyl silyl
TEA	Triethylamine
TMS	Trimethyl silyl
TGA	Thermogravimetric analysis
Tg	Glass transition temperature
THF	Tetrahydrofuran



TREN

UV-Vis

Wt%

XPS

ZnSe

Tris[2-(aminoethyl) amine]

Ultra violet/Visible spectrophotometry

Weight percent

X-ray photoelectron spectroscopy

Zinc selenium

## ACKNOWLEDGEMENTS

This dissertation would not have been possible without the guidance and the help of several individuals who in one way or another contributed and extended their valuable assistance in the preparation and completion of this study.

First and foremost, my gratitude to my supervisor Dr. John F. Kadla, who welcomed me into the Advanced Biomaterials Chemistry Laboratory as his PhD student, for his support, guidance, constructive criticism and for all the knowledge imparted on me through these years.

My sincere gratitude to my committee member Dr. Jayachandran Kizhakkedathu, for his constant support, expertise and guidance, helping me overcome the obstacles of this research project.

I wish to thank my committee member Dr. Shawn Mansfield for his helpful advice, constructive criticism and for his encouraging words in a difficult moment.

The financial support from NSERC and the University of British Columbia is much appreciated.

I would like to express my gratitude to the Faculty of Forestry/Department of Wood Science, staff, members and former-members of the Advanced Biomaterials Chemistry Laboratory. In particular, MSc. Carmen Hsieh, Drs. Reza Korehei, Ian Dallmeyer, William Xu, George Gao, Fadi Asfour, Gernot Marten, Sudip Chowdhury, Jennifer Braun, Michael Hinton, Scott Wasko and Shinsuke Ifuku for sharing their knowledge and for their insightful discussions. A special thank you to Dr. Cindy Prescott for her valuable advice and for her kindness.

I owe my deepest gratitude to my parents, Luísa and Carlos Xavier, for their unconditional love, friendship and for the patience and unwavering faith they have in me.

I am eternally grateful to my loving husband Randolph for his love, support and unwavering strength and for keeping me motivated throughout these challenging years.

I am sincerely thankful to my dear brother and sister, João and Marta Xavier for their unconditional love and for being such a positive influence in my life.

To Yvonne Yuen my gratefulness for her love and believing in me.

I wish to express my gratitude to Dr. Emmanuel Ackom whose friendship, sincerity and encouragement I will never forget.

To my Portuguese friend Dr. Inês Nobre, whom I met in Vancouver, my thank you for saying the right words, at the right time, in the right language, always ready to cheer me up.

During these years I had the opportunity to meet good friends, at UBC and outside UBC, that have inspired me and cheered me in difficult moments, to them my sincerest gratitude.

## DEDICATION

*To  
My Parents,  
Husband and Son*

# 1 INTRODUCTION

Cellulose is an abundant natural, organic compound available in nature. The major sources of cellulose are plant fibres (cotton, jute, hemp, flax and bamboo) and wood. Cellulose was primarily used in the fabrication of cloth and paper but since it was first discovered by Anselme Payen in 1834, cellulose's chemical composition, structure and morphology have been extensively studied. Cellulose is a unique biopolymer with characteristic properties such as hydrophilicity, chirality, chain stiffness and three hydroxyl groups with distinct reactivity. Nowadays demand for innovative and environmentally friendly materials has driven the synthesis of new cellulose derivatives. However, this demand goes along with an increment in complexity when synthesizing new materials. Due to the constant innovation in various disciplines such as, organic chemistry, polymer chemistry and material science the expansion of cellulose into new fields is challenging but very promising. For example, developments in synthetic modification of cellulose using protecting group chemistry enabled the preparation of regioselectively substituted cellulose derivatives<sup>1-3</sup> with special properties.<sup>4-7</sup> On the other hand, modern techniques of controlled radical polymerization, such as atom transfer radical polymerization<sup>8,9</sup> (ATRP), have allowed the grafting of synthetic polymers to obtain well-defined cellulose-based graft copolymers with unique properties. In addition stimuli responsive polymers have been grafted from cellulose derivatives to produce cellulosic smart materials.<sup>10-13</sup> In the present work, it was attempted to “graft-from” cellulose-based materials thermoresponsive polymers. This same concept was applied to the surface of honeycomb films. These are highly attractive materials owing to the wide range of applications, such as: tissue engineering,<sup>14-16</sup> micro-lens arrays,<sup>17</sup> superhydrophobic surfaces<sup>18</sup> and solar cells<sup>19</sup>.

The development of novel cellulose-based materials is becoming more demanding in terms of application and material performance. In order to keep up with the challenging requirements it is necessary to continue exploring new technologies in organic synthesis, controlled polymerization, polymer grafting, surface modification and material characterization. Subsequently, the acquired knowledge will enable the creation of innovative methods to obtain cellulose-based materials with the required set of properties. The introduction (Chapter 1) for the present work includes a literature review of cellulose and cellulose derivatives, polymer grafting and modern polymerization techniques, in particular atom transfer radical polymerization, thermoresponsive polymers and honeycomb films.

## 1.1 Cellulose

Cellulose is a linear hydrophilic polymer consisting of  $\beta$ -(1 $\rightarrow$ 4)-D-anhydroglucopyranose units in the  $^4C_1$  conformation. As shown in Figure 1.1.1 cellulose is a polymer of cellobiose, two anhydroglucopyranose units (AGU) linked through a  $\beta$ -glycosidic bond wherein the two anhydroglucopyranose units have alternating orientation with respect to the bridging oxygen bond. The fully equatorial hydroxyl group conformation of the anhydroglucopyranose residues stabilizes the  $^4C_1$  chair structure. The number of constituent AGUs is expressed as the degree of polymerization (DP) and it depends on the origin and method of isolation. For example, native cotton has a DP of around 13,000<sup>20</sup> and that of native wood cellulose is approximately 10,000<sup>21</sup>.

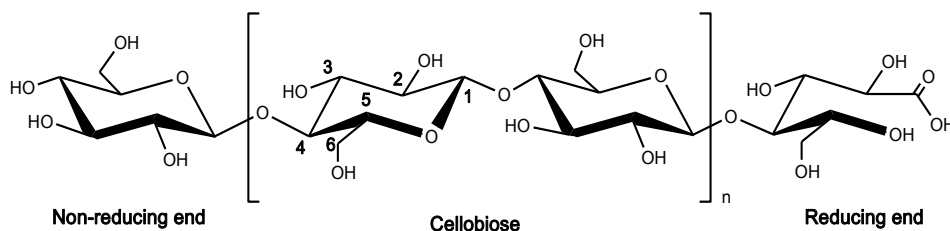


**Figure 1.1.1.** Structural representation of cellulose

Each AGU contains three hydroxyl (OH) groups located at positions 2, 3 and 6. The numbering of the carbons in the AGU is shown in **Figure 1.1.1**. The C6 position is a "primary" hydroxyl group, while the hydroxyl groups at positions 2 (C2) and 3 (C3) are "secondary" hydroxyl groups.

Native cellulose or Cellulose I has a highly ordered parallel cellulose chain structure consisting of crystalline and non-crystalline domains arising from extensive hydrogen bonding and van der Waals forces.<sup>22</sup> Cellulose I exists as a composite of two sub-allomorphs I $\alpha$  and I $\beta$ . Depending on the source of the cellulose the proportions of sub-allomorph (I $\alpha$  and I $\beta$ ) can vary. For example, cellulose derived from algae and bacteria is primarily composed of cellulose I $\alpha$ , while that isolated from higher plants and tunicates is primarily cellulose I $\beta$ .<sup>23</sup> The latter, I $\beta$  can be obtained from the thermal treatment of cellulose I $\alpha$ , which is in a metastable state.<sup>24</sup>

The linear structure of cellulose and the equatorial hydroxyl groups at the C2, C3 and C6 positions of the AGU results in a complex system of inter- and intramolecular hydrogen bonds. **Figure 1.1.2** illustrates the extensive intra- and intermolecular hydrogen bonding in cellulose. Two intramolecular hydrogen bonds in cellulose I are established between the O3-H $\cdots$ O5 and O2-H $\cdots$ O6 of adjoining AGUs, and one intermolecular hydrogen bond between the O6-H $\cdots$ O3' of

adjacent cellulose chains. In cellulose I all hydrogen bonds exist within the same plane, i.e., no interplanar interaction, which gives cellulose I a rigid sheet-like structure.

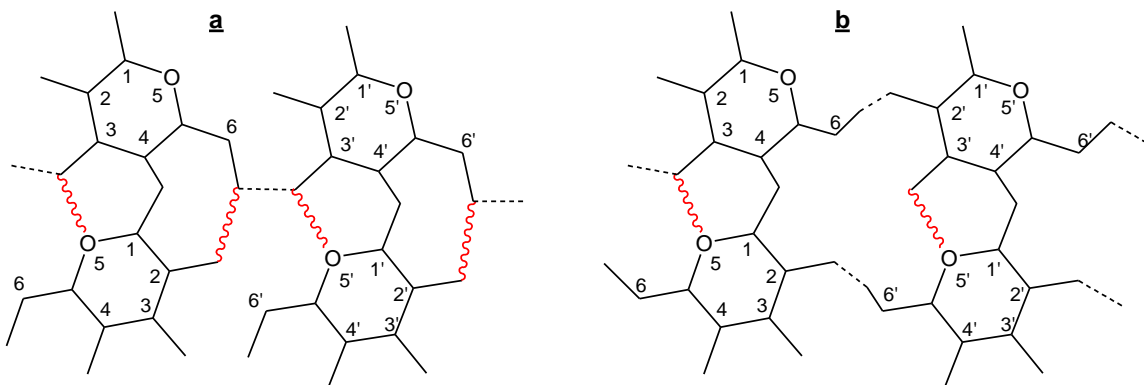


**Figure 1.1.2.** Intra- (red wavy lines) and intermolecular (black dashed lines) hydrogen bonds between adjacent AGU molecules of cellulose I (a) and cellulose II (b).<sup>25–28</sup>

Cellulose II is generated from cellulose I by both swelling in sodium hydroxide solution (mercerization) or dissolution and subsequent recovery (regeneration).<sup>29</sup> This process alters the arrangement of the cellulose strands from parallel to anti-parallel with the C6-OH altering its orientation from trans-gauche (*tg*) to gauche-trans (*gt*), as described by Langan et al.<sup>30</sup> As a result, the intra- and intermolecular hydrogen bonds between the O2-H---O6 and O6-H---O3, respectively, are disrupted although that between the O3-H---O5 is maintained (**Figure 1.1.2**). Two new intermolecular hydrogen bonds are formed, one between the O6-H---O2' in the same plane and one between the O2-H---O2'' in an adjacent plane establishing a 3-D network of hydrogen bonds.<sup>30</sup> In addition, the regeneration of cellulose dramatically reduces the DP to values between 250-500.<sup>31</sup>

As a result of the extensive hydrogen bonding, van der Waals and hydrophobic interactions cellulose is not soluble in most common solvents and is not melt-processable, and as such decomposes before it undergoes melt flow. However, regeneration or functionalization of the hydroxyl groups in cellulose (cellulose derivatives) facilitates its industrial processing. The average number of hydroxyl groups substituted per AGU is known as the degree of substitution (DS) which can be analyzed by nuclear magnetic resonance (NMR) spectroscopy, elemental analysis or hydrolysis and subsequent chromatography.<sup>2,32,33</sup> Higher degrees of substitution, or reaction conditions which disrupt the crystalline regions, can be used to reduce intra- and intermolecular hydrogen bonding and facilitate the processing of cellulose. Furthermore, the distribution of these interactions within the AGU greatly affects the properties of the cellulosic materials; this matter will be further discussed in section 1.3. The primary purpose of cellulose

derivatization is to overcome some of celluloses inherent drawbacks, such as poor solubility in common solvents, poor dimensional stability, lack of thermoplasticity and absence of anti-microbial properties.<sup>34</sup> Therefore, improving the chemical/physical properties of cellulose allows one to produce materials that may be processed into various useful forms, such as three dimensional objects, fibres, and solutions to be used for coating or casting (of films or membranes, for example).

## 1.2 Cellulose Derivatives

Cellulose derivatives are synthesized through functionalization of the hydroxyl groups in the AGU. The properties of the new derivatives are primarily determined by the nature of the functional group, with a significant contribution from the degree of substitution and the degree of polymerization of the cellulose backbone.<sup>35</sup> The most important cellulose derivatives from an application point-of-view are cellulose ethers and esters. The derivatization of cellulose follows standard commercial methods which are generally heterogeneous reactions and in the case of esters might include a subsequent deacylation reaction.<sup>36</sup> Heterogeneous reactions lead to the random insertion of different substituents at the free hydroxyl groups available along the AGU. As the various hydroxyl groups have different reactivities<sup>37,38</sup>, and are found within the crystalline and noncrystalline regions, celluloses with variable physicochemical properties are produced. On the other hand, the production of cellulose derivatives under homogeneous conditions allows one to obtain products with more reproducible properties.

The dissolution of cellulose can be described in three steps: 1) breaking of solute-solute attractions (endothermic process); 2) breaking of solvent-solvent attractions (endothermic process); and 3) forming new solvent-solute attractions (exothermic process). Dissolution occurs if the dissolved state is in a lower energy state than the solid state, which translates into Gibbs free energy change on mixing as  $\Delta G_m = \Delta H_m - T\Delta S_m$  ( $\Delta G$ -Gibbs free energy change on mixing;  $\Delta H$ -enthalpy change on mixing;  $T$ -absolute temperature and  $\Delta S$ -entropy change on mixing). When  $\Delta G$  lower than zero the reaction is favoured, if equal to zero the reaction is under equilibrium and if higher than zero the reaction is not favoured. Apart from the thermodynamics of the solvent/solute system, it is also necessary to consider the kinetics involved in this process. For macromolecules like cellulose the diffusion rate is inversely proportional to the size of the molecules, thus the larger the molecule the slower the dissolution rate. In order to increase the diffusion rate heat may be applied causing a decrease in viscosity.<sup>39</sup> The compatibility between the solute and the solvent may be predicted using Hansen solubility parameters.<sup>40,41</sup> Hansen solubility parameters were developed based on “like dissolves like”. The solvent and solute can be characterized by three parameters,  $\delta_d$  (energy from dispersion forces between molecules),  $\delta_p$

(energy from dipolar intermolecular force between molecules) and  $\delta h$  (energy from hydrogen bonds between molecules). The sum of the energy associated to each type of interaction corresponds to the cohesive energy, which is the increase in the internal energy per mole of the material if all of the intermolecular forces are eliminated. These three parameters define the Hansen space in which the closer the solvent and the solute are, in this three-dimensional space, the more likely they are to dissolve into each other.<sup>41</sup> This methodology has been successfully used for some cellulose derivatives, which include some cellulose acetate with different DS,<sup>42</sup> cellulose acetate butyrate<sup>43</sup> and commercial cellulose ethers<sup>40</sup>. Overall, the dissolution of macromolecules such as cellulose is a multidisciplinary subject requiring knowledge in both organic and inorganic chemistry as well as physical chemistry.

Homogeneous derivatization consists of 3 stages: 1) cellulose activation, 2) dissolution and 3) functionalization of the solubilised cellulose. The objective of the activation step is to increase the accessibility of the cellulose's hydroxyl groups to the reagents through inter- and intracrystalline penetration of the activating agent. The procedure used for this purpose depends on the cellulose structure (DP, purity and crystallinity) therefore, cellulose activation can be done thermally under reduced pressure (successfully used in heterogeneous carboxymethylation)<sup>44</sup>, through an alkali treatment<sup>45</sup> (transforms cellulose I into its polymorph cellulose II, ideal for cellulose with high crystallinity and high DP), or through polar solvent displacement at room temperature<sup>46,47</sup>, which is suitable for most cellulose. The latter consists of washing the cellulose with a series of solvents from water to the solvent that will be employed in the dissolution/derivatization step.<sup>45</sup> This procedure avoids extensive degradation of the cellulose backbone however, it is time consuming and requires different solvents.<sup>46</sup> Another cellulose activation procedure is the thermal treatment of cellulose with the reaction solvent, typically dimethylacetamide (DMA). First proposed by Ekmanis, this process is based upon the fact that the vapor pressure of N,N-dimethyl acetamide (DMA), near its boiling point, is enough to provide swelling and hence an efficient penetration of the reagents.<sup>48</sup> Cellulose dissolution occurs through physical interactions between cellulose and the solvent (non-derivatizing solvents) or through covalent bond formation between the solvent and the cellulose (derivatizing solvent). In the present work, cellulose dissolution was done via a non-aqueous non-derivatizing solvent, and for that reason only the latter will be addressed. The most highly investigated solvent systems involve the dissolution of LiCl in DMA, *N*-methyl-2-pyrrolidinone, or 1,3-dimethyl-2-imidazolidinone, and tetra-*n*-butyl ammonium fluoride trihydrate in DMSO (TBAF/DMSO).<sup>35,45</sup> Of these DMA/LiCl has been extensively used in the synthesis of large variety of cellulose derivatives, mainly due to the fact that this solvent system is colourless, less time- and labor-intensive. A detailed discussion of this matter can be found in the literature.<sup>35,45</sup> The development of solvent systems that disrupt the highly organized hydrogen bonding network within cellulose provides hydroxyl groups with greater reactivity, thus enabling reactions to be



carried out under milder conditions with higher selectivity. This results in better tailoring of physicochemical properties and the development of more homogeneous cellulosic structures.<sup>49,50</sup>

### 1.2.1 Cellulose ethers

Cellulose ethers are non-toxic, soluble in water and/or organic solvents and chemically stable. The processing of these derivatives can be done in a swollen or dissolved state, which is related, to a certain extent, to the nature of the substituents and respective DS. This typically leads to an increase in the viscosity of the solvent and the development of specific rheological profiles, very useful in applications which require a defined consistency in aqueous media and water containing systems.<sup>31</sup> Some of the main cellulose ethers and their fields of application are shown in **Figure 1.2.1** and listed in **Table 1.2.1**.

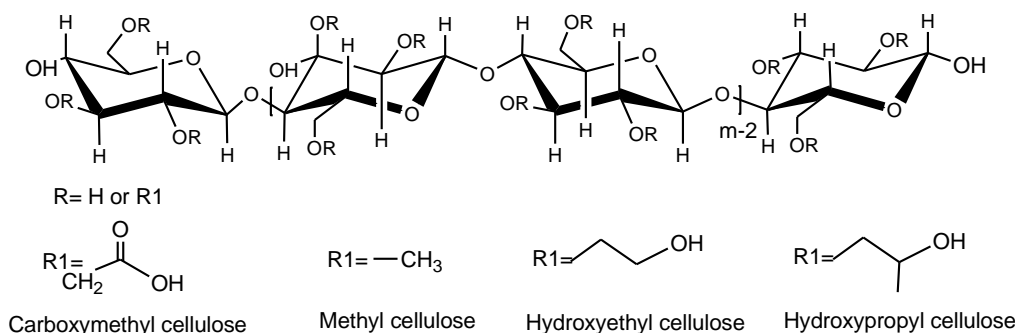


**Figure 1.2.1.** Representative structures of some of the commercially relevant cellulose ethers.

**Table 1.2.1.** Commercially relevant cellulose ethers and their primary applications.<sup>32</sup>

Carboxymethyl Cellulose	Methyl cellulose	Hydroxyethyl cellulose	Hydroxypropyl cellulose
Paper	Tile adhesives	Latex paints	Adhesives
Detergents	Pharmaceutical	Adhesives	Ceramics
Pharmaceutical	Cosmetics	Building materials	Cosmetics
Cosmetics	Wallpaper paste	Cosmetics	Encapsulation
Textile industry	Polymerization	Paper	Food
Food	Food	Agriculture	Polymerization
Coatings	Latex paints	Textile industry	Films
Encapsulation	Plasters/renders	Synthetic resins	

Alkyl cellulose ethers are generally obtained in the presence of strong bases such as sodium hydride (NaH), which ionize (activate) the hydroxyl groups in cellulose and react with an alkyl halide by a nucleophilic substitution ( $S_N2$ ) mechanism, i.e., Williamson ether synthesis. The production of carboxymethylcellulose is also done following Williamson ether synthesis in which the cellulose is activated with an aqueous alkali hydroxide solution (e.g., sodium hydroxide) and converted with monochloroacetic acid or its alkali salt. Hydroxyalkyl ethers can be obtained under aqueous alkaline media and the addition of an epoxide.<sup>31,51</sup> During this reaction there is a possibility of chain growth of the side chains by further addition of alkylene oxides; for that reason the macromolecular characterization of these derivatives (hydroxyethyl cellulose, hydroxypropyl cellulose, for example) includes the DS (average number of hydroxyl groups per AGU involved in the reaction) and molecular substitution (MS) which quantifies the average number of alkylene oxide molecules added per AGU. For example, the importance of these two parameters is reflected in the properties of hydroxypropyl cellulose (HPC); at a MS above 4 the HPC is soluble in cold water, gels at about 40°C and becomes insoluble (precipitates) at 45 °C.<sup>52,53</sup>

## 1.2.2 Cellulose esters

Cellulose esters are widely used in the industry due to their solubility in common organic solvents and processability into objects of various shapes, fibers, films and membranes, for example.<sup>54</sup> Their properties can be controlled through the nature of the ester substituent and the DS. The continuing importance of cellulose esters is stated in the pertinent review paper by Edgar et al.<sup>54</sup> In this review the main fields of application of cellulose esters are highlighted of which some of the general applications include coatings, controlled release devices, optical films and membrane structures. Some of the commercially relevant cellulose esters along with their primary applications are shown in **Figure 1.2.2** and listed in **Table 1.2.2**.

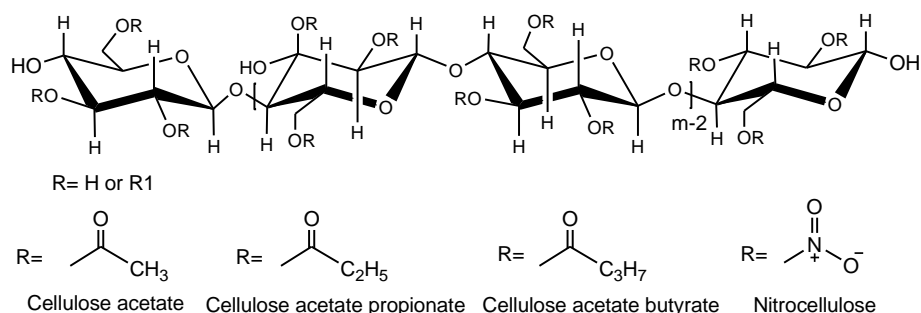


**Figure 1.2.2.** Representative structures of some of the commercially relevant cellulose esters.

**Table 1.2.2.** Commercially relevant cellulose esters and their primary applications.<sup>55</sup>

Cellulose acetate	Cellulose acetate propionate	Cellulose acetate butyrate	Nitrocellulose
Adhesive tape	Plastics	Plastic coating	Coatings
LCD displays	Coating	Metal coating	Explosives
Plastics	Nail care	Plastics	Printing inks
Coating	Printing inks	Drug delivery	Immobilization of
Drug delivery	Drug delivery	Laminating with	proteins
Membrane structures	Covers for television	aluminum foil	Drug delivery
Microfiltration media	screens	Goggles	Lacquers
Chiral separation			Photographic film
Gas-phase separation			

Esters of cellulose can be either organic (e.g., cellulose acetate) or inorganic (e.g., cellulose nitrate) if derived from an organic or inorganic acid, respectively. Homogeneous esterification of cellulose is usually done using acyl chlorides or carboxylic anhydrides in the presence of a base (e.g., pyridine, triethylamine and 4-N,N-dimethylaminopyridine) under homogeneous conditions. This allows for good control of the DS as well as a uniform distribution of the functional groups along the cellulose chains. The first step involves the activation by mild base to form the corresponding highly reactive acylammonium ion, followed by subsequent reaction with the cellulose hydroxyl groups. In the case of acyl chlorides, the base also acts as a scavenger of the formed hydrogen chloride to avoid excessive degradation of the cellulose backbone.<sup>56,57</sup> On the other hand, industrial manufacturing of cellulose esters may be done under acidic conditions in a heterogeneous medium. The process usually involves the addition of an organic or inorganic acid and a catalyst (e.g., sulfuric acid). The mechanism consists of the activation of the carbonyl group by the catalyst followed by the nucleophilic attack of the cellulose hydroxyl group to form the corresponding cellulose ester a water molecule.<sup>58,59</sup>

### 1.3 Regioselective Substitution of Cellulose

The regioselective synthesis of cellulose ethers and esters requires the ability to control the position of the substituents in the AGU, as well as along the chain. It has been shown that the regioselective distribution of functional groups within the AGU of cellulose derivatives plays an influential role in the relative reactivity of hydroxyl groups<sup>60</sup> and resulting physical properties,

such as: solubility<sup>60</sup>, crystallization<sup>60</sup>, gel formation<sup>61,62</sup>, liquid crystallinity,<sup>63</sup> and enzymatic degradation.<sup>64,65</sup>

In order to understand the relationship between the chemical structure of these derivatives and their physical properties, 2,3-*O* and 6-*O* cellulose methyl ethers were synthesized as model compounds to display a specific inter- and intramolecular hydrogen bonding arrangement.<sup>66,67</sup> As illustrated in **Figure 1.3.1**, 2,3-*O*-methylcellulose forms only one intramolecular hydrogen bond between the C6-OH of one AGU and the C2-OMe of an adjacent unit. The same C6-OH is also free to establish an intermolecular hydrogen bond. However, the C3-OMe is precluded from forming a hydrogen bond with the O-5 of the adjacent AGU. On the other hand, the 6-*O*-methylcellulose derivative is still capable of forming the two intramolecular hydrogen bonds found in cellulose, one between the C3-OH of an AGU and the O-5 oxygen in the pyranose ring of an adjacent AGU, and the other between the C2-OH and adjacent C6-OMe. In this case complete methylation of the C6 position disrupts all intermolecular hydrogen bonding.

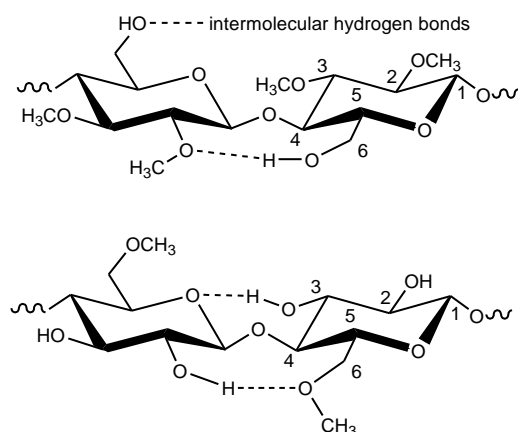


**Figure 1.3.1.** Inter- and intramolecular hydrogen bonding established in 2,3-*O*-methylcellulose (top) and 6-*O*-methylcellulose (bottom).<sup>60</sup>

Kondo<sup>60</sup> studied the correlation between the formation of intra- and intermolecular hydrogen bonds in cellulose and its derivatives and their physical properties such as solubility, hydroxyl reactivity and crystallinity. Solubility of cellulose derivatives is usually related to DP and DS. In general, lower DP and higher DS increases solubility, however, these are not the only factors. The distribution of the substituent groups along the cellulose backbone has been shown to play an important role in the solubility of the cellulose derivatives. It was found that 6-*O*-methylcellulose with a DS = 1 showed higher solubility in organic solvents with different polarities than commercial methylcelluloses with comparable DS, as well as 2,3-*O*-methylcellulose with a DS = 2. Thus, the presence/absence of intermolecular hydrogen bonding involving the C6

hydroxyl group is critical to the solubility of cellulose derivatives.<sup>61,68</sup> In the same study by Kondo<sup>60</sup> it was also found that 2,3-O-methyl cellulose was not soluble in water. However, when Kern et al.<sup>69</sup> improved the regioselectivity of this same derivative they observed that the latter had become water-soluble. This shows how solubility can be further altered by small differences in the distribution of substituents within the AGUs. Furthermore, Kondo<sup>60</sup> also studied films made from solubilised 6-O-methyl cellulose and 2,3-O-methylcellulose in DMA and CHCl<sub>3</sub>/MeOH (4:1 v/v) through X-ray diffraction. Regardless of the homogeneous distribution of the substituent group along the cellulose backbone of 6-O-methylcellulose, the X-ray patterns of the films made from both solvents did not show a crystalline pattern. This might be related to the presence of intramolecular hydrogen bonds. These may induce some chain stiffness in the cellulose backbone and lower the ability to rearrange cellulose chains in a more ordered manner. On the other hand the film obtained from 2,3-O-methyl cellulose showed a crystalline pattern when cast from DMA, but not in that cast from CHCl<sub>3</sub>/MeOH. This shows that crystallization depends not only on structural regularity, but also on chain flexibility and the interactions established between the solvent and the cellulose derivative to allow nucleation through molecular motion.<sup>60</sup>

The distribution of substituents along the cellulose backbone might also affect the reactivity of the hydroxyl groups (C2-OH, C3-OH, C6-OH). Croon and Lindberg<sup>70,71</sup> studied the synthesis of methyl cellulose from alkali cellulose in an aqueous solvent system and found that the relative reactivity of its free OH groups was: C2-OH > C6-OH > C3-OH. With this finding in mind, Kondo<sup>60</sup> analyzed the influence of intramolecular hydrogen bonds in the reactivity of C2-OH and C3-OH. Three cellulose derivatives were synthesized<sup>72</sup>: 6-O-methylcellulose, 6-O-benzylcellulose and 6-O-trityl cellulose. It was assumed that the methylated cellulose had two intramolecular hydrogen bonds (O3-H<sup>···</sup>O5 and O2-H<sup>···</sup>O6) whereas the benzylated analogue had only one between the C3-OH and pyranosidic O5 from the adjacent AGU (O3-H<sup>···</sup>O5) as the intramolecular hydrogen bond between the C2-OH and C6-O-benzyl was disrupted, due to the bulky benzyl group. On the other hand, 6-O-trityl cellulose had the two intramolecular hydrogen bonds C2-OH and C6-O-trityl and C3-OH and pyranosidic O5 disrupted due to the pronounced bulkiness of this group. The three derivatives were then methylated in DMSO under homogeneous conditions and the DS at C2 and C3 determined. In the case of 6-O-methylcellulose the relative reactivities of C2-OH and C3-OH were very similar and the DS values at C2 and C3 were 0.46 and 0.51, respectively. The similar reactivity between both hydroxyl groups might be due to the existence of intramolecular hydrogen bonding in positions C2 and C3 of the AGU, which means that the 6-O-methylcellulose is not completely solvated in DMSO. By contrast, 6-O-benzyl and 6-O-trityl cellulose derivatives exhibited different relative reactivities in the order of C2-OH > C3-OH, with DS at C2/C3 of 0.67/0.38 and 0.74/0.55 respectively. The increment in reactivity of the C2-OH is most likely due to the disruption of intramolecular hydrogen bonding involving that position. Furthermore, the DS in position C3 in 6-O-trityl cellulose was higher than that of the 6-O-benzylcellulose, 0.55 vs. 0.38,

respectively. This was explained as a consequence of the substituent effect, with bulkier functionalities such as the trityl group causing a change in the conformation of the cellulose backbone, disrupting the intramolecular hydrogen bond at C3 and increasing its reactivity.

Thus, substituent distribution has a significant impact on the final properties of the synthesized cellulose derivatives. Better control of these properties has become possible not only due to the development of new solvent systems for cellulose dissolution such as DMA/LiCl<sup>49,73</sup> (less time consuming and less labour-intensive procedure) and ionic liquids (1-buty-3-methylimidazolium chloride ([Bmim]Cl)<sup>74</sup> and 1-allyl-3-methylimidazolium ([Amim]Cl)<sup>75</sup> for its environmentally friendly properties, but also due to advancements in synthetic modification of cellulose using protecting group chemistry, selective cleavage of primary substituents and activating groups which allowed for the preparation of regioselectively substituted cellulose derivatives with improved regioselectivity.<sup>1-3</sup> These not only play an important role in better understanding the structure and property relationships of cellulose derivatives, but also are part of an industry with a demand for “tailor-made” materials.<sup>3,4,6,7,13,50,76</sup> In the present work the focus will be on the regioselective functionalization of cellulose by a protecting group technique. The latter consists in blocking a specific hydroxyl site from further derivatization with a protecting group, leaving the remaining hydroxyl groups free for etherification/esterification reactions. Afterwards the protecting group can be removed. This strategy is based on the differences in reactivity (steric hindrance) of the three hydroxyl groups in the AGU and the higher acidity of the hydroxyl group at the C2 position.<sup>77</sup>

In the regioselective modification of cellulose, “bulky” protecting groups such as the trityl derivatives (trityl and *p*-monomethoxytriphenylmethyl, a more reactive trityl derivative) and silyl derivatives (thexyldimethylsilyl and tert-butyl dimethyl silyl) are commonly used.<sup>3</sup> The trityl derivatives react preferentially with the primary C6-OH rather than the secondary C2- or C3-OH, and are readily removed under mild acidic conditions.<sup>78-81</sup> Using this approach the C2 and C3 positions can be functionalized and the resulting substituents at positions 2,3-O<sup>66,82</sup> and 6-O<sup>67,83</sup> will be different. In the present work, one of the synthetic strategies chosen for our synthesis was based on regioselective silylation. Therefore, this subject will be discussed in more detail. The development of silylation protecting chemistry has produced new regioselectively substituted cellulose derivatives. The use of either heterogeneous or homogeneous media has produced 6-O-protected cellulose derivatives or 2,6-O-diprotected cellulose derivatives, respectively. The first one is produced from swollen cellulose in a mixture of ammonia and DMF or *N*-methylpyrrolidone at -15 or -25 °C, respectively, followed by the addition of thexyltrimethylsilyl chloride to obtain the exclusive silylation of the primary hydroxyl group.<sup>84,85</sup> 2,6-O-Thexyltrimethylsilyl cellulose is obtained under homogeneous conditions in DMA/LiCl with a DS of 1.8,<sup>84</sup> if using pyridine as the base, and a DS of 2 when employing imidazole<sup>2</sup>. The higher effectiveness of imidazole is due to the formation of a highly reactive intermediate, TDMS imidazolidine. After functionalizing the free

hydroxyl groups, deprotection of the silyl groups is performed by the addition of tetrabutylammonium fluoride (TBAF) to produce the corresponding 2,3-O- and 3-O- substituted cellulose derivatives. Etherification of the C3-OH in 2,6-O-thexyldimethylsilyl cellulose is typically done with a strong base (e.g., NaH) and an alkyl iodide, bromide or chloride, followed by the deprotection of the silyl protecting groups.<sup>2,86–89</sup> This method has allowed the successful syntheses of numerous 3-O- derivatives, such as 3-O-hydroxyethyl<sup>90</sup> and hydroxypropyl<sup>91</sup> cellulose with a DS of 1, both soluble in water. Similarly, Kadla et al.<sup>4,92</sup> have synthesized amphiphilic regioselective 3-O-poly(ethylene glycol)-2,6-O-thexyldimethylsilyl celluloses, which have been shown to self assemble into films with honeycomb-like structures.

As with the cellulose ethers, the regioselectively substituted cellulose esters also produce materials with unique properties. For example, Hattori and Tsunashima<sup>93</sup> found that the regioselective distribution of acetyl and trityl groups at the C2, C3 and C6 positions of the AGU play an important role with respect to chain conformation, solubility and associative properties and structures in solution. Furthermore, Tasaka<sup>94</sup> found an improvement in the optical properties of cellulose ester films when producing regioselective cellulose acetate propionates vs. the randomly substituted ones. Following the same protecting group chemistry, regioselectively substituted cellulose esters have been synthesized by acylating 6-O-thexyldimethylsilyl, 2,6-O-thexyldimethylsilyl and 6-O-trityl protected celluloses. Finally, the deprotection of TDMS and trityl groups will produce compounds, such as 2,3-O-acetyl cellulose,<sup>95</sup> 2,3-O-acetyl-6-O-propyl cellulose<sup>95</sup> 6-O-acetyl-2,3-O-propyl cellulose<sup>95</sup> 6-O-acetyl cellulose<sup>96</sup> 2,6-O-acetyl cellulose,<sup>96</sup> 2,3-O-methyl-6-O-acetyl cellulose<sup>84</sup> 3-O-methyl-2,3-O-acetyl cellulose<sup>84</sup> and 3-O-allyl-2,6-acetyl cellulose<sup>2</sup>. Iwata et al. have studied the molecular and crystal structure of 2,3-O-acetyl-6-O-propyl cellulose<sup>95,97</sup> and 6-O-acetyl-2,3-O-propyl cellulose,<sup>95,98</sup> which has a significant impact on its solid state properties. Hsieh and Kadla<sup>99</sup> synthesized regioselectively substituted 2,3-O-acetyl cellulose with different degrees of substitution (DS=2.4 and 2.8) and studied the effect of degree of acetylation and regioselectivity on the viscoelastic behaviour and properties of cellulose acetate gels. It was found that gels made from regioselectively substituted derivatives with DS=2.8 exhibited higher viscoelastic properties than those made with lower DS and random substitution. Based on the data obtained the authors suggest that the C6-OH has a significant effect on the hydrogen bonding networks and therefore the viscoelastic properties of the gels. These studies further support the idea that the position of the substituents in cellulose esters plays a major role on the final properties of the materials formed.

A traditional approach to the synthesis of regioselectively substituted cellulose esters comprises selective deacylation and acylation after protection. This is usually employed in the synthesis of 6-O ester cellulose derivatives. The procedure starts with the dissolution of cellulose in DMA/LiCl followed by the partial acetylation of cellulose with anhydrous pyridine/acetic anhydride; this yields a cellulose acetate preferentially acetylated at the C6. This is followed by

the partial deacetylation at 30 °C in DMSO with an 80 wt% aqueous solution of hydrazine monohydrate to produce the regioselectively substituted 6-O-acetyl cellulose with a DS = 0.6.<sup>96</sup>

Another attempt to synthesize regioselectively substituted cellulose esters was studied by Edgar et al.<sup>77</sup> in which bulky acid chlorides of pivalate, adamantate and 2,4,6-trimethylbenzoate were reacted with cellulose in different solvent systems, DMA/LiCl, [Amim]Cl and DMSO/TBAF. The best solvent system was found to be DMA/LiCl, and the esterification was in most cases selective for the primary hydroxyl group, although some acylation was observed at the secondary hydroxyl groups (C2-OH and C3-OH). Interestingly, the DMSO/TBAF solvent system was found to be ineffective with the bulkier acylation reagents, adamantoyl chloride and 2,4,6-trimethylbenzoate. Based on a recent study by Edgar and Xu<sup>100</sup> the fluoride ion might not be strong enough to deprotonate the acyl moieties in the alpha position to the carbonyl group. The degrees of substitution obtained from the reactions in DMA/LiCl were determined for each of the acylating reagents. Pivaloyl chloride reacted with a maximum DS of 1.82 ( $DS_{C6} = 1$  and  $DS_{C2,3} = 0.82$ ), adamantoyl chloride functionalized cellulose with a maximum DS of 1.74 ( $DS_{C6} = 1$  and  $DS_{C2,3} = 0.74$ ), while 2,4,6-trimethylbenzoyl chloride only produced a DS of 0.63, which might be due to the steric hindrance and the electron withdrawing effect of the three methyl groups of the aromatic ring. The partial distribution of substituents was calculated for a sample with a DS of 0.46 and found to be 0.4 at C6-OH and 0.06 at C2- and C3-OH. Surprisingly, this same reaction in [Amim]Cl gave a higher DS of 1.21 ( $DS_{C6} = 0.83$  and  $DS_{C2,3} = 0.38$ ).

From the literature it is apparent that bulky ethers are more selective for C6-OH substitution than bulky esters. This was explained by Edgar et.al.<sup>77</sup> as a consequence of the bulky ether being one atom closer to the cellulose backbone as well as the smaller bond angle of the  $sp^3$ -hybridized ether bond (109.5°) compared to the  $sp^2$ -hybridized ester bond (120°).

Through the regioselective modification of cellulose a better understanding of the uniqueness of cellulose structure can be obtained. Regioselective modification leads to cellulose derivatives with improved properties by producing materials with a controlled pattern of substitution, and well-defined supramolecular architecture. However, to further expand the application of cellulose into new fields other approaches in combination with regioselective modification are needed, e.g., polymer blending and/or the synthesis of regioselectively substituted copolymers. The introduction of active functionalities allows further modification of cellulose derivatives, in particular grafting from the cellulose backbone polymers with specific properties that will complement those of the initial cellulosic material.



## 1.4 Graft Copolymers

The production of cellulose copolymers through graft polymerization provides an important route to modify physical and chemical properties, such as heat resistance, elasticity, resistance to abrasion and wear, oil and water repellency, ion-exchange capabilities, and antibacterial activity, without destroying the intrinsic properties of cellulose.<sup>34,101–105</sup> The first reported cellulose graft copolymer was synthesized by Ushakov in 1943. He attached allyl or vinyl esters to cellulose and used these sites to initiate a copolymerization with maleic acid esters. However, the products were insoluble and therefore, its full characterization was not possible.<sup>106</sup> Cellulose graft copolymers generally consist of a cellulose backbone to which one or more side chains are chemically linked through covalent bonds. Depending on the end-use, properties can be tailored by using specific polymers with varying degrees of polymerization, initiator density and distribution.<sup>107</sup> The grafting process can be done by three different approaches: “graft-onto”, “graft-through” and “graft-from”. In the “graft-onto” method, a pre-formed polymer with a reactive end-group is coupled with active sites on the cellulose backbone. This approach is restricted, because the preformed polymer is sterically hindered and therefore has limited diffusion to the surface of the cellulose. As a result, the rate and the grafting density are usually low. In “graft-through”, a macromonomer, usually a vinyl cellulose macromonomer, is copolymerized with a low molecular weight co-monomer. The main drawback of this approach is the required synthesis of the cellulose base macromonomer. The most commonly used grafting method is “graft-from” in which the grafted polymer grows from existing initiating sites along the cellulose backbone. The accessibility of the end-group to the reacting monomer allows higher graft densities.<sup>108,109</sup> Cellulose-based grafting copolymers have been synthesized through different polymerization methods such as free radical polymerization<sup>101,110,111</sup>, ionic<sup>112–117</sup> and ring-opening polymerization<sup>118,119</sup> and controlled/“living” radical polymerization<sup>120–123</sup>. Free radical polymerization is applicable to a large number of monomers such as (meth)acrylates,<sup>124</sup> (meth)acrylamides,<sup>101,124</sup> styrene,<sup>125</sup> vinyl acetate<sup>126</sup> and acrylic acid<sup>127</sup>. It is also tolerant towards many solvents, functional groups (OH, NR<sub>2</sub>, COOH, CONR<sub>2</sub>), water and impurities. Furthermore, it can be run in bulk, solution, emulsion, mini-emulsion and suspension under mild reaction conditions. Radical polymerization takes place in three distinct steps: chain initiation, chain propagation and chain termination. The initiation step consists of the formation of cellulose derivative radicals, which can be obtained through chain transfer, directly on the cellulose derivative backbone *via* chemical activation and through radiation with ultraviolet light,  $\gamma$ -rays or plasma treatment. In the second step the monomer adds onto the propagating radical and chain growth occurs by successive addition of monomer units to the end of the growing chain. Finally,

termination occurs when propagating radicals react by combination, disproportionation and chain transfer to monomer, to initiator, to dead polymer, to additives and to impurities.<sup>38,128</sup>

Initiation by chain transfer starts with the formation of a radical ( $R^*$ ) through the addition of an initiator, such as 2,2'-azobisisobutyronitrile or benzoyl peroxide. The newly formed  $R^*$  will react with a monomer (M) to form a propagating radical ( $RM_n^*$ ). This polymerization is then terminated through the abstraction of a hydrogen atom from the cellulose derivative to form the respective radical and initiate chain growth; however, the yields are low. In order to increase the yields, compounds with higher chain activity, such as thiol<sup>110</sup> and xanthate ester<sup>129</sup> groups, may be introduced into the cellulose derivatives before grafting. As a result, a lower amount of homopolymer is formed and higher polymer grafting is observed. On the other hand, initiation through potassium persulfate, also a chain transfer method, requires a swollen cellulose derivative backbone in a solution of potassium persulfate.<sup>130-132</sup> Acrylic acid and acrylamide monomers have been grafted onto carboxymethyl cellulose to produce a super-absorbent cellulose-based material.<sup>127</sup> Redox reaction promoted by Fenton's reagent has also been used in chain transfer free radical polymerization. It consists of a solution of hydrogen peroxide and Fe (II) which is adsorbed on the cellulose derivative substrate. A redox reaction between Fe(II) and hydrogen peroxide will produce hydroxyl radicals and Fe (III).<sup>133</sup> The newly formed radicals will abstract a hydrogen atom from the cellulose derivative to form cellulose derivative radicals. The latter will then initiate polymerization in the presence of a monomer. Homopolymerization may occur but it may be minimized due to the proximity of the adsorbed Fe(III) and the hydroxyl radical to the cellulose derivative substrate.<sup>132</sup>

As previously mentioned, radical formation in graft polymerization can also be done directly on the cellulose derivative backbone by chemical activation. Direct oxidation with ceric (IV) (Ce (IV)) offers many advantages because of its high grafting efficiency and lower amount of homopolymer formation. A simplified description of this mechanism consists of: i) oxidation of the cellulose by the ceric (IV) salts, such as cerium nitrate and cerium sulfate; ii) formation of an intermediate reversible complex between the Ce (IV) and cellulose and iii) formation of Ce (III) and cellulose radicals, which were created by hydrogen abstraction from the cellulose backbone.<sup>102,124,128,134,135</sup>

Doba et al.<sup>136</sup> have proposed that the grafting occurs preferentially at the reducing hemiacetal end-group and at C2 and C3 positions of the AGU rather than at the C6 position. Direct chemical activation can also be done in cellulose derivatives functionalized with peroxides<sup>137</sup>, Barton esters<sup>138</sup> or diazonium salts<sup>139</sup>. These can be decomposed to form radicals and initiate a graft copolymerization. For example, Kubota and Kuwabara<sup>137</sup>, prepared percarboxymethyl cellulose by mixing carboxymethyl cellulose in a hydrogen peroxide and sulfuric acid solution. The radical formation was done through irradiation in the presence of monomer, acrylic acid or methacrylic acid. The synthesized copolymers may be used as cellulosic water absorbents. Finally, as part of the direct radical formation by chemical activation, functionalization of the cellulose backbone with

unsaturated groups such as, allyl and vinyl may also be used to form cellulosic radicals. The double bonds of these functional groups are activated by a free radical initiator enabling the graft copolymerization.<sup>132,140</sup> However, the drawback of this method is the possibility of crosslinking reactions to occur between the double bonds, depending on the degree of substitution and monomer reactivity.<sup>128</sup>

Radiation-induced grafting of cellulose is another method used in free radical polymerization and is usually done using ultraviolet light<sup>125,131,141,142</sup> gamma rays,<sup>143,144</sup> or plasma ion beams<sup>145</sup>. Ultraviolet radiation induced grafting requires a photoinitiator that has the ability to form a radical by hydrogen abstraction when exposed to UV radiation.<sup>146</sup> The newly formed radicals abstract hydrogen from the cellulose to form cellulose radicals to initiate the graft polymerization in the presence of vinyl or acrylic monomers. Examples of photoinitiators include uranyl nitrate, ceric (IV) ammonium nitrate and benzoin ethyl ether.<sup>131,133,141</sup> The lower energy of this radiation prevents the degradation of the cellulose backbone and therefore a better control of the polymerization in comparison to the higher energy,  $\gamma$ -radiation method.<sup>125,141</sup>  $\gamma$ -Irradiation of cellulose derivatives may be performed by two different methods, pre-irradiation and mutual. In the first method, the irradiation of cellulose is done separately and it is followed by the addition of the monomer. One of the advantages of this method is the formation of considerably less homopolymer when comparing to the mutual method.<sup>147</sup> However, the degradation of the cellulose backbone is significantly higher especially in the presence of oxygen.<sup>132,148</sup> On the other hand, in the mutual method the irradiation is done simultaneously on the cellulose backbone and monomer. As previously mentioned, the formation of homopolymer is significantly higher but the degradation of the cellulose fibre is lower.<sup>132,149</sup> The use of high energy radiation in the grafting of cellulose copolymers presents some advantages such as the simplicity of the method and its efficiency, because the modification of cellulose is not required prior to polymerization.<sup>133</sup> Nevertheless, it also presents some disadvantages, for instance the cellulose degradation *via* the splitting of the glycosidic bond<sup>150</sup> causes loss of mechanical strength<sup>151</sup> and the radical formation is unselective because it is dependent on the path of the incident radiation beam.<sup>133</sup>

In conclusion, free radical polymerization presents some advantages and it is one of the most important commercial processes.<sup>128,152</sup> However, the drawbacks such as degradation of the cellulosic backbone, limited control over the molecular weights, high polydispersities, low initiator density associated with high degree of polymerization and potential homopolymerization preclude the use of this method for the synthesis of controlled polymers. Furthermore, the absence of reactive end-groups in the grafted chains excludes the synthesis of block copolymers.<sup>153–156</sup>

Cellulose graft copolymers may also be synthesized through ionic (cationic and anionic) and ring opening polymerization. In general, ionic polymerizations are time- and labour-intensive and require rigorous conditions (low temperature, highly pure reagents, inert atmosphere, anhydrous conditions). Nevertheless, cationic and anionic polymerization methods were successfully used to

obtain well-defined cellulose graft copolymers.<sup>112,114,156–159</sup> However, these methods rely on the “graft-onto” technique and therefore cellulose graft copolymers with limited rate and graft density are obtained. Furthermore, the use of carbanions for grafting requires complete protection of the hydroxyl groups of the cellulose, and the homopolymerization may dominate over graft polymerization.<sup>115,160,161</sup> In the method of ring opening polymerization a reactive centre located in the cellulose reacts with a cyclic monomer, resulting in ring-opening and the formation of a new reactive centre, which can proceed to react with a second monomer, etc. (propagation). If the reactive centre is a cation or an anion the process is called cationic or anionic ring opening polymerization, respectively. If the monomer is a strained cyclic olefinic in the presence of a metal catalyst the process is called ring opening metathesis polymerization. The reaction between these two compounds forms a metal carbene which then attacks the double bond of the strained cyclic olefin. Afterwards a highly strained intermediate is formed favouring the ring opening. As a result, a linear chain with a double bond linked to the metal will react with another monomer (propagation). Ionic and ring opening graft polymerizations are out of the scope of this study and therefore these subjects will not be discussed further. In the present work, controlled/“living” radical polymerization (CRP), in particular atom transfer radical polymerization (ATRP) was used to do the graft copolymerization.

### 1.4.1 Controlled/"living" radical polymerization

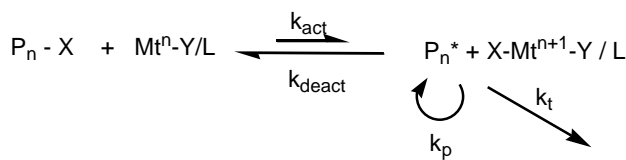
Living polymerization was first demonstrated by M. Szwarc in 1956<sup>162,163</sup> using an anionic polymerization of styrene with an alkali/metal and naphthalene system in THF. According to Szwarc et al.<sup>164</sup> the definition of a "living polymer" is that it "retains its ability to propagate for a long time, and grows to a desired maximum size while the degree of termination or chain transfer is still negligible". Szwarc observed that, for processes in which termination and chain transfer are eliminated, and initiation is fast, polymers of narrow molecular weight distribution could be synthesized.<sup>163</sup> This can be accomplished because the rate of chain initiation is higher than that of chain propagation, and chain termination/chain transfer reactions are negligible. Thus, the polymer chains grow at a more constant rate than seen in traditional chain polymerization, and the chain lengths remain very similar, hence polydispersity indexes (PDI) are low. Overall, living polymerization mechanisms offer advantages that include the ability to control molecular weight, PDI, architecture (e.g., block, graft copolymers), and end group functionalization.<sup>165,166</sup> However, this method is incompatible with a number of functionalities<sup>167</sup> and requires stringent reaction conditions, such as the complete absence of oxygen and water impurities, as well as ultra-pure solvents and reactants. As a consequence, the commercial application of living chain polymerization has been limited to a few systems. On the other hand free radical polymerization is a very versatile and convenient method, however, its products exhibit poor control of DP, end functionalities, chain architectures and compositions. Therefore, the desire to combine the virtues of living polymerization and free radical polymerization led to the development of controlled/"living" radical polymerization (CRP) techniques.<sup>108,168–170</sup> CRP employs the principle of dynamic equilibration between growing free radicals and various types of dormant species. There are three main methods: 1) stable free radical polymerization (SFRP), best represented by nitroxide mediated polymerization (NMP),<sup>171–174</sup> 2) reversible addition-fragmentation chain transfer (RAFT) polymerization,<sup>167,175,176</sup> and 3) reversible termination by ligand transfer to a metal complex, or atom transfer radical polymerization (ATRP).<sup>8,170,177</sup>

ATRP is known for its many advantages such as the wide range of commercially available monomers and (macro)initiators. Its large equilibrium constant means faster polymerization and milder experimental conditions (temperatures range from room temperature to 120 °C). The equilibrium constant can be tuned by altering the initiator, transition metal and ligands. Catalytic amounts of transition metal complexes are used and end-functionalization is possible. Some of the main disadvantages of ATRP include the impossibility of polymerizing acidic monomers and the necessity to remove the transition metal complexes and the green colour of the (co)polymers. This can be done by extraction with water or by treating the reaction mixture with

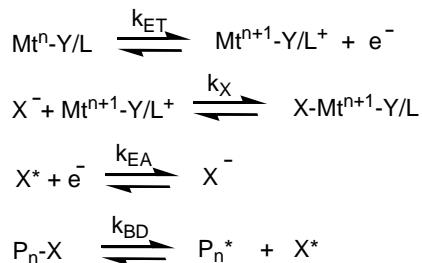
alumina.<sup>170,178,179</sup> The advantages of NMP over ATRP include the fact that purely organic systems can be employed, and it is applicable to many monomers (including acidic monomers). However, the main disadvantages of NMP are the lower equilibrium constants, which require higher reaction temperatures (125-145 °C) and longer reaction times (1 - 3 days). The reagents are expensive, are used in stoichiometric amounts relative to the number of polymer chains, and can include toxic transition metal compounds. Therefore, an extra step is required to remove the transition metal complex after completion of the reaction. As well, the introduction of end functionality to the polymer is challenging.<sup>178,179</sup> As compared to ATRP and NMP the RAFT process has been used with a wider range of monomers, and the systems are frequently mediated by purely organic reagents. However, these processes require a constant supply of radical initiators, which create new polymer chains and may cause termination reactions. Some of the main limitations of RAFT are the lack of commercially available transfer agents, the necessity to remove dithioesters and end groups due to their colour, toxicity and potential odour, and the difficulty associated with end-functionalization.<sup>179</sup> Based on this we chose to proceed with the copolymerization via ATRP.

### 1.4.1.1 Atom Transfer Radical Polymerization (ATRP)

Atom transfer radical polymerization (ATRP) was developed, independently, by Wang and Matyjaszewsky<sup>8</sup> and Kato et al.<sup>9</sup> and is described in **Scheme 1.4.1**.



Contributing Reactions:



$$K_{ATRP} = k_{act}/k_{deact} = K_{ET}K_XK_{EA}K_{BD}$$

$$R_p = k_p K_{eq} [I]_0 [Y] / [XY^*]$$

$$DP = \Delta[M] / [I]_0$$

**Scheme 1.4.1.** General reaction scheme of ATRP and contributing reactions.  $K_{ET}$  - equilibrium constant for electron transfer;  $K_X$  - equilibrium constant for the heterolytic cleavage of the  $Mt^{n+1} - X$  bond;  $K_{EA}$  - equilibrium constant for electron affinity of the halogen;  $K_{BD}$  - equilibrium constant for bond dissociation of the alkyl halide.

The ATRP process consists of a transition metal species ( $Mt^n$ ), with the ability of increasing its oxidation number, a complexing ligand (L), and a counterion (Y) that can form a covalent bond with the metal centre. The complex formed by these species,  $Mt^n - Y/L$  is responsible for the homolytic cleavage of an alkyl halogen bond ( $P_n - X$ ) generating the corresponding higher oxidation state metal halide complex  $X - Mt^{n+1} - Y/L$  (with a rate constant  $k_{act}$ ) and an organic radical  $P_n^*$ . The latter can propagate ( $k_p$ ) with the monomer, terminate as in conventional free radical polymerization ( $k_t$ ), or be reversibly deactivated ( $k_{deact}$ ) in this equilibrium by  $X - Mt^{n+1} - Y/L$  to form a halide-capped dormant polymer chain. The propagating radicals can be terminated by either radical coupling or disproportionation ( $k_t$ ). Termination is suppressed in ATRP as a result of a

persistent radical effect (PRE).<sup>180</sup> Consequently, the equilibrium is strongly shifted toward the dormant species, higher  $k_{\text{deact}}$ , thus the radical concentration is low and termination is suppressed.  $K_{\text{ATRP}}$  can be expressed as the product of the equilibrium constants for electron transfer between metal complexes ( $K_{\text{ET}}$ ), electron affinity of the halogen ( $K_{\text{EA}}$ ), bond dissociation energy of the alkyl halide ( $K_{\text{BD}}$ ) and the equilibrium constant for the heterolytic cleavage of  $\text{Mt}^{n+1}\text{-X}$  bond ( $K_{\text{X}}$ ). The latter is a measure of the “halidophilicity” of the deactivating species, which means that the activity of the catalyst in ATRP depends not only on the redox potential, but also on the halidophilicity of the transition metal complex. For a given catalytic system in the same solvent,  $K_{\text{ET}}$ ,  $K_{\text{EA}}$  and  $K_{\text{X}}$  are constant, which means that  $K_{\text{ATRP}}$  should vary upon the energy for the bond dissociation of the alkyl halide to occur ( $K_{\text{BD}}$ ).<sup>181,182</sup>

An efficient ATRP catalyst should ensure that all polymer chains start to grow simultaneously through a fast and quantitative initiation. The initiation step should not be too fast otherwise a high concentration of radicals is generated causing an increase in radical termination and a decrease in the efficiency of the initiator. When the equilibrium is shifted towards the deactivated species the radical concentration decreases, and the proportion of radical termination reactions is lower in the overall polymerization. A fast deactivation of the radicals by halogen transfer assures that all polymer chains are growing at similar rates producing polymers with a low PDI. The activation of the polymer chains should be done relatively fast in order to provide a reasonable polymerization rate and thus, side reactions such as  $\beta$ -H abstraction or reduction/oxidation of the radical should not occur. Therefore, to prove that a certain system is controlled one should provide a kinetic plot in semilogarithmic coordinates ( $\ln[\text{M}]_0/[\text{M}]$  vs. time) in which a first order reaction with respect to monomer is verified. If acceleration is observed it may indicate slow initiation, on the other hand deceleration might be caused by termination or deactivation of the catalyst. As well a linear progression of molecular weight with conversion should be observed; molecular weights lower than that predetermined by DP may be indicative of chain transfer, while those that are higher indicate inefficient initiation or chain coupling. Finally, PDI should decrease with conversion.

ATRP has been successfully mediated by different transition metals, such as:  $\text{Ti}^{183}$ ,  $\text{Mo}^{184}$ ,  $\text{Re}^{185}$ ,  $\text{Fe}^{186}$ ,  $\text{Ru}^9$ ,  $\text{Os}^{179}$ ,  $\text{Rh}^{187}$ ,  $\text{Co}^{188}$ ,  $\text{Ni}^{189}$ ,  $\text{Pd}^{190}$ , and  $\text{Cu}^{170}$ . Copper complexes were found to be the most efficient catalysts, and are reportedly superior in terms of cost and versatility. Styrenes, meth(acrylates), meth(acrylamides) and acrylonitrile have all been successfully polymerized using copper-mediated ATRP.<sup>191–194</sup> Classes of monomers which are not amenable to ATRP include acid monomers (carboxylic acid side groups react with the metal complexes to form carboxylate salts which are inefficient catalysts for ATRP) olefins, halogenated alkenes, and vinyl acetate (due to their low intrinsic reactivity toward radical polymerization).<sup>170</sup>

The transition metal and the choice of the complexing ligand are critical to the ATRP process. Nitrogen ligands have been widely used in  $\text{Cu}^{195}$  and  $\text{Fe}^{186}$  mediated ATRP, working particularly well for Cu. The role of the ligand is to solubilise the transition-metal salt in the organic medium



and to adjust the redox potential of the metal centre for appropriate reactivity and dynamics for the atom transfer.<sup>170,195</sup> Excessive steric hindrance or the presence of strongly electron-withdrawing substituents around the metal centre or the ligand have a negative effect on the catalytic activity or efficiency.<sup>170,195</sup> Nitrogen based ligands typically used in conjunction with copper include: bidentate bipyridine<sup>196</sup> (bpy), tridentate N,N,N,N,N'-pentamethyldiethylenetriamine<sup>197</sup> (PMDETA), tetradentate tris[2-dimethylamino]ethyl]amine<sup>198</sup> (Me<sub>6</sub>TREN) and tetraazacyclotetradecane<sup>199</sup> (CYCLAM), among other multidentate ligands<sup>200</sup> (Figure 1.4.1).

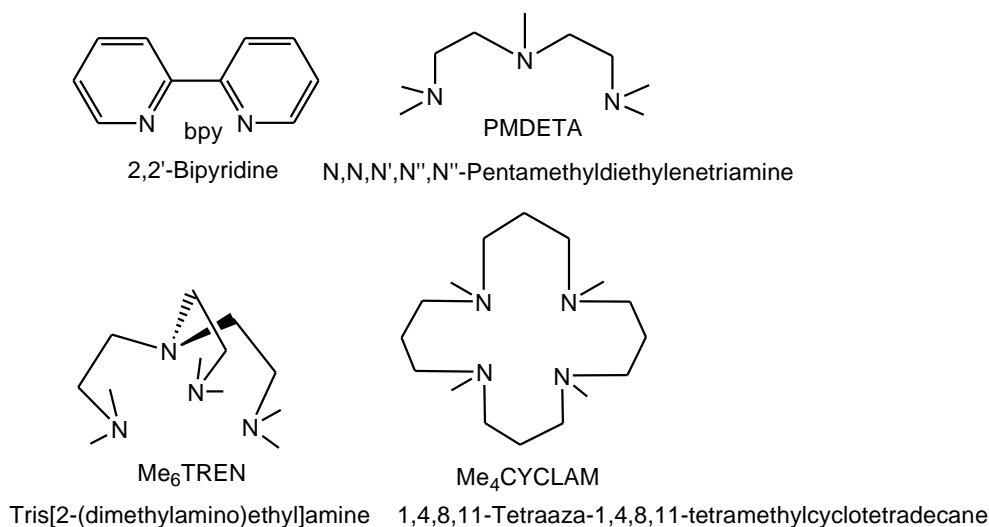


**Figure 1.4.1.** Examples of nitrogen based ligands used in ATRP in conjunction with copper.

The activity of N-based ligands in ATRP decreases as the number of coordinating sites decreases ( $N_4 > N_3 > N_2 > N_1$ ) and the number of linking C-atoms increases ( $C_2 > C_3 > C_4$ ). The nature of the nitrogen substituent also impacts activity with  $R_2N- > R-N= > Ph-N= > Ph-NR-$ . Bridged and cyclic systems are also more active than the linear analogues.<sup>170</sup> Branched tetradentate ligands, such as Me<sub>6</sub>TREN, provide the most strongly reducing ATRP catalysts.<sup>198,200</sup> Cu(I) prefers a tetrahedral or square planar configuration, which can be achieved in the cationic complexes with tetradentate ligands, or with two bidentate ligands. Tridentate ligands, such as PMDETA; presumably form tetrahedral neutral complexes. On the other hand, Cu(II) forms cationic trigonal bipyramidal structures with tetradentate ligands or two bidentate ligands, whereas tridentate ligands form square pyramidal neutral complexes.<sup>170,201</sup>

The main advantages of ATRP over other CRP processes are: the commercial availability of all reagents (alkyl halides, ligands and transition metals); the remarkable tolerance of functional groups; the milder polymerization conditions, and the fact that the dynamic equilibrium between

dormant species and propagating radicals can be easily adjusted by modifying the complexing ligand of the catalyst. It is the most robust CRP method, having been carried out in bulk, solution, suspension, dispersion and emulsion conditions at temperatures ranging from -20 °C to 130 °C.<sup>170</sup> However, despite the potential of the materials synthesized with this technique, the production on an industrial scale is very limited. This has been attributed to: 1) the special handling procedures required to remove all oxygen and oxidants from the systems, 2) catalyst concentrations required by ATRP can approach 0.1M in bulk monomer, and extensive post-polymerization purification of the product is often necessary and expensive,<sup>202</sup> and 3) most of the transition metal species used in this technique are generally considered mildly toxic, which means that the removal/disposal of large quantities of these catalysts may be environmentally harmful.<sup>203</sup> To surpass these limitations several recent ATRP initiation systems have been developed. One is the simultaneous reverse and normal initiation (SR&NI) procedure; it consists of the addition of a larger amount of alkyl halide initiator (normal ATRP) simultaneously with a small amount of radical initiators such as AIBN and the transition metal in its higher oxidation state (reverse ATRP). This procedure allows the use of a higher amount of active catalyst complexes. However, the free radical initiator will form only a small fraction of new polymer chains. Thus, it is not suitable for the preparation of pure block copolymers or systems with a more complex architecture.<sup>204</sup> Another recent development is the initiator for continuous activator regeneration process, ICAR. In this process, the active catalyst is produced by an in-situ reduction of a very small amount of deactivated catalyst (higher oxidation state transition metal) with a thermal radical initiator such as azobis(isobutyronitrile) (AIBN).<sup>205–207</sup> An improvement to SR&NI employs organic reducing agents to considerably lower the amount of required catalyst, and is referred to as AGET<sup>208</sup> (activators generated by electron transfer) and ARGET<sup>209</sup> (activators regenerated by electron transfer). In both systems the Cu(I) activator is quickly generated from the oxidatively stable Cu(II) catalyst precursors with the addition of non-radical generating reducing agents of which zero-valence metals (Cu<sup>0</sup>),<sup>210</sup> and tin(II) 2-ethylhexanoate (Sn(EH)<sub>2</sub>),<sup>211,212</sup> glucose,<sup>209,212</sup> and ascorbic acid<sup>213</sup> are some examples. Moreover, the reducing agents may also behave as oxygen and radical inhibitor scavengers.<sup>209</sup> AGET/ATRP requires a higher concentration of oxidatively stable Cu(II) catalyst, nearly stoichiometric amounts to the reducing agent.<sup>210,214</sup> On the other hand, ARGET/ATRP uses a reduced amount of Cu catalyst and an excess of reducing agent.<sup>209</sup> In these systems, many of the side reactions between the catalyst and chain ends (outer sphere electron transfer or β-hydrogen elimination) that can affect polymer molecular weights and chain end functionality are minimized.<sup>215</sup> Another important process is the addition or formation of a small amount of Cu(II) species at the beginning of the reaction. This enables the deactivation process to occur immediately without requiring its spontaneous formation by termination reactions, thereby providing both higher initiator efficiency and instantaneous control.<sup>216</sup>

#### 1.4.1.2 Cellulose graft copolymers via ATRP

Atom transfer radical polymerization has received increasing interest for its use in the synthesis of cellulose-based graft copolymers under homogeneous or heterogeneous reaction conditions. Homogeneous graft polymerization has been performed in underivatized<sup>11,217</sup> and derivatized celluloses such as cellulose acetate,<sup>123,218</sup> ethyl cellulose,<sup>122,161,219,220</sup> hydroxypropyl cellulose,<sup>120,221</sup> and of particular interest, in regioselectively substituted cellulose<sup>13</sup>. In order to synthesize cellulose graft copolymers through ATRP it is necessary to synthesize a cellulose-based macroinitiator. For example, underivatized cellulose reacted with 2-bromoisobutyryl bromide under homogeneous conditions in 1-allyl-3-methylimidazolium chloride ([Amim]Cl) to obtain an ATRP macroinitiator, 2-bromoisobutyryl-O-cellulose. The cellulose derivatives,  $DS_{2\text{-bromoisobutyryl}} = 0.72$  and  $0.93$ , were used to “graft-from” methyl methacrylate (MMA) in a CuCl/bpy/DMF system, and styrene in a CuCl/bpy/1,4-dioxane system, respectively. Monomer conversion was determined gravimetrically, which is not accurate, and a kinetic plot was built based on these results. An initial curvature was observed in both systems, likely related to the decrease of radical concentration due to partial termination. A linear kinetic regime was verified between 25 and 200 minutes (min) with conversions varying between 3.5 and 18.6% for MMA polymerization and 14.1% for styrene polymerization. The molecular weights of hydrolyzed poly(methyl methacrylate) (PMMA) and polystyrene (PSt) were found to increase linearly with conversion. Polydispersities of the different experiments varied between 1.2 and 1.5 for PMMA and 1.5 for PSt, and in both cases the PDIs decreased with conversion, as expected. These results suggest that both copolymerizations were done under controlled conditions. The authors also found that cellulose-g-PMMA had the ability to aggregate and self-assemble in solution.<sup>217</sup>

In another system Shen et al.,<sup>122</sup> synthesized ethyl cellulose-g-PSt and ethylcellulose-g-PMMA in the presence of CuBr/PMDETA/toluene. Ethylcellulose ( $DS_{\text{ethyl}} = 2.1$ ) was functionalized with 2-bromoisobutyryl bromide to achieve a  $DS_{2\text{-bromoisobutyryl}}$  of 0.5. Conversions of 20% and PDIs of 1.4 were achieved in both cases. PSt and PMMA were hydrolyzed from ethylcellulose and the respective number average molecular weight ( $M_n$ ) and PDI were plotted against conversion. As expected in a controlled copolymerization, the  $M_n$  increased linearly with conversion and the PDI decreased. In a different study done by the same author<sup>161</sup>, ethylcellulose ( $DS_{\text{ethyl}} = 2.1$ ) based macroinitiators with  $DS_{2\text{-bromoisobutyryl}}$  of 0.04 and 0.5 were used to produce EC-g-PSt (CuBr/PMDETA/toluene) with conversions of 10 and 20% and PDIs of 1.3 and 1.4, respectively. Linear kinetic plots confirmed first order reactions with respect to monomer concentration. The PSt side chains were hydrolyzed and the respective  $M_n$  and PDI plotted against conversion. In both cases the  $M_n$  increased linearly with conversion and the PDI decreased to values below 1.25 confirming the controlled character of the ATRP. The authors found that the copolymer

EC<sub>0.5</sub>-g-PSt self-assembled in acetone to form micelles, wherein the micellar diameter and shape regularity increased with increasing concentration.

Shen et al.<sup>123</sup> also produced cellulose diacetate-g-PMMA (CuBr/PMDETA:1,4-dioxane) from a cellulose diacetate with a DS<sub>2-bromoisobutyryl</sub> of 0.43. Conversions were very low (about 5%) and PDI varied between 1.4 and 2, under different experimental conditions. The kinetic plot confirmed a first order reaction. On the other hand, the authors were not able to obtain a linear relation between the Mn of the cellulose base copolymers and the respective conversions. In an attempt to prove that the copolymerization was done under controlled conditions, the authors hydrolyzed the side chains to obtain a low PDI of 1.12, after GPC analysis. Therefore, the authors concluded that the copolymerization was controlled. Although the PDI of the hydrolyzed side chains was low, there was no further confirmation by looking at the plot of Mn vs. conversion to confirm that the polymerization was controlled. Another caveat is that the conversion was too low to produce meaningful conclusions.

Vičák et al.<sup>218</sup> acylated cellulose diacetate (CDA) with 2-bromoisobutyryl bromide to obtain a DS of 0.12 and 0.52. The grafting of styrene was performed from both CDA-Br macroinitiators and as expected, the first led to copolymers with low grafting densities and higher DP (DP = 25), whereas the macroinitiator with higher DS produced densely grafted copolymers with lower DP (DP = 16). Conversions obtained from high and low DS<sub>2-bromoisobutyryl</sub> were found to be similar, 7 and 9%, respectively. PDIs were 1.93 for the lower DS<sub>2-bromoisobutyryl</sub> and 1.74 for the higher DS<sub>2-bromoisobutyryl</sub>. The controlled character of the copolymerization was monitored, and a first order reaction was verified which means that the concentration of active chains was virtually constant within a certain period of time. However, a graph illustrating the relation between Mn/PDI and conversion was not presented. This means that the controlled character of the copolymerization through ATRP was not completely assessed. The authors presented SEC elugrams corresponding to the copolymerization of CDA-Br (DS<sub>2-bromoisobutyryl</sub> = 0.12) at 6, 12 and 20 hours. The copolymer molecular weight increased with time and unimodal traces were observed for the samples measured at 6 and 12 hours. However, the copolymer obtained after 20 hours displayed a bimodal molecular weight distribution, which may have resulted from intermolecular recombination of the growing grafts. Thus, it is important to keep conversions low in order to avoid a possible recombination of the growing grafts. Furthermore, it was interesting to observe that a higher graft density copolymer, obtained from the macroinitiator with DS<sub>2-bromoisobutyryl</sub> of 0.52, generates side chains with a lower DP (DP = 16), compared with the DP (DP = 25) obtained from lower graft density copolymers (DS<sub>2-bromoisobutyryl</sub> = 0.12). On the other hand, conversions from these two experiments were very similar.

Ostmärk et al.,<sup>120</sup> synthesized a densely grafted PMMA from a commercially available hydroxypropyl cellulose (molar substitution of 2.9) substituted with 2-bromoisobutyryl groups (DS<sub>2-bromoisobutyryl</sub> = 2.26). Under typical ATRP conditions (Cu(I)Br:Cu(II)Br:PMDETA:toluene) the

high initiator density, due to the high DS<sub>2-bromoisobutyryl</sub> and the high concentration of radicals lead to radical coupling between growing polymer chains causing gelation. The authors found that by diluting the samples with at least 50 wt% solvent and by decreasing the ratio of Cu(I)/Cu(II) they were able to avoid gelation. Although the highest conversion obtained was 39%, the resulting copolymer PDI was very high (PDI = 3.7). Reducing the initiator DS to 1.13 (e.g., initiator density reduced to half) caused the PDI to increase even further to 4.1 and also decreased the conversion to 10%. The authors also investigated a dendronized hydroxypropyl cellulose (DS = 0.88) with a 2-bromoisobutyryl DS of 1.76. ATRP graft copolymerization resulted in a maximum conversion of 23% and a PDI of 1.2. Again, reducing the initiating sites to approximately half caused a decrease in the conversion to 14.5% and an increment in the PDI to 2. The authors concluded that the ATRP was more efficient when using the dendronized HPC due perhaps to a less crowded macroinitiator. Nevertheless, no detailed assessment of the controlled character of these reactions was provided, i.e., no kinetic or Mn vs. conversion plots were presented. Contrary to what was observed by Vlček et al.<sup>218</sup> conversions decreased substantially when lower graft density copolymers were synthesized. Overall, this work has demonstrated the importance of the reaction mixture concentration and Cu(I)/Cu(II) in gel formation in the synthesis of high graft density copolymers.

#### 1.4.1.2.1 Surface initiated ATRP (SI-ATRP)

Surface initiated ATRP (SI-ATRP) is an efficient and versatile technique that allows one to produce well-defined polymers under different experimental conditions, monomers and surfaces.<sup>222–224</sup> Various surfaces, such as gold<sup>223,225</sup>, silicon<sup>226,227</sup>, silica particles<sup>228</sup>, glass<sup>229</sup>, polyvinyl chloride<sup>230</sup>, and latex particles<sup>191</sup> have been functionalized by SI-ATRP. Cellulosic substrates such as cellulose powder and filter paper have also been modified using SI-ATRP. Coskun and Temüz functionalized the surface of cellulose powder with chloroacetyl groups and its surface grafted with styrene, MMA, methacrylamide and 4-acryloylmorpholine through surface initiated ATRP. These products were studied for thermal stability, water and dye absorption.<sup>231</sup>

Typically, the grafting of polymers from surfaces requires the immobilization of an initiator onto the solid surface. However, in order to conduct a controlled polymer chain growth it is recommended a small initiator, also called sacrificial initiator, is added to the reaction mixture. This allows the generation of a sufficient concentration of deactivator in solution, which contributes to a controlled initiation from the surface.<sup>226</sup> Furthermore, the presence of a soluble initiator allows the reaction to be followed through the monitoring of the homogeneous polymerization of the homopolymer/copolymer from the sacrificial initiator. Although it is not representative of the surface initiated ATRP, it allows one to verify whether the conditions for a controlled polymerization are met or not by analysing the respective products.<sup>154,227,232</sup>

Alternatively, a certain amount of Cu(II) can be added to the reaction mixture to achieve the necessary concentration of deactivator species.<sup>226</sup> The controlled character of the reaction can be assessed through the molecular weight of the polymer cleaved from the grafted surface. On the other hand, if the surface is flat the thickness of the film may also be monitored and it should also increase linearly with time.<sup>233</sup>

Carlmark and Malmström<sup>154</sup> prepared cellulose fibres (filter paper) and surface-grafted with methyl acrylate (MA) by surface initiated ATRP. The polymerization was initiated with the anchored 2-bromoisobutyryl groups and the complex catalyst/ligand Cu(I)Cl/bpy along with the addition of Cu(II)Cl. The halogen-terminated grafts were further copolymerized with 2-hydroxyethyl methacrylate (HEMA), to produce cellulose fibres with amphiphilic poly(MA-*b*-HEMA) surface grafts. This work demonstrated that hydrophilic/hydrophobic behavior of a cellulose surface could be tailored by ATRP.

Lindqvist et al.<sup>234</sup> produced dual responsive polymer brushes from filter paper as the cellulosic surface. The strategy was to first immobilize the initiator on the filter paper and then proceed with the surface initiated ATRP. The dual response was obtained via “grafting-from” block copolymers: poly(N-isopropylacrylamide)-*b*-poly(4-vinylpyridine) (PNIPAM-*b*-P4VP) and P4VP-*b*-PNIPAM. Dual-responsive cellulose surfaces were obtained and found to be reversibly responsive to temperature (PNIPAM) and pH (P4VP). Such materials are part of a wider class of polymers referred to as stimulus-responsive or “smart” polymers which can be classified according to the stimuli they respond to, as: thermo-<sup>101</sup>, pH-<sup>235</sup>, light or radiation-<sup>236</sup>, electric<sup>237</sup> - and magnetic field-<sup>238</sup> responsive. The uniqueness of these materials lies not only in the fast macroscopic reversible changes occurring in their structure, but also the reversible changes in the microstructure from a hydrophilic to a hydrophobic state. The responses are manifested as changes in: shape, surface characteristics, solubility, formation of an intricate molecular assembly such as sol-gel transition and others. These properties have attracted much interest for application in the fields of medicine and biotechnology,<sup>239</sup> for their use as drug delivery systems,<sup>240,241</sup> and for the immobilization of enzymes<sup>242</sup> and cells<sup>243</sup>.

## 1.5 Thermoresponsive Polymers

As previously mentioned, polymers that have the ability to respond to external temperature changes are known as thermoresponsive polymers. Temperature-sensitive polymers may exhibit upper or lower critical solution temperature (UCST or LCST, respectively) behaviour where phase separation is induced by surpassing a certain temperature threshold. In the present work we will be focusing our discussion on thermoresponsive polymers with LCST behaviour. This type of polymer undergoes a thermally induced, reversible phase transition; they are commonly soluble

in a solvent (water) at low temperatures becoming insoluble as the temperature rises above the lower critical solution temperature.<sup>244</sup> Thermoresponsive polymers can be classified into different groups: a) poly(vinyl ether)s, of which poly(vinyl methylether) (PVME) is an example with a LCST around 36 °C. It is usually synthesized by living polymerization techniques which require demanding experimental conditions;<sup>245</sup> b) poly(N-alkyl substituted acrylamides) e.g., poly(N-isopropylacrylamide) PNIPAM with a LCST of 32 °C,<sup>246</sup> it has been synthesized via free radical<sup>247</sup> as well as the advantageous controlled radical polymerization<sup>248</sup>; and c) poly(N-vinylalkylamides) e.g., poly(N-vinylcaprolactam) has a LCST of 32-35 °C and has been prepared through free radical polymerization.<sup>249</sup> There are other types of thermoresponsive polymers such as hydroxypropylcellulose (HPC), with a LCST of 42 °C as a result of a hydrophilic/hydrophobic interaction<sup>250-252</sup> and poly(ethylene oxide)<sub>106</sub>-poly(propylene oxide)<sub>70</sub>-poly(ethylene oxide)<sub>106</sub> copolymer,<sup>253</sup> with the trade name of Pluronic® F127; a solution with 25% (w/v) concentration shows a sol-gel transition around 20 °C. Recent studies have also investigated the potential of non-linear poly(ethylene glycol) analogues as thermoresponsive materials.<sup>254</sup>

One of the most studied thermoresponsive polymers is PNIPAM which exhibits thermoresponsive behaviour close to body temperature in aqueous solution; the insensitivity of its LCST to environmental conditions has attracted much attention. In fact, slight variations of pH, concentration or chemical environment generally affect the LCST by only a few degrees.<sup>247</sup> PNIPAM hydrogels have been explored for biomedical applications,<sup>255,256</sup> including controlled sorption and release of solutes,<sup>240,241,257</sup> control of enzyme activity,<sup>258</sup> and protein separation.<sup>259,260</sup>

PNIPAM typically adopts a hydrated random coil structure when dissolved in water at room temperature. As the temperature rises and approaches the phase transition point, the intermolecular hydrogen bonds formed around the polymer coil between water molecules and the N-H or C=O groups of the polymer are disrupted and intramolecular hydrogen bonding becomes predominant. Simultaneously, the hydrophobic isopropyl groups are also exposed to the outer layer forming a hydrophobic globule. These interactions may be responsible for the molecular structure of PNIPAM in water below and above the LCST (**Figure 1.5.1**).<sup>261-264</sup>

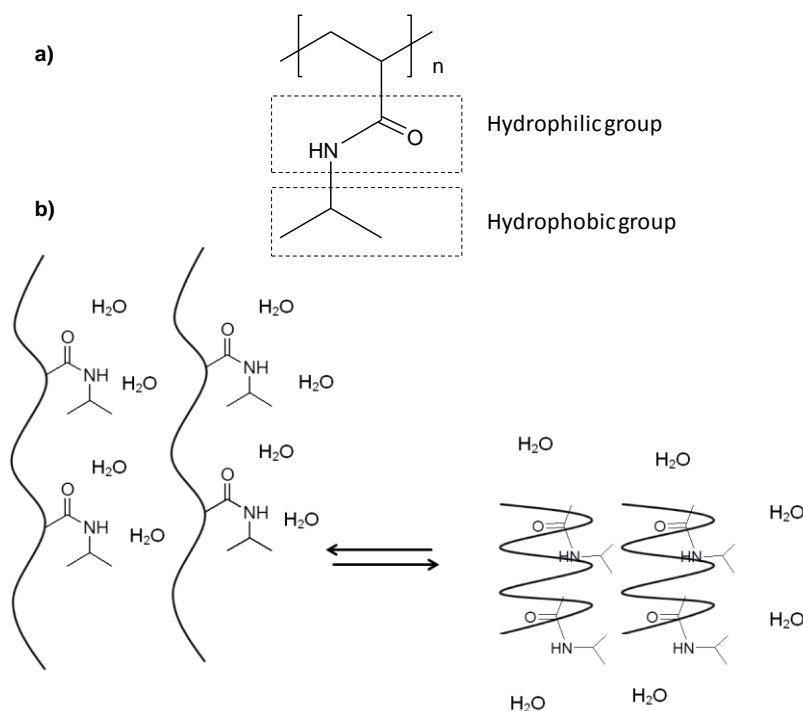


**Figure 1.5.1. a)** Molecular structure of PNIPAM and identification of the hydrophilic and hydrophobic groups; **b)** Thermoresponsive behaviour of PNIPAM below and above the LCST<sup>265</sup>.

The first attempts to polymerize meth/acrylamides such as NIPAM by ATRP were challenging, as polymerizations were not controlled and/or conversions were too low.<sup>266</sup> The use of Me<sub>4</sub>CYCLAM as a ligand produced polymers with a higher conversion but the polymerization was not controlled, which was attributed to the slow deactivation rate of the catalytic system. When using ligands with lower catalytic activity, such as unsubstituted bipyridines and the linear ligand, PMDETA, the conversions were too low (< 10%), which might have been due to slow activation in conjunction with fast deactivation. The poor control in the polymerizations was studied in detail and a combination of three plausible reasons has been discussed in the literature:<sup>266</sup> 1) complexation of copper by the amide group<sup>267,268</sup> in the forming polymer of meth(acrylamide) may slow down or even stop the polymerization. However, if the ligand employed has a high complexation constant for copper, such as 1,4,8,11-tetraaza-1,4,8,11-tetramethylcyclotetradecane (Me<sub>4</sub>CYCLAM) for example, then it will compete against the formation of the polymer-copper complex; 2) establishment of a strong bond between the terminal meth(acrylamide) unit in the growing polymer and the bromine atom which might cause a slower activation in conjunction with a fast deactivation. However, this does not explain the occurrence of termination reactions; and finally 3) nucleophilic displacement of the terminal bromine atom by the amide group, which will lead to the loss of initiating sites, hence irreversible deactivation of the



initiator. These consist of cyclization reactions and are accelerated in the presence of bromine, polar solvents and higher temperatures.

Teodorescu and Matyjaszewski reported the controlled polymerization of (meth)acrylamides by ATRP using Me<sub>6</sub>TREN as ligand in conjunction with CuCl and methyl 2-chloropropionate as the initiator.<sup>248</sup> The kinetic plot showed a fast rate of initiation followed by the loss of linearity, which is indicative of termination reactions. Limited conversion was also observed and it was found that the higher the ratio of catalyst: initiator the higher the conversion. Incomplete conversion might be caused by deactivation of the growing polymer chains. However, the low polydispersities (< 1.3) show that the deactivation is not extensive. Therefore, the loss of linearity in the kinetic plots might be due to deactivation of the catalyst rather than loss of initiating sites. Furthermore, the use of a bromine-based initiating system caused a significant decrease in conversion.

In 2005 Masci et al.<sup>269</sup> successfully polymerized NIPAM by ATRP using a solvent system of dimethyl formamide (DMF): water (75:25), Me<sub>6</sub>TREN as the ligand and ethyl 2-chloropropionate as the initiator. A linear kinetic plot was obtained at 92% conversion in only 35 min. This is indicative of a constant number of radicals and therefore, negligible termination and side reactions. Furthermore, the Mn increased linearly with conversion and a final PDI of 1.2 was obtained. Similarly, Xia et al.<sup>270</sup> also successfully polymerized NIPAM in different alcohols (methanol, ethanol, *n*-propanol, *i*-propanol and *t*-butanol) using methyl 2-chloropropionate and Me<sub>6</sub>TREN as the ligand. Polymerization in methanol (MeOH) turned blue with the addition of initiator indicating high concentration of Cu(II). A plateau was reached after 2 hours with a conversion of 32% and a low PDI of 1.13. On the other hand, ATRP in ethanol and *n*-propanol achieved higher conversions, ~ 65% where after 6 hours a plateau was reached. The final products revealed low PDIs (~ 1.1), which means that the curvature might be related to loss of catalyst and not initiating sites. In *t*-butanol the polymerization had a similar behaviour; however, the conversion further increased to 76% although the PDI was slightly higher (PDI ~ 1.2). The highest conversion was obtained from the branched alcohol *i*-propanol with 91% conversion in 7 hours and a PDI of 1.1. The dependence of Mn and conversion was found to be linear for polymerizations in *i*-propanol and *t*-butanol. In conclusion, Xia et al.<sup>270</sup> showed that by using the right combination of solvent, ligand and catalyst it was possible to polymerize an acrylamide like NIPAM under controlled polymerization conditions.

The adjustment of LCST is possible through the addition of additives. When saccharides were added to an aqueous PNIPAM solution a decrease in the LCST was observed, likely because of the increment in hydrophobic interactions between the polymer chains.<sup>271</sup> This behaviour was also observed with the addition of sodium chloride (NaCl), which was explained as a consequence of the salting-out effect, the water-structuring ability of salt ions decreasing the temperature at which phase separation occurs. On the other hand, surfactants contribute to a

better solubilisation of PNIPAM in water, resulting in an increase in the phase separation temperature.<sup>272</sup>

Another method used to adjust the LCST of PNIPAM is copolymerization. Virtanen et al.<sup>273</sup> grafted PNIPAM with varying amounts of poly(ethylene oxide) (PNIPAM-*g*-PEO) and found that the LCST increased with the number of PEO grafts as well as the dilution of the solution. Ifuku and Kadla,<sup>13</sup> developed a regioselectively substituted thermoresponsive 6-O-poly(*N*-isopropylacrylamide)-*g*-2,3-O-methylcellulose prepared via ATRP. The copolymers with DPs of PNIPAM of 19 and 29 displayed LCSTs of 27.8 and 28.5 °C, respectively. As expected, these were lower than the homopolymer's LCST of 32 °C, due to the hydrophobicity of the cellulose-based macroinitiator. However, for the copolymer with higher DP we would have expected a lower LCST compared to the LCST of the copolymer with lower DP, as demonstrated in work by Lutz et al.<sup>274</sup>

Some of the most interesting applications of PNIPAM are found in the biomedical field, therefore it is critically important to evaluate the toxicity of PNIPAM and its derivatives to cells (cytotoxicity).<sup>275–277</sup> Hsiue et al.<sup>275,276</sup> have used PNIPAM in eye drop preparations and no *in vitro* cytotoxicity was found. PNIPAM has also been used as a new embolic material in neurosurgery and no acute toxicity in mice was observed.<sup>277</sup> Vihola et al.<sup>278</sup> tested the cytotoxicity (cell viability and membrane integrity) of PNIPAM in intestinal and pulmonary cells and found the polymers to be relatively non-toxic during short exposure times. However, the monomer *N*-isopropyl acrylamide (NIPAM) was found to be highly cytotoxic.<sup>278–280</sup> As a result, considerable efforts have been made in search of non-toxic and biocompatible thermoresponsive materials.

As previously mentioned, one class of compounds of particular interest for biocompatible thermoresponsive materials are the ethylene glycol methacrylate analogues. Like the linear polyethylene glycol (PEG) macromolecules which are known for being highly soluble, uncharged, non-toxic and can be completely removed from the body,<sup>281,282</sup> the non-linear PEG analogues retain many of these desirable properties.<sup>283–285</sup> These macromolecules are built from oligo(ethyleneglycol) macromonomers and could become a viable thermoresponsive material for biomedical applications.<sup>274</sup> In a recent work developed by Lutz et al.<sup>286</sup>, random copolymers of 2-(2-methoxyethoxy)ethyl methacrylate (DEGMA) and oligo(ethyleneglycol) methacrylate (OEGMA,  $M_n = 475$  g/mol) were prepared by ATRP and exhibited thermoresponsive behaviour with an LCST adjustable between 26 and 90 °C by simply varying the co-monomer composition, **Table 1.5.1.**

**Table 1.5.1.** LCST of poly(OEGMA-co-DEGMA) prepared by ATRP.

[DEGMA]/[OEGMA]	LCST (°C) <sup>a</sup>
0:100	90
70:30	59
80:20	49
85:15	44
90:10	39
92:8	37
95:5	32
100:0	28

<sup>a</sup>) LCST observed in pure water with a concentration of 3 mg/mL.

In a study by Lutz et al.<sup>274</sup> PNIPAM and P(DEGMA<sub>95</sub>-co-OEGMA<sub>5</sub>) samples were prepared by ATRP with similar DPs and LCSTs. The PNIPAM samples exhibited a very sharp phase transition when heated, followed by a broad hysteresis in the cooling process; attributed to an irreversible coil-to-globule transition.<sup>274</sup> On the other hand P(DEGMA<sub>95</sub>-co-OEGMA<sub>5</sub>) showed comparable heating and cooling cycles. The cloud point of both polymers was decreased by 3 °C when placed in physiological medium at a polymer concentration of 3 mg/mL. Likewise, varying the polymer concentration between 1-10 mg/mL affected the LCST of the two polymers simultaneously, both increasing a few degrees with dilution. However, altering the DP only affected significantly the phase transition of PNIPAM; PNIPAM samples (3 mg/mL aqueous solutions) with long and short polymer chains displayed differences in LCST of 7 °C, the higher the DP the lower the LCST.<sup>270,287</sup> On the other hand, little influence of DP on the phase transition of P(DEGMA<sub>95</sub>-co-OEGMA<sub>5</sub>) samples was found. These novel P(DEGMA-co-OEGMA) copolymers have the potential to produce thermoresponsive materials with tailored LCSTs. However, to extend their use in biomedical applications more studies are necessary to systematically evaluate their properties.

The growing interest of grafting stimuli-responsive polymers from cellulose is widening the field of application of this biodegradable and biocompatible polysaccharide.<sup>128,288</sup> In particular, the synthesis of thermoresponsive cellulose-based graft-copolymers with well-defined architecture by ATRP is one of the current topics in biomaterials research. For example, Li et al.<sup>10</sup> successfully grafted OEGMA (M<sub>n</sub> = 300 g/mol) through ATRP, from commercially available ethyl cellulose (DS = 2.1) functionalized with 2-bromoisobutryl (DS of 0.02 and 0.2). Kinetic plots confirmed a first order reaction with respect to monomer, as well as a constant concentration of active species during the polymerization. The variation of M<sub>n</sub> vs. conversion was found to be linear.

The macroinitiator with a low degree of substitution ( $DS_{2\text{-bromoisobutyryl}} = 0.02$ ) attained a slightly higher final conversion when compared to the higher  $DS_{2\text{-bromoisobutyryl}}$  (0.2) macroinitiator, 62% vs. 56%, respectively. Moreover, the low  $DS_{2\text{-bromoisobutyryl}}$  (0.02) macroinitiator took almost twice as long to reach a similar conversion (62%) to that of the higher  $DS_{2\text{-bromoisobutyryl}}$  (0.2) sample, 14 hours vs. 8 hours, respectively. Nevertheless, both polymerizations were controlled. As expected, the DP of the copolymer with lower graft density ( $DS_{2\text{-bromoisobutyryl}} = 0.02$ ) was significantly higher (DP = 185) than the DP of the copolymer with higher graft density ( $DS_{2\text{-bromoisobutyryl}} = 0.2$ ) (DP = 28). The LCST values were also determined through plots of transmittance vs. temperature and found to be 64 ( $DS_{2\text{-bromoisobutyryl}} = 0.2$ ) and 67 °C ( $DS_{2\text{-bromoisobutyryl}} = 0.02$ ), showing that DS and DP had only a small effect on the LCST values. The LCST plots showed no hysteresis which is in accordance with Lutz's work.<sup>286</sup> Interestingly, the EC-*g*-P(OEGMA) graft copolymers were found to self-assemble into thermoresponsive spherical micelles in water.

In another study by Porsch et al.<sup>221</sup>, ATRP-ARGET was used to polymerize DEGMA and OEGMA ( $M_n = 300$  g/mol) individually and as a copolymer, from a hydroxypropylcellulose (HPC) macroinitiator with a DS of initiator (2-bromoisobutyryl) of 0.6.  $HPC_{0.6}\text{-}g\text{-P(}DEGMA\text{)}$  was obtained with 21% conversion,  $HPC_{0.6}\text{-}g\text{-P(OEGMA)}$  with 35% conversion and  $HPC_{0.6}\text{-}g\text{-P(DEGMA}_{48}\text{-co-OEGMA}_{52}\text{)}$  with 28% conversion. When the DS of 2-bromoisobutyryl in HPC was increased to 1.4 the OEGMA and P(DEGMA-co-OEGMA) could not be successfully grafted from the macroinitiator; this might have been caused by the higher density of initiators causing termination reactions. However, DEGMA could be grafted from the HPC ( $HPC_{1.4}\text{-}g\text{-P(DEGMA)}$ ) with a conversion of 20%. No kinetic or  $M_n$  vs. conversion plots were given, nor were the respective PDIs reported. Therefore, the authors did no real assessment of the controlled character of the ATRP. Regardless, some interesting observations were done in this work. The decrease in the DS of 2-bromoisobutyryl from 1.4 to 0.6 in the HPC caused only a 1 °C increase in the LCST, which is not a significant increment. Micelles were formed using the  $HPC_{1.4}\text{-}g\text{-DEGMA}$  and  $HPC_{0.6}\text{-}g\text{-DEGMA}$  copolymers and it was found that the critical micelle concentration decreased with the higher grafting density.

## 1.6 Honeycomb Films

Ordered porous films are of great interest in areas such as chemical sensors,<sup>289</sup> tissue engineering,<sup>14–16</sup> photonic crystals,<sup>290</sup> microreactors or microarray chips<sup>291</sup> and catalyst supports for fuel cells.<sup>292</sup> The honeycomb patterning of surfaces has been widely studied and several methods have been developed, of which, lithography, microcontact printing, bottom-up technologies have been studied.<sup>293,294</sup> Lithography is complicated and expensive, while microcontact printing is a simple method, the combination of molecular self-assembly and photolithography.<sup>295</sup> Finally, the bottom-up technique mimics biological self-assembly and self-organization to produce patterned structures.<sup>293</sup> Included in the latter is the “breath-figures” method, based on the findings of Aitken<sup>296,297</sup> and Rayleigh<sup>298,299</sup>, it is one the most simple and robust methods available.<sup>300–302</sup>

François et al.<sup>303–305</sup> first reported self-assembled honeycomb morphologies from star polystyrene and poly(para-phenyl-ene)-*b*-poly(styrene) when a drop of the respective solutions in carbon disulfide was exposed to a flow of moist air. Although a single mechanism explaining the formation of “breath figures” does not exist, it is generally recognized that the formation and subsequent “crystallization” of the “breath-figures” is the basic cause for the hexagonal arrays in polymer films.<sup>298,299,306</sup> François et al.<sup>303</sup> stated that the formation of “breath-figure arrays” is due to a Marangoni convection of condensed water droplets. Marangoni convection is fluid motion caused by a surface tension gradient arising from a temperature gradient within the polymer solution. If the temperature gradient is sufficiently large the water droplets will not coalesce.<sup>307</sup> Under a humid air-flow the surface temperature of an evaporating polymer solution can reach - 6 °C.<sup>306,308–310</sup> Water droplets condense on the surface of the polymer solution. The droplets start to nucleate and subsequently grow which can either coalesce or organize on the surface into a highly ordered and mobile hexagonal array. The ordered array of water droplets starts to sink into the polymer solution and according to Pitois and François<sup>304,305</sup> an interfacial polymer layer keeps them from coalescing. The process starts again with a second layer of water droplets nucleating again on the surface of the polymer solution. The final step consists of the evaporation of the solvent and water droplets leaving behind highly ordered porous 2D (monolayer) or 3D (multi-layer) polymeric films.

Srinivasarao et al.<sup>306</sup> explained the formation of “breath-figure” arrays as a combination of Marangoni convection and thermocapillary effects. Thermocapillary effects arise from the motion of droplets of liquid A (water) in a bulk liquid B (water immiscible solvent) to the free surface due to a temperature gradient in liquid B. The water droplets are stabilized on or at the polymer solution surface and will eventually sink into solution at a later stage.<sup>306,311</sup> Similarly Shimomura et

al.<sup>310</sup> proposed a mechanism in which Marangoni convection and thermocapillary effect cause the water droplets to submerge into the organic solution adopting a hexagonal array.

The detailed mechanism for the formation of “breath-figure” arrays is not fully known and may be in fact a combination of different mechanisms depending on the particular system. Bunz<sup>311</sup> has discussed in detail the proposed mechanisms and has conducted a critical review on the effectiveness of the “breath-figure” method to produce highly ordered honeycomb arrays. A simplified mechanism is shown in **Figure 1.6.1**.

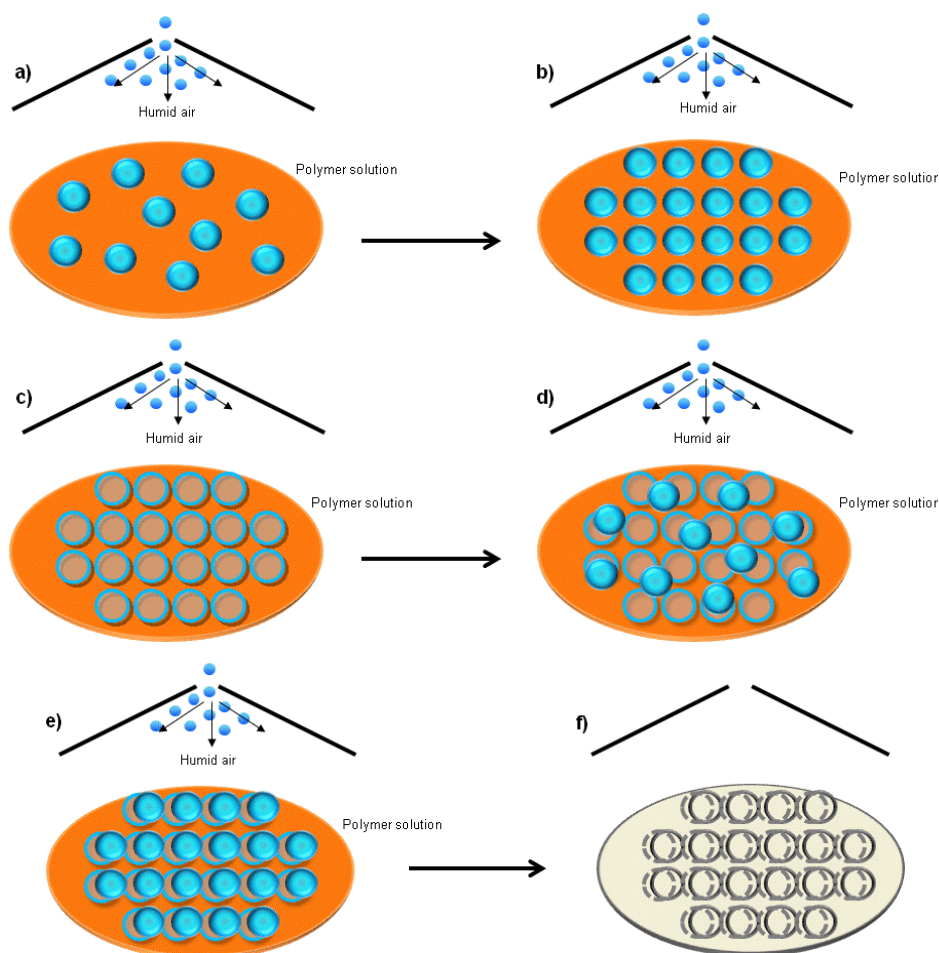


**Figure 1.6.1.** Simplified mechanism for the formation of honeycomb films through “breath-figure” method; a) nucleation of water droplets; b) water droplets in close packed array; c) water droplets in close packed array sink into solution; d) nucleation of new water droplets; e) formation of a close packed array of water droplets; f) solvent and water evaporation with simultaneous precipitation of polymer around water droplets and formation of honeycomb film.<sup>306</sup>

To form honeycomb films with high regularity it is reported that it is essential for the polymer to adopt a spherical shape in solution.<sup>303,312</sup> This could be a star-shaped polymer such as poly(styrene), a block copolymer which is able to aggregate in the solution, or polymers that contain an insoluble block, polar head groups, or polar side chains and are, therefore, capable of association into a spherical shape in the solvent.<sup>303,304,309,312,313</sup> Additionally, in this process, a fast nucleation of the water droplets combined with a slow growth rate contribute to a smaller and more uniform pore size distribution. Processing conditions such as air flow, humidity and concentration may contribute to attain this equilibrium between nucleation and growth rate. For example, increasing humidity and reducing air-flow causes growth rate to increase forming larger pore-sizes.<sup>306,310</sup> On the other hand, as the humid air flow is applied on the surface, water

droplets start to nucleate at a certain rate on the surface of the polymer solution. Simultaneously, the solvent starts to evaporate as well forming a gradient of temperature and an increase in polymer concentration, which decreases the growth rate of water droplets, thus smaller pore size. At a certain point the solubility will pass the saturation point and the process of phase-inversion from liquid to solid is accelerated and, ideally, a honeycomb film will be formed.<sup>314,315</sup> Nevertheless, it has also been found that star polymers are less sensitive to concentration.<sup>312</sup>

The surface tension of the organic polymer solution is a function of the amphiphilic nature of the polymer; hence a small modification of the polymer should affect honeycomb formation. An increment in the hydrophilic character of the polymer could correspond to smaller pore sizes within the honeycomb.<sup>312</sup> Amphiphilic block copolymers with hydrophilic and hydrophobic blocks are known to form inverse structures in organic solvents. Upon contact with water, these inverse micelles start interacting with water, leading to the rearrangement of the block copolymer around the water droplets. With the evaporation of the solvent and water, the formation of pores enriched with hydrophilic functionality is expected. On the other hand, the surface of the film should remain hydrophobic.<sup>316</sup> Nygard et al.<sup>317</sup> tested this hypothesis by synthesizing a temperature-responsive block copolymer, polystyrene-*block*-poly(N-isopropylacrylamide) (PSt-*b*-PNIPAM). The authors measured the contact angle of the honeycomb surface and the underlying honeycomb structure, after careful surface removal, at temperatures between 25 and 45 °C. The underlying honeycomb structure showed an arrangement of bowls (bowl structure) where PNIPAM enrichment was expected, due to the interaction between the hydrophilic polymer and the water droplets during the casting process. The contact angle measurements made on the honeycomb surface revealed no thermoresponsive behaviour remaining at ~ 90°. On the other hand, the bowl structure with nanometer-sized walls revealed, according to the authors, thermoresponsive behaviour as the contact angle increased from ~ 87 to 91° when the temperature increased from 25 to 45°C.

More recently, Xu and Kadla<sup>318</sup> were able to produce honeycomb films with site specific-functionalization in the pores. A regioselectively substituted amphiphilic cellulose azide, 3-O-azidopropoxypoly(ethylene glycol)-2,6-O-thexyldimethylsilyl cellulose<sup>319</sup> was used to prepare the honeycomb structures. These films were functionalized with biotin followed by the addition of fluorescent avidin. Confocal fluorescence microscopy images of the honeycomb films showed that avidin was mainly located inside the pores. To further confirm the preferential allocation of the azido groups inside the pores, quantum dots were linked to the honeycomb films. Once again, confocal fluorescence microscopy images of the honeycomb films showed clearly the fluorescent quantum dots located inside the pores.

Since the discovery of breath figures by Aitken<sup>296,297</sup> and Rayleigh<sup>298,299</sup> and the production of honeycomb films from star polystyrene and, rod-coil block copolymers, poly(para-phenyl-ene)-*block*-poly(styrene),<sup>303–305</sup> different polymers have also shown the ability to form regular structured films, such as poly(l-lactide),<sup>320</sup> polystyrene-*b*-poly(dimethylmethacrylamide),<sup>321</sup>



poly[dodecylacrylamide-*b*-( $\omega$ -carboxyhexylacrylamide)],<sup>322</sup> among others. Cellulose derivatives have been used to fabricate honeycomb-patterned materials. For example, honeycomb-shaped films were reported using cellulose acetates,<sup>323,324</sup> but again the corresponding films were extremely irregular with pore sizes varying between 1 to 100  $\mu\text{m}$ .

Kadla et al.,<sup>4</sup> have reported the formation of uniform honeycomb films from regioselectively modified 3-O-poly(ethyleneglycol)<sub>n</sub>-2,6-thexylmethyldimethylsilyl cellulose (3-EG<sub>n</sub>-2,6-TDMS cellulose). It was found that altering the amphipilicity of the polymer, by increasing the length of the ethylene glycol segments from 3 to 16, improved significantly the pore uniformity however, no significant change in pore size was observed. This was contrary to what had been described by Stenzel et al.<sup>325</sup> wherein side chains with a higher DP led to an increase in pore size. The discrepancy of results was explained by the authors as potentially due to the low DS of the cellulose derivative, the hydrophilic nature of the side chain and its relatively low molecular weight and/or the regioselectivity of substitution.

Xu and Kadla<sup>318</sup> and Xu et al.<sup>319</sup> prepared uniform honeycomb films from 3-O-azidopropoxypoly(ethylene glycol)-2,6-O-thexyldimethylsilyl cellulose with different DS (0.07 to 0.47) and DP of polyethylene glycol (PEG) (4 to 22). Unlike the observations of Stenzel,<sup>325</sup> pore size decreased with increasing DP<sub>PEG</sub> in polymers with similar DS. As well, polymers with lower DP<sub>PEG</sub> formed porous films in which the pore size increased with increasing DS. Therefore, polymers with a higher DP<sub>PEG</sub> formed porous films wherein the pore size decreased slightly with increasing DS. Furthermore, the surface of this cellulosic honeycomb film was modified via biotinylation through a heterogeneous surface “click reaction”. ATR-FTIR analysis of the films before and after confirmed a successful reaction in particular with the films produced with the longer PEG<sub>22</sub> side chains.

Honeycomb films have also been successfully obtained from graft copolymers with well-defined architectures synthesized through well known controlled radical polymerization techniques such as RAFT and ATRP. One of the first reports was using polystyrene comb polymers built on hydroxyisopropyl cellulose.<sup>325,326</sup> It was found that the regularity of the porous films increased with the density of branches and with the increasing length of each branch; however, poor quality films were obtained. Stenzel et al.<sup>325</sup> synthesized a cellulose-based polystyrene copolymer via RAFT polymerization, [hydroxyisopropylcellulose-co-(3-benzylsulfanylthiocarbonylsulfanylpropionyloxy) isopropylcellulose]-*g*-polystyrene, and claimed it suitable to prepare porous films with regular arrays, however, no images of the films were given by the authors. The effect of concentration of the casting solution (from 2.5 to 20 mg/mL) was also studied for this particular copolymer and found to have little effect, pore size varied from 0.3 to ~ 1  $\mu\text{m}$ , respectively. The latter is not in accordance with what was found in the same work with other carbohydrate based polymers as well as from what is reported in the literature,<sup>312,327–329</sup> in

which the increment of concentration causes a significant decrease of the pore size, in particular for amphiphilic polymers or other polymers that tend to form aggregates in solution.

Liu et al.<sup>329</sup> employed ATRP to synthesize cellulose-based copolymers ethylcellulose-*g*-polystyrene (EC<sub>0.5</sub>-*g*-PSt) with different chain lengths and ethylcellulose-*g*-poly(poly(ethylene glycol) methyl ether) (EC<sub>0.02</sub>-*g*-P(OEGMA<sub>4.5</sub>)<sub>57</sub>). The effect of relative humidity, concentration, chain length and type of side chain on the formation of honeycomb films was studied. EC-*g*-PSt was shown to form honeycomb-like ordered porous films. Increasing the relative humidity during casting increased the pore size, likely due to the formation of larger water droplets with increasing relative humidity. At the lowest polymer concentration (1 mg/mL) the water droplets were not stabilized due to the low concentration/viscosity, coalescing and forming a poor quality film. As the concentration increased the pore size decreased and the films became relatively ordered; the best honeycomb films were obtained at 10 mg/mL. The films formed at a polymer concentration of 20 mg/mL revealed shallow pores, indicating the water droplets stayed at the surface of the solution due to the high concentration/viscosity. The copolymer with the longest PSt chain length, EC<sub>0.5</sub>-*g*-PSt<sub>256</sub> produced very poor quality honeycomb films, while those prepared from EC<sub>0.5</sub>-*g*-PSt<sub>162</sub> and EC<sub>0.5</sub>-*g*-PSt<sub>20</sub> were well ordered, with the pore size decreasing with increasing side-chain length. As previously mentioned Liu et al.<sup>329</sup> also synthesized EC<sub>0.02</sub>-*g*-P(OEGMA<sub>4.5</sub>)<sub>57</sub> through ATRP to study the effect of the side-chain on the rate of precipitation. The authors claim that due to the long hydrophilic side-chain (DP<sub>OEGMA</sub>=57) the rate of precipitation is slow. Therefore, the ability of the side chain to stabilize the water droplets is very poor. The honeycomb films had no ordered porous structure and the pores were very large.

The preparation of honeycomb films by the “breath-figures” method is still very challenging. Experimental parameters such as, air flow, humidity and polymer concentration, play an important role in whether or not a certain polymer is able to form uniform honeycomb films. Additionally, the nature of the backbone polymer, the hydrophilic/hydrophobic character of the side chain and its respective length, add extra complexity to the whole process. Therefore, a more in depth study of these properties would allow designing polymers with the ability of forming uniform honeycomb films.

Wong et al.<sup>316</sup> studied the ability of amphiphilic copolymers to form honeycomb films and determine how the hydrophilic block can interfere with condensing water droplets affecting the rate of precipitation. An optimal balance between the hydrophilic and hydrophobic block is essential in the formation of a well structured honeycomb film. Amphiphilic copolymers are interesting materials for the formation of honeycomb films because the pores are hydrophilic and the remaining surface is mostly hydrophobic.<sup>316,330</sup> This special arrangement has been confirmed by X-ray photoelectron spectroscopy (XPS)<sup>331</sup>, contact angle measurements<sup>317</sup> and bacterial studies.<sup>328</sup> However, if an ideal balance cannot be achieved a honeycomb film will not be formed. A potential alternative is to have a honeycomb film made from the hydrophobic block, e.g.,

cellulose-based macroinitiator, and then graft-from the surface the hydrophilic polymer. In work developed by Stenzel et al.<sup>332</sup> PNIPAM was grafted-from a honeycomb surface made from comb-PSt and a random copolymer made from polystyrene and 2-hydroxyethyl methacrylate (PSt-*ran*-PHEMA) through RAFT polymerization. Mild reaction conditions were used (aqueous media at room temperature) allowing for surface modification without damaging the honeycomb surface. The successful grafting of PNIPAM to the honeycomb surface was confirmed by contact angle measurements. Fibroblast cells were then attached to the surface. The authors suggested that these materials might be used as switchable thermoresponsive surfaces with hydrophilic and hydrophobic properties below and above PNIPAM's LCST, respectively. Furthermore, these properties might be particularly interesting for the control of protein adsorption and cell growth studies.<sup>332</sup>

The use of honeycomb films for tissue growth has also been the focus of recent studies. These films provide tissue growth without affecting adhesion and proliferation of the cells.<sup>14,16,333,334</sup> Furthermore, it was found that cell morphology is affected by the architecture of the films. Flattened films produced flat chondrocyte and hepatocyte cells, which makes them unsuitable for use in tissue engineering. On the other hand, macropatterned films form cells with spherical shape, making them potentially suitable for use in tissue engineering, as illustrated in **Figure 1.6.2.**<sup>14,334</sup>

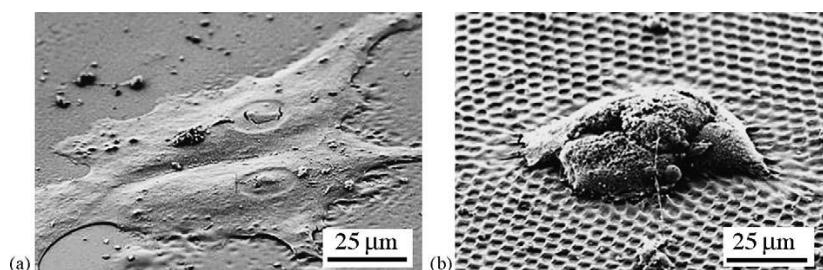


**Figure 1.6.2.** SEM images of hepatocytes 72 h after culture on (a) flat film and (b) honeycomb film.<sup>334</sup>

Note: Reprinted from *Colloids and Surfaces A: Physicochemical and Engineering Aspects*, 284-285, Tanaka, M.; Nishikawa, K.; Okubo, H.; Kamachi, H.; Kawai, T.; Matsushita, M.; Todo, S.; Shimomura, Control of hepatocyte adhesion and function on self-organized honeycomb-patterned polymer film, 464-469, Copyright (2006), with permission from Elsevier.

## 1.7 Hypothesis/Goals

### 1.7.1 Synthesis of 6-O-(2-bromoisobutyryl) TMS-O-cellulose for the preparation of thermoresponsive honeycomb patterned films via surface initiated ATRP

The use of regioselectively and non-regioselectively substituted cellulose derivatives for the production of honeycomb films has been studied (Section 1.6). To the best of my knowledge the grafting of polymers from these surfaces through ATRP has not yet been reported.

It is hypothesized that the films made from the regioselectively substituted derivatives form homogeneous honeycomb patterned films and would be able to keep a homogeneous pore distribution after ATRP. An ordered allocation of initiating sites on the surface of the honeycomb film may allow a uniform distribution of the newly grafted polymers and potentially a more controlled polymerization.

As given in **section 3.1** the objectives are: 1) to synthesize, for the first time, regioselectively and non-regioselectively substituted cellulose derivatives, 6-O-(2-bromoisobutyryl) TMS-O-cellulose and (2-bromoisobutyryl) TMS-O-cellulose, respectively; 2) to study the ability of these derivatives to form honeycomb films; 3) to study the effect of some of the experimental parameters as well as the role of regioselectivity and DS of 2-bromoisobutyryl in the formation of honeycomb patterned films; 4) to “graft-from” a uniform honeycomb film a thermoresponsive polymer (PNIPAM); 5) to characterize the films.

The goal is to produce a uniform honeycomb patterned film to be used as an ATRP active film for design of “stimuli-responsive” surfaces.

### **1.7.2 Synthesis of 3-O-(2-bromoisobutyryl) 2,6-O-TDMS cellulose and 2,3-O-(2-bromoisobutyryl) 2,6-O-TDMS cellulose for the preparation of thermoresponsive honeycomb patterned films via ATRP**

Regioselectively substituted 3-O-poly(ethyleneglycol)<sub>n</sub>-2,6-thexylmethyldimethylsilyl cellulose and 3-O-azidopropoxypoly(ethylene glycol)-2,6-O-thexyldimethylsilyl 3-O-cellulose derivatives have been used to produce homogeneous honeycomb films.<sup>4,318,319</sup>

It is hypothesized that the films made from the regioselectively substituted derivatives form homogeneous honeycomb films regardless of the position of 2-bromoisobutyryl group in the cellulose backbone (C6 vs. C3). The ordered structure of 3-O-(2-bromoisobutyryl) 2,6-O-TDMS cellulose favours the formation of homogeneous honeycomb films. Thus, it is expected the non-regioselectively substituted 2,3-O-(2-bromoisobutyryl) 2,6-O-TDMS cellulose to not form homogeneous honeycomb films.

In **section 3.2** the objectives are: 1) to synthesize for the first time regioselectively and non-regioselectively substituted cellulose derivatives 3-O-(2-bromoisobutyryl) 2,6-O-TDMS cellulose and 2,3-O-(2-bromoisobutyryl) 2,6-O-TDMS cellulose, respectively; 2) to verify the ability for both compounds to form homogeneous honeycomb films; 3) to “graft-from” a homogeneous honeycomb film thermoresponsive polymer (PNIPAM); 4) to characterize the films.

The goal is to verify the effect of regioselectivity in the formation of honeycomb films and to modify the properties of those surfaces through the grafting of a polymer via surface initiated ATRP.

### **1.7.3 Homogeneous ATRP of thermoresponsive copolymers from 3-O-(3-O-(2-bromoisobutyryl)-hydroxypropyl)-2,6-O-TDMS cellulose**

Homogeneous ATRP of homopolymers or copolymers grafted from small initiators have been obtained through controlled polymerization with high conversions, as discussed in section 1.4.1.1.

However, when “grafting-from” homopolymers or copolymers from macromolecules such as cellulose, the results vary and a controlled polymerization is not always achieved. For example, polymers have been successfully grafted from cellulose<sup>217</sup> and ethyl-cellulose<sup>122,161</sup> however, the successful grafting of polymers from other cellulose derivatives such as cellulose diacetate<sup>218</sup> and commercially available hydroxypropyl cellulose<sup>120,221</sup> by homogenous ATRP has not yet been fully proven.

It is hypothesized, that the regioselective allocation of initiating sites in a hydroxypropyl cellulose derivative macroinitiator may minimize termination reactions, even in cellulose based macroinitiators with high initiator density. Therefore, a controlled polymerization may be attained.

In **section 3.3** the objectives are: 1) to synthesize regioselectively substituted 3-O-(3-O-(2-bromoisobutyryl)-hydroxypropyl)-2,6-O-TDMS cellulose with different degrees of substitution of 2-bromoisobutyryl; 2) to run homogeneous ATRP reactions of these derivatives based on the linear kinetic regime and conversion; 3) to test the effect of DS of 2-bromoisobutyryl in the ATRP; 4) to characterize the cellulose-based copolymers.

The goal is to synthesize regioselectively modified thermoresponsive cellulose-based copolymer via homogeneous ATRP.

## 2 EXPERIMENTAL

### 2.1 Materials

Cellulose diacetate (Mw=30K, 39.8 wt% acetyl content (DS=2.5), anhydrous lithium chloride (LiCl), anhydrous pyridine (Py), triethylamine (TEA), imidazole, sodium hydride (NaH), 60% dispersion in mineral oil), 2-bromoisobutyryl bromide, hexamethyldisilazane (HMDS), allyl chloride, bromooctane, isopropanol, 9-borabicyclo (3.3.1) nonane (9-BBN), hydrogen peroxide (H<sub>2</sub>O<sub>2</sub>) 30%, N-isopropylacrylamide (NIPAM), di(ethylene glycol) methyl ether methacrylate (DEGMA) and oligo(ethylene glycol) methyl ether methacrylate (OEGMA), copper (I) chloride (CuCl), copper (II) chloride (CuCl<sub>2</sub>), copper (Cu) and tris[2-(aminoethyl) amine] (TREN) were purchased from Sigma-Aldrich. Anhydrous lithium chloride was dried under vacuum for 2 hours prior to use. NIPAM was recrystallized from a mixture of hexane and toluene (35:65). DEGMA and OEGMA were filtered through alumina to remove inhibitors. CuCl was washed with glacial acetic acid and then washed 3 times with ethanol to remove CuCl<sub>2</sub>, according to previous work.<sup>335</sup> Tris[2-(dimethylamino)ethyl]amine (Me6TREN) was synthesized based on a procedure described in the literature from commercially available TREN.<sup>336</sup> The remaining reagents were used as received. Potassium hydroxide, anhydrous N,N-dimethyl acetamide (DMA), chloroform (CHCl<sub>3</sub>), MeOH, hydrochloric acid (37%), ethyl ether, tetrahydrofuran (THF), potassium phosphate monobasic (KH<sub>2</sub>PO<sub>4</sub>), potassium phosphate dibasic (K<sub>2</sub>HPO<sub>4</sub>), and sodium hydroxide (NaOH) were purchased from Fisher Scientific and used as received with the exception of THF which was dried in a mixture of sodium metal and benzophenone under nitrogen atmosphere, prior to use. NMR solvents were purchased from Cambridge Isotope Laboratories.

### 2.2 Methods

Fourier-Transform Infrared (FTIR) spectra were recorded on a Perkin Elmer Spectrum One FTIR spectrometer. For CHCl<sub>3</sub> soluble polymers films were deposited on zinc selenium (ZnSe) plates using 2-3 drops of 5% w/w CHCl<sub>3</sub> solutions. The wavenumber range was 4000-600 cm<sup>-1</sup> at a resolution of 4 cm<sup>-1</sup> and a minimum of 16 scans recorded. For solid samples attenuated total reflectance (ATR) FTIR was used and 32 scans recorded.

<sup>1</sup>H-, <sup>13</sup>C- and quantitative <sup>13</sup>C nuclear magnetic resonance (NMR) spectra were recorded using a 300 MHz Bruker Avance Ultrashield NMR spectrometer (300.13 and 75.03 MHz, respectively) at 25 °C in deuterated chloroform and acetone and 40 °C in deuterated benzene

and dimethylsulfoxide (DMSO). Chemical shifts were referenced to tetramethyl silane (TMS; 0 ppm). The  $^1\text{H}$ -NMR spectra were recorded with a 7 s relaxation delay (d1) to ensure complete relaxation of TDMS protons and a total of 64 scans were recorded. The quantitative  $^{13}\text{C}$ -NMR analyses were done in the presence of relaxation agent chromium (III) acetylacetonate ( $\text{Cr(III)acac}$ ) at a concentration of 0.1 M, a relaxation delay of 11 s, based on the methine proton of TDMS group and a total of thirty thousand scans were recorded.<sup>92</sup>

Gel permeation chromatography (GPC) - multiangle light scattering (MALS) analyses were performed using an Agilent 1100 Series GPC Analysis System equipped with a Wyatt Dawn Heleos-II multiangle light scattering (MALS) detector to determine number average and weight average molecular weight ( $M_n$ ,  $M_w$ ) and polydispersity index (PDI). Styragel HR-1, HR-2 and HR-5E column (Waters Corp., Milford, USA) were used with THF as the eluting solvent at a flow rate of 0.5 ml/min at 35 °C. The injection volume was 100  $\mu\text{L}$ , and polymers were dissolved in HPLC-grade THF at concentrations of 1.5 mg/ml.

Contact angles were measured in triplicate using a KSV CAM 101 instrument (KSV Instruments Ltd., Finland). A 5  $\mu\text{L}$  droplet of distilled water was placed on the surface of the honeycomb film and the contact angle was measured after 60 seconds. The average and respective standard deviation of the triplicates were calculated.

Turbidity measurements were done through ultra violet-visible (UV-Vis) spectroscopy (Varian-Cary 4000) to measure the lower critical solution temperature temperatures of the various copolymers. The turbidities of the aqueous solutions (3 mg/mL) were obtained at 670 nm with heat/cool cycles from 15 to 70 °C at 1 °C/min and expressed as absorbance curves.

Surface morphology of the honeycomb films was observed with optical microscopy (Olympus BX41 microscope), scanning electron microscopy (SEM) using a Hitachi S-2600N variable pressure scanning electron microscope (VPSEM) as well as atomic force microscopy (AFM); Veeco Multimode coupled with a Nanoscope V Controller. The moduli of the honeycomb film surfaces were measured in triplicate using the AFM PeakForce QNM (Quantitative NanoMechanics mapping) mode. The spring constant (0.44 N/m) and deflection sensitivity (40.5 nm/V) of a Scanasyt-Air silicon tip on nitride cantilever were calibrated with a Sapphire-15M standard (Veeco).

Thermal gravimetric analyses (TGA) were carried out using a TA Instruments Q500 TGA. A typical procedure consisted of weighing approximately 4 mg of sample in a calibrated platinum pan and measuring the weight loss as the sample was subjected to a temperature ramp from 25-600 °C at 10 °C/min under nitrogen. The decomposition temperatures were then taken from the peak maxima of the derivative of the weight loss curve (DTGA). Differential scanning calorimetry (DSC) measurements were carried out on a TA Instruments Q1000 DSC calibrated against indium. All experiments were run with approximately 3 mg of sample in sealed aluminum hermetic pans using a heat/cool/heat method at a heating/cooling rate of 10 °C/min; samples were heated



from room temperature to 200 °C, cooled to – 90 °C and subsequently heat to 200 °C. TGA and DSC measurements were done in duplicate.

For all synthesized compounds purity was evaluated qualitatively by FTIR and NMR by the observed absence/presence of impurity peaks.

## **2.3 Synthesis**

### **2.3.1 Regenerated cellulose**

In the present work, regenerated cellulose was prepared from a commercial cellulose acetate to obtain a starting material with a more homogeneous molecular weight and polydispersity. The more homogeneous starting material helps assure a valid comparison between the different cellulose derivatives synthesized and contributes to a final product with more consistent properties.

Cellulose diacetate (60 g; 0.22 mol) was suspended in a solution of MeOH (1.4 L) and potassium hydroxide (84 g, 1.5 mol) and stirred overnight at room temperature. The alkaline mixture was then neutralized with 70 mL (0.85 mol) of hydrochloric acid and filtered through Whatmann qualitative filter paper. The regenerated cellulose residue was washed with water (1.5 L) and MeOH (2 × 500 mL), stirred in MeOH (1 L) for 30 min and washed with 500 mL of ethyl ether. The residue was dried under vacuum (1 mmHg) at 40 °C overnight.

### **2.3.2 Synthesis of 6-O-(2-bromoisobutyryl) cellulose**

In this study, when dissolving the cellulose by heat activation<sup>2</sup> we could not get a reproducible dissolution of cellulose. Therefore, based on work described elsewhere<sup>99</sup>, we decided to add a polar medium exchange<sup>46</sup> step to the cellulose dissolution. The objective was to have the polymer chains adopt a more relaxed conformation allowing the diffusion of solvent into the less accessible crystalline regions. Therefore, the first solvent to be used was water which swells the polymer and disrupts the hydrogen bonding between the AGU protons. The second was methanol, a more non-polar solvent; it removes residual water from the system and finally DMA which prevents the re-establishment of hydrogen bonding. The heat activation<sup>46</sup> was done at 120 °C creating enough vapour pressure to swell the polymer further assuring complete dissolution. A detailed description of the dissolution procedure is described as follows. Regenerated cellulose (1 g, 6 mmol) in 40 mL deionized water, which was mixed at room temperature for 1 min. The suspension was then centrifuged (15 min and 3,000 g), the water decanted off and replaced by

MeOH (40 mL). The MeOH/cellulose suspension was mixed for 1 min, centrifuged and repeated a second time with fresh MeOH (40 mL). This was followed by repeated washing with N,N-dimethyl acetamide (DMA) (4 x 40 mL). Finally, 25 mL of DMA were added to cellulose and left stirring overnight under an argon atmosphere. The following day cellulose was dissolved as per the synthesis of 2,6-O-TDMS cellulose.<sup>2</sup> Cellulose/DMA suspension was heated to 120 °C and stirred for 2 hours. The reaction was then cooled to 100 °C, and 1.5 g (35.4 mmol) of lithium chloride (LiCl) was added. The reaction was stirred for 10 min and then cooled to room temperature and left stirring overnight under an argon atmosphere to completely dissolve the cellulose. The next day 0.32 mL (3.7 mmol) of pyridine was added to the cellulose solution and it was stirred for 10 min. The reaction was then placed in an ice/water bath and stirred for 5 min at which point 0.38 mL (3.1 mmol) of 2-bromoisobutyryl bromide was added dropwise over a period of 3 min. The reaction proceeded at room temperature for 19 hours at which point the product was precipitated from the reaction mixture by slow addition to excess of acetone (100 mL). The precipitate was filtered through Whatmann qualitative filter paper and dried in a vacuum oven (1 mmHg) at 40 °C overnight. Unpurified yield: 1.86 g (> 132%). FTIR (CHCl<sub>3</sub>, cm<sup>-1</sup>), 3510 (ν<sub>O-H</sub>), 2956, 2901 (ν<sub>CH<sub>3</sub></sub>, ν<sub>CH<sub>2</sub></sub>), 1747 (ν<sub>C=O</sub>), 1460, 1375 (δ<sub>CH<sub>3</sub></sub>), 1248 (ν<sub>C-O-C</sub>, ester), 1122, 1084 (ν<sub>C-O-C</sub>, ether). <sup>1</sup>H-NMR (10% in DMSO-d<sub>6</sub>, ppm, 313 K): δ = 1.76 (C(CH<sub>3</sub>)<sub>2</sub>Br), δ = 3.1 (OH), δ = 3.4 (H6), δ = 3.5-3.8 (H2, H3, H5), δ = 4.34 (H6 if 2-bromoisobutyryl at C6, H4), δ = 4.53 (H1). <sup>13</sup>C-NMR (10% in DMSO-d<sub>6</sub>, ppm, 313 K): δ = 29.8 (C(CH<sub>3</sub>)<sub>2</sub>Br), δ = 60.7 (C6), 64.9 (C(CH<sub>3</sub>)<sub>2</sub>Br), δ = 73.0-81.0 (C5, C4, C3, C2), δ = 103.2 (C1), δ = 170.8 (C=O).

### 2.3.3 Synthesis of 6-O-(2-bromoisobutyryl)-acetyl-O-cellulose

6-O-(2-bromoisobutyryl) cellulose (0.5 g, 2.2 mmol) was dissolved in anhydrous pyridine (9.8 g, 124 mmol) and acetic anhydride (1.4 g, 13.7 mmol) of acetic anhydride was added dropwise, under argon atmosphere. The reaction proceeded at 90 °C for 48 hours. The brown reaction mixture was then precipitated in 300 mL of methanol and stirred for 5 minutes. The solution was filtered and a brown precipitate was obtained and dried in a vacuum oven (1 mmHg) at 40 °C overnight. The crude product was purified by dissolving in CHCl<sub>3</sub> (200 mL), filtering through Whatman qualitative filter paper and reprecipitating from MeOH (700 mL). The purified compound was recovered by filtration and dried as previously described. Purified yield: 0.39 g (65%), DS<sub>acetyl</sub> = 1.7. <sup>1</sup>H-NMR (10% in CDCl<sub>3</sub>, ppm, 313 K): δ = 1.76 (C(CH<sub>3</sub>)<sub>2</sub>Br), δ = 1.9, 2.0, 2.1 (CH<sub>3</sub>(C=O)O if acetyl in positions C2, C3 and C6), δ = 3.52 (H5); δ = 3.73 (H5), δ = 4.04 and 4.35 (H6<sub>α,β</sub> if acetyl at C6), δ = 4.2 and 4.4 (H6<sub>α,β</sub> if 2-bromoisobutyryl at C6), δ = 4.46 (H1), δ = 4.8 (H2 if acetyl at C2 group), δ = 5.1 (H3 if 2-bromoisobutyryl or acetyl at C3). <sup>13</sup>C-NMR (10% in CDCl<sub>3</sub>, ppm, 313 K). δ = 23.8 (CH<sub>3</sub> acetyl), δ = 29.8 (C(CH<sub>3</sub>)<sub>2</sub>Br), δ=60.7 and 63.6 (C6 of the AGU if acetyl and 2-bromoisobutyryl at C6); δ = 62.9 (C(CH<sub>3</sub>)<sub>2</sub>Br), δ = 73.4 (C2, C3), δ = 78.4 (C4, C5), δ = 101.2

(C1),  $\delta = 169.2$  ( $\text{CH}_3\text{C}(\underline{\text{C}}=\text{O})$  at C2),  $\delta = 169.5$  ( $\text{CH}_3\text{C}(\underline{\text{C}}=\text{O})$  at C3),  $\delta = 170.2$  ( $\text{CH}_3\text{C}(\underline{\text{C}}=\text{O})$  at C6),  $\delta = 170.8$  ( $\text{CH}_3\text{C}(\underline{\text{C}}=\text{O})$  at C2).

### 2.3.4 Synthesis of 6-O-(2-bromoisobutyryl)-trimethylsilyl-O-cellulose

6-O-(2-bromoisobutyryl) cellulose (1 g, 44 mmol) was dissolved in 40 mL of anhydrous DMA and 5.8 mL (0.66 mol) of anhydrous pyridine was added under an argon atmosphere. The mixture was stirred for 10 min and then cooled in an ice/water bath. After 5 min of cooling 1,1,1,3,3,3-hexamethyldisilazane (0.132 mol, 2.8 mL) was added dropwise over 10 min. The mixture was left stirring in the ice/water bath for 10 min and then heated to 90 °C and left stirring for 24 hours. The reaction mixture was cooled and the product precipitated from acetone (500 mL); MeOH (500 mL) was used for the higher DS products. The filtered precipitate was dried in a vacuum oven (1 mmHg) at 40°C overnight. The crude product was purified by dissolving in  $\text{CHCl}_3$  (200 mL), filtering through Whatman qualitative filter paper and reprecipitating from MeOH (1L). The purified compound was recovered by filtration and dried as previously described. Purified yield: 0.93 g (70%),  $\text{DS}_{\text{Br-isobutyryl}} = 0.5$  FTIR ( $\text{CHCl}_3$ ,  $\text{cm}^{-1}$ ), 3510 ( $\nu_{\text{O-H}}$ ); 2956, 2901 ( $\nu_{\text{CH}_3}$ ,  $\nu_{\text{CH}_2}$ ); 1747 ( $\nu_{\text{C=O}}$ ); 1460, 1375 ( $\delta_{\text{CH}_3}$ ,  $\delta_{\text{CH}_2}$ ); 1248 ( $\delta_{\text{Si-C}}$ ,  $\nu_{\text{C-O-C}}$ , ester); 1122, 1084 ( $\nu_{\text{C-O-C}}$ , ether); 746 ( $\gamma_{\text{Si-CH}_3}$ ).  $^1\text{H-NMR}$  (10% in  $\text{CHCl}_3$ , ppm, 313 K):  $\delta = 0.16$  ( $\text{Si}(\underline{\text{CH}_3})_3$ ),  $\delta = 1.82$  ( $\text{C}(\underline{\text{CH}_3})_2\text{Br}$ ),  $\delta = 3.3$  ( $\underline{\text{OH}}$ ),  $\delta = 3.4$  (H6 if OH at C6 of the AGU is free),  $\delta = 3.7\text{-}3.9$  (H2, H3, H5),  $\delta = 4.21$  (H4),  $\delta = 4.4$  (H6 if OH group at C6 of the AGU has been functionalized with a bromoisobutyryl group),  $\delta = 4.6$  (H1).  $^{13}\text{C-NMR}$  (10% in  $\text{CHCl}_3$ , ppm, 313 K):  $\delta = 0.49$  ( $\text{Si}(\underline{\text{CH}_3})_3$ ),  $\delta = 29.8$  ( $\text{C}(\underline{\text{CH}_3})_2\text{Br}$ ),  $\delta = 60.7$  (C6); 64.5 ( $\underline{\text{C}}(\text{CH}_3)_2\text{Br}$ ),  $\delta = 73.0\text{-}81.0$  (C5, C4, C3, C2),  $\delta = 102.9$  (C1),  $\delta = 170.9$  (C=O).

### 2.3.5 Preparation of honeycomb films

Honeycomb films were prepared by dissolving the macroinitiators in toluene at a concentration of 2mg/mL and then applying 10  $\mu\text{L}$  of the solution onto a clean glass slide under a flow of humid air at a defined flow and relative humidity (flow: 0.3-0.8 g/l; relative humidity: 70-80%) and temperature ( $20 \pm 1$  °C). The films were left to dry before microscopic observation. The humidity was measured with a humidity temperature pen (Thermo-Hygrometer, Fisher Scientific). The surface morphology of the cast films was observed by optical microscopy (BX41, Olympus) and scanning electron microscopy (SEM; JEOL JSM-5900LV). Pore size, respective average and standard deviation were measured from the SEM images at 4 K magnification ( $n = 11$ ). An illustration of the casting apparatus is given in **Figure 3.1.7**.

### 2.3.6 Surface initiated ATRP of NIPAM from honeycomb films made from 6-O-(2-bromoisobutyryl)-trimethylsilyl-O-cellulose

A 100 mL Schlenk flask was charged with 10 mL of a 10 wt% NIPAM/H<sub>2</sub>O solution and degassed through four freeze-pump-thaw (FPT) cycles (the reaction flask was sealed and submerged in liquid nitrogen until the solution was visibly frozen. A vacuum of 0.02 mmHg was then pulled on the system. The reaction flask was then removed from the liquid nitrogen and thawed. The cycle was repeated three more times). In the fourth cycle, while frozen, the reaction flask was opened and CuCl (3.6 mg, 2.5  $\mu$ mol/mL), CuCl<sub>2</sub> (8.3 mg, 3.7  $\mu$ mol/mL), Cu (0.95 mg, 1.5  $\mu$ mol/mL) and Me<sub>6</sub>TREN (40 mg, 0.17 mmol) and the honeycomb film previously cast on top of a glass slide were added. During this process special care was taken to keep the reaction solution frozen. The Schlenk flask was sealed again and another four FPT cycles were completed. In the last cycle, the thawed reaction solution was blanketed with argon. The reaction proceeded at room temperature overnight under an argon atmosphere. The reaction was terminated by exposure to air; the film was removed, thoroughly washed (3 x 100 mL) with distilled water and dried in a vacuum oven (1 mmHg) overnight.

### 2.3.7 Synthesis of 2,6-O-thexyldimethylsilyl cellulose

Regenerated cellulose was first activated by solvent exchange as described in **section 2.3.2**. The synthesis of 2,6-O-TDMS cellulose was done according to the procedure of Koschella et al.<sup>2</sup> A suspension of cellulose/DMA (1 g/25 mL) was heated to 120 °C and stirred for 2 hours. The reaction was then cooled to 100 °C, and 1.5 g (35.4 mmol) of lithium chloride (LiCl) was added. The reaction was stirred for 10 min and then cooled to room temperature and left stirring overnight under an argon atmosphere to completely dissolve the cellulose. Imidazole (2.0 g, 30 mmol) was then added to the cellulose/DMA/LiCl solution and stirred for 15 min under argon, followed by the addition of 4.7 mL (24 mmol) of thexyldimethylsilyl chloride (TDMS-Cl). The reaction mixture was heated to 100 °C for 24 hours under an argon atmosphere and constant stirring. The reaction mixture was then poured into buffer solution (7.14 g K<sub>2</sub>HPO<sub>4</sub> and 3.54 g KH<sub>2</sub>PO<sub>4</sub> in 1000 mL of distilled water). The precipitate was then collected by filtration, washed with distilled water (3 x 250 mL) and ethanol (3 x 250 mL) and dried under vacuum (1 mmHg) at 30 °C. The crude product was purified by dissolving it in CHCl<sub>3</sub> (300 mL) and then filtered through Whatman qualitative filter paper. The filtrate was precipitated from MeOH (1 L). The purified colorless compound was recovered by filtration and dried as previously described. Purified yield: 2.5g (91%). DS ~ 2.1. FTIR (CHCl<sub>3</sub>, cm<sup>-1</sup>), 3517 ( $\nu_{O-H}$ ); 2957, 2871 ( $\nu_{CH_3}$ ,  $\nu_{CH_2}$ ); 1465, 1377 ( $\delta_{CH_3}$ ,  $\delta_{CH_2}$ ); 1251 ( $\delta_{Si-C}$ ), 1116, 1078 ( $\nu_{C-O-C}$ , ether); 835 ( $\nu_{Si-C}$ ); 777 ( $\gamma_{Si-CH_3}$ ). <sup>1</sup>H-NMR (10% in CDCl<sub>3</sub>,

ppm, 313 K):  $\delta$  = 0.15 (Si-CH<sub>3</sub>),  $\delta$  = 0.89 (Si-C(CH<sub>3</sub>)<sub>2</sub>CH(CH<sub>3</sub>)<sub>2</sub>),  $\delta$  = 1.66 (Si-C(CH<sub>3</sub>)<sub>2</sub>CH(CH<sub>3</sub>)<sub>2</sub>),  $\delta$  = 3.34 (OH),  $\delta$  = 3.71 (H-6),  $\delta$  = 3.8 (H-2),  $\delta$  = 3.9 (H-5,4,3),  $\delta$  = 4.4 (H-1). <sup>13</sup>C-NMR (10% in CDCl<sub>3</sub>, ppm, 313 K):  $\delta$  = - 2.5 (Si-(CH<sub>3</sub>)<sub>2</sub>),  $\delta$  = 18.6 (Si-C(CH<sub>3</sub>)<sub>2</sub>CH(CH<sub>3</sub>)<sub>2</sub>),  $\delta$  = 20.4 (Si-C(CH<sub>3</sub>)<sub>2</sub>CH(CH<sub>3</sub>)<sub>2</sub>), 25.2 (Si-C(CH<sub>3</sub>)<sub>2</sub>CH(CH<sub>3</sub>)<sub>2</sub>),  $\delta$  = 34.3 (Si-C(CH<sub>3</sub>)<sub>2</sub>CH(CH<sub>3</sub>)<sub>2</sub>),  $\delta$  = 60.3 (C6),  $\delta$  = 75.02 (C4),  $\delta$  = 101.9 (C1).

### 2.3.8 Synthesis of 3-O-(propanoyl)-2,6-O-TDMS cellulose

This procedure was based in a procedure to esterify polysaccharides developed by Biswas et al.<sup>337</sup> 2,6-O-TDMS cellulose (0.2 g, 0.44 mmol) and iodine (0.012 g, 0.044 mmol) were suspended in propionic anhydride (6.12 g, 47 mmol) and stirred at 40 °C for 64 hours under argon atmosphere. Afterwards 9 mL of a saturated aqueous solution of sodium thiosulfate was added to the reaction mixture and stirred for 15 minutes. The mixture colour changed from dark brown to colourless, indicating the transformation of iodine to iodide. The mixture was then filtered and the precipitate washed 3 times with 125 mL of water. The precipitate was resuspended in 200 mL of methanol and stirred for 5 minutes. Finally the mixture was filtered and the white precipitate dried under vacuum (1 mmHg, 30 °C). The crude product was purified by dissolving it in CHCl<sub>3</sub> (100 mL) and then filtered through Whatman qualitative filter paper. The filtrate was precipitated from MeOH (500 mL). The purified colorless compound was recovered by filtration and dried as previously described. Purified yield: 0.18 g (80%). DS<sub>propyl</sub> = 0.6. <sup>1</sup>H-NMR (10% in CDCl<sub>3</sub>, ppm, 313 K):  $\delta$  = 0.15 (Si-CH<sub>3</sub>),  $\delta$  = 0.89 (Si-C(CH<sub>3</sub>)<sub>2</sub>CH(CH<sub>3</sub>)<sub>2</sub>),  $\delta$  = 1.2 (CH<sub>3</sub>CH<sub>2</sub>(C=O)O),  $\delta$  = 1.66 (Si-C(CH<sub>3</sub>)<sub>2</sub>CH(CH<sub>3</sub>)<sub>2</sub>),  $\delta$  = 2.32 (CH<sub>3</sub>CH<sub>2</sub>(C=O)O),  $\delta$  = 3 – 4.8 (AGU protons),  $\delta$  = 5 (H-3 if propyl in position C3). <sup>13</sup>C-NMR (10% in CDCl<sub>3</sub>, ppm, 313 K):  $\delta$  = - 2.5 (Si-(CH<sub>3</sub>)<sub>2</sub>),  $\delta$  = 9.6 (CH<sub>3</sub>CH<sub>2</sub>(C=O)O),  $\delta$  = 18.6 (Si-C(CH<sub>3</sub>)<sub>2</sub>CH(CH<sub>3</sub>)<sub>2</sub>),  $\delta$  = 20.4 (Si-C(CH<sub>3</sub>)<sub>2</sub>CH(CH<sub>3</sub>)<sub>2</sub>), 25.2 (Si-C(CH<sub>3</sub>)<sub>2</sub>CH(CH<sub>3</sub>)<sub>2</sub>),  $\delta$  = 27.4 (CH<sub>3</sub>CH<sub>2</sub>(C=O)O),  $\delta$  = 34.3 (Si-C(CH<sub>3</sub>)<sub>2</sub>CH(CH<sub>3</sub>)<sub>2</sub>),  $\delta$  = 60.3 (C6),  $\delta$  = 70 – 83 (AGU carbons),  $\delta$  = 101.9 (C1),  $\delta$  = 173.5 (CH<sub>3</sub>CH<sub>2</sub>(C=O)O).

### 2.3.9 Synthesis of 3-O-(2-bromoisobutyryl)-2,6-O-TDMS cellulose

2,6-O-TDMS cellulose (1 g, 2.2 mmol) was suspended in 25 mL of freshly distilled THF and 3.7 mL (46.2 mmol) of anhydrous pyridine under argon atmosphere. The reaction solution was cooled to 0 °C with an ice/water bath and 2.9 mL (44 mmol) of 2-bromoisobutyryl bromide was added dropwise over 15 min. The ice/water bath was removed and the reaction mixture was allowed to react for 19 hours at room temperature under argon atmosphere. The reaction mixture was precipitated from MeOH (300 mL), filtered and dried in a vacuum oven (1 mmHg) at 40 °C. The crude product was purified by dissolving it in CHCl<sub>3</sub> (300 mL) and filtered through a Whatman

qualitative filter paper. The product was precipitated from MeOH (1 L) and filtered through Whatman filter paper and dried under vacuum (1 mmHg, 30 °C). The crude product was purified by dissolving it in CHCl<sub>3</sub> (300 mL) and then filtered through Whatman qualitative filter paper. The filtrate was precipitated from MeOH (1 L). The purified colorless compound was recovered by filtration and dried as previously described. Purified yield: 1.25 g (82%). DS = 0.3. FTIR (CHCl<sub>3</sub>, cm<sup>-1</sup>); 3530 (ν<sub>O-H</sub>); 2957, 2871 (ν<sub>CH3</sub>, ν<sub>CH2</sub>); 1751 (ν<sub>C=O</sub>); 1465, 1377 (δ<sub>CH3</sub>, δ<sub>CH2</sub>); 1252 (δ<sub>Si-C</sub>, ν<sub>C-O-C</sub>, ester); 1117, 1075 (ν<sub>C-O-C</sub>, ether); 835 (ν<sub>Si-C</sub>); 777 (γ<sub>Si-CH3</sub>). <sup>1</sup>H-NMR (10% in CDCl<sub>3</sub>, ppm, 313 K): δ = 0.15 (Si-CH<sub>3</sub>), δ = 0.89 (Si-C(CH<sub>3</sub>)<sub>2</sub>CH(CH<sub>3</sub>)<sub>2</sub>), δ = 1.66 (Si-C(CH<sub>3</sub>)<sub>2</sub>CH(CH<sub>3</sub>)<sub>2</sub>), δ = 1.95 (C(CH<sub>3</sub>)<sub>2</sub>Br), δ = 3.3 (OH), δ = 3.7 (H-6), δ = 3.8 (H-2, 5), δ = 4.0 (H-4), δ = 4.4 (H-1, 3). <sup>13</sup>C-NMR (10% in CDCl<sub>3</sub>, ppm, 313 K): δ = -2.5 (Si-(CH<sub>3</sub>)<sub>2</sub>), δ = 18.6 (Si-C(CH<sub>3</sub>)<sub>2</sub>CH(CH<sub>3</sub>)<sub>2</sub>), δ = 20.4 (Si-C(CH<sub>3</sub>)<sub>2</sub>CH(CH<sub>3</sub>)<sub>2</sub>), δ = 25.2 (Si-C(CH<sub>3</sub>)<sub>2</sub>CH(CH<sub>3</sub>)<sub>2</sub>), δ = 34.3 (Si-C(CH<sub>3</sub>)<sub>2</sub>CH(CH<sub>3</sub>)<sub>2</sub>), δ = 60.3 (C6), δ = 75.02 (C4), δ = 101.9 (C1).

### 2.3.10 Synthesis of 3-O-octyl-2,6-O-TDMS cellulose

First, 188 mg (7.8 mmol) of NaH (60% dispersion in mineral oil) was washed with 20 mL of freshly distilled THF. The process was done in the reaction flask under argon atmosphere. The mixture of THF and NaH was stirred for 15 min. Once the two components were separated (30 min) the THF layer was removed with a syringe and any NaH present in it destroyed in MeOH. This procedure was repeated four times. Then 10 mL of freshly distilled THF were added to the washed NaH together with 0.25 g (0.55 mmol) of 2,6-O-TDMS cellulose and left stirring for 30 min under an argon atmosphere at room temperature. Bromooctane (1.1 mL, 5.5 mmol) was then added dropwise to the reaction mixture in an ice bath. The mixture was stirred for 1 day at room temperature and 3 more days at 50 °C. The reaction was quenched by addition of isopropanol (10 mL) and poured into 100 mL of phosphate buffer solution (714 mg K<sub>2</sub>HPO<sub>4</sub> and 354 mg KH<sub>2</sub>PO<sub>4</sub> in 100 mL of distilled water). The precipitate was collected by filtration with Whatman qualitative paper filter. The precipitate was washed with 50 mL of distilled water and 50 mL of MeOH and dried in a vacuum oven (1 mmHg) overnight at 40 °C. DS ~ 1. FTIR (CHCl<sub>3</sub>, cm<sup>-1</sup>); 2923, 2857 (ν<sub>CH3</sub>, ν<sub>CH2</sub>); 1462, 1378 (δ<sub>CH3</sub>, δ<sub>CH2</sub>); 1252 (δ<sub>Si-C</sub>); 1140, 1030 (ν<sub>C-O-C</sub>, ether); 831 (ν<sub>Si-C</sub>); 777 (γ<sub>Si-CH3</sub>). <sup>1</sup>H-NMR (10% in CDCl<sub>3</sub>, ppm, 313 K): δ = 0.14 (Si-CH<sub>3</sub>), δ = 0.89 (Si-C(CH<sub>3</sub>)<sub>2</sub>CH(CH<sub>3</sub>)<sub>2</sub>), δ = 1.3 (Si-C(CH<sub>3</sub>)<sub>2</sub>CH(CH<sub>3</sub>)<sub>2</sub> (O-CH<sub>2</sub>CH<sub>2</sub> (CH<sub>2</sub>)<sub>5</sub>CH<sub>3</sub>), δ = 1.6 (O-CH<sub>2</sub>CH<sub>2</sub> (CH<sub>2</sub>)<sub>5</sub>CH<sub>3</sub>), δ = 2.8-4.4 AGU protons and (O-CH<sub>2</sub>CH<sub>2</sub> (CH<sub>2</sub>)<sub>5</sub>CH<sub>3</sub>). (H-6), δ = 3.8 (H-2), δ = 3.9 (H-5,4,3), δ = 4.4 (H-1).

### 2.3.11 Synthesis of 3-O-acetyl-2,6-O-TDMS cellulose

2,6-O-TDMS cellulose (0.25 g, 0.55 mmol) was weighed into a reaction flask to which 5 mL (62 mmol) of anhydrous pyridine was added and stirred until dissolved. The solution was then cooled in an ice bath for 5 min followed by the slow dropwise addition of acetyl bromide (0.42 mL; 5.5 mmol). The reaction mixture was left stirring under an argon atmosphere at room temperature (RT) for 1 day. The reaction mixture was then poured into MeOH (100 mL) and the product recovered as a precipitate. The final product was purified by dissolving it in  $\text{CHCl}_3$  (20 mL) and filtering the solution through a Whatman qualitative paper filter. The solution was poured into 100 mL of MeOH and the precipitate recovered by filtration (Whatman qualitative paper filter), washed with MeOH (50 mL) and dried in a vacuum oven (1 mmHg) overnight at 40 °C. DS = 0.3. FTIR ( $\text{CHCl}_3$ ,  $\text{cm}^{-1}$ ), 3514 ( $\nu_{\text{O-H}}$ ); 2956, 2868 ( $\nu_{\text{CH}_3}$ ,  $\nu_{\text{CH}_2}$ ); 1752 ( $\nu_{\text{C=O}}$ ); 1463, 1375 ( $\delta_{\text{CH}_3}$ ,  $\delta_{\text{CH}_2}$ ); 1251 ( $\delta_{\text{Si-C}}$ ,  $\nu_{\text{C-O-C}}$ , ester); 1150, 1037 ( $\nu_{\text{C-O-C}}$ , ether); 832 ( $\nu_{\text{Si-C}}$ ); 777 ( $\gamma_{\text{Si-CH}_3}$ ).  $^1\text{H-NMR}$  (10% in  $\text{CDCl}_3$ , ppm, 313 K):  $\delta$  = 0.13 ( $\text{Si-CH}_3$ ),  $\delta$  = 0.89 ( $\text{Si-C}(\text{CH}_3)_2\text{CH}(\text{CH}_3)_2$ ),  $\delta$  = 1.64 ( $\text{Si-C}(\text{CH}_3)_2\text{CH}(\text{CH}_3)_2$ ),  $\delta$  = 2.27 ( $\text{CH}_3\text{CO}$ ),  $\delta$  = 2.82-4.6 AGU protons.

### 2.3.12 Synthesis of 3-O-(2-bromo-2-methylpropyl)-2,6-O-TDMS cellulose

NaH (188 mg, 7.8 mmol) was washed four times with 20 mL of freshly distilled THF, as per the synthesis of 3-O-octyl-2,6-O-TDMS cellulose (section 2.3.10). Then 10 mL of THF was added to the washed NaH together with 0.25 g (0.55 mmol) of 2,6-O-TDMS cellulose and left stirring for 30 min under an argon atmosphere. 1,2-Dibromo-2-methylpropane (0.7 mL, 5.5 mmol) was then slowly added dropwise over 5 min to the stirring mixture at room temperature. The reaction mixture was stirred for 1 day at room temperature and 3 more days at 50 °C. The reaction was quenched by addition of isopropanol (10 mL) and poured into 100 mL of phosphate buffer solution (714 mg  $\text{K}_2\text{HPO}_4$  and 354 mg  $\text{KH}_2\text{PO}_4$  in 100 mL of distilled water). The precipitate was collected by filtration (Whatman qualitative paper filter), washed with 50 mL of distilled water and 50 mL of MeOH, and dried in a vacuum oven (1 mmHg) overnight at 40 °C. FTIR ( $\text{CHCl}_3$ ,  $\text{cm}^{-1}$ ), 3500 ( $\nu_{\text{O-H}}$ ); 2956, 2868 ( $\nu_{\text{CH}_3}$ ,  $\nu_{\text{CH}_2}$ ); 1462, 1380 ( $\delta_{\text{CH}_3}$ ,  $\delta_{\text{CH}_2}$ ); 1251 ( $\delta_{\text{Si-C}}$ ); 1149, 1034 ( $\nu_{\text{C-O-C}}$ , ether); 831 ( $\nu_{\text{Si-C}}$ ); 777 ( $\gamma_{\text{Si-CH}_3}$ ).  $^1\text{H-NMR}$  (10% in  $\text{CDCl}_3$ , ppm, 313 K):  $\delta$  = 0.14 ( $\text{Si-CH}_3$ ),  $\delta$  = 0.89 ( $\text{Si-C}(\text{CH}_3)_2\text{CH}(\text{CH}_3)_2$ ),  $\delta$  = 1.66 ( $\text{Si-C}(\text{CH}_3)_2\text{CH}(\text{CH}_3)_2$ ),  $\delta$  = 1.94 ( $\text{CBr}(\text{CH}_3)_2$ ),  $\delta$  = 2.98-4.7 AGU protons and ( $\text{C}(\text{CH}_2)\text{-O}$ ).

### 2.3.13 Synthesis of 2,3-O-(2-bromoisobutyryl)-2,6-O-(thexyldimethylsilyl) cellulose

2,6-O-TDMS-cellulose (1 g, 2.2 mmol) with a total DS of 1.3 was suspended in 25 mL of freshly distilled THF and 3.7 mL (46.2 mmol) of anhydrous pyridine under an argon atmosphere. The reaction solution was cooled to 0 °C with an ice/water bath and 2.9 mL (44 mmol) of 2-bromoisobutyryl bromide was added dropwise over 15 min. The ice/water bath was removed and the reaction mixture was allowed to react for 19 hours at room temperature. The reaction mixture was precipitated into MeOH (300 mL), filtered (Whatman qualitative filter paper) and dried in a vacuum oven (1 mmHg) at 40 °C. The crude product was purified by dissolving it in 300 mL of CHCl<sub>3</sub>, and filtered through Whatman qualitative filter paper. The filtrate was then poured into MeOH (1 L) and the precipitate dried under vacuum (1 mmHg, 40 °C). Purified yield: 1.25 g (82%). FTIR (CHCl<sub>3</sub>, cm<sup>-1</sup>), 3530 (ν<sub>O-H</sub>); 2957, 2871 (ν<sub>CH<sub>3</sub></sub>, ν<sub>CH<sub>2</sub></sub>); 1751 (ν<sub>C=O</sub>); 1465, 1377 (δ<sub>CH<sub>3</sub></sub>, δ<sub>CH<sub>2</sub></sub>); 1252 (δ<sub>Si-C</sub>, ν<sub>C-O-C</sub>, ester); 1117, 1075 (ν<sub>C-O-C</sub>, ether); 835 (ν<sub>Si-C</sub>); 777 (γ<sub>Si-CH<sub>3</sub></sub>). <sup>1</sup>H-NMR (10% in CDCl<sub>3</sub>, ppm, 313 K): δ = 0.15 (Si-CH<sub>3</sub>), δ = 0.89 (Si-C(CH<sub>3</sub>)<sub>2</sub>CH(CH<sub>3</sub>)<sub>2</sub>), δ = 1.66 (Si-C(CH<sub>3</sub>)<sub>2</sub>CH(CH<sub>3</sub>)<sub>2</sub>), δ = 1.95 (C(CH<sub>3</sub>)<sub>2</sub>Br), δ = 3.3 (OH), δ = 3.7 (H-6), δ = 3.8 (H-2, 5), δ = 4.0 (H-4), δ = 4.3 (H-3 if TDMS in C2 and 2-bromoisobutyryl in C3), δ = 4.7 (H-1 if 2-bromoisobutyryl in position C2), δ = 4.8 (H-1 if TDMS in position C2), δ = 5.0 (H2 if 2-bromoisobutyryl in position C2), δ = 5.2 (H3 if 2-bromoisobutyryl in position C2). <sup>13</sup>C-NMR (10% in CDCl<sub>3</sub>, ppm, 313 K): δ = -2.5 (Si-(CH<sub>3</sub>)<sub>2</sub>), δ = 18.6 (Si-C(CH<sub>3</sub>)<sub>2</sub>CH(CH<sub>3</sub>)<sub>2</sub>), δ = 20.4 (Si-C(CH<sub>3</sub>)<sub>2</sub>CH(CH<sub>3</sub>)<sub>2</sub>), 25.2 (Si-C(CH<sub>3</sub>)<sub>2</sub>CH(CH<sub>3</sub>)<sub>2</sub>), δ = 34.3 (Si-C(CH<sub>3</sub>)<sub>2</sub>CH(CH<sub>3</sub>)<sub>2</sub>), δ = 60.3 (C6), δ = 75.02 (C4), δ = 101.9 (C1), δ = 169.6 (C13, if 2-bromoisobutyryl in position C2), δ = 170.8 (C13, if 2-bromoisobutyryl in position C3).

### 2.3.14 Synthesis of 3-O-allyl-2,6-O-TDMS cellulose

The synthesis of 3-O-allyl-2,6-O-TDMS cellulose was executed according to the procedure of Koschella et al.<sup>2</sup> NaH (0.753 g, 24 mmol, or 10 mol/mol modified AGU) was washed four times with 80 mL of freshly distilled THF, as per the synthesis of 3-O-octyl-2,6-O-TDMS cellulose (section 2.3.10). Then 40 mL of freshly distilled THF was added along with 1.0 g (24 mmol) of 2,6-O-TDMS cellulose and the reaction was stirred for 30 min. The flask was then placed in an ice bath and 1.84 mL (24 mmol) of allyl chloride was added dropwise over 5 min, under vigorous stirring. The mixture was stirred for 1 day at room temperature and 3 more days at 50 °C. The reaction was quenched by addition of isopropanol (40 mL) and poured into 300 mL of phosphate buffer solution (2.14 g K<sub>2</sub>HPO<sub>4</sub> and 1.1 g KH<sub>2</sub>PO<sub>4</sub> in 300 mL of distilled water). The precipitate was collected by filtration (Whatman qualitative filter paper) and washed with 200 mL of distilled



water and 150 mL of MeOH and dried in a vacuum oven (1 mmHg) overnight at 40 °C. Crude yield: 1.25 g (80%). FTIR (CHCl<sub>3</sub>, cm<sup>-1</sup>), 3513 (ν<sub>O-H</sub>); 3078 (ν<sub>=CH</sub>); 2957, 2871 (ν<sub>CH3</sub>, ν<sub>CH2</sub>); 1647 (ν<sub>C=C</sub>); 1465, 1379 (δ<sub>CH3</sub>, δ<sub>CH2</sub>); 1252 (δ<sub>Si-C</sub>); 1119, 1086 (ν<sub>C-O-C</sub>, ether); 835 (ν<sub>Si-C</sub>); 777 (γ<sub>Si-CH3</sub>). <sup>1</sup>H-NMR (10% in CDCl<sub>3</sub>, ppm, 313 K) δ = 0.15 (Si-CH<sub>3</sub>), δ = 0.89 (Si-C(CH<sub>3</sub>)<sub>2</sub>CH(CH<sub>3</sub>)<sub>2</sub>), δ = 1.68 (Si-C(CH<sub>3</sub>)<sub>2</sub>CH(CH<sub>3</sub>)<sub>2</sub>), δ = 3.2 (H-6), δ = 3.9 (H-2, 5), δ = 4 (H-4), δ = 4.5 (O-CH<sub>2</sub>-CH=CH<sub>2</sub>), δ = 5.2 (O-CH<sub>2</sub>-CH=CH<sub>2</sub>), δ = 6.0 (O-CH<sub>2</sub>-CH=CH<sub>2</sub>). <sup>13</sup>C-NMR (10% in CDCl<sub>3</sub>, ppm, 313 K): δ = - 2.5 (Si-(CH<sub>3</sub>)<sub>2</sub>), δ = 18.6 (Si-C(CH<sub>3</sub>)<sub>2</sub>CH(CH<sub>3</sub>)<sub>2</sub>), δ = 20.4 (Si-C(CH<sub>3</sub>)<sub>2</sub>CH(CH<sub>3</sub>)<sub>2</sub>), 25.2 (Si-C(CH<sub>3</sub>)<sub>2</sub>CH(CH<sub>3</sub>)<sub>2</sub>), δ = 34.3 (Si-C(CH<sub>3</sub>)<sub>2</sub>CH(CH<sub>3</sub>)<sub>2</sub>), δ = 61.5 (C6), δ = 68.1 (O-CH<sub>2</sub>-CH=CH<sub>2</sub>), δ = 72-74.4 (C2, C4, C5, O-CH<sub>2</sub>-CH=CH<sub>2</sub>), δ = 82.3 (C3), δ = 101.6 (C1), δ = 116 (O-CH<sub>2</sub>-CH=CH<sub>2</sub>), δ = 135.8 (O-CH<sub>2</sub>-CH=CH<sub>2</sub>).

### 2.3.15 Synthesis of 3-O-(3-hydroxypropyl)-2,6-O-TDMS cellulose

The synthesis of 3-O-(3-hydroxypropyl)-2,6-O-TDMS cellulose performed as described by Schumann et al.<sup>91</sup> 3-O-allyl-2,6-O-TDMS cellulose (1 g, 2.1 mmol) was dissolved in 40 mL of freshly distilled THF, once dissolved the flask was cooled in an ice bath and 42 mL (0.5 M solution in THF; 21 mmol) of 9-borabicyclo (3.3.1) nonane (9-BBN) were slowly added dropwise over 20 min under an argon atmosphere. The reaction mixture was left stirring for 10 min, removed from the ice bath, warmed to room temperature and then heated to 80 °C and stirred for 5 hours. The reaction was then cooled to 0 °C and excess 9-BBN was hydrolyzed by the addition of 16.5 mL of water, followed by 40.9 mL of a 3 M aqueous solution of NaOH and 35 mL of H<sub>2</sub>O<sub>2</sub> (30%). The reaction mixture was left stirring at room temperature, overnight. THF was then removed by rotary evaporation causing the product to precipitate, which was recovered by filtration (Whatman qualitative filter paper) and washed with water (100 mL) and MeOH (150 mL). The isolated product was dried overnight in a vacuum oven (1 mmHg) at 40 °C. Recovered yield: 0.73 g (70%). FTIR (CHCl<sub>3</sub>, cm<sup>-1</sup>), 3465 (ν<sub>OH</sub>); 2957, 2871 (ν<sub>CH3</sub>, ν<sub>CH2</sub>); 1465, 1379 (δ<sub>CH3</sub>, δ<sub>CH2</sub>); 1251 (δ<sub>Si-C</sub>); 1117, 1081 (ν<sub>C-O-C</sub>, ether); 835 (ν<sub>Si-C</sub>); 777 (γ<sub>Si-CH3</sub>). <sup>1</sup>H-NMR (10% in CDCl<sub>3</sub>, ppm, 313 K) δ = 0.17 (Si-CH<sub>3</sub>), δ = 0.89 (Si-C(CH<sub>3</sub>)<sub>2</sub>CH(CH<sub>3</sub>)<sub>2</sub>), δ = 1.67-1.78 (Si-C(CH<sub>3</sub>)<sub>2</sub>CH(CH<sub>3</sub>)<sub>2</sub>, OCH<sub>2</sub>CH<sub>2</sub>CH<sub>2</sub>OH), δ = 3.1-4.5 (H-1-H-6, OCH<sub>2</sub>CH<sub>2</sub>CH<sub>2</sub>OH). <sup>13</sup>C-NMR (10% in CDCl<sub>3</sub>, ppm, 313 K) δ = - 2.37 (Si-(CH<sub>3</sub>)<sub>2</sub>), δ = 18.6 (Si-C(CH<sub>3</sub>)<sub>2</sub>CH(CH<sub>3</sub>)<sub>2</sub>), δ = 20.5 (Si-C(CH<sub>3</sub>)<sub>2</sub>CH(CH<sub>3</sub>)<sub>2</sub>), 24.8 (Si-C(CH<sub>3</sub>)<sub>2</sub>CH(CH<sub>3</sub>)<sub>2</sub>), δ = 32.7 (OCH<sub>2</sub>CH<sub>2</sub>CH<sub>2</sub>OH), δ = 33.8 (Si-C(CH<sub>3</sub>)<sub>2</sub>CH(CH<sub>3</sub>)<sub>2</sub>), δ = 59.3 (O-CH<sub>2</sub>CH<sub>2</sub>CH<sub>2</sub>OH), δ = 61.5 (O-CH<sub>2</sub>-CH<sub>2</sub>CH<sub>2</sub>OH), δ = 69.8 (C6), δ = 73-79 (C2, C5, C4), δ = 84.1 (C3), δ = 101.5 (C1).

### 2.3.16 Synthesis of 3-O-propyl-(2-bromoisobutyryl)-2,6-O-TDMS cellulose

3-O-(3-hydroxypropyl)-2,6-O-TDMS cellulose (1 g, 1.98 mmol) was dissolved in 30 mL of freshly distilled THF to which 0.45 g (6.6 mmol) of imidazole was added. The reaction was cooled to 0 °C under an argon atmosphere and 0.54 mL (4.4 mmol) of 2-bromoisobutyryl bromide was added under constant stirring. The reaction was warmed to room temperature and left to proceed overnight. The reaction was precipitated into MeOH (200 mL), filtrated (Whatman qualitative filter paper) and washed with MeOH (3 x 50 mL). The product was dried overnight in a vacuum oven (1 mmHg) at 40 °C. Recovered Yield: 0.73 g (70%). FTIR ( $\text{CHCl}_3$ ,  $\text{cm}^{-1}$ ), 3465 ( $\nu_{\text{O-H}}$ ); 2957, 2871 ( $\nu_{\text{CH}_3}$ ,  $\nu_{\text{CH}_2}$ ); 1738 ( $\nu_{\text{C=O}}$ ); 1465, 1379 ( $\delta_{\text{CH}_3}$ ,  $\delta_{\text{CH}_2}$ ); 1251 ( $\delta_{\text{Si-C}}$ ,  $\nu_{\text{C-O-C}}$ , ester); 1117, 1082 ( $\nu_{\text{C-O-C}}$ , ether); 835 ( $\nu_{\text{Si-C}}$ ); 777 ( $\gamma_{\text{Si-CH}_3}$ ).  $^1\text{H-NMR}$  (10% in  $\text{CDCl}_3$ , 313 K)  $\delta$  = 0.16 (Si- $\text{CH}_3$ ),  $\delta$  = 0.88 (Si- $\text{C}(\text{CH}_3)_2\text{CH}(\text{CH}_3)_2$ ),  $\delta$  = 1.67 (Si- $\text{C}(\text{CH}_3)_2\text{CH}(\text{CH}_3)_2$ ),  $\delta$  = 1.93 ( $\text{OCH}_2\text{CH}_2\text{CH}_2\text{OCOC}(\text{CH}_3)_2\text{Br}$ ),  $\delta$  = 3.1-4.25 (H-1-H-6,  $\text{OCH}_2\text{CH}_2\text{CH}_2\text{OCOC}(\text{CH}_3)_2\text{Br}$ ).  $^{13}\text{C-NMR}$  (10% in  $\text{CDCl}_3$ , ppm, 313 K):  $\delta$  = -2.37 (Si- $\text{C}(\text{CH}_3)_2$ ),  $\delta$  = 18.6 (Si- $\text{C}(\text{CH}_3)_2\text{CH}(\text{CH}_3)_2$ ),  $\delta$  = 20.4 (Si- $\text{C}(\text{CH}_3)_2\text{CH}(\text{CH}_3)_2$ ),  $\delta$  = 25.1 (Si- $\text{C}(\text{CH}_3)_2\text{CH}(\text{CH}_3)_2$ ),  $\delta$  = 29.2 ( $\text{OCH}_2\text{CH}_2\text{CH}_2$ ),  $\delta$  = 30.9 ( $\text{O}(\text{CO})\text{CBr}(\text{CH}_3)_2$ ),  $\delta$  = 33.8 (Si- $\text{C}(\text{CH}_3)_2\text{CH}(\text{CH}_3)_2$ ),  $\delta$  = 55.7 ( $\text{O}(\text{CO})\text{CBr}(\text{CH}_3)_2$ ),  $\delta$  = 63.6 ( $\text{O-CH}_2\text{-CH}_2\text{CH}_2\text{OH}$ ),  $\delta$  = 70.5 (C6),  $\delta$  = 73-79 (C2, C5, C4),  $\delta$  = 84.3 (C3),  $\delta$  = 101.4 (C1),  $\delta$  = 171.4 ( $\text{O}(\text{CO})\text{CBr}(\text{CH}_3)_2$ ).

### 2.3.17 Homogeneous polymerization of NIPAM from 3-O-propyl-(2-bromoisobutyryl)-2,6-O-TDMS cellulose through ATRP

3-O-propyl-(2-bromoisobutyryl)-2,6-O-TDMS cellulose (100 mg; 0.15 mmol) and NIPAM (1.7 g, 15 mmol) were dissolved in 10 mL of freshly distilled THF in a 50 mL Schlenk flask (mixture 1). The mixture was degassed by four FPT as per the surface initiated ATRP of NIPAM from honeycomb films made from 6-O-(2-bromoisobutyryl) trimethylsilyl-O-cellulose (section 2.3.6). In a second 50 mL Schlenk flask 1.2 g of dimethyl formamide (DMF; 16 mmol) as an internal standard and 0.5 mL of MeOH (12.3 mmol) were added and degassed (four FPT cycles) (mixture 2). Then CuCl (14.85 mg, 0.15 mmol), Cu(II)Cl<sub>2</sub> (1 mg, 0.0075 mmol), and Me<sub>6</sub>TREN (41.4 mg, 0.18 mmol) were added to the degassed MeOH/DMF mixture while frozen. The mixture was then subjected to further degassing by four FPT cycles (as described in section 2.3.6). The reaction was started by adding the initiator in mixture 1 through a degassed syringe under argon to the 50 mL Schlenk flask containing the catalyst (mixture 2). The reaction proceeded at room temperature, under an argon atmosphere with constant stirring. During the course of the reaction, aliquots were withdrawn at specific time intervals. The reaction was terminated by exposure to air. The reaction mixture was precipitated in water (100 mL), which was heated above the LCST of PNIPAM to remove unreacted NIPAM and catalyst, and was repeated four times. The final

product was dried in a vacuum oven (1 mmHg) at 40 °C overnight and purified by dissolving the crude product (50 mg) in THF (20 mL) and precipitating it in water (100 mL). Again the precipitate was washed with water (3 x 50 mL) and finally freeze-dried. FTIR (ATR,  $\text{cm}^{-1}$ ), 3302 ( $\nu_{\text{N-H}}$ ); 3064 ( $\nu_{\text{CH}}$ ); 2966, 2868 ( $\nu_{\text{CH}_3}$ ,  $\nu_{\text{CH}_2}$ ); 1724 ( $\nu_{\text{C=O}}$ ); 1644 ( $\nu_{\text{C=O}}$ , PNIPAM); 1538 ( $\delta_{\text{N-H}}$ ); 1458 ( $\delta_{\text{CH}_3}$ ,  $\delta_{\text{CH}_2}$ ); 1385 and 1365 ( $\delta_{\text{CH}_3}$ , PNIPAM); 1251 ( $\delta_{\text{Si-C}}$ ,  $\nu_{\text{C-O-C}}$ , ester); 1168 and 1042 ( $\nu_{\text{C-O-C}}$ , ether); 832 ( $\nu_{\text{Si-C}}$ ); 776 ( $\gamma_{\text{Si-CH}_3}$ ).  $^1\text{H-NMR}$  (10% in  $\text{CDCl}_3$ , 313 K)  $\delta$  = 0.08 (Si-CH<sub>3</sub>);  $\delta$  = 0.87 (Si-C(CH<sub>3</sub>)<sub>2</sub>CH(CH<sub>3</sub>)<sub>2</sub>),  $\delta$  = 1.16 (CH<sub>3</sub>)<sub>2</sub>-CH-NH);  $\delta$  = 1.3-2.4 (CH<sub>2</sub>CHCH<sub>2</sub>)(CH)Br), (Si-C(CH<sub>3</sub>)<sub>2</sub>CH(CH<sub>3</sub>)<sub>2</sub>) OCH<sub>2</sub>CH<sub>2</sub>CH<sub>2</sub>OCOC(CH<sub>3</sub>)<sub>2</sub>);  $\delta$  = 2.9-4.6 (AGU protons, (OCH<sub>2</sub>CH<sub>2</sub>CH<sub>2</sub>OCOC(CH<sub>3</sub>)<sub>2</sub>) ((CH<sub>3</sub>)<sub>2</sub>-CH-NH);  $\delta$  = 6.3 (N-H).  $^{13}\text{C-NMR}$  (10% in  $\text{CDCl}_3$ , ppm, 313 K):  $\delta$  = 18.7 (Si-C(CH<sub>3</sub>)<sub>2</sub>CH(CH<sub>3</sub>)<sub>2</sub>),  $\delta$  = 20.6 (Si-C(CH<sub>3</sub>)<sub>2</sub>CH(CH<sub>3</sub>)<sub>2</sub>),  $\delta$  = 22.6 (CH<sub>3</sub>)<sub>2</sub>-CH-NH);  $\delta$  = 24.8 (O(CO)CBr(CH<sub>3</sub>)<sub>2</sub>),  $\delta$  = 30.3 (OCH<sub>2</sub>CH<sub>2</sub>CH<sub>2</sub>O),  $\delta$  = 34.2 (Si-C(CH<sub>3</sub>)<sub>2</sub>CH(CH<sub>3</sub>)<sub>2</sub>),  $\delta$  = 41.3 (CH<sub>3</sub>)<sub>2</sub>-CH-NH),  $\delta$  = 174 (HN-(CO)CH).

### 2.3.18 Homogeneous copolymerization of DEGMA and OEGMA from 3-O-propyl-(2-bromoisobutyryl)-2,6-O-TDMS cellulose

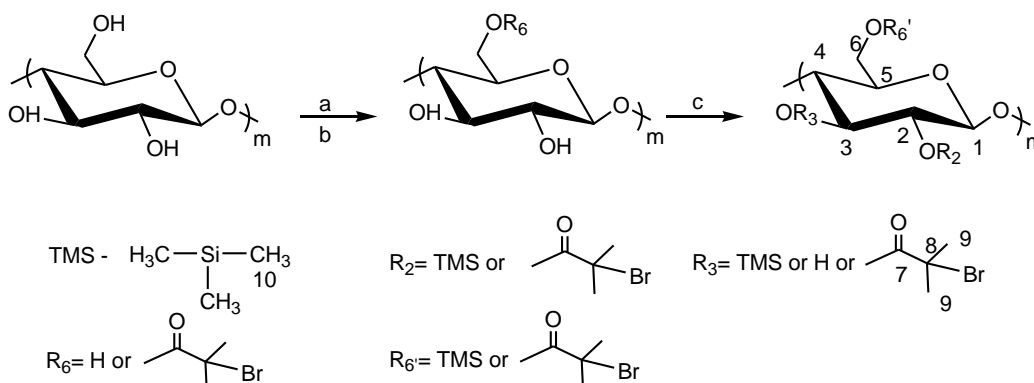
3-O-propyl-(2-bromoisobutyryl)-2,6-O-TDMS cellulose (49 mg, 0.075 mmol) was dissolved in 5 mL of freshly distilled THF in a 50 mL Schlenk flask (mixture 1). In a second 100 mL Schlenk flask a mixture of OEGMA (0.178 mg, 0.375 mmol), DEGMA (1.3 g, 7.125 mmol), Me<sub>6</sub>TREN (20.7 mg, 0.09 mmol) and DMF (1.2 g, 16 mmol) as internal standard were mixed with 5 mL of freshly distilled THF (mixture 2). Both mixtures were degassed by four FPT cycles and blanketed with argon, as per the surface initiated ATRP of NIPAM from honeycomb films made from 6-O-(2-bromoisobutyryl) trimethylsilyl-O-cellulose (section 2.3.6). CuCl (7.425 mg, 0.075 mmol) and CuCl<sub>2</sub> (2.0 mg, 0.015 mmol) were introduced in the DEGMA and OEGMA mixture, while frozen, and again degassed (four FPT cycles). The reaction was started by adding the initiator mixture 1 using a degassed syringe under argon. The reaction mixture was placed in an oil bath at 55 °C and stirred under argon. During the reaction aliquots were withdrawn at specific time intervals. The reaction was terminated by exposure to air and the catalyst was removed by passing the reaction mixture through a short alumina column, followed by dialysis (membrane cut off 3,500 g/mol) in water for 72 hours. The product was then obtained as a dry powder after lyophilization. FTIR (ATR,  $\text{cm}^{-1}$ ), 2915, 2873 ( $\nu_{\text{CH}_3}$ ,  $\nu_{\text{CH}_2}$ ); 1726 ( $\nu_{\text{C=O}}$ ); 1470 ( $\delta_{\text{CH}_2}$ ), 1452 ( $\delta_{\text{CH}_3}$ ); 1246 ( $\delta_{\text{Si-C}}$ ,  $\nu_{\text{C-O-C}}$ , ester); 1106 ( $\nu_{\text{C-O-C}}$ , ether); 835 ( $\nu_{\text{Si-C}}$ ); 777 ( $\gamma_{\text{Si-CH}_3}$ ).  $^1\text{H-NMR}$  (10% in  $\text{CDCl}_3$ , 313 K)  $\delta$  = 0.08 (Si-CH<sub>3</sub>),  $\delta$  = 1.0 CH<sub>3</sub>-C(CO)(CH<sub>2</sub>)<sub>2</sub>);  $\delta$  = 1.9 (CH<sub>2</sub>(C(CO)CH<sub>3</sub>)<sub>2</sub>);  $\delta$  = 3.4 ((CH<sub>2</sub>)OCH<sub>3</sub>);  $\delta$  = 3.6-3.7 ((CH<sub>2</sub>)OCH<sub>3</sub>);  $\delta$  = 4.1 ((CO)OCH<sub>2</sub>CH<sub>2</sub>).  $^{13}\text{C-NMR}$  (10% in  $\text{CDCl}_3$ , ppm, 313 K):  $\delta$  = 17.3 (CH<sub>3</sub>-C(CO)(CH<sub>2</sub>)<sub>2</sub>),  $\delta$  = 44.8 (CH<sub>2</sub>(C(CO)CH<sub>3</sub>)<sub>2</sub>);  $\delta$  = 54.1 (CH<sub>3</sub>CH<sub>2</sub>C(CO));  $\delta$  = 59.0 (OCH<sub>3</sub>),  $\delta$  = 63.9 ((CO)OCH<sub>2</sub>CH<sub>2</sub>);  $\delta$  = 68.5-77.1 (O(CH<sub>2</sub>)<sub>2</sub>),  $\delta$  = 176.5, 177.2, 177.6 (C(CO)O(CH<sub>2</sub>)<sub>2</sub>).

### 3 RESULTS AND DISCUSSION

#### 3.1 Synthesis of 6-O-(2-Bromoisobutyryl)-TMS-O-Cellulose for Preparation of Thermoresponsive Honeycomb Patterned Films via Surface Initiated ATRP

Regioselectively substituted 6-O-(2-bromoisobutyryl)-TMS-O-cellulose was synthesized with different DS, and its structure confirmed by FTIR,  $^1\text{H}$ - and  $^{13}\text{C}$ -NMR. The ability of the newly synthesized cellulose derivative to form honeycomb patterned films was evaluated. The effect of parameters, such as concentration, flow/humidity, DS and regioselectivity in the film formation was studied. This ATRP active honeycomb film surface was modified through the grafting of thermoresponsive PNIPAM and its surface morphology and properties evaluated by SEM, AFM and contact angle measurements. The ability of 6-O-(2-bromoisobutyryl)-TMS-O-cellulose to form honeycomb patterned films makes it a very interesting material which provides the opportunity to tailor its surface properties to meet the requirements of specified end-use applications.

##### 3.1.1 Synthesis and characterization of 6-O-(2-bromoisobutyryl)-2,3-O-TMS cellulose



**Scheme 3.1.1.** Proposed synthetic scheme to synthesize 6-O-(2-bromoisobutyryl)-TMS-O-cellulose: a. DMA-LiCl, TDMS-Cl, imidazole; b. 2-bromoisobutyryl bromide, anhydrous pyridine; c. DMA, anhydrous pyridine, HMDS-Cl.

The regioselectively substituted cellulose derivatives were synthesized by introducing a 2-bromoisobutyryl group at position 6 according to **Scheme 3.1.1**. The selective modification of the C6 position was based on the preferential reactivity of the hydroxyl group in this position<sup>96</sup> and through control of reaction stoichiometry. The solubility of these derivatives varied according to DS, which was calculated through quantitative <sup>13</sup>C-NMR as described below. The low (0.26) and medium (0.52) DS derivatives were soluble in DMA, but not soluble in water, acetone, THF or CHCl<sub>3</sub>. The high (0.80) DS derivative was soluble in CHCl<sub>3</sub>, THF and DMA, but not in water or acetone. Therefore, to improve the solubility of the cellulose derivatives the unreacted hydroxyl groups in positions 2, 3 and 6 were silylated with trimethyl silyl (TMS) groups. In **Table 3.1.1** the experimental conditions used to obtain these derivatives is described along with the respective DS of 2-bromoisobutyryl, Mn and PDIs. The Mn was determined by GPC-MALS to monitor the degradation of the cellulose backbone. Mn and DSs analyses were conducted in duplicate, respective relative percent differences (RPDs%) were determined as per **Equation 3.1.1** and found to be no higher than 4%. A table with respective duplicate values and RPDs is presented in **APPENDIX-Duplicates and respective RPDs%**.

$$\text{RPD (\%)} = [(x_1 - x_2) / x_{\text{avg}}] \times 100 \quad \text{Equation 3.1.1}$$

$x_1, x_2$ — measured values

$x_{\text{avg}}$  — average of measured values

**Table 3.1.1.** Effect of molar equivalents of 2-bromoisobutyryl bromide (BribuBr) on the degree of substitution (DS), Mn and PDI of 6-O-(2-bromoisobutyryl)-TMS-O-cellulose derivatives.

C6 derivative	Molar equivalents BribuBr	DS <sub>2-bromoisobutyryl</sub> <sup>(a)</sup>	Mn (g/mol) <sup>(b)</sup>	PDI <sup>(b)</sup>
L	0.4	0.26	5.5*10 <sup>4</sup>	1.1
M	0.6	0.52	5.9*10 <sup>4</sup>	1.2
H	0.8	0.80	5.9*10 <sup>4</sup>	1.2
Non-regioselective	6	2.24	7.0*10 <sup>4</sup>	1.2

<sup>(a)</sup> DS determined from quantitative <sup>13</sup>C-NMR. <sup>(b)</sup> Mn and PDI determined by GPC-MALS.

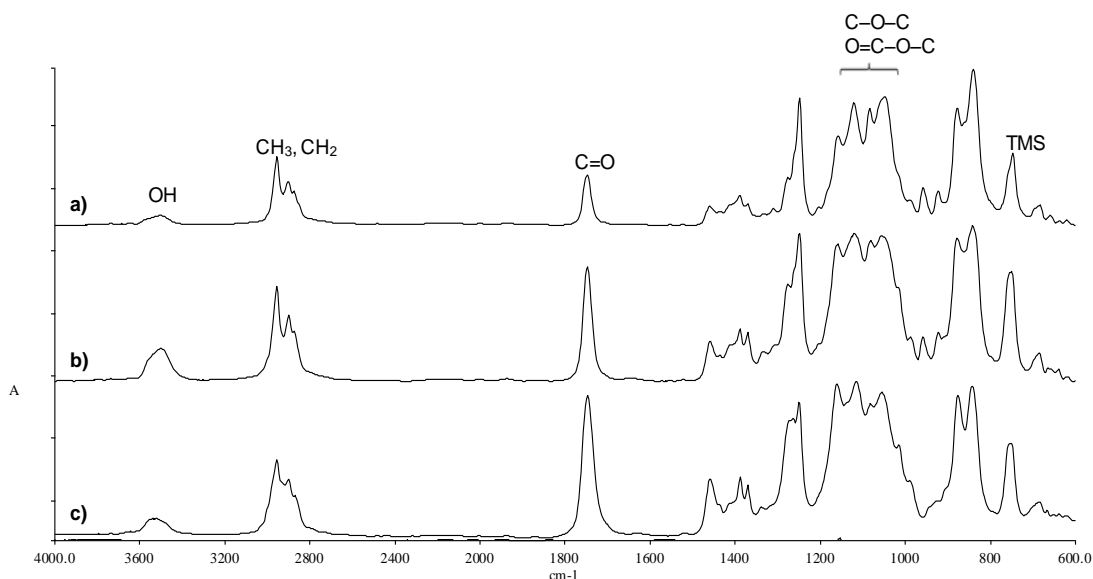


**Figure 3.1.1.** Comparison of FTIR spectra of 6-O-(2-bromoisobutyryl) TMS-O-cellulose with different DS; a) low DS (0.24); b) medium DS (0.50); c) high DS (0.80).

FTIR spectra of the C6 derivatives (**Figure 3.1.1**) confirmed the introduction of functional group 2-bromoisobutyryl in the cellulose backbone (detection of C=O peak at  $1740\text{ cm}^{-1}$  ( $\nu_{\text{C=O}}$ ), C-O-C ester peak at  $1248\text{ cm}^{-1}$  ( $\nu_{\text{C-O-C}}$ ) and C-O-C ether at  $1122$  and  $1084\text{ cm}^{-1}$  ( $\nu_{\text{C-O-C}}$ ). The existence of TMS was also confirmed by the presence of a peak at  $746\text{ cm}^{-1}$  ( $\nu_{\text{Si-C}}$ ).

The molecular structure of 6-O-(2-bromoisobutyryl) cellulose with a DS of 0.26 and the regioselective substitution in position C6 was done by two dimensional NMR (2D-NMR). In order to obtain well resolved spectra, 6-O-(2-bromoisobutyryl) cellulose was first acetylated with acetic anhydride in anhydrous pyridine to avoid the peak broadening caused by inter- and intramolecular interactions.<sup>2</sup> Signals assignments were determined by crosspeak correlations using heteronuclear single-quantum correlation (HSQC, **Figure 3.1.2**), homonuclear correlation spectroscopy (COSY, **Figure 3.1.3**) and heteronuclear multiple-bond correlation spectroscopy (HMBC, **Figure 3.1.4**).

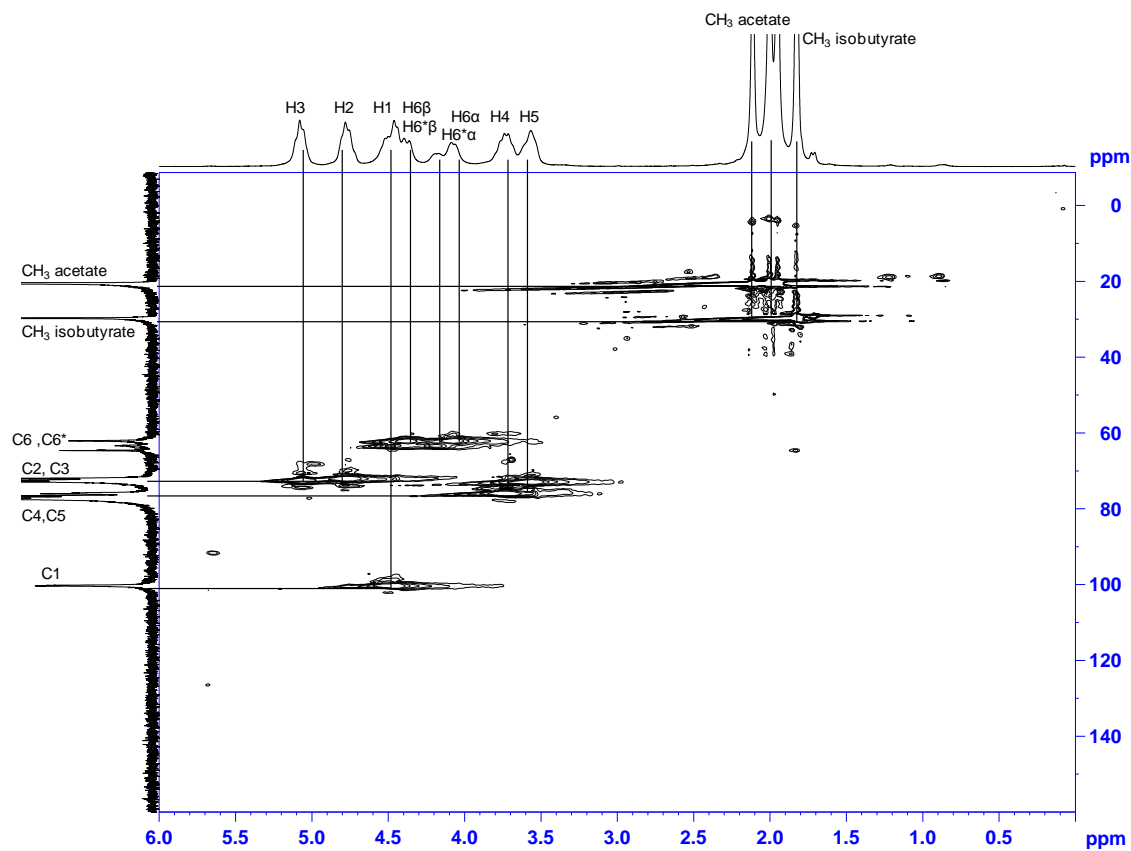


**Figure 3.1.2.**  $^1\text{H}/^{13}\text{C}$  heteronuclear single-quantum correlation spectroscopy (HSQC) of 6-O-(2-bromoisobutyryl)-2,3,6-O-acetyl cellulose.

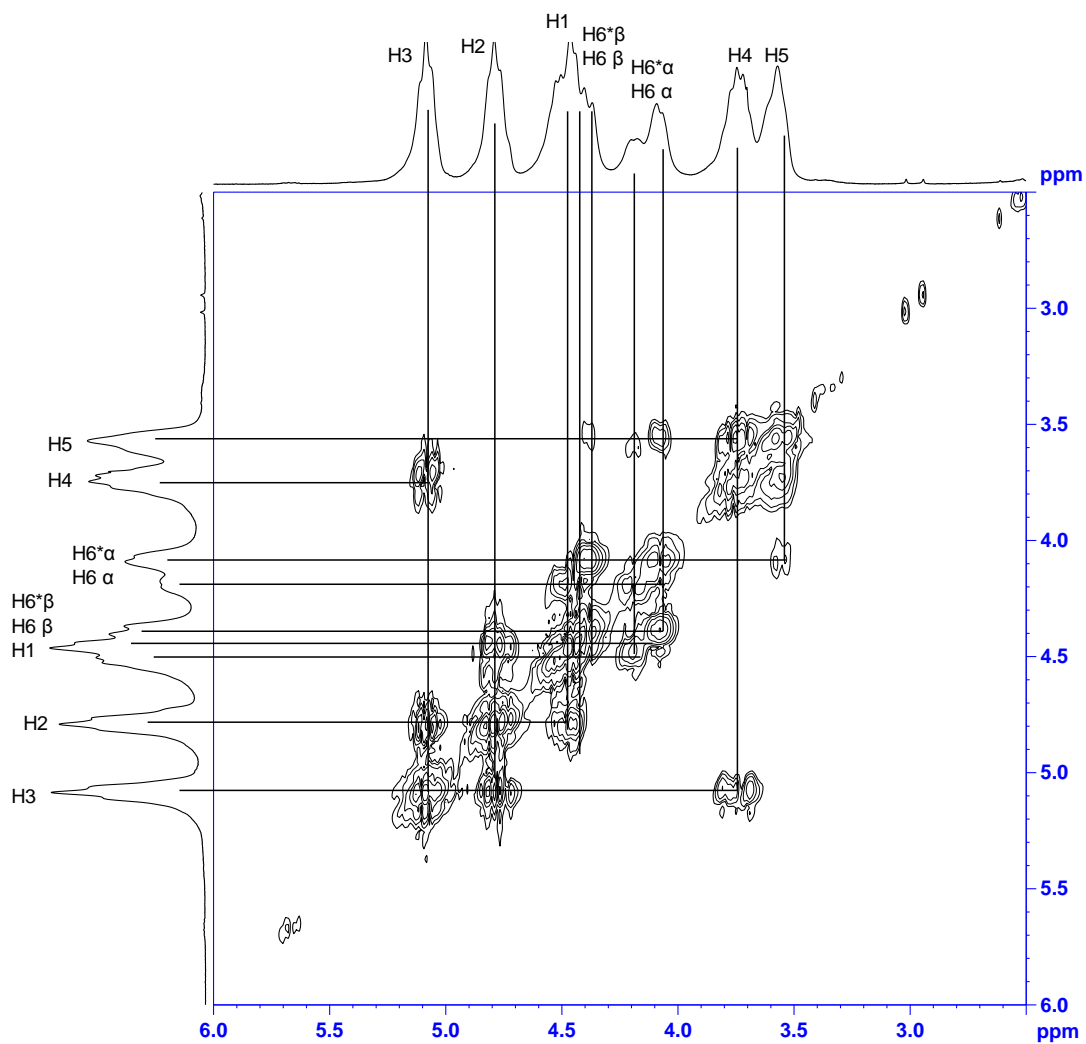


**Figure 3.1.3.**  $^1\text{H}/^1\text{H}$  homonuclear correlation spectroscopy (COSY) of 6-O-(2-bromoisobutryl)-2,3,6-O-acetyl cellulose.



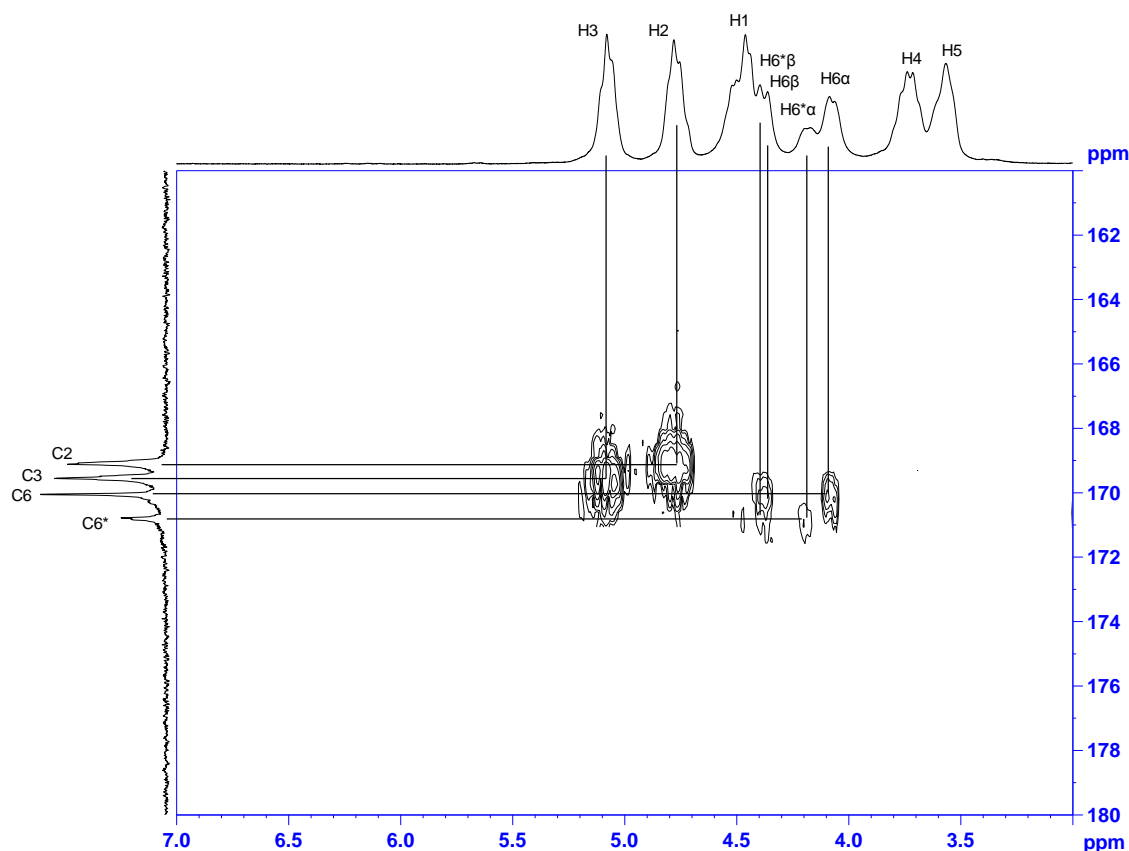


**Figure 3.1.4.**  $^1\text{H}/^{13}\text{C}$  heteronuclear multiple-bond correlation spectroscopy (HMBC) of 6-O-(2-bromoisobutyryl)-2,3,6-O-acetyl cellulose.

Accordingly, H1, H6 were assigned by correlations in the HSQC spectrum (**Figure 3.1.2**)  $\delta\text{H}/\delta\text{C}$ ; H1/C1  $\sim 4.5/102$ ; H6<sub>acetate/2-bromoisobutyryl</sub>/C6<sub>acetate/2-bromoisobutyryl</sub>  $\sim 4.1\text{--}4.4/61\text{--}64$ . COSY spectrum (**Figure 3.1.3**) correlations assigned H2 ( $\sim 4.8$  ppm), H3 ( $\sim 5.1$  ppm), H4 ( $\sim 3.7$  ppm) and H5 ( $\sim 3.55$  ppm) by crosspeak correlation with H1, H2, H3 and H(4 and 6), respectively. Once the protons were identified, it was possible to assign the remaining carbons by correlations in the HSQC spectrum  $\delta\text{H}/\delta\text{C}$ ; H2/C2  $\sim 4.8/70\text{--}73$ ; H3/C3  $\sim 5.1/70\text{--}73$ ; H4/C4  $\sim 3.7/75\text{--}78$ ; H5/C5  $\sim 3.55/75\text{--}78$ . As the DS of 2-bromoisobutyryl was 0.26 the acetylated product produced two signals for H6/C6 which were identified through correlations in the HMBC spectrum (**Figure 3.1.4**)  $\delta\text{H}/\delta\text{C}$ ; H6<sub>acetate</sub>/C6<sub>acetate</sub>  $\sim 4.1\text{--}4.35/170$  H6<sub>2-bromoisobutyryl</sub>/C6<sub>2-bromoisobutyryl</sub>  $\sim 4.2\text{--}4.4/171$ . Furthermore, the remaining carbonyl peaks were assigned as follows:  $\delta = 169.5$  ppm (C3( $\text{C}=\text{O}$ )) and  $\delta = 169$  ppm (C2( $\text{C}=\text{O}$ )). All peaks and correlations found from 2D NMR techniques HSQC, COSY and HMBC are in agreement with the structure 6-O-(2-bromoisobutyryl) 2,3,6-O-acetyl cellulose (DS = 0.26). Therefore, to verify the regioselective substitution of 6-O-(2-bromoisobutyryl) TMS-O-cellulose with DS of 0.52 (medium DS) and 0.80 (high DS) a comparison between the different

$^1\text{H}$ - and  $^{13}\text{C}$ -NMR spectra, **Figure 3.1.5** and **Figure 3.1.6**, respectively, was done against the regioselectively substituted cellulose derivative with a DS = 0.26 (low DS) and a non-regioselectively substituted 2,3,6-O-(2-bromoisobutyryl) TMS cellulose, synthesized for this purpose.

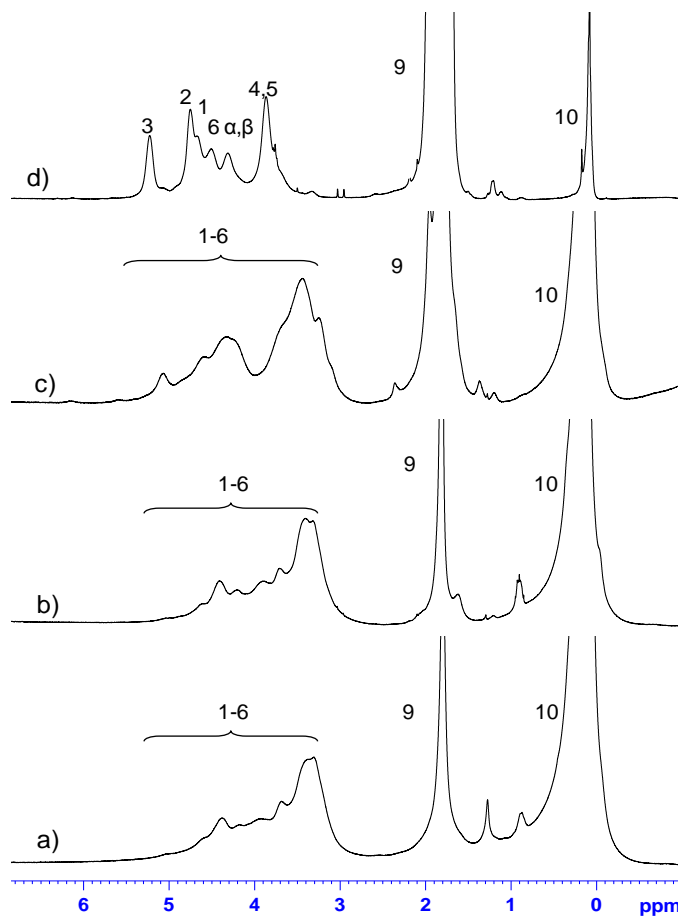


**Figure 3.1.5.** Comparison of  $^1\text{H}$ -NMR spectrum of 6-O-(2-bromoisobutyryl)-TMS-O-cellulose; a) low DS, b) medium DS, c) high DS, d) non-regioselectively substituted 2,3,6-O-(2-bromoisobutyryl)-TMS-O-cellulose.

$^1\text{H}$ -NMR spectra of 6-O-(2-bromoisobutyryl) TMS-O-cellulose with different DS (**Figure 3.1.5 a), b) and c)**) were compared against the respective non-regioselectively substituted derivative (**Figure 3.1.5 d)**). The synthesis of a random C6 derivative with a DS = 1 was attempted but positions C6 and C2 were preferentially functionalized. We also considered using protecting group chemistry but it was extremely difficult because the 2-bromoisobutyryl group is sensitive to the deprotection conditions of TMS, TDMS and trityl. Therefore, it was decided to synthesize a

non-regioselectively substituted 2,3,6-O-(2-bromoisobutyryl)-O-TMS cellulose for comparison. The latter was synthesized following the same procedure as described for the regioselectively substituted derivatives, employing an excess of 6 mole equivalents of 2-bromoisobutyryl bromide. The identification of the peaks was done based on what was found earlier for 6-O-(2-bromoisobutyryl)-2,3,6-O-acetyl-O-cellulose and from work by Heinze et al.<sup>338</sup> and Iwata et al.<sup>95</sup>. The AGU region of the 6-O-(2-bromoisobutyryl)-TMS-O-cellulose with a medium DS in **Figure 3.1.5 b)** is very similar to the AGU region of the low DS cellulose derivative confirming the regioselective substitution of the C6 position with a calculated DS of 0.52. In the <sup>1</sup>H-NMR spectrum of the cellulose derivative with high DS (**Figure 3.1.5 c)**) a new peak was detected at 5.1 ppm which could potentially be due to the presence of 2-bromoisobutyryl in position C2. If confirmed, this would mean that the high DS derivative might not have been regioselectively substituted exclusively in position C6. Furthermore, the AGU region shows a slight alteration when compared against the AGU regions of the cellulose derivatives with medium and low DS. This difference might be due to the increment of the DS in position C6. Based on these observations it is not possible to determine whether this cellulose derivative with high DS has been regioselectively substituted or not. The <sup>13</sup>C-NMR analysis might bring some more information on this matter. On the other hand, the <sup>1</sup>H-NMR spectrum of the non-regioselective cellulose derivative (**Figure 3.1.5 d)**) clearly shows two peaks at 5.4 and 4.7 ppm which were assigned as H3 and H2 when 2-bromoisobutyryl is present at positions C2 and C3 of the AGU. In order to confirm the structure of these cellulose derivatives and the respective DS<sub>isobutyryl</sub> quantitative <sup>13</sup>C-NMR was performed (**Figure 3.1.6**).

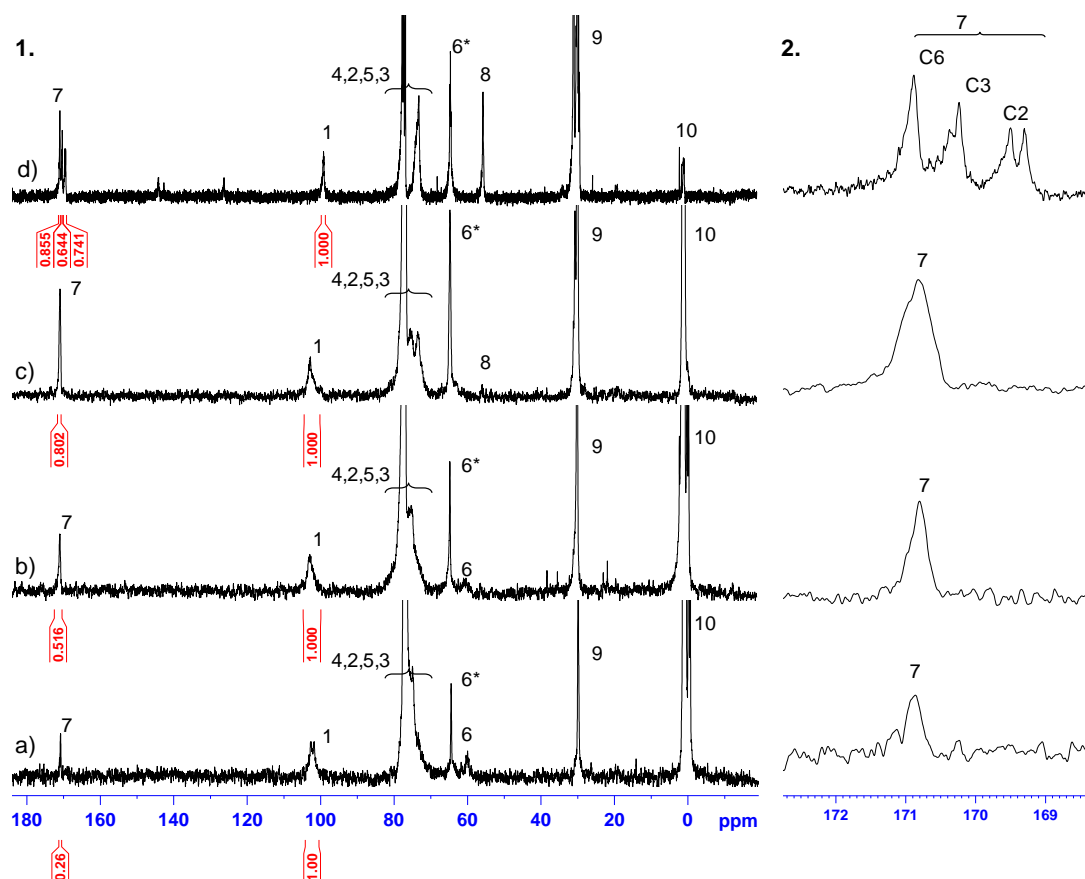


**Figure 3.1.6.** 1: Comparison of  $^{13}\text{C}$ -NMR spectrum of 6-O-(2-bromoisobutyryl)-TMS-O-cellulose; a) low DS, b) medium DS, c) high DS, d) non-regioselectively substituted with high DS; 2: Zoom-in of respective carbonyl region.

The comparison of  $^{13}\text{C}$ -NMR spectra further confirmed the synthesis of the regioselectively substituted derivatives with low and medium DS (**Figure 3.1.6 a)** and **b)**) in which, a single carbonyl peak at 170.8 ppm was detected. In the spectrum of the high DS derivative (**Figure 3.1.6 c)**) one single carbonyl peak at 170.8 ppm was detected, and not the two peaks that would have been expected if 2-bromoisobutyryl had been in positions C6 and C2. The absence of a second carbonyl peak might be due to the low DS at C2 position, confirmed by the low intensity of peak at 5.1 ppm, **Figure 3.1.5 c)**. Therefore, for the present study, derivative 6-O-(2-bromoisobutyryl) TMS-O-cellulose with high DS (DS = 0.8) will be treated as regioselectively substituted and the DS of 2-bromoisobutyryl in C2 position considered negligible. On the other hand, the spectrum of the non-regioselectively substituted derivative (**Figure 3.1.6 d)**) exhibited three carbonyl peaks at 170.8, 170.2 and 169.4 ppm, confirming the isobutyrylation at positions C6, C3 and C2 of the AGU. As expected peak 9, which corresponds to the methyl groups of 2-bromoisobutyryl, increased as the DS increased. Similarly, peak 10, from the methyl groups in the

TMS groups, decreased as the DS of 2-bromoisobutyryl increased. The degree of substitution of 2-bromoisobutyryl was determined by setting the integral value for C1 carbon of the AGU to 1.0 and compared against peak 7 (carbonyl group from the 2-bromoisobutyryl), see **Table 3.1.1**.

In the following section, the newly synthesized 6-O-(2-bromoisobutyryl) TMS-O-cellulose with different DS was used to produce honeycomb films and the different parameters studied in order to obtain good quality films.

### 3.1.2 Preparation of honeycomb films from 6-O-(2-bromoisobutyryl) TMS-O-cellulose derivatives with different DS

The experimental work done in this section was part of a preliminary study with the objective to prepare uniform honeycomb films with homogeneous distribution of pore sizes. Therefore, experimental parameters were varied, such as flow/humidity, concentration of the polymer solution and DS<sub>2-bromoisobutyryl</sub>, which are known to influence the formation of uniform honeycomb films. Ideally a statistically designed study to obtain the optimal experimental conditions for honeycomb formation would have been desired; however time and equipment limitations prevented this study from being executed. Nevertheless, this has been proposed as future work.

Regioselectively substituted 6-O-(2-bromoisobutyryl) TMS-O-cellulose with high, medium and low DS were solubilised in toluene, which was previously shown to be a very good solvent for honeycomb film formation from cellulose derivatives.<sup>4,319</sup> **Figure 3.1.7** is a cartoon describing the experimental set up for the film formation.

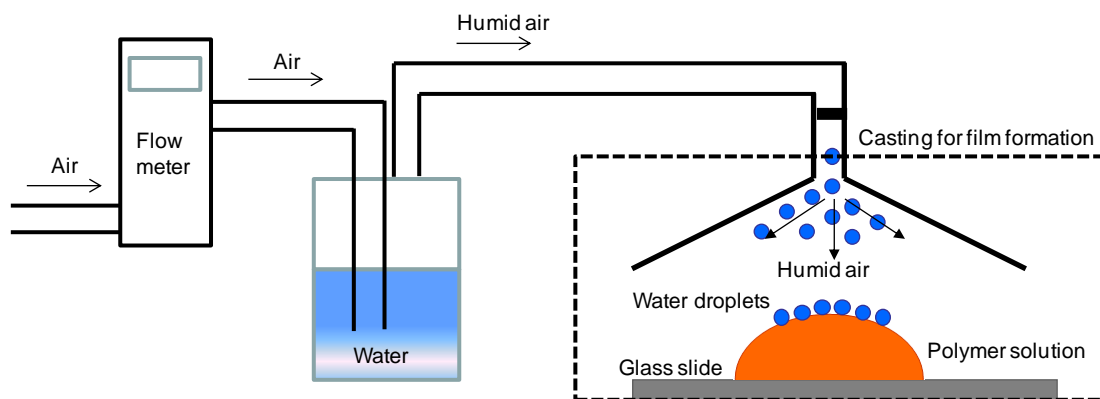


**Figure 3.1.7.** Experimental setup for formation of honeycomb films.

In short, a stream of air, with a known flow rate, was passed through water to produce a flow of humid air. The humidity was found to be directly proportional to the flow rate. Accordingly, a 10  $\mu$ L drop of polymer solution, with a specific concentration was cast on top of a glass slide and exposed to the humid airflow. As the solvent evaporated a film was produced; whether or not it was a honeycomb film was dependent on the conditions used. 6-O-(2-Bromoisobutyryl) TMS-O-cellulose solutions with different concentration and DS were tested under different flow rate/humidity conditions for the production of honeycomb films.

#### Flow rate/Humidity

In **Table 3.1.2**, 6-O-(2-bromoisobutyryl) TMS-O-cellulose derivatives with low (0.26) and medium (0.52) DS were used at a concentration of 2 mg/mL but different flow rates. As previously mentioned, increasing the flow rate causes an increase in the humidity. From previous work,<sup>306,310,314</sup> it was found that the higher the flow rates the smaller the pores, however in our case the accompanying increase in humidity resulted in an increase in the pore size. Therefore, in this particular experimental set up, flow rate and humidity have an opposite effect in the pore size. The chosen flow rates correspond to the minimum humidity required for honeycomb formation, about 50%,<sup>312</sup> and a medium and a high value, of 70 and 90% (**Table 3.1.2**, **Figure 3.1.8** and **Figure 3.1.9**)

**Table 3.1.2.** Experimental conditions used in the production of honeycomb films from 6-O-(2-bromoisobutyryl) TMS-O-cellulose with low and medium DS and different flow/humidity.

Expt #	DS	H(%)	C(mg/ml)	F(L/min)	Pore size
1	0.26	50	2	0.5	3.1 $\pm$ 1.0 $\mu$ m
2	0.26	88	2	0.9	2.4 $\pm$ 0.4 $\mu$ m
3	0.52	69	2	0.7	3.3 $\pm$ 0.2 $\mu$ m
4	0.52	90	2	0.9	2.5 $\pm$ 0.5 $\mu$ m

Note: The Expt #s correspond to the numbers in **Figure 3.1.8** and **Figure 3.1.9**. Pore size measurements, n = 11.

Honeycomb films formed from the low (0.26) DS derivative at 0.5 L/min were not uniform, and evidence of coalescence was observed at 1 K and 4 K magnification (**Figure 3.1.8**). The large pore size (3.1  $\pm$  1.0  $\mu$ m) observed was possibly due to the slower rate of solvent evaporation. Increasing the flow rate to 0.9 L/min narrowed and decreased the pore size distribution to 2.4  $\pm$  0.4  $\mu$ m. This behaviour might be related to the higher rate of solvent evaporation and not higher

humidity as no increase in pore size was observed. However, the pore shape was not as uniform as at the lower flow rate. In order to improve the quality of these films an intermediate flow rate of 0.7 L/min was tested. Unfortunately, the corresponding films showed a similar pattern to the ones prepared at the lower flow rate (0.5 L/min) when observed under the optical microscope (**APPENDIX-Selected optical micrograph**). As a result the SEM analysis was not performed on this sample.

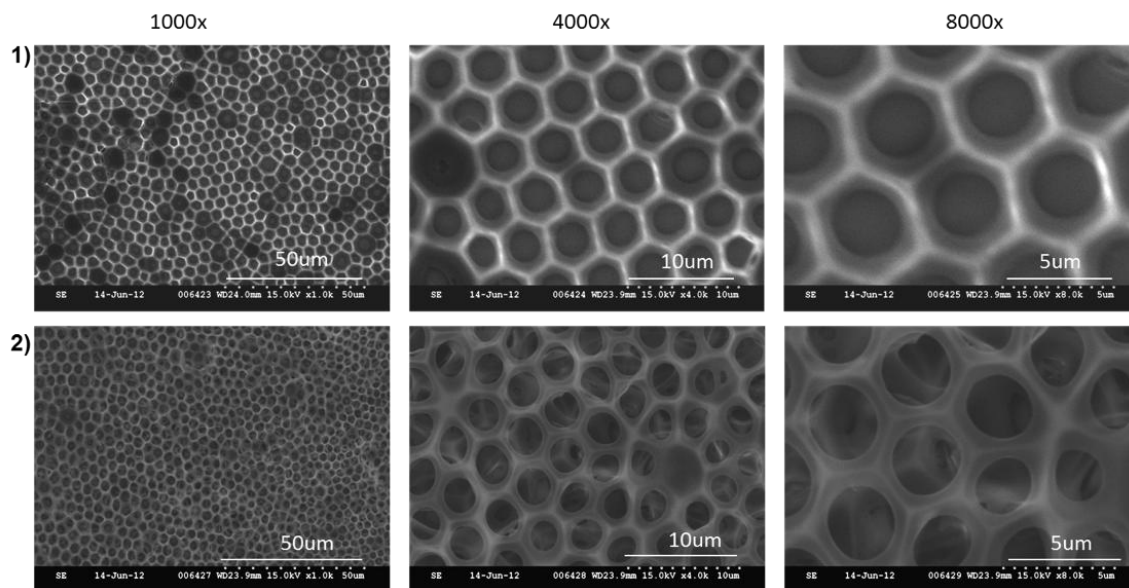


**Figure 3.1.8.** SEM images of honeycomb films from 6-O-(2-bromoisobutryl) TMS-O-cellulose with low (0.26) DS at different flow/humidity: 1) 0.5 L/min and 2) 0.9 L/min.

The effect of flow rate on honeycomb film formation using the medium (0.52) DS 6-O-(2-bromoisobutryl) TMS-O-cellulose derivatives was also studied (**Figure 3.1.9**).

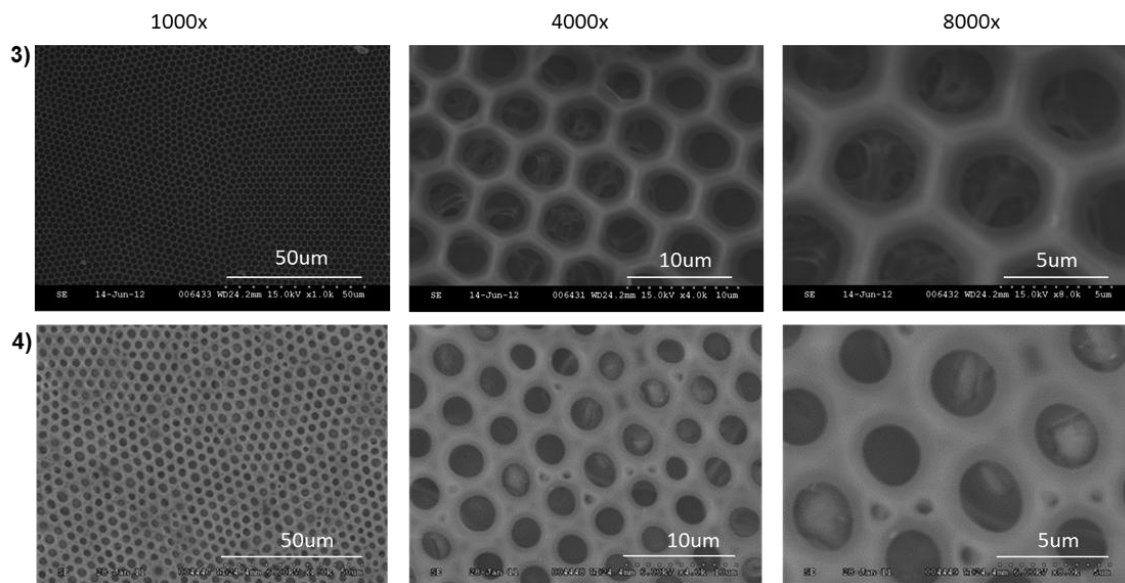


**Figure 3.1.9.** SEM images of honeycomb films from 6-O-(2-bromoisobutryl) TMS-O-cellulose with medium DS (0.52) at different flow/humidity; 3) 0.7 L/min; 4) 0.9 L/min.

Unlike those prepared using the low (0.26) DS derivative, the medium (0.52) DS 6-O-(2-bromoisobutryl) TMS-O-cellulose formed honeycomb films with higher uniformity. At a flow rate of 0.7 L/min films were formed with a pore size of  $3.3 \pm 0.2 \mu\text{m}$ . Increasing the flow rate to 0.9 L/min decreased the pore size to  $2.5 \pm 0.5 \mu\text{m}$ , but also increased the pore size distribution with small pores being formed on the walls of the larger pores.

### Concentration

Concentration is another parameter that allows the pore size to be controlled. Generally, the higher the concentration, the smaller the pores.<sup>314</sup> Stenzel observed a correlation between concentration ( $c$ ) and pore size ( $ps$ ) which is close to  $ps = k/c$ , where  $k$  is a constant dependent upon the material employed.<sup>312</sup> This has been observed in amphiphilic polymers or other polymers that tend to form aggregates in solution, such as star shaped PSt.<sup>312,327–329</sup> On the other hand, star polymers are not as sensitive to a variation in concentration.<sup>312,314,325,328</sup> Based on the aforementioned results a flow rate of 0.7 L/min was used and the concentration of the solutions was varied between 3-8 mg/mL; 2-5 mg/mL and 2-4 mg/mL for the low (0.26), medium (0.52) and high (0.8) DS derivatives, respectively (**Table 3.1.3**).



**Table 3.1.3.** Experimental conditions used in the production of honeycomb films from 6-O-(2-bromoisobutryl) TMS-O-cellulose with different DS and concentration.

Expt #	DS	H(%)	C(mg/mL)	F(L/min)	Pore size
5	0.24	68	3	0.7	3.4 ± 0.4 µm
6	0.24	68	4	0.7	3.6 ± 0.4 µm
7	0.24	68	8	0.7	N/A
8	0.5	69	2	0.7	3.3 ± 0.2 µm
9	0.5	69	3	0.7	3.9 ± 0.3 µm
10	0.5	69	4	0.7	4.3 ± 0.1 µm
11	0.5	67	5	0.7	1.7 ± 0.1 µm
12	0.8	69	2	0.7	1.1 ± 0.5 µm
13	0.8	68	3	0.7	1.8 ± 0.5 µm
14	0.8	68	4	0.7	1.2 ± 0.4 µm

Note: The Expt #s correspond to the numbers in Figure 3.1.10-Figure 3.1.12. Pore size measurements, n = 11.

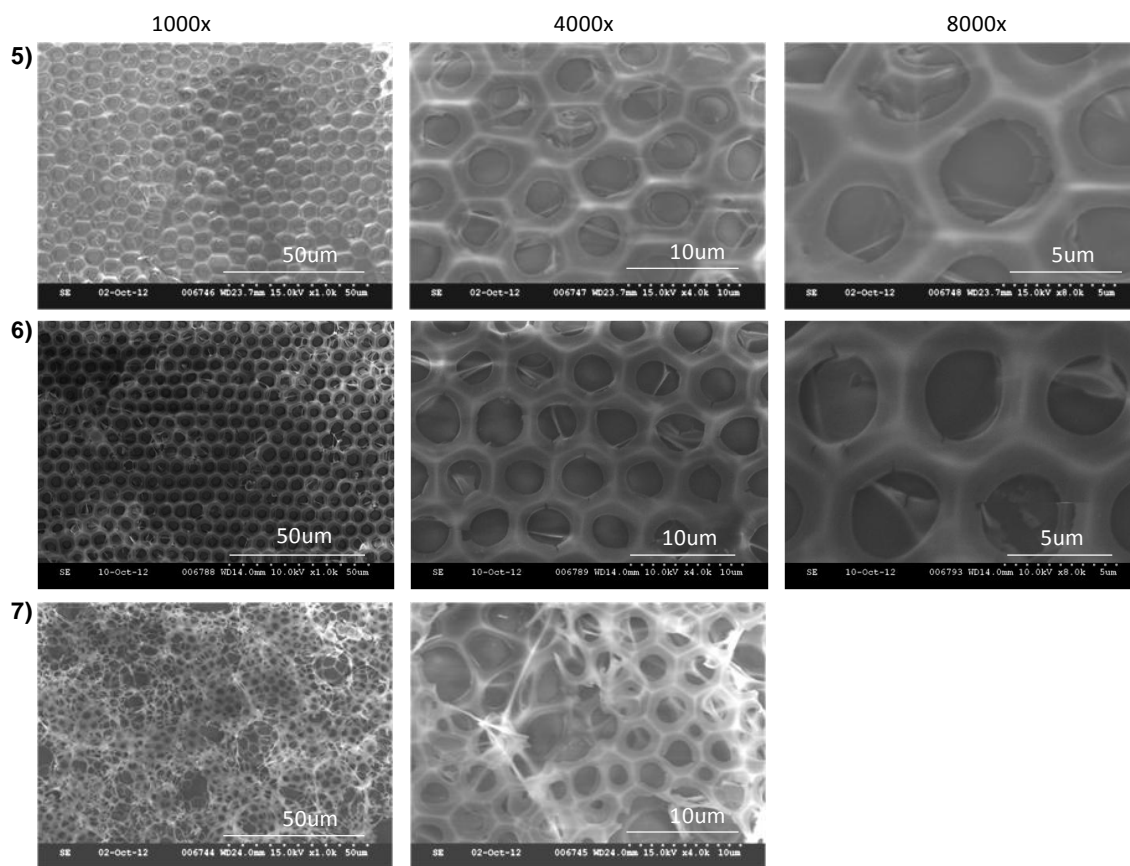


**Figure 3.1.10.** SEM images of honeycomb films from 6-O-(2-bromoisobutryl) TMS-O-cellulose with low (0.26) DS at different concentrations: 5) 3mg/mL; 6) 4 mg/mL and ;7) 8 mg/mL.

The concentration of solutions made from the cellulose derivative with low (0.26) DS was increased from 3 to 4 mg/mL and better film formation was observed. However, the pore size did not decrease, as expected. As a matter of fact, the pore size did not change significantly,  $3.4 \pm 0.4 \mu\text{m}$  and  $3.6 \pm 0.4 \mu\text{m}$ , respectively. The further increase in concentration from 4 to 8 mg/mL caused a substantial decrease in the quality of the films formed (**Figure 3.1.10 - 7**). These unexpected observations might be related to the low DS of the polymer and its interactions with the solvent used.

In **Figure 3.1.11** the effect of the concentration of the polymer solution on film formation was studied in C6 derivatives with medium (0.52) DS.

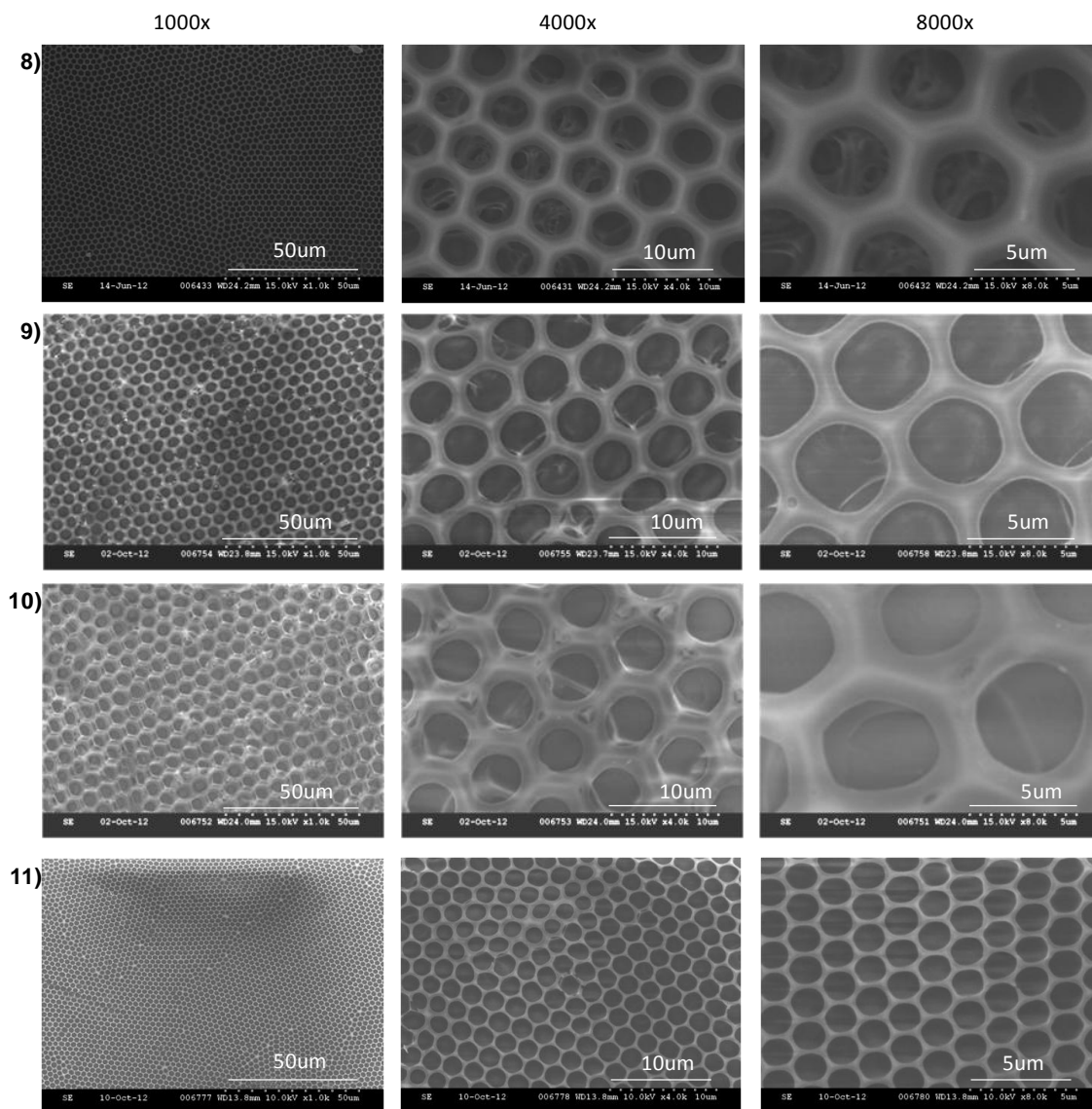


**Figure 3.1.11.** SEM images of honeycomb films from 6-O-(2-bromoisobutyryl) TMS-O-cellulose with medium (0.52) DS at different concentrations; 8) 2 mg/mL; 9) 3 mg/mL; 10) 4 mg/mL; 11) 5 mg/mL.

In general, the films exhibited a uniform pore distribution. Increasing the concentration from 2 to 4 mg/mL for the medium (0.52) DS derivative did not cause a decrease in pore size, as expected from Stenzel's equation<sup>312</sup>, and in fact the pore size increased from  $3.3 \pm 0.2 \mu\text{m}$  to

4.3±0.1  $\mu\text{m}$ . As previously mentioned, the concentration effect on the pore size was mainly verified in amphiphilic polymers or other polymers, such as star shaped PSt, which tend to aggregate in solution. This was not the case for the cellulose derivatives used in this study at 2-4 mg/mL. However, when increasing the concentration from 4 to 5 mg/mL (**Figure 3.1.11 - 11**) the pore size decreased dramatically (from 4.3  $\pm$  0.1  $\mu\text{m}$  to 1.7  $\pm$  0.1  $\mu\text{m}$ ). This might be indicative of polymer chain aggregation above a certain polymer concentration. As mentioned above, an increase in the concentration of polymer solutions that tend to form aggregates causes a decrease in the pore size. In order to confirm the occurrence of aggregation or not, a measurement of the size particles would be necessary. This could be done by dynamic light scattering but due to lack of time, it was not possible to do it. The formation of honeycomb films from 6-O-(2-bromoisobutyryl) TMS-O-cellulose with high (0.80) DS at different concentrations was also studied (**Figure 3.1.12**).

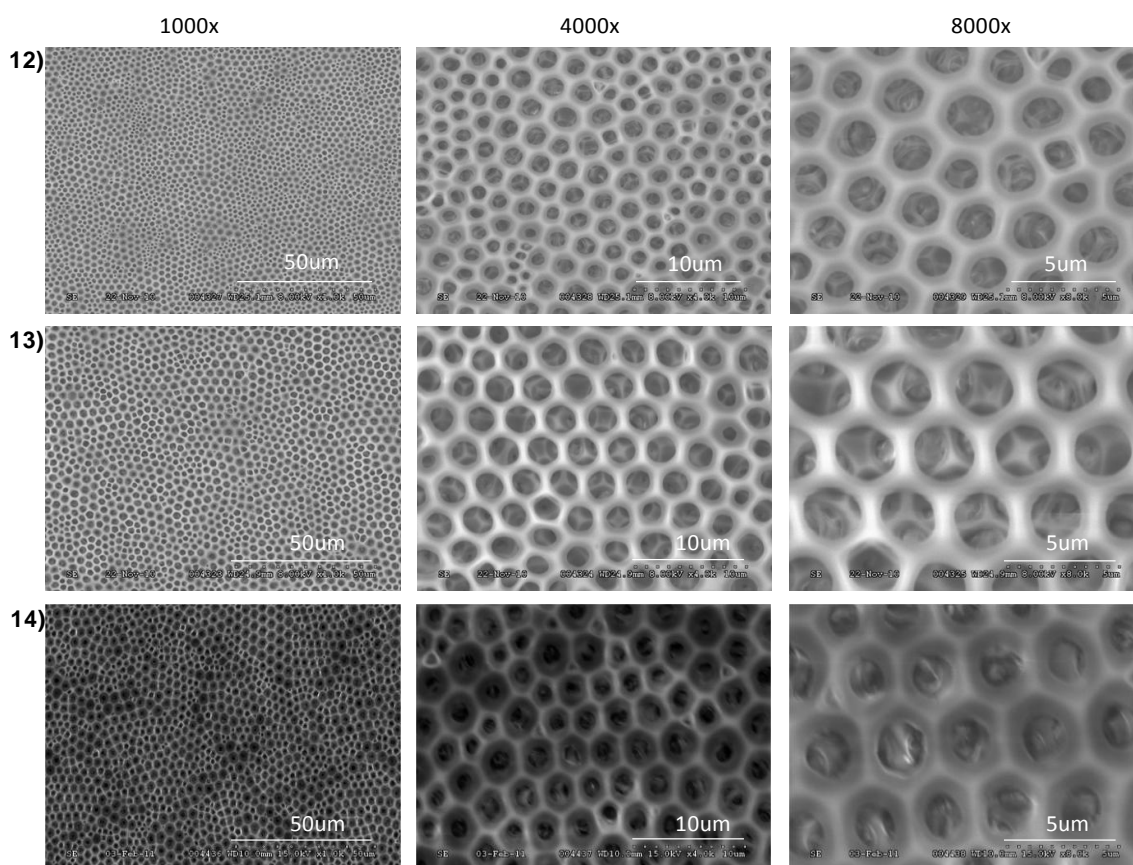


**Figure 3.1.12.** SEM images of honeycomb films from 6-O-(2-bromoisobutyryl) TMS-O-cellulose with high (0.80) DS at different concentrations. 12) 2 mg/mL; 13) 3 mg/mL; 14) 4 mg/mL.

The 6-O-(2-bromoisobutryl) TMS-O-cellulose with high (0.80) DS formed relatively uniform honeycomb films at a concentration of 2 mg/mL with an average pore size of  $1.1 \pm 0.5 \mu\text{m}$ . Increasing the concentration to 3 mg/mL caused a small increase in pore size from  $1.1 \pm 0.5 \mu\text{m}$  to  $1.8 \pm 0.5 \mu\text{m}$ . A further increase to 4 mg/mL caused a decrease in pore size to  $1.2 \pm 0.4 \mu\text{m}$  however; the uniformity of the honeycomb film was lost. Additionally, a multi-layered honeycomb film was clearly observed in the SEM images (**Figure 3.1.12**).

#### Degree of substitution

The DS of the 2-bromoisobutryl groups and its effect on honeycomb film formation was assessed. Regioselectively substituted 6-O-(2-bromoisobutryl) TMS-O-cellulose samples with DS of 0.26 (low), 0.52 (medium) and 0.8 (high) as well as a non-regioselectively substituted derivative with a DS of 2.2 were studied (**Table 3.1.4** and **Figure 3.1.13**).

**Table 3.1.4.** Experimental conditions used in the production of honeycomb films from 6-O-(2-bromoisobutryl) TMS-O-cellulose with different DS.

Expt #	DS	Solvent	H(%)	C(mg/ml)	F(L/min)	Pore size
5	0.26	Toluene	68	3	0.7	$3.4 \pm 0.4 \mu\text{m}$
9	0.52	Toluene	69	3	0.7	$3.9 \pm 0.3 \mu\text{m}$
13	0.8	Toluene	68	3	0.7	$1.8 \pm 0.5 \mu\text{m}$
15	2.2	$\text{CHCl}_3$ :Toluene <sup>(a)</sup>	70	3	0.7	$0.5 \pm 0.2 \mu\text{m}$

<sup>(a)</sup> Ratio = 2:1 ( $\text{CHCl}_3$ :Toluene)

**Note:** The Expt #s correspond to the numbers in Figure 3.1.13. Pore size measurements, n = 11.

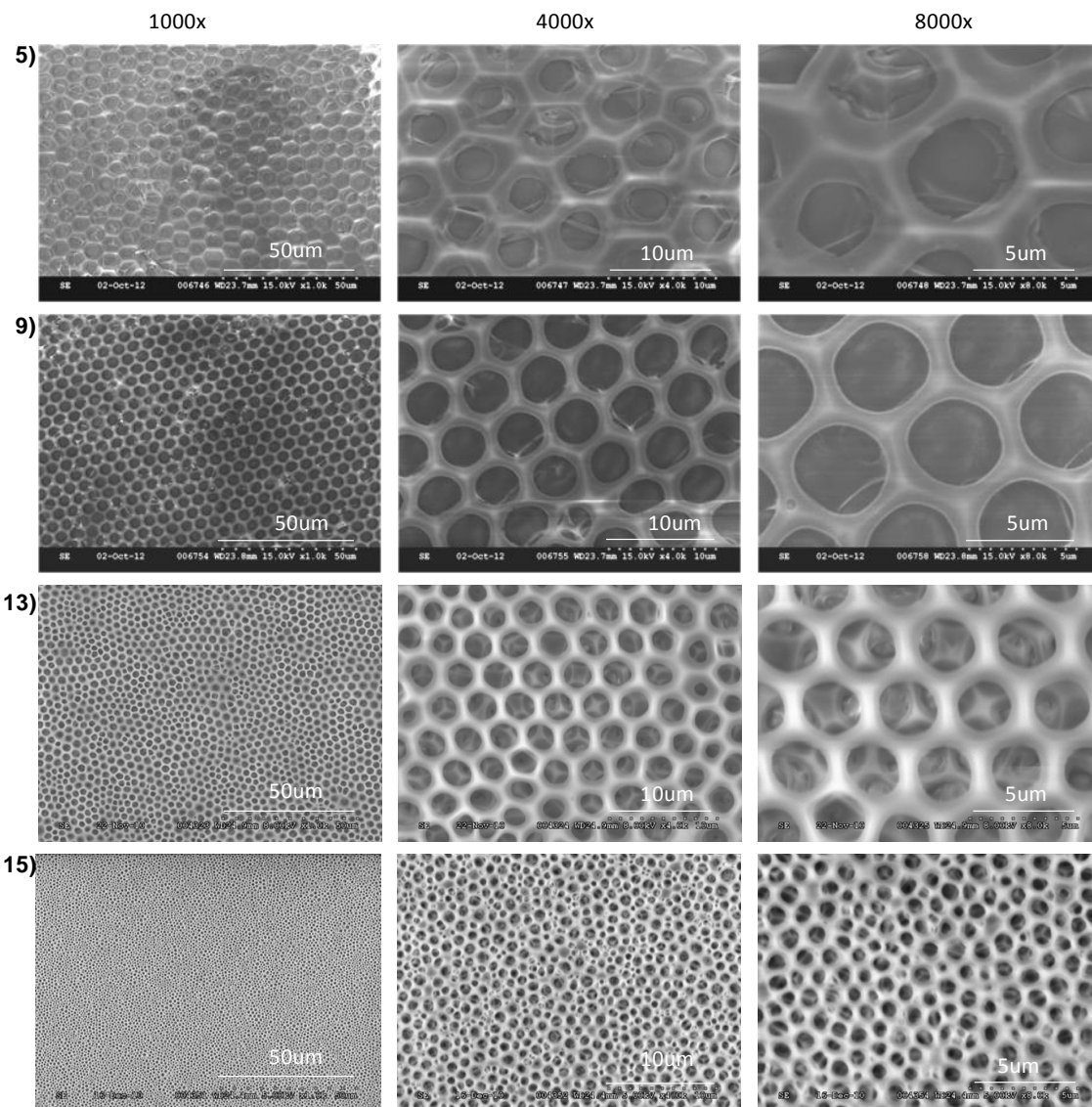


**Figure 3.1.13.** SEM images of honeycomb films from 6- O-(2-bromoisobutryl) TMS- O-cellulose with different DS at a concentration of 3mg/mL. 5) DS = 0.26; 9) DS = 0.52; 13) DS = 0.8; 15) DS=2.2.

The DS of the 2-bromoisobutryl moiety showed a significant influence on the pore size. A significant decrease in pore size from  $3.4 \pm 0.4 \mu\text{m}$  to  $1.8 \pm 0.5 \mu\text{m}$  was observed with an increase in DS from 0.26 to 0.8 (**Table 3.1.4**). At the higher DS of 2.2 the film obtained from the non-regioselectively substituted derivative showed a substantial decrease in pore size ( $0.5 \pm 0.2 \mu\text{m}$ ) and uniformity of the pores. This observation could be related to the insolubility of the latter in toluene; which required a mixture of  $\text{CHCl}_3$  and toluene (2:1) to be used. It is known that different solvent systems evaporate at different rates, influence the molecular shape adopted by a polymer in solution, and therefore affect the uniformity of film formation.<sup>329</sup> The addition of  $\text{CHCl}_3$

increased the vapor pressure of the solvent system and consequently the rate of evaporation, and ultimately to a rapid cooling of the surface of the polymer solution. As a result, the condensation of water vapor increases forming larger water droplets and an increase in pore size.<sup>329</sup> However, that was not observed, the pore size was the smallest obtained so far for these derivatives. Therefore, the lower pore size and lack of uniformity could be due to a combination of factors such as the significantly higher DS, the non-regioselective derivative and the molecular interactions between the cellulose derivative and the solvent system. Furthermore, the increased hydrophilic character of the non-regioselectively substituted cellulose derivative, due to the lower amount of TMS groups and higher amount of 2-bromoisobutyryl groups, might also contribute to the observed behaviour.<sup>318</sup>

### 3.1.3 Surface modification of honeycomb films made from regioselectively substituted cellulose derivative via surface initiated ATRP

Hernández-Guerrero et al.<sup>332</sup> modified the surface of honeycomb films made from PSt and polystyrene-*ran*-poly(hydroxyethyl methacrylate) (PSt-*ran*-PHEMA) by “grafting-from” PNIPAM through RAFT polymerization. To the best of our knowledge, surface modification of cellulosic honeycomb films through ATRP polymerization has not been done. In the present work, PNIPAM was “grafted-from” the surface of the honeycomb film made from 6-O-(2-bromoisobutyryl)-TMS-O-cellulose, with medium (0.52) DS (section 3.1.2) through surface initiated ATRP. The choice of this honeycomb film was based on the uniform pore size distribution and the lower density of initiator on the surface. A lower distribution of initiators on the surface would minimize potential interactions between growing chains, which could lead to termination. The polymerization was performed in aqueous media and Me<sub>6</sub>TREN/CuCl was used as a catalyst; experimental conditions were based on previous work<sup>230</sup> (**Table 3.1.5**).

**Table 3.1.5.** Experimental conditions used in surface initiated ATRP of NIPAM from the surface of honeycomb film.

NIPAM:Solvent	Solvent	Cu(I)Br mmol/mL	Cu(II)Br mmol/mL	Cu(0) mmol/mL	Me <sub>6</sub> TREN mmol/mL
1:100	H <sub>2</sub> O	2.5	3.7	1.5	8.7

Note: The final product was washed 3 times with distilled water and then dried in a vacuum oven overnight.

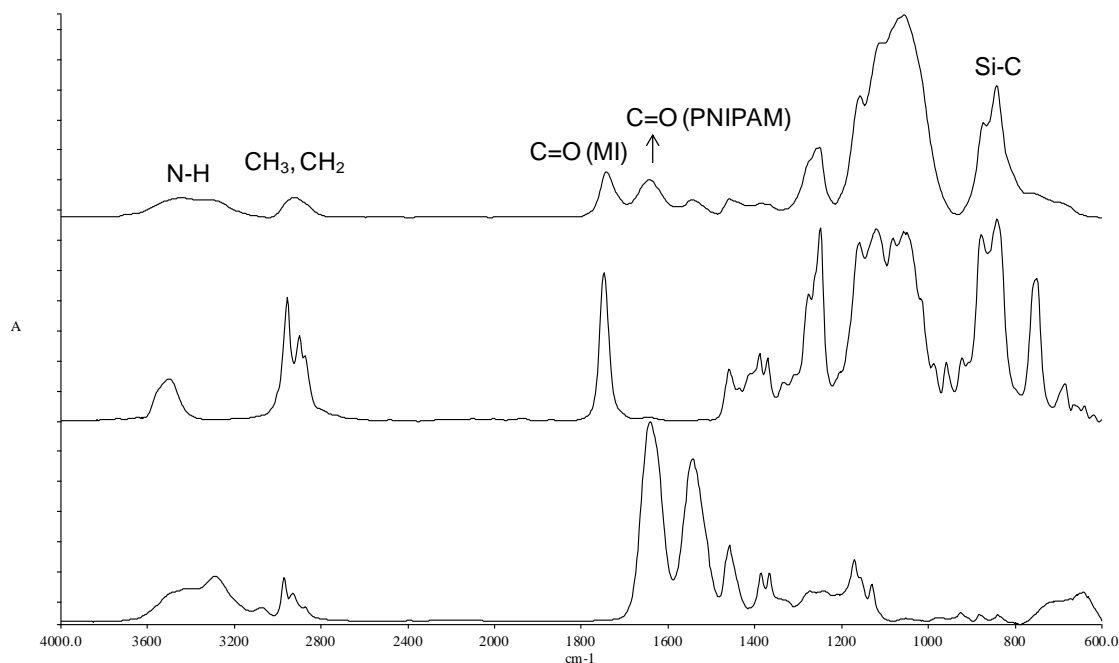


**Figure 3.1.14.** Comparison of ATR-FTIR spectra of PNIPAM (bottom), 6-O-(2-bromoisobutyryl) TMS-O-cellulose (middle) and honeycomb film from 6-O-(2-bromoisobutyryl)-TMS-O-cellulose medium DS (top) after surface initiated ATRP.

After surface initiated ATRP the film was extensively washed with water to remove any adsorbed homopolymer of PNIPAM from the surface. The successful grafting of PNIPAM from the surface of the honeycomb film was confirmed by ATR-FTIR (**Figure 3.1.14**). The film made from 6-O-(2-bromoisobutyryl)-TMS-O-cellulose (middle spectrum **Figure 3.1.14**) clearly shows the carbonyl stretching band ( $\nu_{\text{C=O}}$ ) at  $1734\text{ cm}^{-1}$  associated with isobutyryl moieties, and that of the TMS groups ( $\nu_{\text{Si-C}}$ ) at  $746\text{ cm}^{-1}$ . The corresponding spectrum after PNIPAM was grafted-from the honeycomb film surface and thoroughly washed, displayed the appearance of new peaks at  $3302\text{ cm}^{-1}$  ( $\nu_{\text{N-H}}$ ) and  $1644\text{ cm}^{-1}$  ( $\nu_{\text{C=O}}$ ) associated with the PNIPAM side-chain. This result confirms that the peaks detected from PNIPAM are grafted from the cellulose-based macroinitiator.

The effect of SI-ATRP of NIPAM on the honeycomb film surface was analyzed by optical microscopy (**Figure 3.1.15**) and AFM (**Figure 3.1.16**). From the optical micrographs, it is clear that the grafting of PNIPAM from the surface of the films did not dramatically affect the morphology of the pores. The two images appear virtually identical.



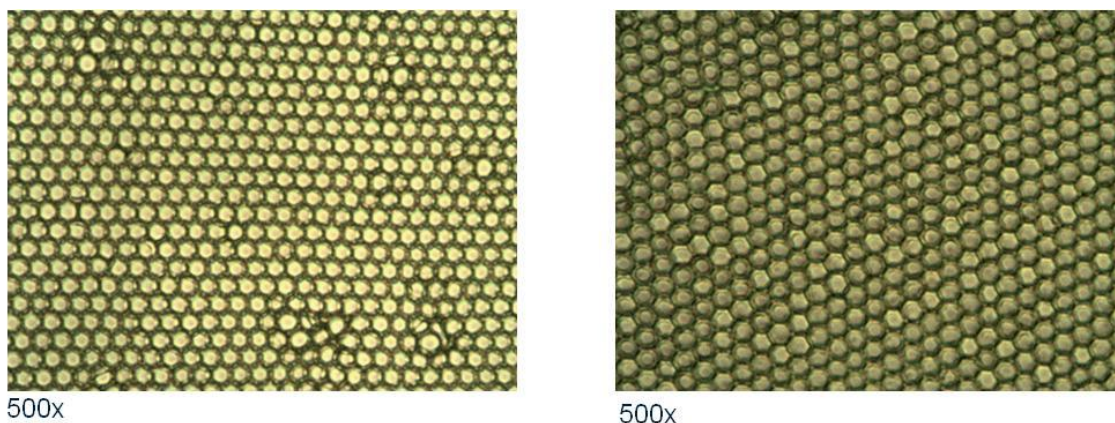


**Figure 3.1.15.** Optical micrographs of honeycomb films from 6-O-(2-bromoisobutryl) TMS-O-cellulose with medium DS before (left) and after (right) surface initiated ATRP.

AFM analysis of the films before and after ATRP appears to show some difference between the two 3D images (**Figure 3.1.16**). The surface of the films may have been modified, however, the width of the pores before ( $3.0 \pm 0.3 \mu\text{m}$ ) and after ( $2.9 \pm 0.3 \mu\text{m}$ ) ATRP did not change. Likewise, pore depth did not increase significantly (from  $2.2 \pm 0.1 \mu\text{m}$  to  $2.3 \pm 0.08 \mu\text{m}$ ).

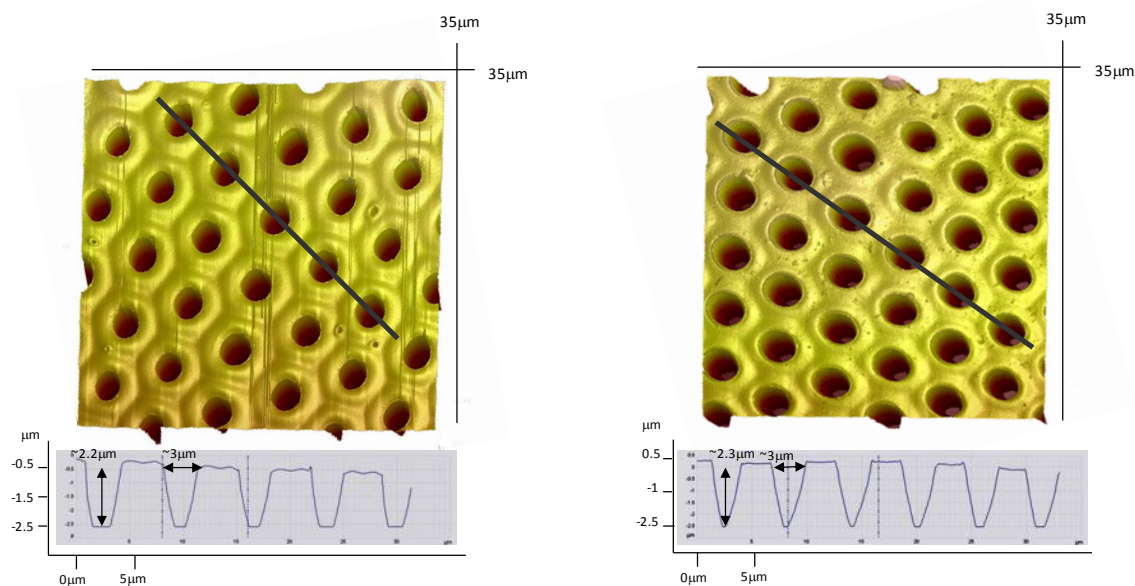


**Figure 3.1.16.** AFM 3D height images of the honeycomb film from 6-O-(2-bromoisobutryl) TMS-O-cellulose with medium DS before (left) and after (right) surface initiated ATRP. Pore depth and width measurements,  $n = 4$ .

The surface properties were further studied by AFM in peak force/quantitative nanomechanical mapping mode (QNM) to determine the elastic modulus of the honeycomb films before and after surface initiated ATRP (**Figure 3.1.17**).

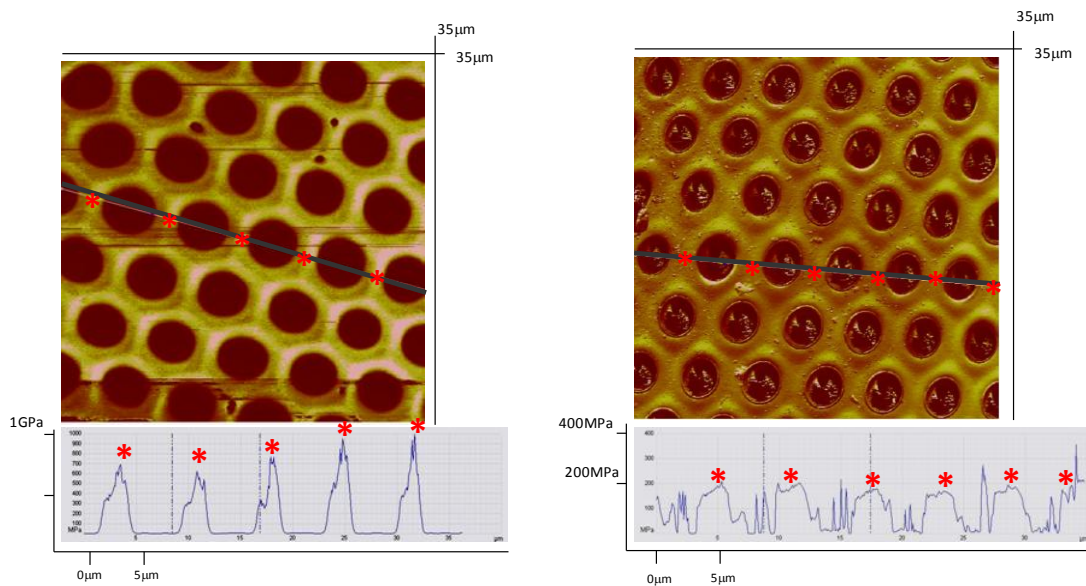


**Figure 3.1.17.** AFM 2D modulus images of the honeycomb film from 6-O-(2-bromoisobutryl) TMS-O-cellulose with medium DS before (left) and after (right) surface initiated ATRP. Modulus measurements,  $n = 5$ .

The elastic modulus of the honeycomb film surface before surface initiated ATRP was measured to be  $824 \pm 162$  MPa, but after ATRP the elastic modulus of the surface decreased dramatically to  $202 \pm 15$  MPa, **Figure 3.1.17**. This observation is consistent with the ATR-FTIR results and confirm the modification of the surface.

Further confirmation of the surface modification and grafting of PNIPAM via surface initiated ATRP can be seen from overlaying the 3D AFM elastic modulus image on top of the 3D height image (**Figure 3.1.18**). The overlaid images clearly showed the PNIPAM modification of the surface of the film, wherein the grafting occurred consistently across the surface between the pores and not preferentially in or around the edges of the pores. This is consistent with the distribution of the initiator evenly throughout the film and not around the pores, as observed for other amphiphilic copolymers<sup>316–318</sup>. Furthermore, the pore size distribution of the honeycomb films made from 6-O-(2-bromoisobutryl)-TMS-O-cellulose remained homogeneous after surface initiated ATRP.

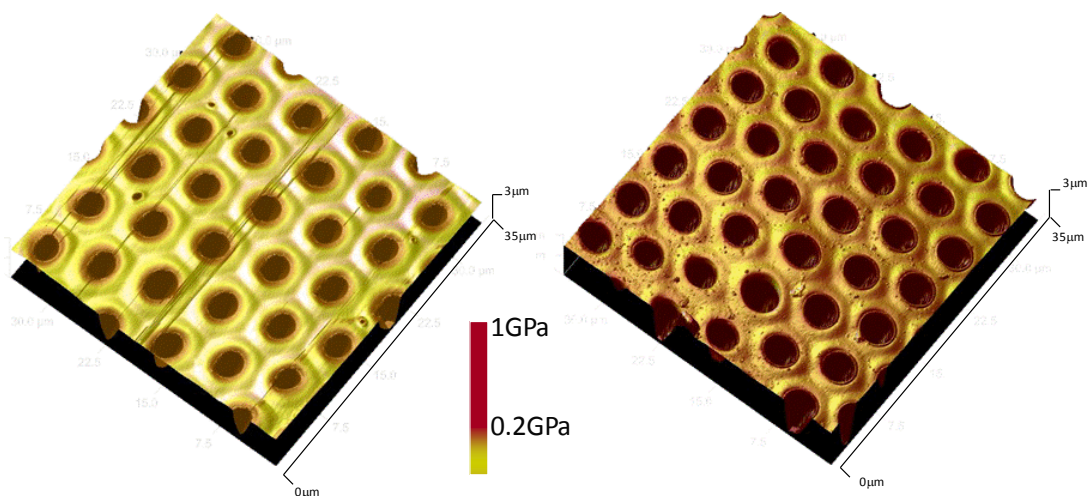


**Figure 3.1.18.** AFM 3D image of elastic modulus overlaid on top of height, before (left) and after (right) ATRP.

The surface modification was also assessed by contact angle measurements (**Figure 3.1.19**). In general, a surface with a contact angle above  $90^\circ$  is considered more hydrophobic and below  $90^\circ$  more hydrophilic.<sup>339</sup> The contact angle of the honeycomb surface changed dramatically from  $105 \pm 3^\circ$ , before surface initiated ATRP, to  $66 \pm 1^\circ$ , after PNIPAM modification. This implies that the surface became more hydrophilic, confirming the successful grafting of PNIPAM from the honeycomb film surface.

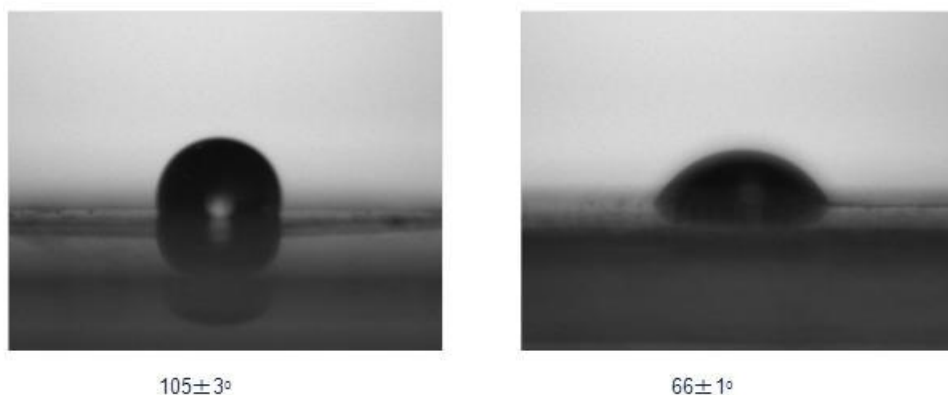


**Figure 3.1.19.** Contact angle analysis of honeycomb film surface from 6-O-(2-bromoisobutryl) TMS-O-cellulose with medium DS before (left) and after (right) surface initiated ATRP. Measurements were done in triplicate.

### 3.1.4 Conclusions

Regioselectively substituted 6-O-(2-bromoisobutryl) TMS-O-cellulose, an ATRP macroinitiator, was successfully synthesized with different DS, which was confirmed by FTIR,  $^1\text{H}$ - and  $^{13}\text{C}$ -NMR. This derivative was found to form honeycomb patterned films by the breadth-figures method. Film casting parameters such as air flow/humidity, polymer concentration and the DS of the 2-bromoisobutryl moiety influenced honeycomb film structure. Air flow/humidity affected pore size and uniformity. Three different air flow/humidity values were tested and  $0.7 \text{ L min}^{-1}$  / 70% RH was found to be the best. The effect of concentration was found to vary depending on the DS of the 2-bromoisobutryl moieties in the cellulose derivative. For example, the low (0.24) DS derivative did not appear to change in pore size at concentrations of 3 or 4 mg/mL, but lost its ability to form good quality honeycomb films when the concentration was increased to 8 mg/mL. On the other hand, the honeycomb films made from the derivative with medium (0.5) DS had increased pore size ( $3.3 \pm 0.2 \mu\text{m}$  to  $4.3 \pm 0.1 \mu\text{m}$ ), when increasing the concentration from 2 to 4 mg/mL. Further increasing the polymer concentration to 5 mg/mL caused a dramatic decrease in pore size to  $1.7 \pm 0.1 \mu\text{m}$ . Finally, the high (0.8) DS macroinitiator required much lower concentrations and produced the smallest pore diameter films. Increasing the concentration from 2 to 3 mg/mL caused a small increment in pore size ( $1.1 \pm 0.5 \mu\text{m}$  to  $1.8 \pm 0.5 \mu\text{m}$ ). On the other hand, a further increase in concentration to 4 mg/mL decreased the pore size to  $1.2 \pm 0.4 \mu\text{m}$ , resulting in a loss of the honeycomb film uniformity. Increasing the DS to 2.2 (non-regioselectively substituted derivative) decreased the pore-diameter to  $0.5 \pm 0.2 \mu\text{m}$ , however; the honeycomb pattern distribution was not uniform. This could be due to the significantly higher DS, the non-regioselectivity of the cellulose derivative and/or to the fact that a different solvent system ( $\text{CHCl}_3$ :toluene (2:1)), needed to be used because of solubility issues. The solvent system affects the rate of evaporation, and hence film formation.<sup>329</sup>

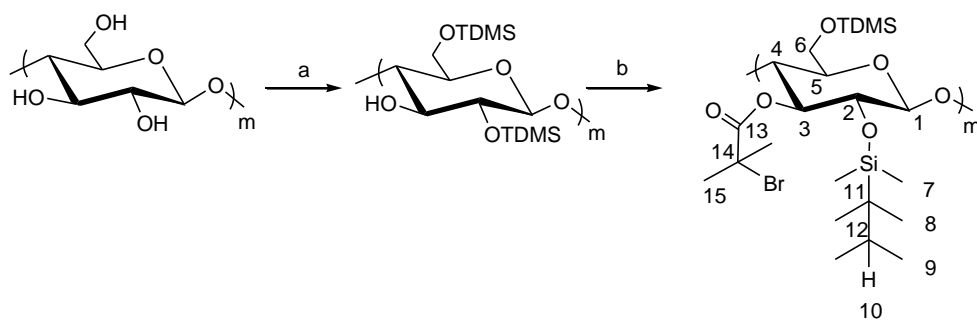
The surface modification of the honeycomb films was achieved by grafting the PNIPAM via surface initiated ATRP. The film was analyzed by ATR-FTIR, which confirmed successful grafting. Contact angle analysis indicated a change in the surface's properties from more hydrophobic to more hydrophilic, consistent with the grafting of PNIPAM. Optical and atomic force microscopy (AFM) confirmed that the honeycomb pattern was preserved after the surface modification. Although AFM height analysis revealed the pore size remained the same after grafting, AFM quantitative nanomechanical mapping (AFM/QNM) analysis showed that the elastic modulus of the surface was dramatically altered ( $824 \pm 162 \text{ MPa}$  to  $202 \pm 15 \text{ MPa}$ ). The AFM results also demonstrated that the initiators were distributed throughout the surface of the film and not exclusively around the pores as observed in amphiphilic copolymers.<sup>316,317</sup> Finally, the pore size distribution remained homogeneous after ATRP. Unfortunately, it was not possible to assess the

thermore sponsiveness of the PNIPAM modified films in the present study due to the absence of adequate instrumentation.

### 3.2 Synthesis of 3-O-(2-Bromoisobutyryl)-2,6-O-TDMS-cellulose and 2,3-O-(2-Bromoisobutyryl)-2,6-O-TDMS-cellulose for the Preparation of Thermoresponsive Honeycomb Patterned Films via ATRP

In the previous section it was demonstrated that 6-O-(2-bromoisobutyryl)-2,6-O-TDMS cellulose, an ATRP cellulose based macroinitiator, forms homogeneous honeycomb films. Herein, it is hypothesized that this ability might be related to the regioselective substitution of the cellulose derivative. Therefore, 3-O-(2-bromoisobutyryl)-2,6-O-TDMS cellulose (regioselectively substituted) and 2,3-O-(2-bromoisobutyryl)-2,6-O-TDMS cellulose (non-regioselectively substituted), also ATRP cellulose based macroinitiators, were synthesized and their aptitude to form homogeneous honeycomb films tested. The conditions used in this study were based on the results obtained from the preceding section. The final objective of the present section is to modify the surface of a homogeneous honeycomb film by “grafting-from” a thermoresponsive polymer (PNIPAM) through ATRP while maintaining the honeycomb pattern.

#### 3.2.1 Synthesis of 3-O-(2-bromoisobutyryl)-2,6-O-TDMS cellulose



**Scheme 3.2.1.** Synthetic scheme for the synthesis of 3-O-(2-bromoisobutyryl)-2,6-O-TDMS cellulose; a) DMA/LiCl, TDMS-Cl, imidazole b) anhydrous pyridine, 2-bromoisobutyryl bromide, THF.

In the present study, macroinitiator 3-O-(2-bromoisobutryl)-2,6-O-TDMS cellulose was prepared by reacting 2-bromoisobutryl bromide with 2,6-O-TDMS-cellulose in the presence of a base (imidazole) and THF (Scheme 3.2.1). The regioselective modification of cellulose was performed according to Koschella et al.<sup>2</sup> Cellulose was reacted with TDMS-Cl and imidazole in DMA/LiCl. The resulting 2,6-O-TDMS cellulose was analyzed by quantitative <sup>13</sup>C-NMR and is shown in **Figure 3.2.1**. The degree of substitution of the TDMS group was determined by setting the integral value for peak 1, C1 of the AGU, to 1.00. The corresponding TDMS carbon integrals at 7 (Si-CH<sub>3</sub>), 8 and 9 (C-CH<sub>3</sub>) were 4.07, 4.46 and 4.31, respectively and 2.02 and 2.12 for carbons 11 and 12, corresponding to a TDMS DS of ~ 2.1. It is acknowledged that the spectrum is rather noisy and signal intensity rather weak, but all efforts were made to analyze each spectrum in the same manner as to provide consistency and some level of accuracy

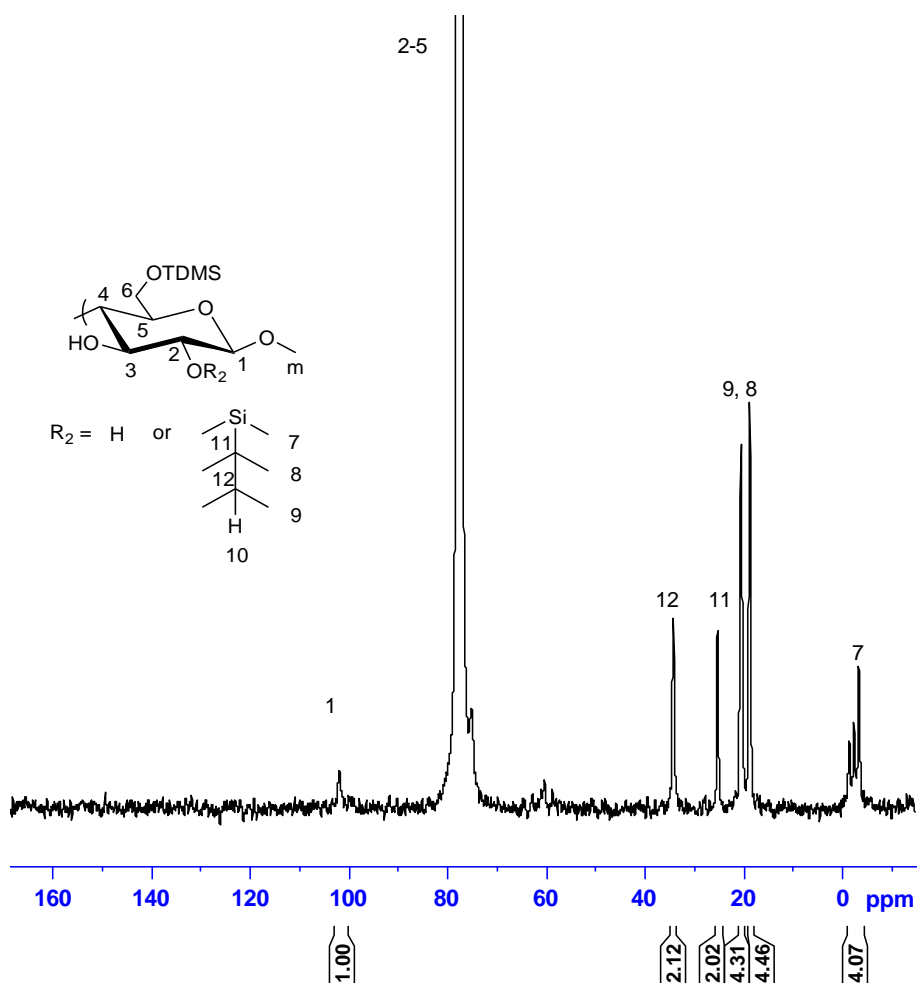


**Figure 3.2.1.** Quantitative <sup>13</sup>C-NMR of 2,6-O-TDMS cellulose with DS ~ 2.1.



As previously mentioned, the synthesis of 2,6-O-TDMS cellulose was based on well established experimental procedures found in the literature.<sup>2,91</sup> The effectiveness of this procedure has been extensively proven through 2D-NMR (COSY, HSQC and HMBC).<sup>2,87,90,92,340</sup> To assure that the precursor 2,6-O-TDMS cellulose with DS ~ 2.1, had been regioselectively substituted, the procedure described in the literature<sup>2</sup> was followed and the latter propionylated, based on procedure described elsewhere<sup>337</sup>. The <sup>1</sup>H- and <sup>13</sup>C-NMR of the propionylated precursor were compared against a propionylated non-regioselectively substituted 2,6-O-TDMS cellulose (**Figure 3.2.2** and **Figure 3.2.3**).

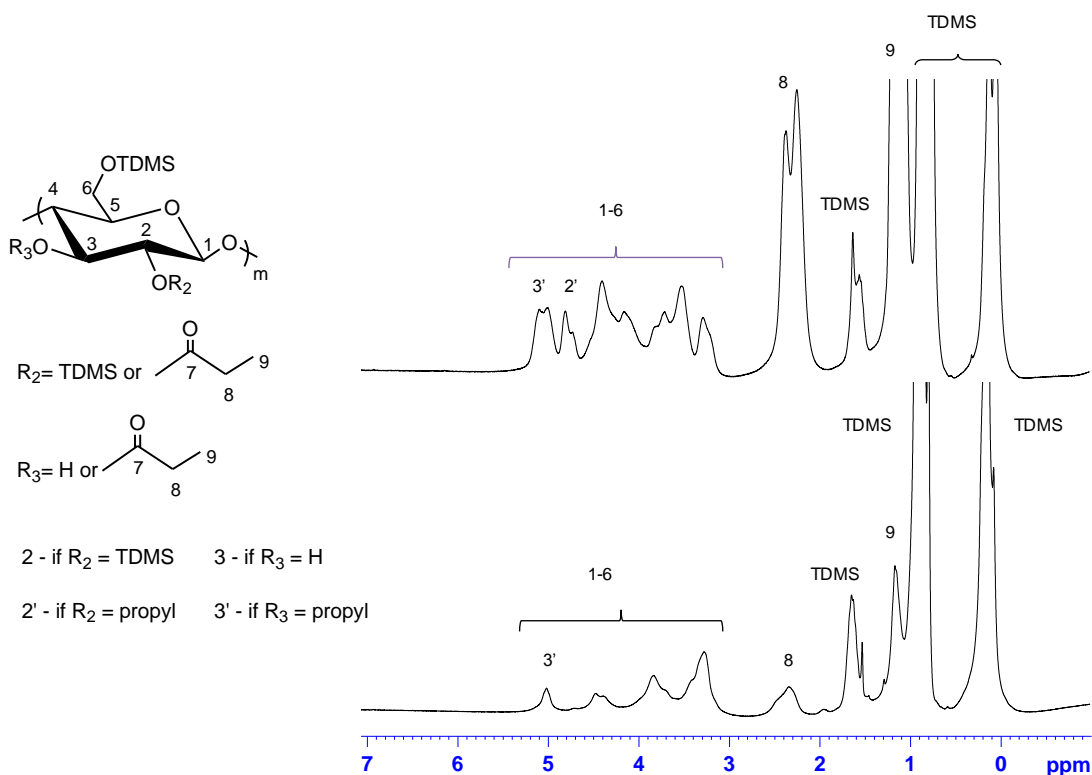


**Figure 3.2.2.** Comparison of <sup>1</sup>H-NMR of 3-O-propanoyl-2,6-O-TDMS cellulose (bottom) and 2,3-O-propanoyl-2,6-O-TDMS cellulose (top).

The <sup>1</sup>H-NMR spectrum of the propionylated non-regioselective 2,6-O-TDMS cellulose (**Figure 3.2.2**, top spectrum) shows clearly 2 peaks identified as 3' (5 ppm) and 2' (5.2 ppm) which correspond to protons in positions C3 and C2 when functionalized with 2-bromoisobutyrate, respectively. On the other hand, the spectrum of the propionylated regioselectively substituted precursor shows only one peak in the 5 ppm region confirming the exclusive functionalization with



2-bromoisobutyryl in position C3 (**Figure 3.2.2**, bottom spectrum). This observation was also confirmed by  $^{13}\text{C}$ -NMR (**Figure 3.2.3**).

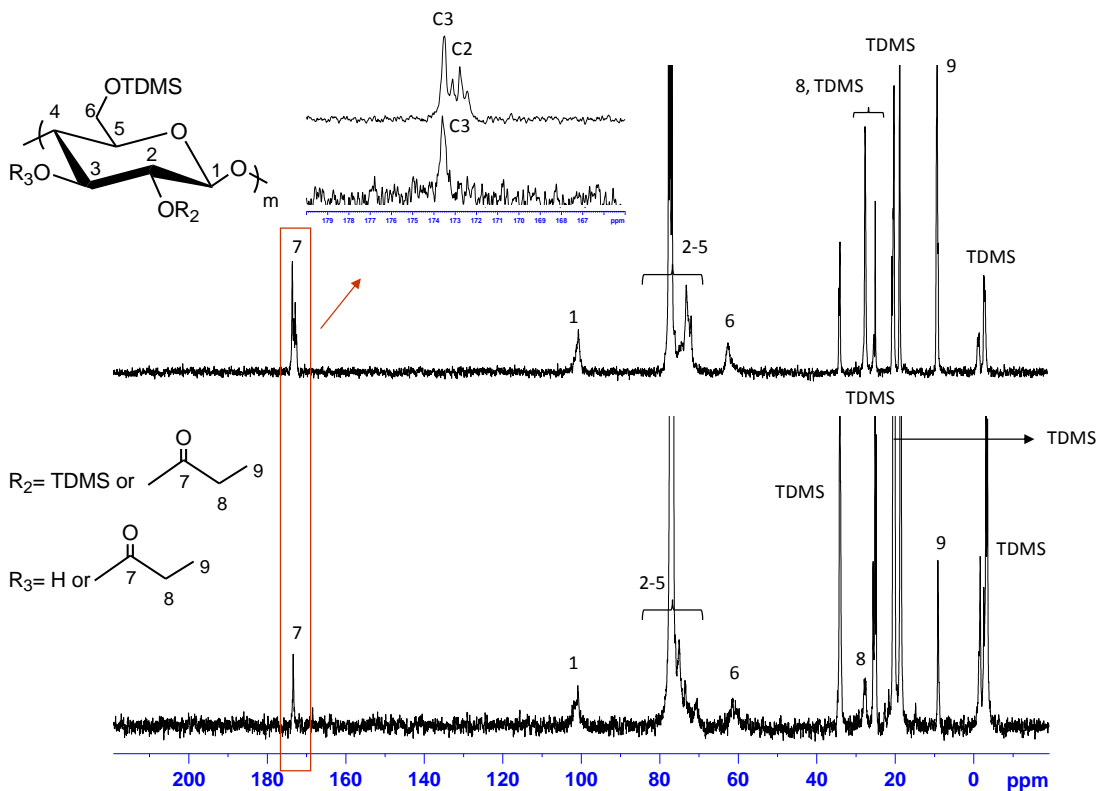


**Figure 3.2.3.** Comparison of  $^{13}\text{C}$ -NMR of 3-O-propanoyl-2,6-O-TDMS cellulose (bottom) and 2,3-O-propanoyl-2,6-O-TDMS cellulose (top).

The comparison of  $^{13}\text{C}$ -NMR spectra (**Figure 3.2.3**) confirms the regioselective substitution of 2,6-O-TDMS cellulose previously synthesized with a DS of  $\sim 2.1$  as it can be observed by the existence of one single carbonyl peak against 2 peaks from the  $\text{C}=\text{O}$  groups in positions C2 and C3 in 2,3-O-propanoyl-2,6-O-TDMS cellulose.

After confirming the regioselective substitution of the precursor the next step was to functionalize position C3 with 2-bromoisobutyryl group. Different reaction conditions were attempted in order to maximize the 2-bromoisobutyryl DS while minimizing the extent of degradation of the cellulose backbone. **Table 3.2.1** lists the different experimental conditions, which included the ratio of base and 2-bromoisobutyryl bromide, as well as temperature, time, and base. The  $M_n$  were determined by GPC-MALS, and used to monitor the degradation of the cellulose backbone. The refractive index increment ( $dn/dc$ ) was calculated for 3-O-(2-bromoisobutyryl) 2,6-O-TDMS cellulose and found to be  $0.083 \text{ mL/g}$ . The  $M_n$ , DS and  $dn/dc$

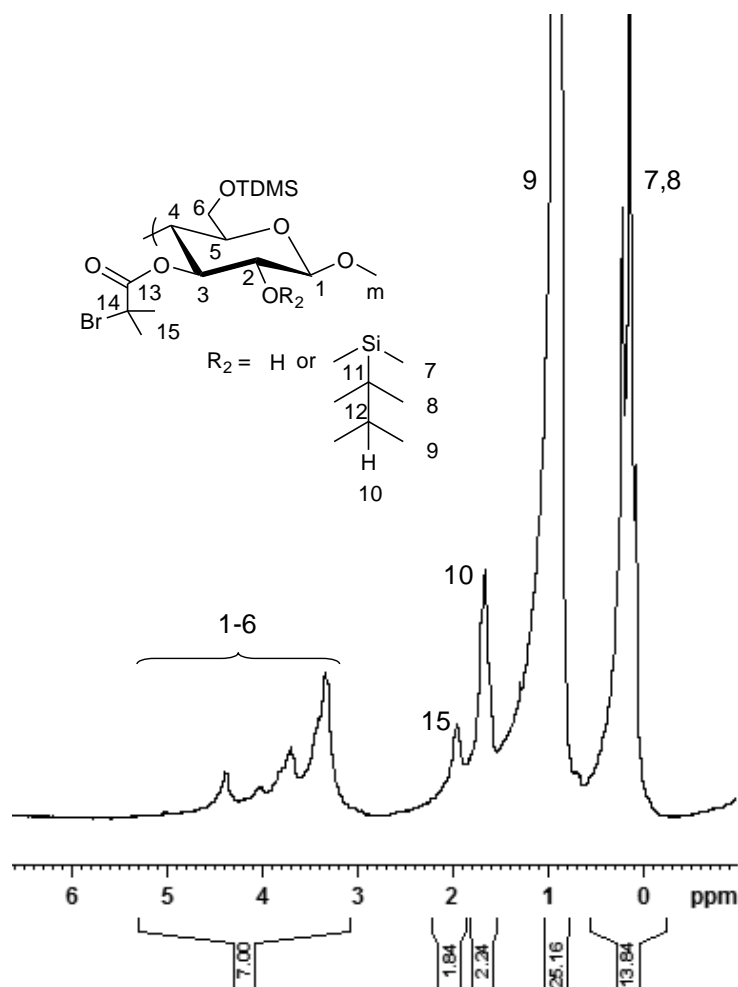
measurements were done in duplicate. The RPDs% (**Equation 3.1.1**) for the Mn and DS were no higher than 7% and the RPD% for dn/dc was 1%. A table with respective duplicate values and RPDs is presented in **APPENDIX-Duplicates and respective RPDs%**.

**Table 3.2.1.** Experimental conditions used in the synthesis of 3-O-(2-bromoisobutyryl) 2,6-O-TDMS cellulose.

T (°C)	Time (h)	Base	Ratio	DS	Mn (g/mol)	PDI	DP
2,6-O-TDMS cellulose					3.9*10 <sup>4</sup>	2.5	88
RT	19	Py	1:11:10:0	0.16	3.3*10 <sup>4</sup>	1.2	70
RT	19	Py	1:21:20:0	0.21	3.0*10 <sup>4</sup>	1.2	63
Refl	19	Pyr	1:11:10:0	0.22	2.6*10 <sup>4</sup>	1.3	55
RT	48	Py	1:11:10:0	0.28	3.0*10 <sup>4</sup>	1.3	61
RT	19	Im	1:11:10:0	<0.1	3.1*10 <sup>4</sup>	1.2	67
RT	19	NaH	1:10:10:0	<0.1	N/A	N/A	N/A
Refl	19	Pyr	1:20:20:0.05	0.26	N/A	N/A	N/A

RT = room temperature; Refl = Reflux; Py=anhydrous pyridine; Im=imidazole; Ratio= 2,6-O-TDMS-cellulose:base:2-bromoisobutyryl bromide: *N,N*-dimethyl-4-aminopyridine

The degree of 2-bromoisobutyryl substitution (DS) was calculated based on the <sup>1</sup>H-NMR spectrum by comparing the integral areas of the signals for the methyl protons of the isobutyryl group (~2.0 ppm) with the area of the AGU protons (3.0-5.5 ppm) calibrated to 7. **Figure 3.2.5** shows a representative <sup>1</sup>H NMR spectrum for a 3-O-(2-bromoisobutyryl)-2,6-O-TDMS cellulose macroinitiator. Despite varying the reaction parameters and conditions, the highest DS was found to be ~ 0.3, substantially lower than anticipated. The use of a stronger base such as NaH did not improve the DS which was lower than 0.1. *N,N*-dimethylaminopyridine, also a strong base, was used under extreme conditions: 1:20:20:0.05 (2,6-O-TDMS cellulose:2-bromoisobutyryl bromide: anhydrous pyridine:*N,N*-dimethyl-4-aminopyridine), reflux for 19 hours but no improvement was observed ( DS = 0.26).

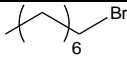
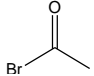
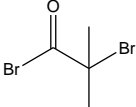
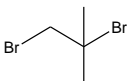


**Figure 3.2.4.**  $^1\text{H}$ -NMR spectrum of 3-O-(2-bromoisobutyryl)-2,6-O-TDMS cellulose.

The unexpectedly poor reactivity of the 2,6-O-TDMS cellulose may be a result of steric and electronic effects arising from the bulky hexyldimethylsilyl protecting groups, particularly that at position C2 of the AGU. The results obtained in this set of experiments (**Table 3.2.1**) were very similar to those presented in **Figure 3.2.4**. The reactivities of the AGU's hydroxyl groups in positions C2, C3 and C6 are influenced by pKa (10, 12, 14, respectively),<sup>37,38</sup> steric hindrance, electronic effects and experimental conditions. The primary OH in the C6 position is the most reactive due to its steric availability, followed by the C2 position and then the C3 position. It is believed that the steric hindrance and electronic interactions between the different species involved in the reaction play an important role in the DS at the C3 position.

In order to verify and try to understand why such low DS were obtained in the C3 position when 2,6-O-TDMS cellulose reacts with 2-bromoisobutyryl bromide, another set of experiments was performed using linear and branched alkyl halides as well as short chain and branched bromo esters (**Table 3.2.2**).

**Table 3.2.2.** Functional groups used to synthesize 3-O-2,6-O-TDMS cellulose derivatives.

Reagent	Ratio	Base	DS <sup>(a)</sup>
	1:10:10	NaH	~1
	1:10:10	Pyridine	0.3
	1:10:10	Pyridine	0.3
	1:10:10	NaH	< 0.1

<sup>(a)</sup> Determined by <sup>1</sup>H-NMR. Ratio - 2,6-O-TDMS cellulose:base:reagent. The pyridine used in this study was anhydrous

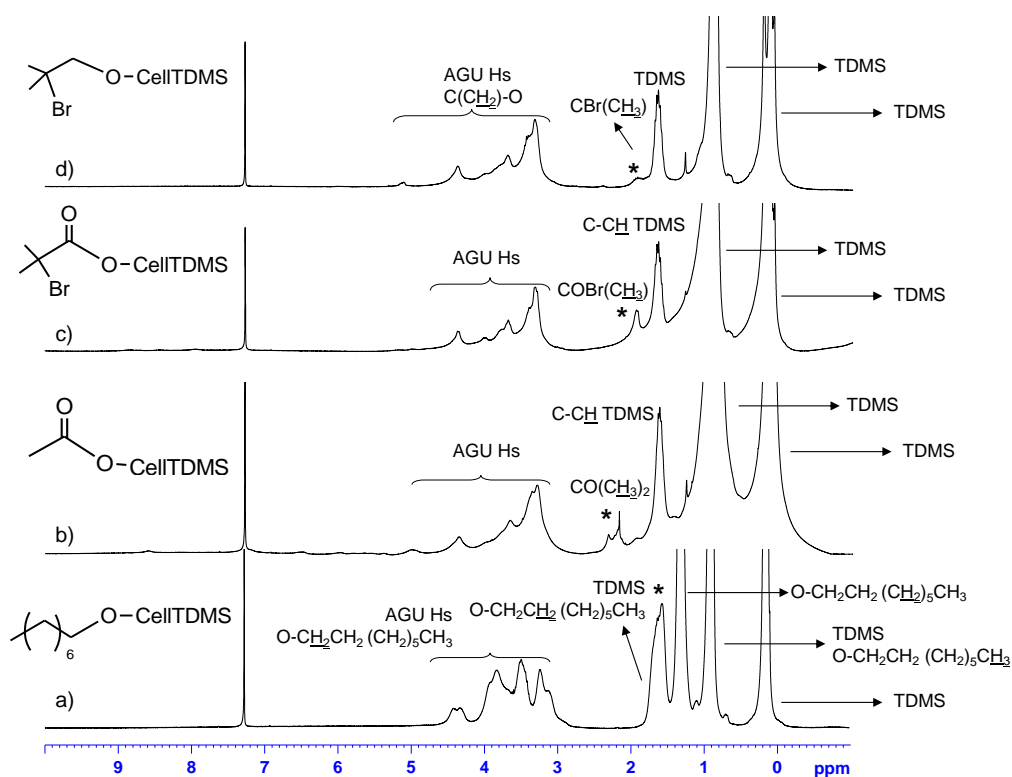


**Figure 3.2.5.** Comparison of <sup>1</sup>H-NMR spectra of a) 3-O-octyl-2,6-O-TDMS cellulose, b) 3-O-acetyl-2,6-O-TDMS cellulose, c) 3-O-(2-bromoisobutyryl)-2,6-O-TDMS cellulose and d) 3-O-(2-bromo-2-methylpropyl)-2,6-O-TDMS cellulose.

The DS (**Table 3.2.2**) of each compound was calculated by integrating specific peaks (marked with a \* in **Figure 3.2.5**) against the peak corresponding to the Si-(CH<sub>3</sub>), calibrated to 12 protons. The peak used to calculate the DS of 3-O-octyl-2,6-O-TDMS cellulose overlaps with the proton from the methine in TDMS which was taken into consideration. As one can see the linear ether, 3-O-octyl-2,6-O-TDMS cellulose, was successfully obtained with a high DS ~ 1. It was hypothesized that, in the presence of NaH, the functionalization of 2-bromooctane in position C3 of the AGU occurs preferentially via a S<sub>N</sub>2 mechanism.<sup>341</sup> RO<sup>-</sup>, a strong nucleophile, attacks the less sterically hindered sp<sup>3</sup> primary carbon centre of bromooctane, followed by the release of bromine as the leaving group to finally achieve a DS of ~ 1. When reacting 2,6-O-TDMS cellulose with acetyl bromide a DS of 0.3 was obtained. This substrate is not sterically hindered, but does have a C=O group with the ability to establish electronic interactions between the different species involved in the reaction which may lower its reactivity. Based on the latter, we would have expected to observe a further decrease in the DS of the branched ester, 2-bromoisobutyryl due to the added steric hindrance of this compound. However, the DS at the C3 position was the same (DS = 0.3). In this particular case, the larger angle established by the sp<sup>2</sup>-hybridized linkage (120°) might have minimized the effect of the bulkier 2-bromoisobutyryl group. On the other hand, the functionalization of the C3-OH with branched ether, 1,2-dibromo-2-methylpropane, in the presence of NaH produced 3-O-(2-bromo-2-methylpropyl)-2,6-O-TDMS cellulose with a very low DS (DS < 0.1). In this case, the occurrence of a nucleophilic substitution via a two step S<sub>N</sub>1 mechanism might have been favoured.<sup>341</sup> The first step comprises the formation of a tertiary carbocation, formed by the loss of leaving group bromine, and the second step the nucleophilic attack to the carbocation. Therefore, the effect of the steric hindrance caused by the bulkiness of 1,2-dibromo-2-methylpropane and the lower angle of the sp<sup>3</sup>-hybridized ether bond (109.5°) may not favour this reaction. Additionally, it was also hypothesized that the presence of a fully substituted C2 position in the cellulose backbone with a bulky TDMS group might have also contributed to the low DS. Therefore, we attempted to reduce the impact of the latter by decreasing the DS of the TDMS group at the C2 position (see section 3.2.2).

### 3.2.2 Synthesis of 2,3-O-(2-bromoisobutryl)-2,6-O-TDMS-cellulose

To synthesize 2,3-O-(2-bromoisobutryl) 2,6-O-TDMS cellulose we first had to decrease the DS at the C2 position of the 2,6-O-TDMS cellulose precursor. The experimental procedure followed that described in the synthesis of 2,6-O-TDMS cellulose (section 2.3.7) with some modifications: lower equivalents of TDMS-Cl (ratio of TDMS-Cl:imidazole:cellulose 2:3:1) and lower temperature, 90 °C.

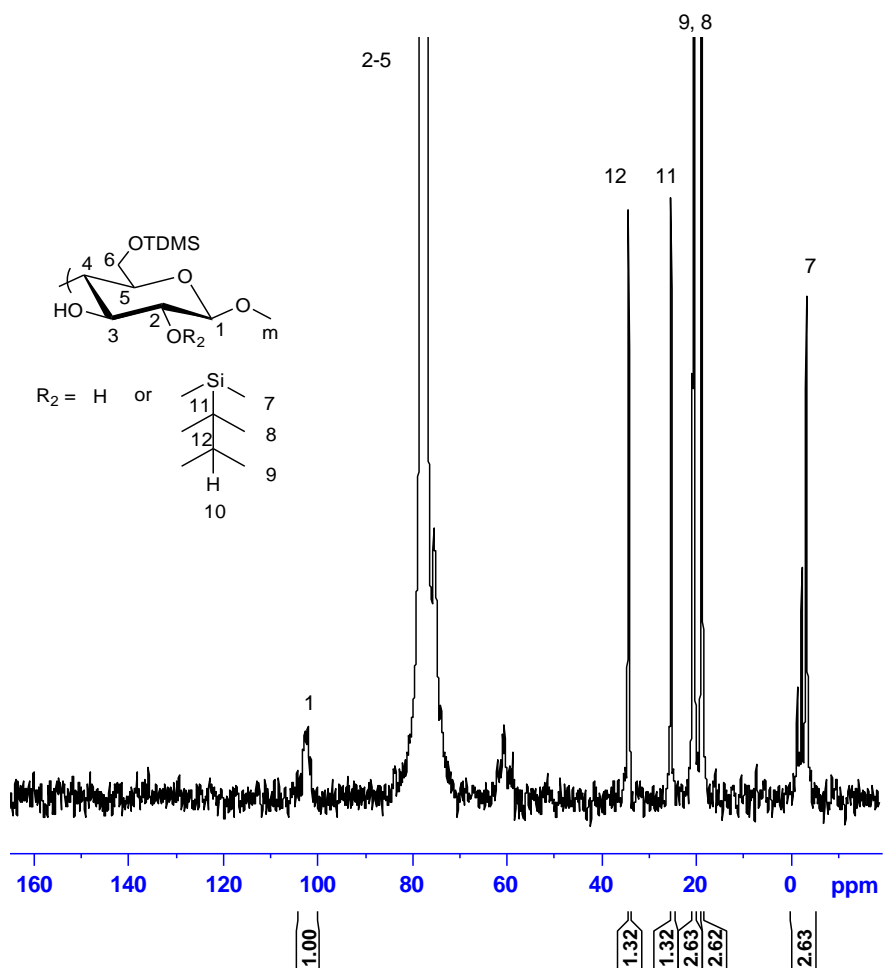


Figure 3.2.6. Quantitative  $^{13}\text{C}$ -NMR of 2,6-O-TDMS cellulose with DS = 1.3.

A 2,6-O-TDMS cellulose with lower DS was obtained and analyzed by quantitative  $^{13}\text{C}$ -NMR analysis (**Figure 3.2.6**). The DS of TDMS was determined by setting the integral value for peak 1 (C1 of the AGU) to 1.00. The corresponding TDMS carbon integrals at 7 ( $\text{Si}-\text{CH}_3$ ), 8 and 9 ( $\text{C}-\text{CH}_3$ ) were 2.63, 2.62 and 2.63, respectively and 1.32 for 11 and 12, corresponding to a TDMS DS of 1.3. It is acknowledged that the spectrum is rather noisy, but all efforts were made to analyze each spectrum in the same manner as to provide consistency and some level of accuracy. This lower DS 2,6-O-TDMS cellulose was then subjected to acylation by reacting with 2-bromoisobutyryl bromide as per that of the 3-O-(2-bromoisobutyryl)-2,6-O-TDMS cellulose (section 2.3.9).

Three different bases were investigated: pyridine, imidazole and triethylamine, and the effect on the DS of the 2-bromoisobutyryl moiety as well as polymer Mn are shown in **Table 3.2.3**. The DS and Mn were determined in duplicate and the respective RPDs% calculated as per **Equation 3.1.1**. A table with respective duplicate values and RPDs is presented in **APPENDIX-Duplicates and respective RPDs%**. The RPDs% found for the DS and Mn duplicates were no higher than 8%.

**Table 3.2.3.** Effect of base on the synthesis of 2,3-O-(2-bromoisobutyryl)-2,6-O-TDMS cellulose.

Exp#	Base	Ratio	DS	Mn(g/mol)	PDI	DP
2,6-O-TDMS-cellulose				$5.4 \times 10^4$	2.4	121
1	Pyridine	1:5:5	0.30	$4.6 \times 10^4$	2.4	94
2	Imidazole	1:5:5	0.10	$5.3 \times 10^4$	2.2	115
3	Triethylamine	1:5:5	0.13	$4.6 \times 10^4$	2.2	99
4	Pyridine	1:5:10	0.35	$5.3 \times 10^4$	1.9	115

Experimental conditions: room temperature (RT) for 19 hours; Ratio= 2,6-O-TDMS cellulose:base:2-bromoisobutyryl bromide. The pyridine used in this study was anhydrous.

Reactions run with anhydrous pyridine showed the highest 2-bromoisobutyryl DS (0.35), accompanied with a slight decrease in molecular mass. Imidazole and triethylamine produced products with very low DS of 2-bromoisobutyryl, 0.10 and 0.13, respectively. The molecular weight did not significantly decrease in the reaction with imidazole, whereas that in TEA caused a drop in molecular weight. Increasing the ratio of base:2-bromoisobutyryl bromide (Exp # 1 vs. 4) did not significantly improve DS (0.3 vs. 0.35), but slightly reduced cellulose degradation, as measured by Mn analysis.

**Table 3.2.4.** Effect of time and temperature on the synthesis of 2,3-*O*-(2-bromoisobutyryl) 2,6-*O*-TDMS cellulose.

Exp#	Temp (° C)	Time (h)	Ratio	DS	Mn (g/mol)	PDI	DP
4	RT	19	1:5:10	0.35	5.3*10 <sup>4</sup>	1.9	115
5	Reflux	6	1:5:10	0.43	3.1*10 <sup>4</sup>	2.2	61
6	Reflux	19	1:5:10	0.53	2.7*10 <sup>4</sup>	2.4	51
7	Reflux	48	1:5:10	0.83	2.1*10 <sup>4</sup>	3.4	37
8	Reflux	19	1:5:10	0.53	2.7*10 <sup>4</sup>	2.4	51

RT = room temperature; Ratio = 2,6-*O*-TDMS cellulose:base:2-bromoisobutyryl bromide).

Increasing the reaction temperature resulted in a substantial increase in DS, but a significant drop in Mn was observed (**Table 3.2.4**). Refluxing the reaction mixture for 48 hours produced a 2,3-*O*-(2-bromoisobutyryl) 2,6-*O*-TDMS cellulose with the highest DS (0.83), but also the lowest Mn. The decrease of the Mn at a higher temperature and longer reaction times was caused by the harsh conditions, which caused degradation of the cellulosic backbone. The GPC-MALS and DS analyses were done in duplicate and the different RPDs% were calculated (**Equation 3.1.1**) and found to be below 5%. A table with respective duplicate values and RPDs is presented in **APPENDIX-Duplicates and respective RPDs%**.

The impact of the various reaction parameters was further investigated by varying the equivalents of 2-bromoisobutyryl bromide to 2,6-*O*-TDMS cellulose from 1 to 20 equivalents (**Table 3.2.5**). The GPC-MALS and DS analyses were done in duplicate and the different RPDs% were calculated (**Equation 3.1.1**) and found to be below 8%. A table with respective duplicate values and RPDs is presented in **APPENDIX-Duplicates and respective RPDs%**.



**Table 3.2.5.** Effect of changing the mole equivalents of 2-bromoisobutyryl bromide and anhydrous pyridine in the synthesis of 2,3-O-(2-bromoisobutyryl) 2,6-O-TDMS cellulose.

Exp#	Base	Ratio	DS	Mn (g/mol)	PDI	DP
9	Pyridine	1:10:1	0.39	$5.4 \times 10^4$	2.6	107
10	Pyridine	1:10:5	0.35	$5.3 \times 10^4$	2.4	106
11	Pyridine	1:10:10	0.58	$5.1 \times 10^4$	2.6	96
12	Pyridine	1:10:20	0.67	$4.2 \times 10^4$	2.8	77
13	Pyridine	1:20:20	0.78	$3.7 \times 10^4$	2.1	66

Temperature – room temperature for 19 hours; Ratio = 2,6-O-TDMS cellulose:base:2-bromoisobutyryl bromide). The pyridine used in this study was anhydrous.

Increasing the molar equivalents increased the DS (Exps # 9 to 12). Exp # 12 showed the best results with regards to DS, however, again a decrease in Mn was observed. A further increase in DS was observed when the molar equivalents of anhydrous pyridine was increased to 20 molar equivalents relative to 2,6-O-TDMS cellulose (Exp #13). This resulted in a DS of 0.8 and a PDI of 2.1 with a further drop in Mn to  $3.7 \times 10^4$  g/mol. Once again, the harsh conditions used in this study (excess of base and 2-bromoisobutyryl bromide) might have been the cause for the decrease in Mn. Although the DS obtained using the 2,6-O-TDMS cellulose:base:2-bromoisobutyryl bromide of 1:20:20 increased the DS (~0.8), a significant number of hydroxyl groups were still unreacted (~0.9 based on a 2,6-O-TDMS cellulose with a DS of ~1.3). Therefore, the effect of sequential reaction cycles on the DS was evaluated, and the results obtained are presented in **Table 3.2.6**. The GPC-MALS and DS analyses were done in duplicate and the different RPDs% were calculated as per **Equation 3.1.1**, and found to be below 10%. A table with respective duplicate values and RPDs is presented in **APPENDIX-Duplicates and respective RPDs%**.

**Table 3.2.6.** Effect of 2<sup>nd</sup> reaction cycle in the synthesis of 2,3-O-(2-bromoisobutyryl) 2,6-O-TDMS cellulose.

Exp#	1 <sup>st</sup> cycle	2 <sup>nd</sup> cycle	DS	Mn (g/mol)	PDI	DP
14	19h,RT	19h,RT	0.84	$2.4 \times 10^4$	2.6	42
15	19h,RT	3h, reflux	0.82	$2.3 \times 10^4$	1.9	40

RT = room temperature; Ratios= 2,6-O-TDMS cellulose : base : 2-bromoisobutyryl bromide, 1:20:20).

The addition of a second reaction cycle, whether at room temperature (RT) or at reflux did not improve the DS, but dramatically decreased the Mn. Thus, the highest DS (~ 0.8) of 2,3-O-(2-bromoisobutyryl) 2,6-O-TDMS cellulose with a Mn of  $3.7 \times 10^4$  g/mol was obtained by reacting 2,6-O-TDMS cellulose with 2-bromoisobutyryl bromide for 19 hours in the presence of anhydrous pyridine, at room temperature with a 2,6-O-TDMS cellulose:anhydrous pyridine:2-bromoisobutyryl bromide ratio of 1:20:20 (**Table 3.2.6**).

As mentioned above, 50% of the available hydroxyl groups ( $DS_{\text{freeOH}} \sim 0.9$ ) were not derivatized, even under the most extreme conditions investigated; high temperature, base and time. In the 3-O-(2-bromoisobutyryl) 2,6-O-TDMS cellulose a maximum DS of 0.3 or 30% conversion was obtained. Therefore, the allocation of the 2-bromoisobutyryl groups at the C2 and C3 positions of the AGU were analyzed to see if there was an increase in DS at the C3 position by decreasing the DS of TDMS at the C2 position of the AGU. **Figure 3.2.7** shows the  $^1\text{H-NMR}$  of 2,3-O-(2-bromoisobutyryl) 2,6-O-TDMS cellulose.

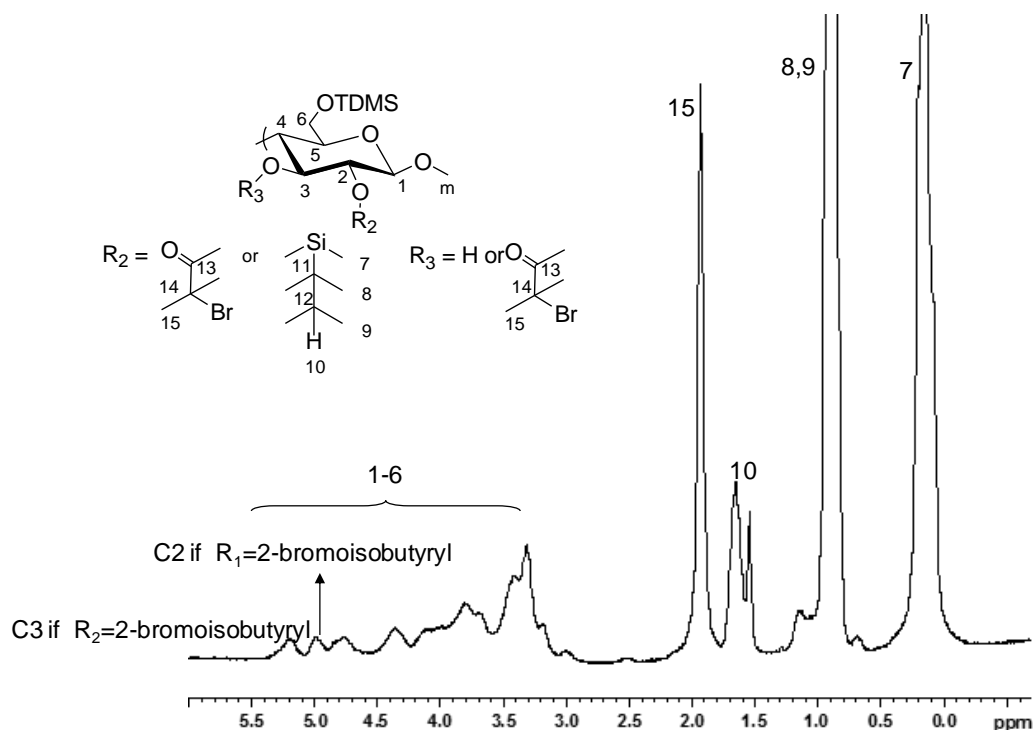


**Figure 3.2.7.**  $^1\text{H-NMR}$  spectrum of 2,3-O-(2-bromoisobutyryl)2,6-O-TDMS cellulose in  $\text{CDCl}_3$ .

In addition to the various signals associated with the 2,6-O-TDMS cellulose and the methyl protons from 2-bromoisobutyryl moiety, two new signals were detected at 5 and 5.2 ppm. Based

on work by Heinze et al.<sup>338</sup> and Iwata et al.<sup>95</sup> we have assigned these signals as the protons at C2 and C3 positions when respective C-OH is functionalized with 2-bromoisobutyryl groups.

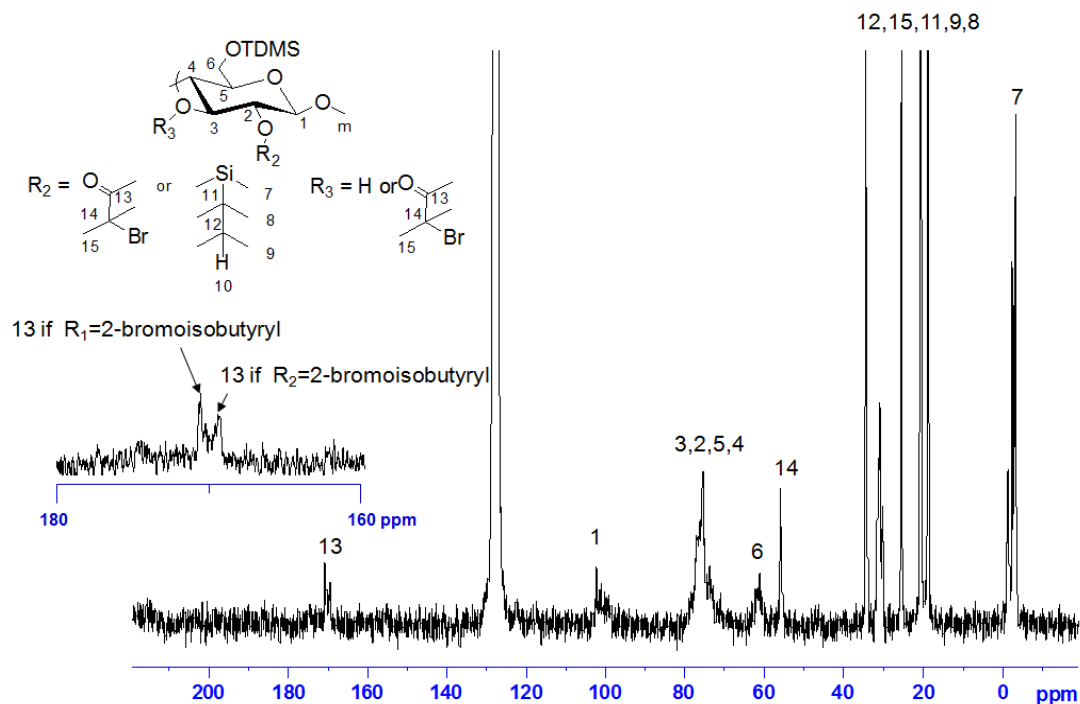


**Figure 3.2.8.** Quantitative  $^{13}\text{C}$ -NMR spectrum of 2,3-O-(2-bromoisobutyryl)2,6-O-TDMS-cellulose in benzene.

The quantitative  $^{13}\text{C}$ -NMR spectrum (**Figure 3.2.8**) clearly showed the two different carbonyl peaks associated with 2-bromoisobutyryl substitution at the C2 and C3 positions (peak 13). The DS of the 2-bromoisobutyryl at the C2 and C3 positions were calculated by calibrating the integral value of C1 to 1.0 against the integral value of the respective carbonyl peaks. It is acknowledged that the spectrum is rather noisy and signal intensity rather weak but all efforts were made to analyze each spectrum in the same manner as to provide consistency and some level of accuracy. The results obtained for C2 (0.5) and C3 (0.3) showed that an increase in DS was completely due to substitution at the C2 position. Thus steric and electronic effects arising from the C2 position are not responsible for the low DS attained at the C3 position.

### 3.2.3 Honeycomb Film Formation

Honeycomb films were prepared from 3-O-(2-bromoisobutyryl)-2,6-O-TDMS cellulose and 2,3-O-(2-bromoisobutyryl)-2,6-O-TDMS cellulose. It should be noted that both polymers have the same C3 DS  $\sim 0.3$ ; the 2,3-O-(2-bromoisobutyryl)-2,6-O-TDMS cellulose has a total 2-bromoisobutyryl DS  $\sim 0.8$  ( $DS_{C3} \sim 0.3$ ,  $DS_{C2} \sim 0.5$ ). As with the previously reported ethyleneglycol-modified 2,6-O-TDMS cellulose both 3-O-(2-bromoisobutyryl)-2,6-O-TDMS cellulose and 2,3-O-(2-bromoisobutyryl)-2,6-O-TDMS cellulose were soluble in toluene.<sup>4</sup>

**Figure 3.2.9** shows optical microscope images of the films obtained from 3-O-(2-bromoisobutyryl)-2,6-O-TDMS-cellulose and 2,3-O-(2-bromoisobutyryl)-2,6-O-TDMS cellulose using the conditions found for honeycomb film formation: 3 mg/mL in toluene, 75% humidity, air flow of 0.7 L/min. Unlike the 2,6-O-TDMS cellulose which did not form honeycomb patterned films,<sup>4</sup> both 3-O-(2-bromoisobutyryl)- and 2,3-O-(2-bromoisobutyryl)-2,6-O-TDMS cellulose did form patterned films. However, despite our best efforts, the regioselectively substituted 3-O-(2-bromoisobutyryl)-2,6-O-TDMS cellulose did not produce a uniform honeycomb like structure.

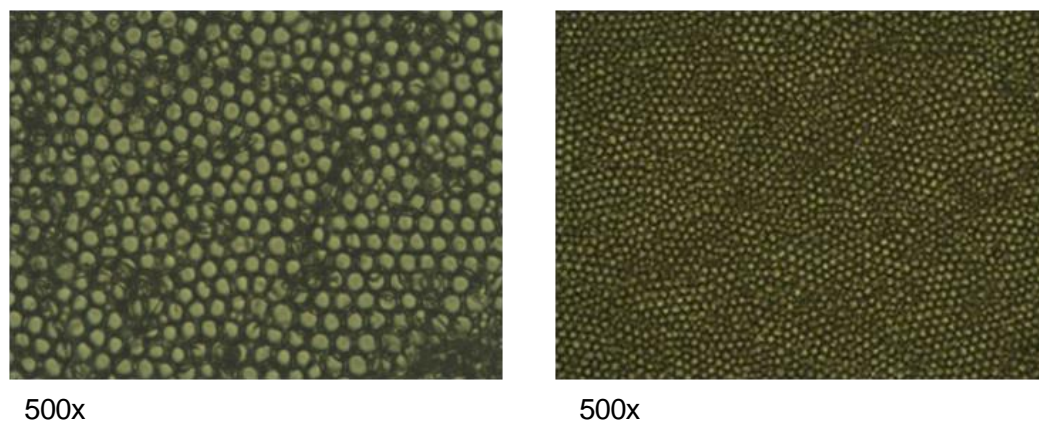


**Figure 3.2.9.** Optical microscope images of honeycomb films formed from 3-O-(2-bromoisobutyryl)-2,6-O-TDMS-cellulose (left) and 2,3-O-(2-bromoisobutyryl)-2,6-O-TDMS cellulose (right).

In 2,6-O-TDMS cellulose the hydroxyl group at the C3 position is available to interact through hydrogen bonding with the pyranose ring C5 oxygen, thereby affecting the rigidity and perhaps the ability to form the necessary spherical shape required for honeycomb film formation.<sup>342</sup> By substituting the C3 position these intramolecular interactions may be reduced and honeycomb-like structures thus produced. However, the limiting DS may preclude uniform film formation. By

contrast the 2,3-*O*-(2-bromoisobutyryl)-2,6-*O*-TDMS-cellulose formed more regular honeycomb-structured films. Perhaps changing the substitution pattern at the C2 from TDMS to 2-bromoisobutyryl further impacted the intra- and intermolecular interactions and thus molecular shape, resulting in better pattern formation.

**Figure 3.2.10** shows the SEM images of 2,3-*O*-(2-bromoisobutyryl)-2,6-*O*-TDMS-cellulose honeycomb films; the pores are approximately  $1.1 \pm 0.3 \mu\text{m}$  in diameter.

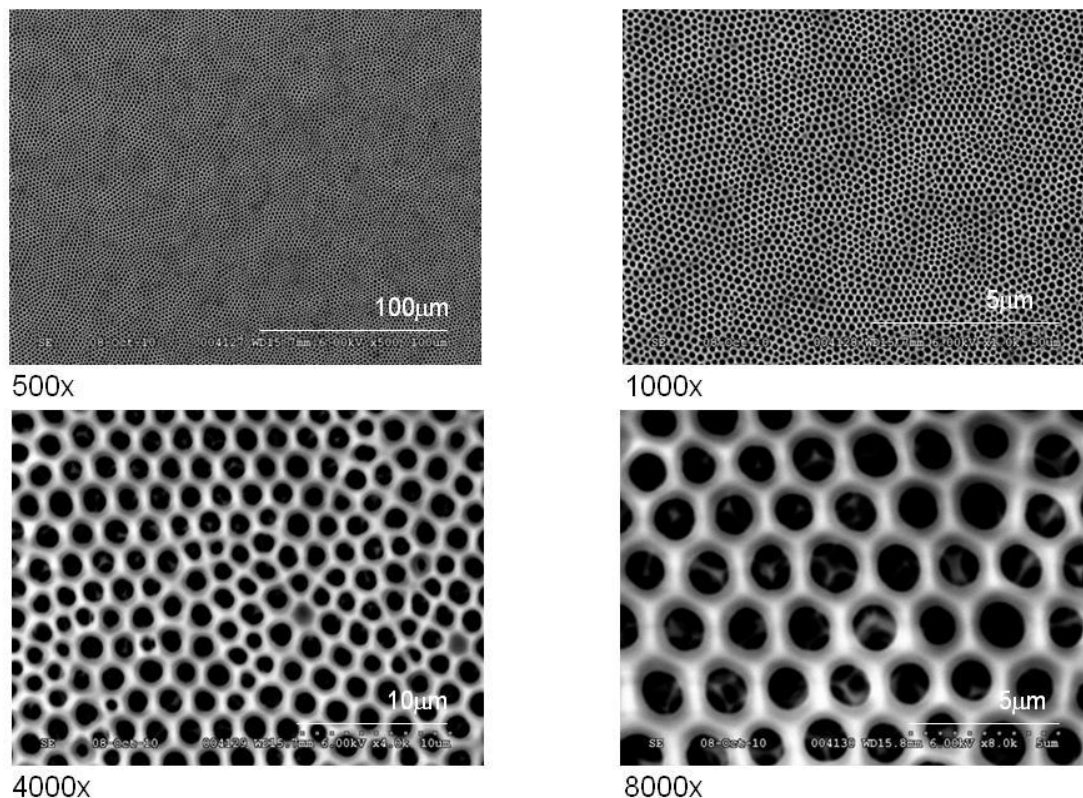


**Figure 3.2.10.** SEM images of the 2,3-*O*-(2-bromoisobutyryl)-2,6-*O*-TDMS-cellulose honeycomb films.

### 3.2.4 Surface initiated ATRP

The 2,3-O-(2-bromoisobutyryl)-2,6-O-TDMS-cellulose honeycomb patterned films were modified by surface initiated ATRP of NIPAM. The experimental conditions were based on previous work,<sup>230</sup> and are described in **Table 3.2.7**.

**Table 3.2.7.** Experimental conditions used in the surface initiated ATRP.

NIPAM/H <sub>2</sub> O	CuBr	CuBr <sub>2</sub>	Cu <sup>0</sup>	Me <sub>6</sub> TREN
1:10	2.5µmol/mL	3.7µmol/mL	1.5µmol/mL	8.7µmol/mL
0.1:10	2.5µmol/mL	3.7µmol/mL	1.5µmol/mL	8.7µmol/mL

**Figure 3.2.11** shows the SEM images of the 2,3-O-(2-bromoisobutyryl)-2,6-O-TDMS-cellulose honeycomb patterned films before and after surface initiated ATRP using 1 wt% and 10 wt% NIPAM/H<sub>2</sub>O solutions. At the higher monomer concentration (10 wt%), the grafted PNIPAM chains covered the honeycomb film surface, completely obscuring the honeycomb film pattern (**Figure 3.2.11 bottom-right**). On the other hand, after surface initiated ATRP with 1 wt% NIPAM:H<sub>2</sub>O (**Figure 3.2.11 top-right**) the honeycomb film was able to keep a porous pattern but the uniformity was lost. The pore size decreased from  $1.1 \pm 0.3 \mu\text{m}$ , before ATRP, to  $0.7 \pm 0.4 \mu\text{m}$  (after ATRP), see **Figure 3.2.11 left**.

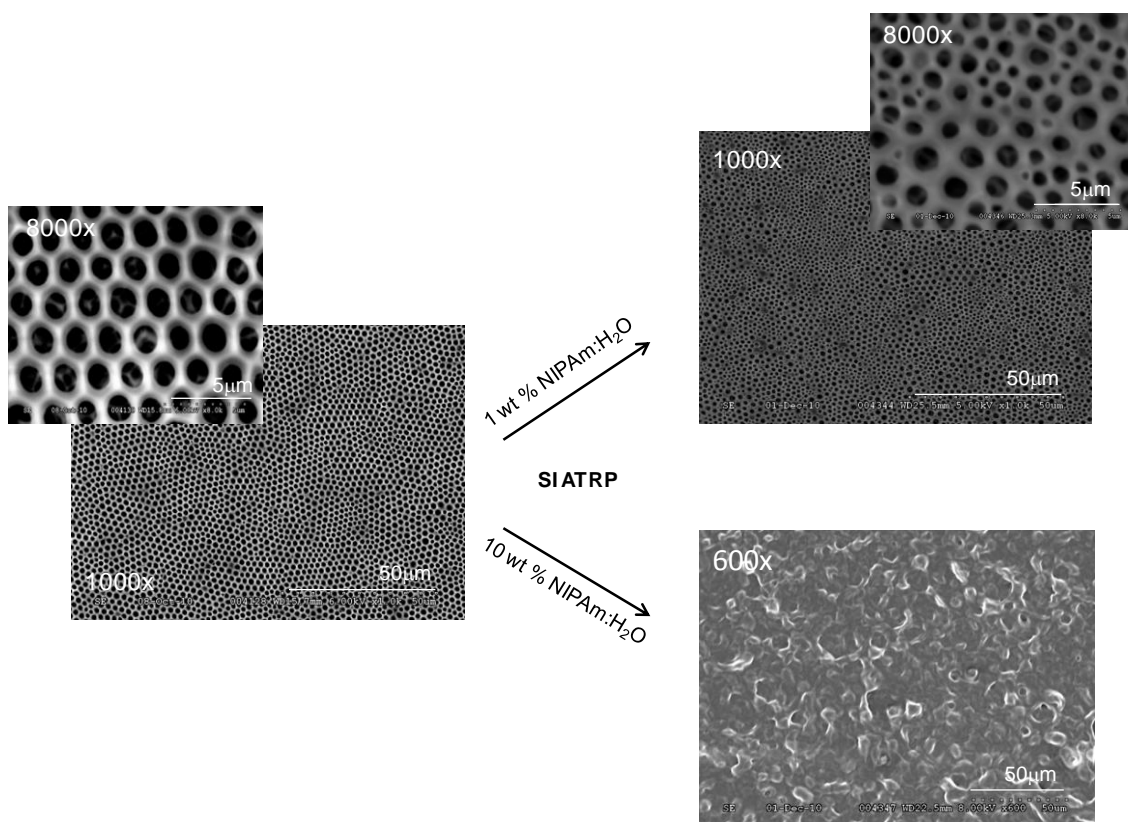


**Figure 3.2.11.** SEM images of honeycomb films from 2,3-O-(2-bromoisobutryl)-2,6-O-TDMS cellulose before (left) and after surface initiated ATRP (right) with 1 wt% (top) and 10 wt% (bottom) NIPAM/H<sub>2</sub>O solutions.

In addition to SEM analysis, the effect of PNIPAM on surface hydrophilicity was measured by contact angle (**Figure 3.2.12**). As expected, the originally hydrophobic 2,3-O-(2-bromoisobutryl)-2,6-O-TDMS-cellulose honeycomb surfaces became more hydrophilic after surface initiated ATRP with NIPAM, as the contact angle changed from  $100 \pm 4^\circ$  to  $73 \pm 4^\circ$ . Again, increasing the amount of PNIPAM on the surface dramatically changed the surface energy, resulting in a contact angle of  $55 \pm 2^\circ$ . Although the surface was successfully modified, the lack of uniformity in the pore size distribution might have a negative impact in the final properties of the honeycomb films and therefore should be improved. Further studies are necessary in order to understand this phenomenon and improve the uniformity of these films after ATRP.

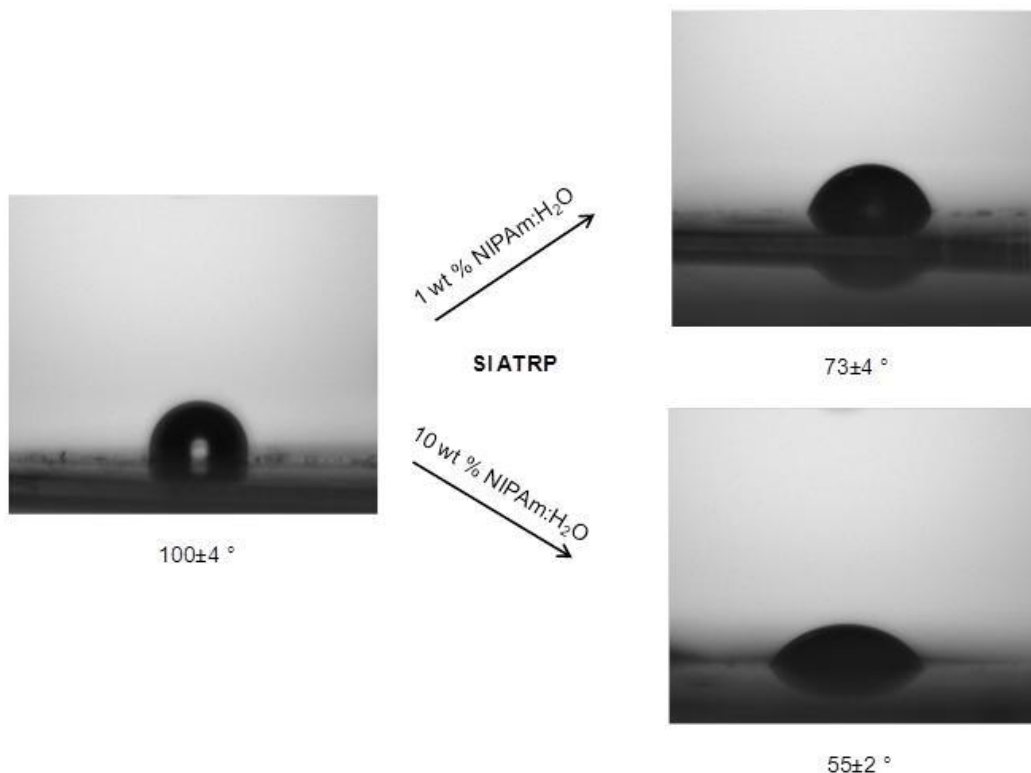


**Figure 3.2.12.** Contact angle measurements of honeycomb films from 2,3-O-(2-bromoisobutyryl)-2,6-O-TDMS-cellulose before (left) and after SI ATRP (right) with 1 wt% (top) and 10 wt% (bottom) of NIPAM/H<sub>2</sub>O (see **Table 3.2.7** for details). Measurements were done in triplicate.

### 3.2.5 Conclusions

The synthesis of 3-O-(2-bromoisobutyryl) 2,6-O-TDMS-cellulose was successfully accomplished with a maximum DS of 2-bromoisobutyryl in position C3 of 0.3. By decreasing the TDMS substitution at the C2 position of the 2,6-O-TDMS-cellulose, 2,3-O-(2-bromoisobutyryl)-2,6-O-TDMS-cellulose with a higher 2-bromoisobutyryl DS values (max ~ 0.8) was produced. However, the increase in DS was only due to the substitution of the free hydroxyl groups at the C2 position.

Honeycomb patterned films were produced from both the regio- and non-regioselectively substituted cellulose derivatives. The film obtained from the non-regioselectively substituted cellulose-based macroinitiator was much more uniform than that produced from the regioselective derivative. Therefore, surface-initiated ATRP was performed on the non-regioselectively substituted 2,3-O-(2-bromoisobutyryl)-2,6-O-TDMS-cellulose honeycomb film. PNIPAM polymer chains were effectively grafted from the honeycomb surface, the properties of which depended on



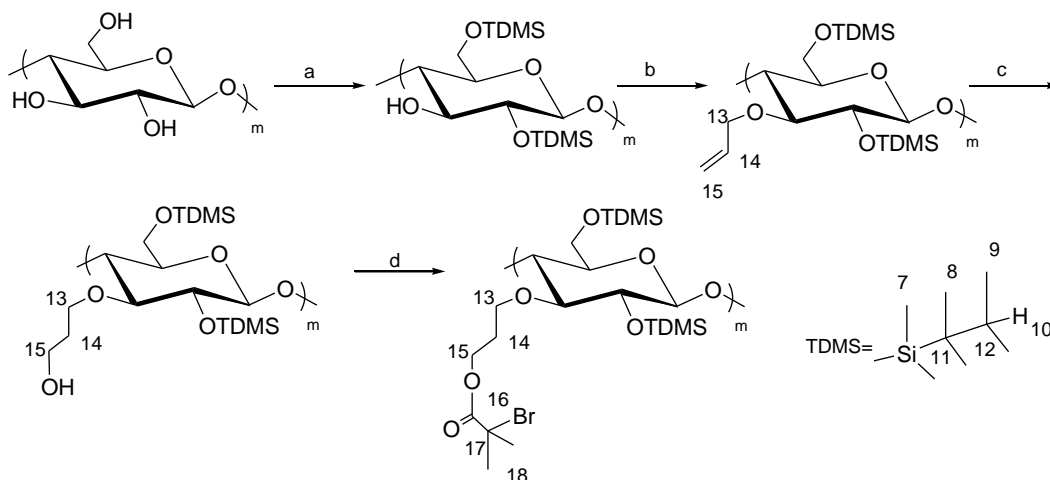
the monomer concentration used. At higher NIPAM concentration (10 wt% NIPAM/H<sub>2</sub>O) the porous honeycomb structure was lost, and a rough continuous hydrophilic surface was formed. At much lower NIPAM concentration (1 wt% NIPAM/H<sub>2</sub>O) the honeycomb structure was maintained, albeit much less regular in structure, which might be due to lack of control during ATRP. Surface initiated ATRP of NIPAM decreased the contact angle of the 2,3-O-(2-bromoisobutryl)-2,6-O-TDMS-cellulose films from  $100 \pm 4^\circ$  to  $73 \pm 4^\circ$  (1 wt% NIPAM/H<sub>2</sub>O) to  $55 \pm 2^\circ$  (10 wt% NIPAM/H<sub>2</sub>O). The thermoresponsiveness of the films was not tested due to the absence of adequate instrumentation.

### 3.3 Homogeneous ATRP of Thermoresponsive Copolymers from Regioselectively Substituted 3-O-(3-O-(2-Bromoisobutyryl)-hydroxypropyl)-2,6-O-TDMS cellulose

As discussed in section 3.2 and to the best of our knowledge, it is not possible to synthesize macroinitiator, 3-O-(2-bromoisobutyryl)-2,6-O-TDMS with a high initiator density due to the low 2-bromoisobutyryl DS. Therefore an alternative synthetic path has been developed allowing the grafting of thermoresponsive copolymers from a macroinitiator with high and low initiating site density. We have synthesized, for the first time, 3-O-(3-O-(2-bromoisobutyryl)-hydroxypropyl)-2,6-O-TDMS cellulose-*g*-PNIPAM, a regioselectively substituted cellulose-based macroinitiator for ATRP with high, medium and low degrees of substitution. Thermoresponsive copolymers, PNIPAM and poly(di(ethylene glycol) methyl ether methacrylate-*co*-oligo(ethylene glycol) methyl ether methacrylate) (P(DEGMA<sub>95</sub>-*co*-OEGMA<sub>5</sub>)) were “grafted-from” the newly synthesized cellulosic macroinitiators via homogeneous ATRP. Regioselective functionalization and the degree of substitution (DS) of the initiator in the cellulose backbone on ATRP were investigated with these new cellulosic macroinitiators. The effects of parameters such as solvent, addition of Cu(II), temperature, ligand, halogen and monomer concentration on ATRP were also studied. The results were discussed based on the respective conversion and kinetic plots.

#### 3.3.1 Synthesis of 3-O-(3-O-(2-bromoisobutyryl)-hydroxypropyl)-2,6-O-TDMS cellulose

As discussed in section 3.2, as well as elsewhere<sup>343</sup> the functionalization of the C3-OH with 2-bromoisobutyryl moieties could only be done with a maximum DS of 0.3. As one of our objectives in this thesis was to produce an ATRP macroinitiator with a flexible range of DS to enable the synthesis of high or low densely grafted cellulose-based copolymers, a new approach was needed. Although esterification of the C3 position appears to be limited, etherification is not. Therefore, to achieve complete substitution of the C3 position, i.e., a DS of 1, we would first introduce a spacer in position 3. This was achieved by C3 allylation followed by the oxidation of the double bond to form an anti-Markovnikov alcohol, as described by Heinze et al.,<sup>91</sup> followed by functionalization of the latter to the corresponding 2-bromoisobutyryl (**Scheme 3.3.1**).



**Scheme 3.3.1.** Synthetic scheme to synthesize 3-O-(3-O-(2-bromoisobutyryl)-hydroxypropyl)-2,6-O-TDMS cellulose: a. DMA-LiCl, TDMS-Cl, imidazole; b. Allyl-Cl; NaH; c. i) 9-BBN; ii) NaOH, H<sub>2</sub>O<sub>2</sub>; d. 2-bromoisobutyryl bromide, anhydrous pyridine.

As per **Scheme 3.3.1** synthesis of the 3-O-(3-O-(2-bromoisobutyryl)-hydroxypropyl)-2,6-O-TDMS cellulose-*g*-PNIPAM was initiated by the regioselective protection of the C2 and C6 positions of the AGU with bulky TDMS protecting groups. The resulting 2,6-O-TDMS cellulose was then reacted with allyl chloride to form the corresponding 3-O-allyl-2,6-O-TDMS cellulose. From the <sup>1</sup>H-NMR the peaks corresponding to the TDMS groups, 7, 8, 9 and 10 as well as those associated with the allyl group, 13, 14, and 15 are clearly evident (**Figure 3.3.1 a**). Peak 13 corresponds to the allyl methylene group (overlaps with the AGU region (peaks 1-6)) while peaks 14 and 15 correspond to the vinyl protons (**Figure 3.3.1 a**) which now overlap with the protons linked to the tertiary carbon of the TDMS groups (peak 10) and the protons in the AGU region, respectively (**Figure 3.3.1 b**). Functionalization of the newly formed primary OH group with a 2-bromoisobutyryl group introduces peak 18 associated with the protons of the isobutyryl methyl groups (**Figure 3.3.1 c**).

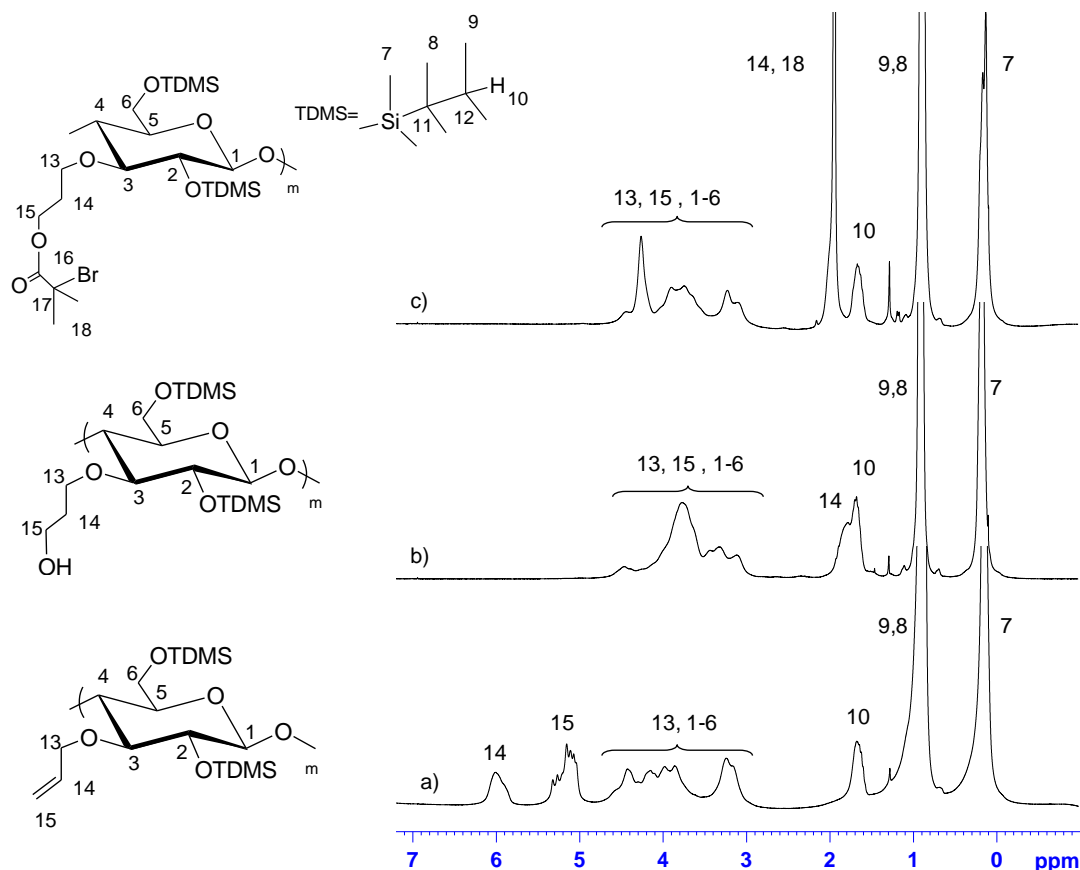


**Figure 3.3.1.** Comparison of  $^1\text{H}$ -NMR spectra of a) 3-O-allyl-2,6-O-TDMS cellulose, b) 3-hydroxypropyl 2,6-O-TDMS cellulose and c) 3-O-(3-O-(2-bromoisobutyryl)-hydroxypropyl)-2,6-O-TDMS cellulose-g-PNIPAM, see **Scheme 3.3.1**.

$^{13}\text{C}$ -NMR analysis (**Figure 3.3.2**) further confirmed the successful synthesis of the intermediates and final product as described in **Scheme 3.3.1**. Allylation produced two peaks 14 and 15 at lower field corresponding to the carbons involved in the double bond. The peak from the methylene carbon of the allyl group (peak 13) was not very visible, but it should be found between 60 and 70 ppm. Oxidation of the double bond caused a shift to higher field of carbons 14 and 15 overlapping with peak 10 (TDMS) and peak 6 (C6 AGU), respectively. 2-Bromoisobutyrylation of the newly formed OH group introduced 3 new peaks, peak 16 (the carbonyl group), peak 17 (the tertiary carbon of the isobutyryl group) and peak 18 (the carbons of the isobutyryl methyl groups).

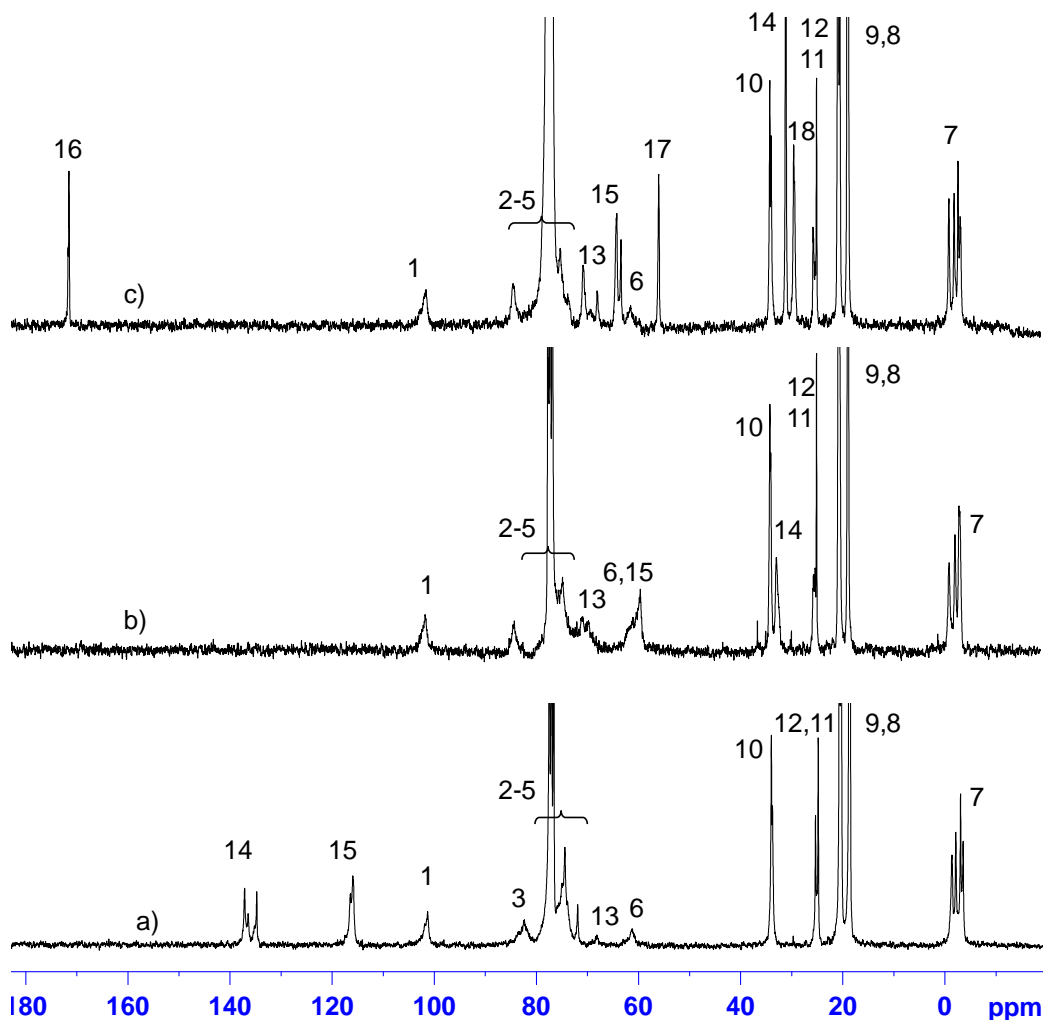


**Figure 3.3.2.** Comparison of quantitative  $^{13}\text{C}$ -NMR spectra of a) 3-O-allyl-2,6-O-TDMS cellulose, b) 3-O-hydroxypropyl-2,6-O-TDMS cellulose and c) 3-O-(3-O-(2-bromoisobutyryl)-hydroxypropyl)-2,6-O-TDMS cellulose, see **Figure 3.3.1** for peak identification.

Varying the number of molar equivalents of allyl chloride enables different degrees of substitution to be obtained (**Table 3.3.1**). Our objective was to obtain C3 derivatives with low, medium and high DS. The DS was calculated from quantitative  $^{13}\text{C}$ -NMR of the macroinitiator in which the carbonyl peak 16 was integrated against the C1 carbon peak 1 of the AGU, which was calibrated to 1.0. TDMS deprotection of the macroinitiator was not performed because the fluoride ion associated with the deprotecting agent tetra-*n*-butylammonium fluoride (TBAF) causes the elimination of the bromine from the 2-bromoisobutyryl, deactivating the ATRP initiator.<sup>100</sup>

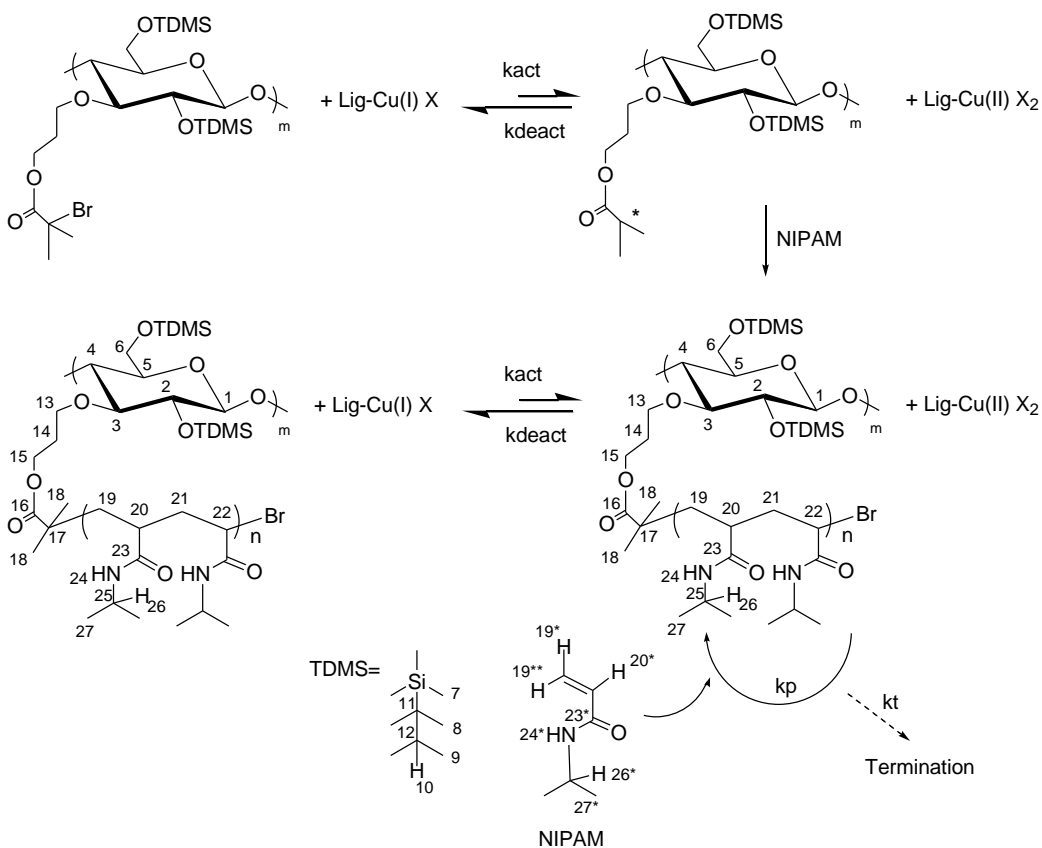
**Table 3.3.1.** Molar equivalents of allyl chloride used in the synthesis of macroinitiator 3-O-(3-O-(2-bromoisobutyryl)-hydroxypropyl)-2,6-O-TDMS cellulose (Scheme 3.3.1, step b) with different DS.

	<b>2,6-O-TDMS Cellulose</b>	<b>Allyl-Cl</b>	<b>DS</b>
	<b>(molar equivalents)</b>	<b>(molar equivalents)</b>	<b>macroinitiator</b>
<b>Low DS</b>	1	1	0.2
<b>Medium DS</b>	1	3	0.6
<b>High DS</b>	1	10	1

Note: DSs were determined in duplicate and respective RPD% calculated as per **Equation 3.1.1**. RPDs% were no higher than 9%. Duplicate and RPD% values are presented in **APPENDIX-Duplicates and respective RPDs%**.

### 3.3.2 Homogeneous polymerization of NIPAM from 3-O-(3-O-(2-bromoisobutyryl)-hydroxypropyl)-2,6-O-TDMS cellulose

The homogeneous polymerization of NIPAM from 3-O-(3-O-(2-bromoisobutyryl)-hydroxypropyl)-2,6-O-TDMS cellulose was attempted as per **Scheme 3.3.2**.



**Scheme 3.3.2.** Schematic illustration of the polymerization of NIPAM from 3-O-(3-O-(2-bromoisobutyryl)-hydroxypropyl)-2,6-O-TDMS cellulose.

To assess the success of the different ATRP reactions, it is necessary to prove that the copolymerization occurred in a controlled manner. The main conditions to be verified were: i) the reaction is first order relative to monomer concentration; ii) the molecular weight increases linearly with conversion, and iii) a narrow distribution of molecular weight, which decreases with conversion.<sup>170</sup> The effects of the concentration of macroinitiator, temperature, Cu(II), ATRP through activator regenerated by electron transfer (ARGET) and degree of substitution in the ATRP reactions were assessed (**Table 3.3.2**).

**Table 3.3.2.** Experimental conditions used in the ATRP of NIPAM from 3-O-(3-O-(2-bromoisobutryl)-hydroxypropyl)-2,6-O-TDMS cellulose and respective conversions.

Exp#	MI	Cu <sup>I</sup> Cl	Cu <sup>II</sup> Cl <sub>2</sub>	Me <sub>6</sub> TREN	T(°C)	Time <sup>(a)</sup>	Conv <sup>(b)</sup>
Molar equivalents based on MI							%
I <sup>(c)</sup>	1	1	0.05	1.2	RT	30 min	7
II <sup>(d)</sup>	1	1	0.05	1.2	RT	30 min	8
III <sup>(d)</sup>	1	1	0.05	1.2	55	30 min	6
IV <sup>(d)</sup>	1	1	0.2	1.2	RT	60 min	19
V <sup>(d),(e)</sup>	1	0	0.01	0.1	RT	90 min	4
VI <sup>(d),(f)</sup>	1	1	0.2	1.2	RT	60 min	19

Experimental conditions: MI:NIPAM:Me<sub>6</sub>TREN:CuCl:CuCl<sub>2</sub> = (1:100:x:y:z) molar equivalents for exp# I (0.15:15:0.18:0.15:0.0075) mmol; solvent – THF/MeOH; MI – Exp# I to V macroinitiator with high DS and Exp#VI macroinitiator with low DS; RT-room temperature. <sup>(a)</sup> Time within linear kinetic regime was observed; <sup>(b)</sup> Conv. (%) =  $\Delta[M]/[M]$  (calculated from kinetic plots) – maximum conversion attained within the linear kinetic regime; <sup>(c)</sup> MI/solvent = 0.1 wt%; <sup>(d)</sup> MI/solvent = 0.05 wt%; <sup>(e)</sup> ARGET – Sn(EH)<sub>2</sub> 0.1 equivalent; <sup>(f)</sup> MI with low DS. For further information see section 2.3.17.

In this study, the kinetic plots ( $\ln([M]_0/[M])$  vs. time, where  $[M]_0$  is the initial concentration of monomer and  $[M]$  is the monomer concentration at time t) were used to assess the effect of the different parameters. Accordingly, aliquots were collected from the reaction mixture at different reaction intervals and then diluted in acetone and analyzed by <sup>1</sup>H-NMR (**Figure 3.3.3**). The objective was to obtain the highest conversion and the longest linear kinetic regime possible.



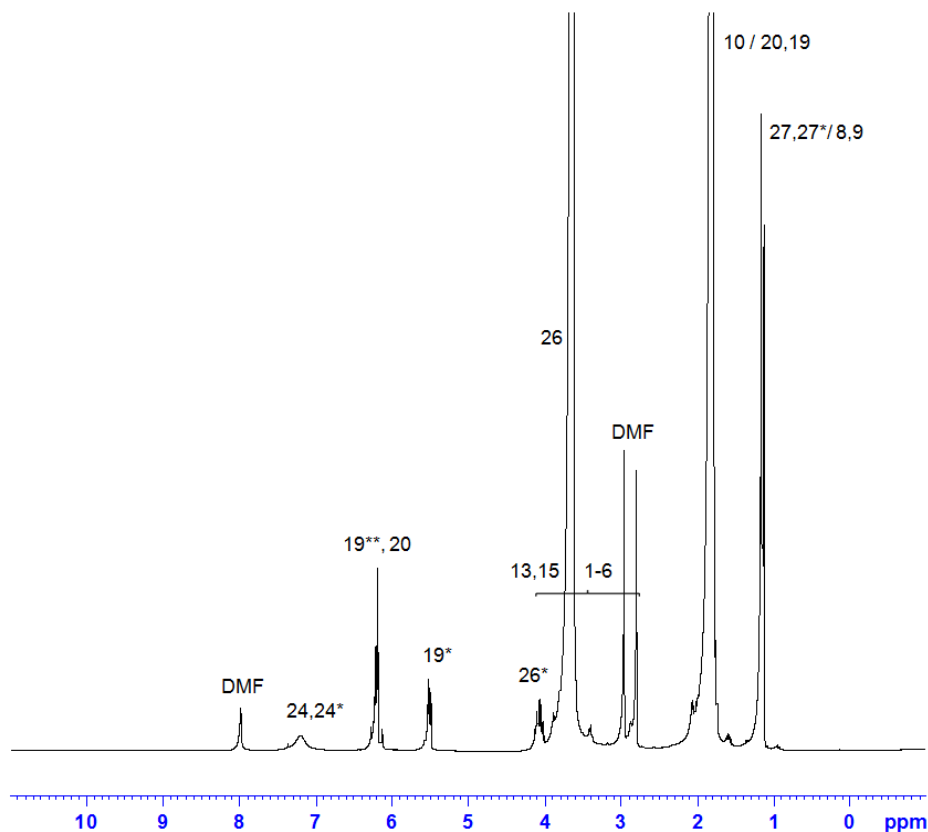


**Figure 3.3.3.**  $^1\text{H}$ -NMR spectrum of 30 min aliquot obtained from homogeneous polymerization of NIPAM from the macroinitiator with high DS, see **Scheme 3.3.2** for identification of the peaks.

To determine the initial concentration of monomer ( $[\text{M}]_0$ ) and the concentration of monomer consumed ( $[\text{M}]$ ), a known concentration of DMF was used as an internal standard. The integral for the peak from the proton in the alpha position relative to the carbonyl group of DMF at 8 ppm was set to 1.0 and compared to the integral areas of the signals for the protons in the double bond of the unreacted NIPAM monomer at 5.5 (peak 19\*) and 6.2 ppm (peaks 19\*\*, 20\*). The kinetic plots for each experimental condition (**Figure 3.3.4**) were in general very similar to what was observed previously for NIPAM<sup>269,270</sup> as well as other meth(acrylamides).<sup>248,266</sup> Plots from Exps # I to III formed a plateau after only 30 min of reaction. On the other hand, a linear kinetic regime was observed in Exps # IV to VI (as illustrated by dashed line in **Figure 3.3.4 c**) after which a plateau was formed. The latter suggests that the concentration of radicals in solution is not constant throughout the polymerization, or the catalytic sites have been deactivated.<sup>270</sup>

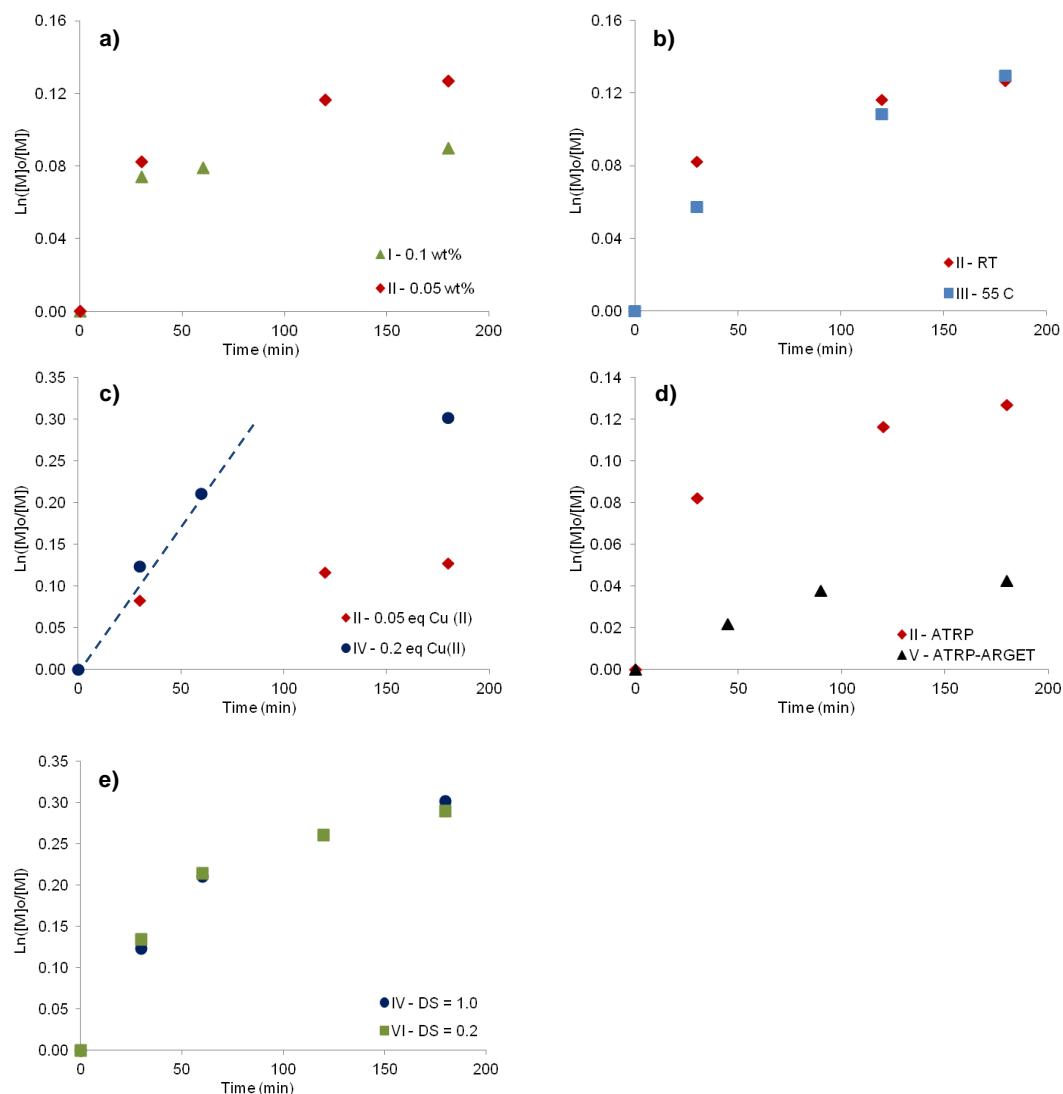


**Figure 3.3.4.** Semi-logarithmic plots of NIPAM polymerization under different experimental conditions, using the cellulose-based macroinitiator with high DS. MI:NIPA:Me<sub>6</sub>TREN:Cu(I)Cl:Cu(II)Cl<sub>2</sub> - 1:100:x:y:z; solvent: THF/MeOH; [MeOH] = 5 wt%; MI – macroinitiator with high DS. (a) Concentration of MI wt%, I – 0.1; II – 0.05.; (b) Temperature, II – RT; III – 55 °C. (c) Molar equivalents of Cu(II), II – 0.05 ; IV – 0.2. (d) Effect of ATRP, II – ATRP; V – ATRP-ARGET, tin<sup>II</sup> 2-ethylhexanoate (Sn(EH)<sub>2</sub>) = 0.1 molar equivalents and Cu(II) = 0.1 molar equivalents; (e) MI with low DS, IV – MI DS = 1; VI – MI DS = 0.2.

The decrease in macroinitiator (MI) concentration from 0.1 to 0.05 wt%, (**Figure 3.3.4 a**) did not affect the rate of polymerization or conversion (7 vs. 8%). On the other hand, an increase in temperature from RT to 55 °C, (**Figure 3.3.4 b**) caused a slight decrease in the conversion from 8 to 6%. This might be due to a higher concentration of radicals being produced at the higher temperature. The addition of a higher amount of Cu(II), (**Figure 3.3.4 c**) extended the linear

kinetic regime, from 30 min to 1 hour. Thus, the conversion of NIPAM was also higher 19% compared to 8% (Exp # II). The increase in Cu(II) might have increased the deactivation constant, which caused the concentration of radicals to decrease, resulting in less termination reactions. In Exp # V (**Figure 3.3.4 d**) ATRP-ARGET was applied and the reducing agent  $\text{Sn}(\text{EH})_2$  was used to regenerate the deactivator. The rate decreased substantially, but the linear kinetic regime was prolonged from 30 to 90 min. Unfortunately, the conversion remained very low, reaching a maximum value of only 4%. Finally, in Exp # VI (**Figure 3.3.4 e**) a macroinitiator with lower DS was used under comparable conditions to Exp # IV (macroinitiator with high DS). The rate of polymerization was maintained, as well as the period of linear kinetic regime, 60 min, and the conversion remained at 19%. Considering the lower initiator density of this macroinitiator, the PNIPAM DP should be considerably higher than the one with the higher initiator density.

Overall, the ATRP reactions were not complete, only achieving conversions within the linear kinetic regime of between 4 and 19%. These values are considered low compared to the homopolymerization of NIPAM, which can be as high as  $\sim 90\%$ .<sup>269,270</sup> The observed behaviour in this system could be attributed to: i) the size of the macroinitiator, the initiator was a bulky macromolecule and/or ii) the solvent system used. The homopolymerization of NIPAM was found to be successful in DMF:water<sup>269</sup> (75:25) or 2-propanol,<sup>270</sup> however, the cellulose-based macroinitiator was not soluble in any of these solvents. Therefore, an alternative solvent system had to be used (THF) which might not be ideal.

To verify whether NIPAM polymerizes by itself an ATRP polymerization was done in the absence of macroinitiator under the exact same conditions as Exp # IV. The reaction mixture was analyzed by  $^1\text{H-NMR}$ , which showed exclusively unreacted NIPAM, the spectrum can be found in **APPENDIX-Selected NMR spectra**.

To confirm the successful grafting of PNIPAM from the cellulose-based macroinitiator the copolymers were analyzed after 3 hours of reaction by FTIR and  $^1\text{H-NMR}$ . The spectra obtained were similar therefore representative FTIR (**Figure 3.3.5**) and  $^1\text{H-NMR}$  (**Figure 3.3.6**) spectra are shown.

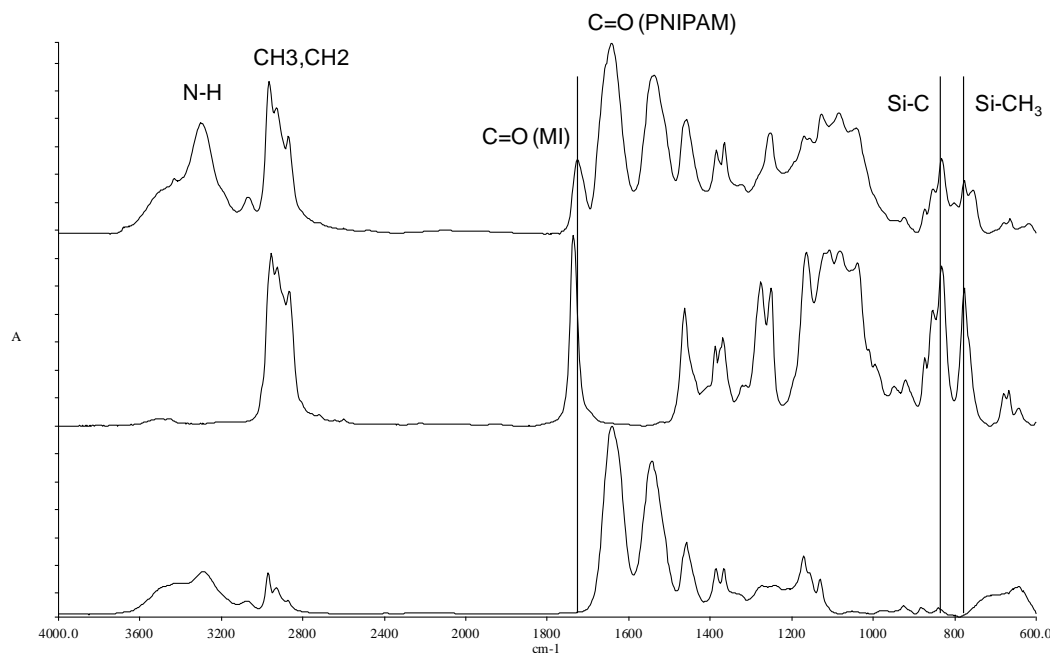


**Figure 3.3.5.** Comparison of FTIR spectra of PNIPAM (bottom), cellulose-based macroinitiator with high DS (middle) and the synthesized 3-O-(3-O-(2-bromoisobutyryl)-hydroxypropyl)-2,6-O-TDMS cellulose-g-PNIPAM (top).

The FTIR spectrum of the synthesized cellulose-based copolymer showed clearly peaks from the macroinitiator,  $\nu_{\text{C=O}}$  peak at  $1724\text{ cm}^{-1}$  and both peaks from the TDMS groups ( $\nu_{\text{Si-C}}$  at  $832\text{ cm}^{-1}$  and  $\nu_{\text{Si-CH}_3}$  at  $776\text{ cm}^{-1}$ ), as well as those from PNIPAM:  $\nu_{\text{N-H}}$  at  $3302\text{ cm}^{-1}$ ,  $\nu_{\text{C=O}}$  at  $1644\text{ cm}^{-1}$ , and  $\delta_{\text{CH}_2}$  and  $\delta_{\text{CH}_3}$  bending peaks at  $1538$  and  $1385\text{ cm}^{-1}$ . The cellulose-based copolymer was also analyzed by  $^1\text{H-NMR}$ , Figure 3.3.6.

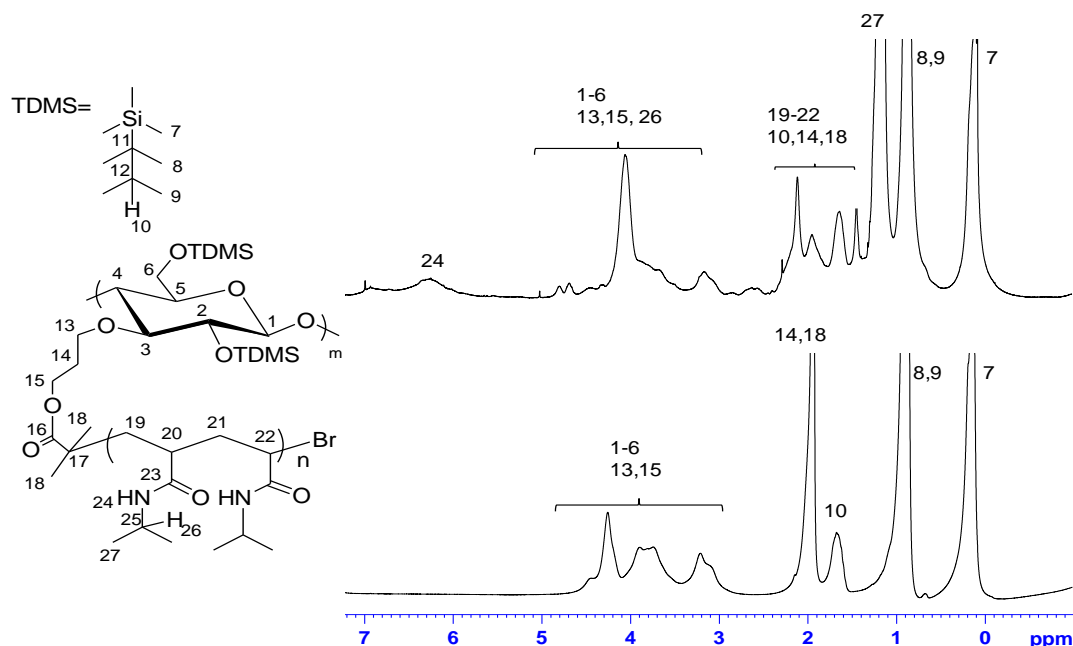


**Figure 3.3.6.** Comparison of <sup>1</sup>H-NMR spectra of cellulose-based macroinitiator with high DS (bottom) and the synthesized 3-O-(3-O-(2-bromoisobutryl)-hydroxypropyl)-2,6-O-TDMS cellulose-g-PNIPAM (top).

The spectrum of the cellulose-based copolymer (**Figure 3.3.6-top**) showed peaks from the macroinitiator and PNIPAM. In particular, note the AGU protons, the TDMS CH<sub>3</sub> proton peaks at 0.08 and 0.87 ppm (peaks 7-9) and a peak at 1.16 ppm from the two CH<sub>3</sub> protons from the PNIPAM isopropyl groups. Additionally, the N-H peak of PNIPAM was also detected at 6.3 ppm. The remaining PNIPAM peaks overlapped with those from the macroinitiator. These results are indicative of a successful grafting of PNIPAM from the cellulose-based macroinitiator. However, to prove that the PNIPAM peaks detected by FTIR and <sup>1</sup>H-NMR are from the grafted polymer and not from PNIPAM associated to the cellulose-based macroinitiator, we dissolved the latter and PNIPAM in THF and added water causing the formation of a white precipitate which was isolated and analyzed by <sup>1</sup>H-NMR. The spectrum (see **APPENDIX-Selected NMR spectra**) showed exclusively the cellulose-based macroinitiator. Therefore, the PNIPAM detected earlier is grafted to the cellulose-based macroinitiator.

The dn/dc of the macroinitiator and copolymer III were determined in duplicate and found to be 0.0873 and 0.091 mL/g, respectively. The copolymers were analyzed by GPC-MALS to determine number Mn and PDI (**Table 3.3.3**). The dn/dc and GPC-MALS analyses were done in duplicate and the RPDs% of the dn/dc and Mn were calculated as per **Equation 3.1.1**, and found to be below 1% and 10%, respectively. A table with the values of the duplicates and respective RPDs% can be found in **APPENDIX-Duplicates and respective RPDs%**.

**Table 3.3.3.** Mn<sub>(th)</sub>, Mn<sub>(GPC-MALS)</sub>, PDI, conversion and DP of macroinitiators and respective cellulose-based graft copolymers after 3 hours of reaction.

Exp#	Mn <sub>(th)</sub> <sup>(a)</sup>	Mn <sub>(GPC-MALS)</sub> (g/mol)	PDI	Conv% <sup>(b)</sup>	DP <sup>(c)</sup>
MI-High DS		4.4*10 <sup>4</sup>	1.5		
MI-Low DS		4.3*10 <sup>4</sup>	1.3		
I	1.1*10 <sup>5</sup>	1.3*10 <sup>5</sup>	1.2	9	9
II	1.3*10 <sup>5</sup>	1.6*10 <sup>5</sup>	1.1	12	12
III	1.4*10 <sup>5</sup>	1.3*10 <sup>5</sup>	1.1	12	13
IV	2.7*10 <sup>5</sup>	1.1*10 <sup>5</sup>	1.1	26	28
V <sup>(d)</sup>	7.7*10 <sup>4</sup>	N/A <sup>(e)</sup>	N/A	4	4
VI <sup>(f)</sup>	2.4*10 <sup>5</sup>	1.7*10 <sup>7</sup>	1.8	25	130
		4.3*10 <sup>4</sup>	1.2		

<sup>(a)</sup> Mn<sub>(th)</sub> after 3 hours = Mn<sub>(MI)</sub> + (MM<sub>NIPAM</sub> \* DP \* I.S.); MI = macroinitiator, MM = molar mass, DP after 3 hours = degree of polymerization =  $\Delta[M] / ([MI] * DS)$ , I.S. = initiating sites = Mn<sub>(MI)</sub> / MM<sub>(Repeating unit)</sub> \* DS; <sup>(b)</sup> Conv. (%) after 3 hours =  $\Delta[M] / [M]$ , calculated from kinetic plots; <sup>(c)</sup> DP after 3 hours =  $\Delta[M] / ([MI] * DS)$ , base on conversion obtained from kinetic plots; <sup>(d)</sup> ATRP-ARGET; <sup>(e)</sup> sample not soluble in THF; <sup>(f)</sup> MI with low DS. See **Table 3.3.2** for information on the experimental conditions.

**Note:** To facilitate the discussion, the copolymers obtained from experiments I-VI will be called copolymers # I-VI.

The theoretical number average molecular weight (Mn<sub>(th)</sub>) of copolymers # I, II and III were not very close to the number average molecular weight obtained from GPC-MALS (Mn<sub>(GPC-MALS)</sub>) but presented low polydispersities suggesting a controlled polymerization. The slight discrepancy might have been caused by the loss of catalytic sites before termination reactions became predominant.<sup>270</sup> As previously discussed elsewhere<sup>266</sup> and in section 1.5, the side reactions

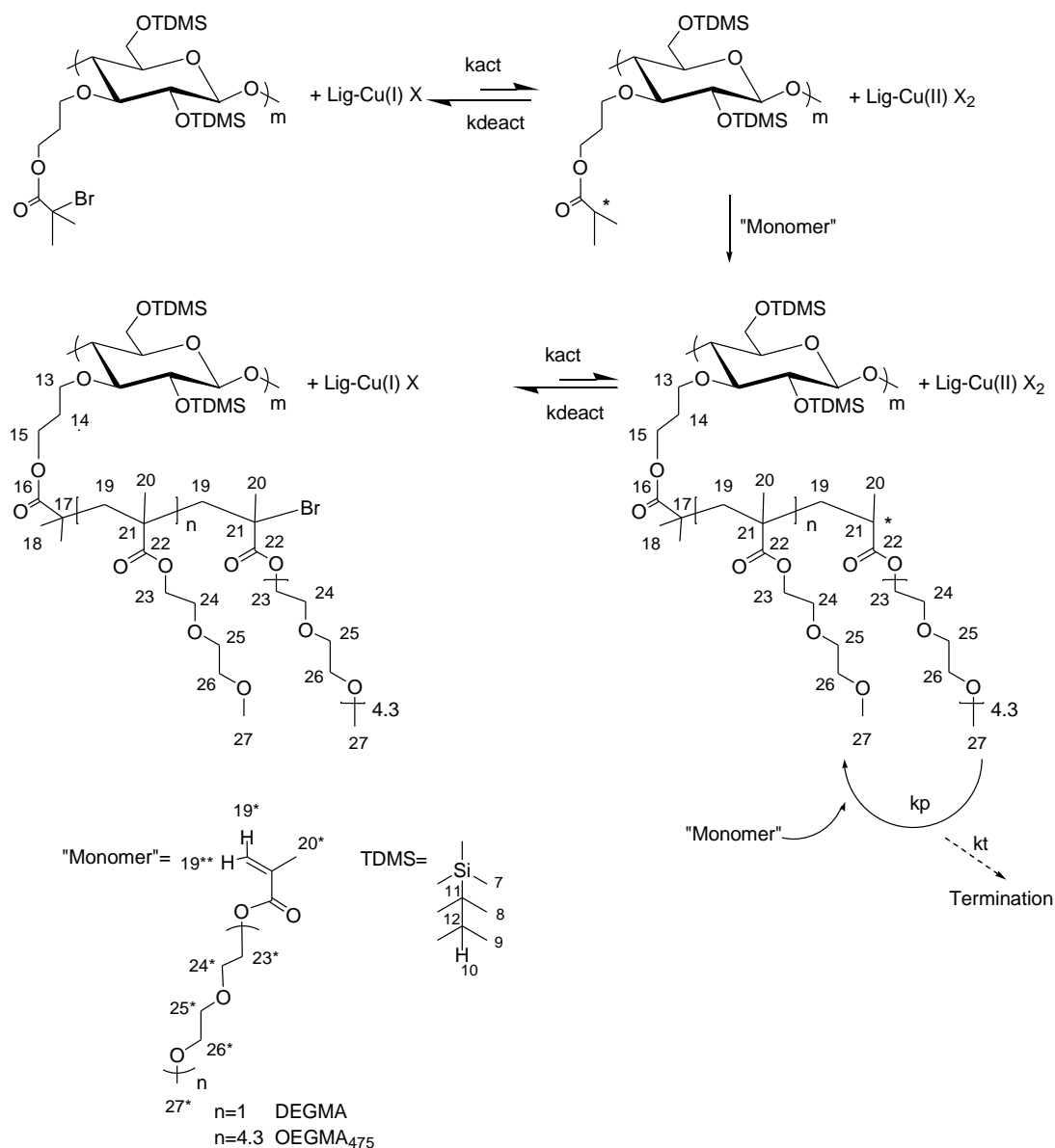
observed in the ATRP of (meth)acrylamides could be responsible for the loss of catalytic sites. The  $Mn_{(th)}$  of copolymer # IV is substantially higher than that determined by GPC-MALS, which may be indicative of chain transfer that occurred outside the linear kinetic regime. In the kinetic plot of copolymer # VI (**Figure 3.3.4 e**), the initial rate of polymerization is relatively high and very close to the rate of polymerization of copolymer # IV. The GPC-MALS analysis of copolymer # VI revealed two distinct peaks. The first had an extremely high  $Mn$  ( $1.7 \times 10^7$  g/mol) and high PDI (1.8), which might be due to radical coupling reactions between growing polymer chains. The second peak ( $Mn = 4.3 \times 10^4$  g/mol and PDI = 1.2) likely corresponds to unreacted macroinitiator. Copolymer # V was not soluble in THF and therefore no GPC-MALS analysis was conducted. Overall, the polymerization of NIPAM from the cellulose-based macroinitiator produced copolymers with low conversions. As previously discussed, the use of PNIPAM presents some drawbacks which include a challenging ATRP due to the loss of catalytic sites<sup>344</sup> caused by certain side reactions<sup>266</sup>. Recently, P(DEGMA<sub>95</sub>-co-OEGMA<sub>5</sub>) a new thermoresponsive copolymer was discovered, with a similar LCST as PNIPAM and with some advantages over the latter, as previously discussed in section 1.5.<sup>254,274,345</sup> Therefore, homogeneous copolymerization of P(DEGMA<sub>95</sub>-co-OEGMA<sub>5</sub>) from 3-O-(3-O-(2-bromoisobutryl)-hydroxypropyl)-2,6-O-TDMS cellulose was attempted.

### 3.3.3 Homogeneous copolymerization of DEGMA and OEGMA from 3-O-(3-O-(2-bromoisobutyryl)-hydroxypropyl)-2,6-O-TDMS cellulose

The macroinitiator with high DS (1.0) was used for the homogeneous ATRP under different experimental conditions. This study was based solely on the kinetic plots with the following objectives: higher conversion and longer linear kinetic regime. After the synthesis selected copolymers were isolated from the linear kinetic regime and characterized by ATR-FTIR, TGA and DSC. Copolymers that were soluble in  $\text{CHCl}_3$  were analyzed by  $^1\text{H}$ - and  $^{13}\text{C}$ -NMR, and those soluble in THF were analyzed by GPC-MALS to determine  $M_n$  and PDI. Additionally, a macroinitiator with low DS (0.2) was used to study the effect of initiating sites/graft density on the ATRP and respective properties.

The copolymer  $\text{P}(\text{DEGMA}_{95}\text{-co-OEGMA}_5)$  was grafted from the C3 position of a regioselectively substituted cellulose-based macroinitiator via ATRP (**Scheme 3.3.3**).





**Scheme 3.3.3.** Schematic illustration of the copolymerization of P(DEGMA<sub>95</sub>-co-OEGMA<sub>5</sub>) from 3-O-(3-O-(2-bromoisobutryl)-hydroxypropyl)-2,6-O-TDMS cellulose.

In one set of experiments (**Table 3.3.4**) the effects of parameters such as solvent, ratio Cu(I)/Cu(II), temperature, absence of Cu(II), ligand, catalyst and dilution were studied. In another set of experiments (**Table 3.3.5**), the impact of DEGMA and OEGMA concentration was studied.

**Table 3.3.4.** Experimental conditions used in the ATRP of P(DEGMA<sub>95</sub>-co-OEGMA<sub>5</sub>) from 3-O-(3-O-(2-bromoisobutyryl)-hydroxypropyl)-2,6-O-TDMS cellulose and the resulting conversions.

Exp#	[MI]	CuX	CuCl <sub>2</sub>	Solv	T(°C)	Lig	Time <sup>(a)</sup>	Conv <sup>(b)</sup>
Molar equivalents based on MI								%
1	1	Cl	0.2	THF/MeOH	RT	Me <sub>6</sub> TREN	5 min	13
2	1	Cl	0.2	THF	RT	Me <sub>6</sub> TREN	30 min	26
3	1	Cl	0.1	THF	RT	Me <sub>6</sub> TREN	30 min	26
4	1	Cl	0.1	THF	55	Me <sub>6</sub> TREN	1 h	44
5 <sup>(c)</sup>	1	Cl	0	THF	55	Me <sub>6</sub> TREN	1 h	45
6	1	Cl	0	THF	RT	Me <sub>6</sub> TREN	1 h	29
7	1	Cl	0	THF	55	PMDETA	2 h	23
8 <sup>(c)</sup>	1	Br	0	THF	55	Me <sub>6</sub> TREN	30 min	36
9 <sup>(d)</sup>	1	Cl	0	THF	55	Me <sub>6</sub> TREN	1 h	38
10 <sup>(e)</sup>	1	Cl	0	THF	55	Me <sub>6</sub> TREN	30 min	10

Experimental conditions: MI:(DEGMA+OEGMA):Ligand:CuX:CuCl<sub>2</sub> = (1:100:1.2:1) molar equivalents, for Exp # 1 (0.075:7.5:0.09:0.075:) mmol; MI/solvent = 0.5 wt% in Exp # 1-8, 0.25 wt% in Exp # 9 and 0.125 wt% in Exp # 10; MI – macroinitiator with high DS, DME02MA:OEGMA = 95:5. <sup>(a)</sup> Time within linear kinetic regime was observed; <sup>(b)</sup> Conv. (%) =  $\Delta[M] / [M]$ , maximum monomer conversion attained within linear kinetic regime, calculated from kinetic plots; <sup>(c)</sup> gel formation; <sup>(d)</sup> MI/solvent = 0.25 wt%; <sup>(e)</sup> MI/solvent = 0.125 wt%. For further information see section 2.3.18.

**Table 3.3.5.** Experimental conditions used in the ATRP of P(DEGMA<sub>95</sub>-co-OEGMA<sub>5</sub>) from 3-O-(3-O-(2-bromoisobutyryl)-hydroxypropyl)-2,6-O-TDMS cellulose and respective conversions.

Exps#	[MI]wt%	MI	"M" <sup>(a)</sup>	Time <sup>(b)</sup>	Conv <sup>(c)</sup>
Molar equivalents relative to MI					%
11	0.5	1	50	30min	32
12	0.5	1	25	1h	30
13	0.5	1	10	1h	24

Experimental conditions: MI:(OEGMA+DMEOMA):Ligand:CuX = (1:100:1.2:1); MI – macroinitiator, DEGMA:OEGMA = 95:5; <sup>(a)</sup> "M" – DEGMA (95%) and OEGMA (5%) <sup>(b)</sup> Time within linear kinetic regime was observed; <sup>(c)</sup> Conv.% =  $\Delta[M] / [M]$ , maximum monomer conversion attained within linear kinetic regime, calculated from kinetic plots. For further information see section 2.3.18.

To verify when the reactions follow a first order kinetic regime with respect to monomer concentration it is necessary to build kinetic plots of  $\ln([M_0]/[M])$  vs. time. In order to calculate the concentration of "monomer" (DEGMA and OEGMA) aliquots of reactions were collected from the reaction mixture at defined times and analyzed by <sup>1</sup>H-NMR.

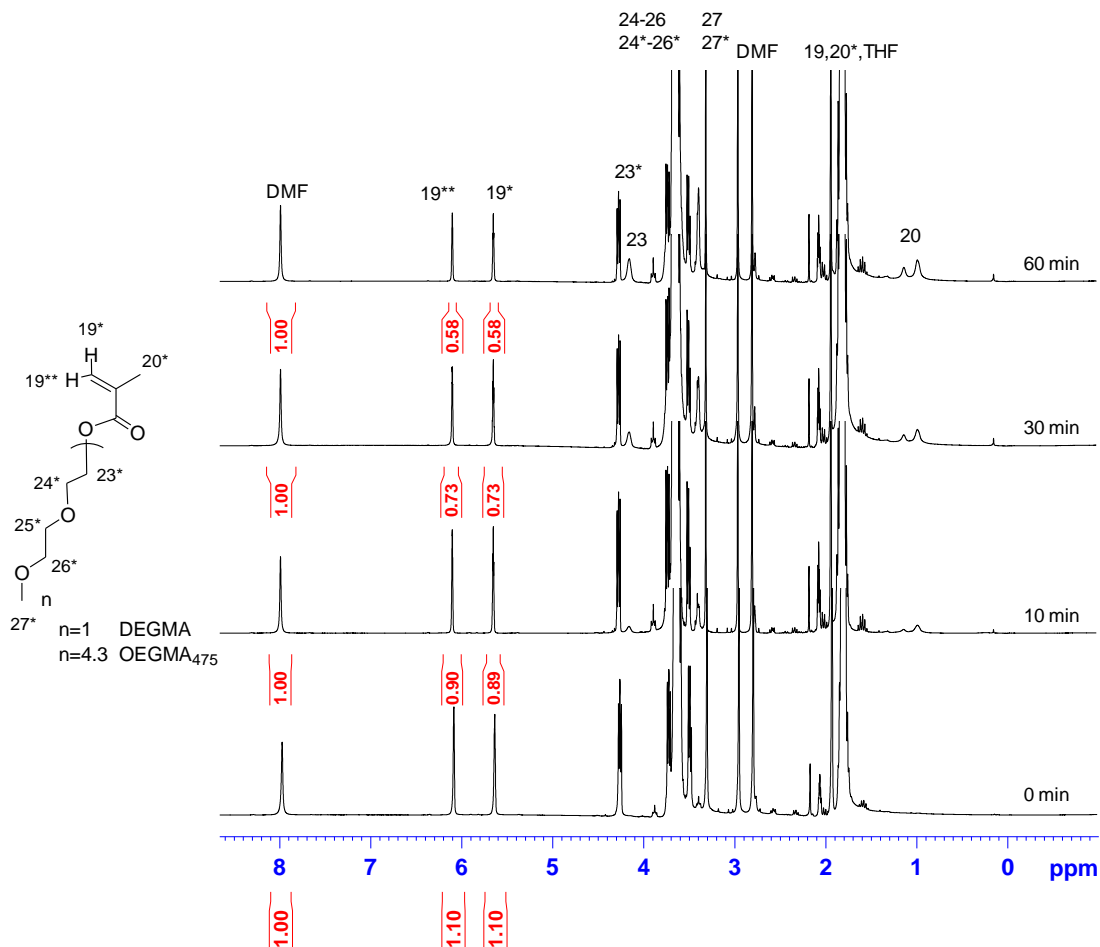


**Figure 3.3.7.**  $^1\text{H}$ -NMR spectra of different aliquots collected at 0, 10, 30 and 60 min, obtained from experiment 5. See **Scheme 3.3.3** for the identification of the peaks.

A comparison of  $^1\text{H}$ -NMR spectra of the different aliquots are shown in **Figure 3.3.7**. As expected, a decrease in the intensity of the peaks corresponding to DEGMA and OEGMA (in particular the two peaks at 5.6 and 6.1 ppm) identified as protons 19\* and 19\*\* were apparent. “Monomer” consumption was quantified by integrating the peaks at 5.6 and 6.1 ppm against the peak at 8 ppm, calibrated as 1.0 proton. The latter is the alpha proton relative to the carbonyl group of DMF (internal standard). **Figure 3.3.8** shows the corresponding kinetic plots obtained for the copolymerization of DEGMA and OEGMA under the different experimental conditions used.

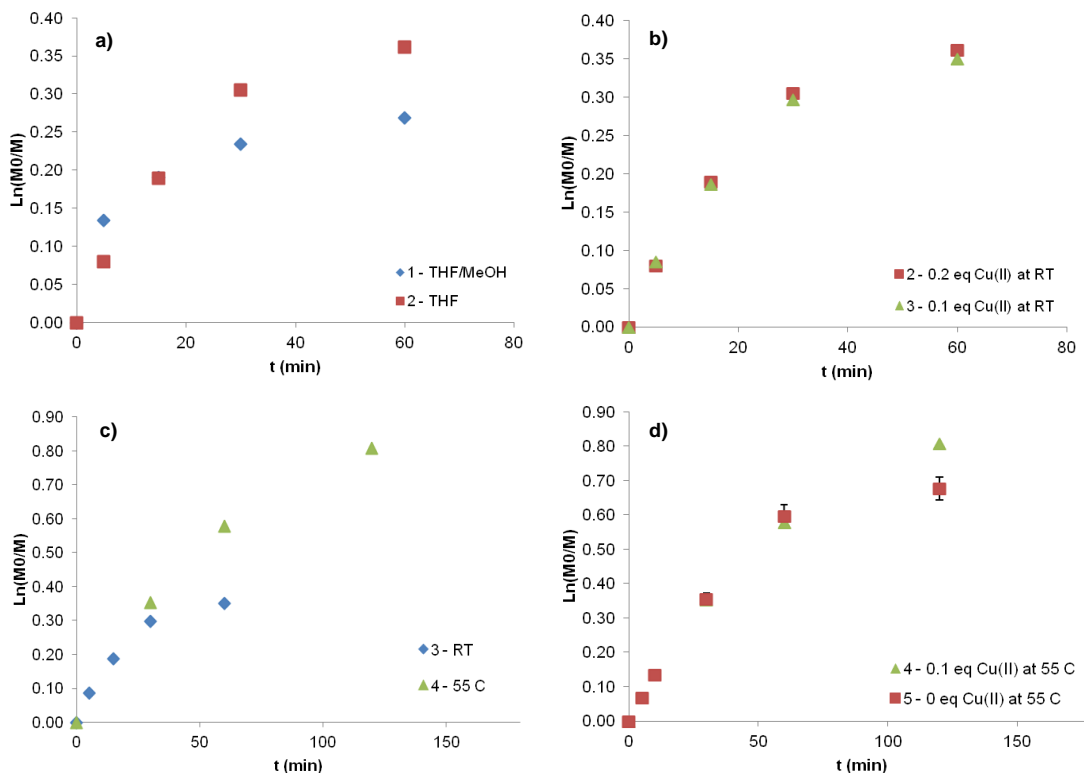


**Figure 3.3.8.** Semi-logarithmic plots of copolymerization of DEGMA and OEGMA, under different experimental conditions, from cellulose-based macroinitiator with high DS. (MI:(DEGMA+OEGMA):Ligand:CuX - 1:100:1.2:1, DEGMA:OEGMA=95:5; solvent: THF) **a)** Effect of Solvent: Exp # 1: THF/MeOH, Exp # 2: THF; **b)** Molar equivalents of Cu(II) at RT: Exp # 2: Cu(II)=0.2; Exp # 3: 0.1; **c)** Effect of Temperature using 0.1 molar equivalents of Cu(II): Exp # 3: RT, Exp # 4: 55 °C; **d)** Effect of Molar equivalents of Cu(II) at 55 °C: Exp # 4: Cu(II) = 0.1, Exp # 5: Cu(II) = 0.

When using the THF/MeOH (Exp # 1) solvent system a plateau began to form after just 5 min of reaction and a conversion of 13%. The plateau is indicative of termination, which can occur via radical coupling reactions. Removing MeOH and using only THF as the solvent (Exp # 2) dramatically affected the reaction kinetics; a first order reaction was observed for almost 30 min, and the conversion was increased to 26% (**Figure 3.3.8 a**). Decreasing the amount of Cu(II) from 0.2 to 0.1 molar equivalents (Exp # 3) did not affect the kinetics or conversion, remaining identical to that of Exp # 2 (**Figure 3.3.8 b**). An increase in temperature from RT to 55 °C (Exp # 4) extended the linear kinetic regime from 30 min to 1 hour. Additionally, monomer conversion increased from 26 to 44% (**Figure 3.3.8 c**). In the absence of Cu(II) (Exp # 5) the kinetic plot (**Figure 3.3.8 d**) showed a similar behaviour to the one with Cu(II) (Exp # 4). However, gel formation was observed, which might be indicative of coupling reactions between propagating

polymer chains. The presence of Cu(II) may have contributed to an increase in the deactivation constant which decreased the concentration of radicals in solution avoiding gel formation. Studies have shown<sup>226,346,347</sup> that gelation may be prevented via the addition of a deactivator or the use of lower reaction temperature. This contributes to a decrease in the rate of polymerization, and thus, a lower concentration of propagating radicals.

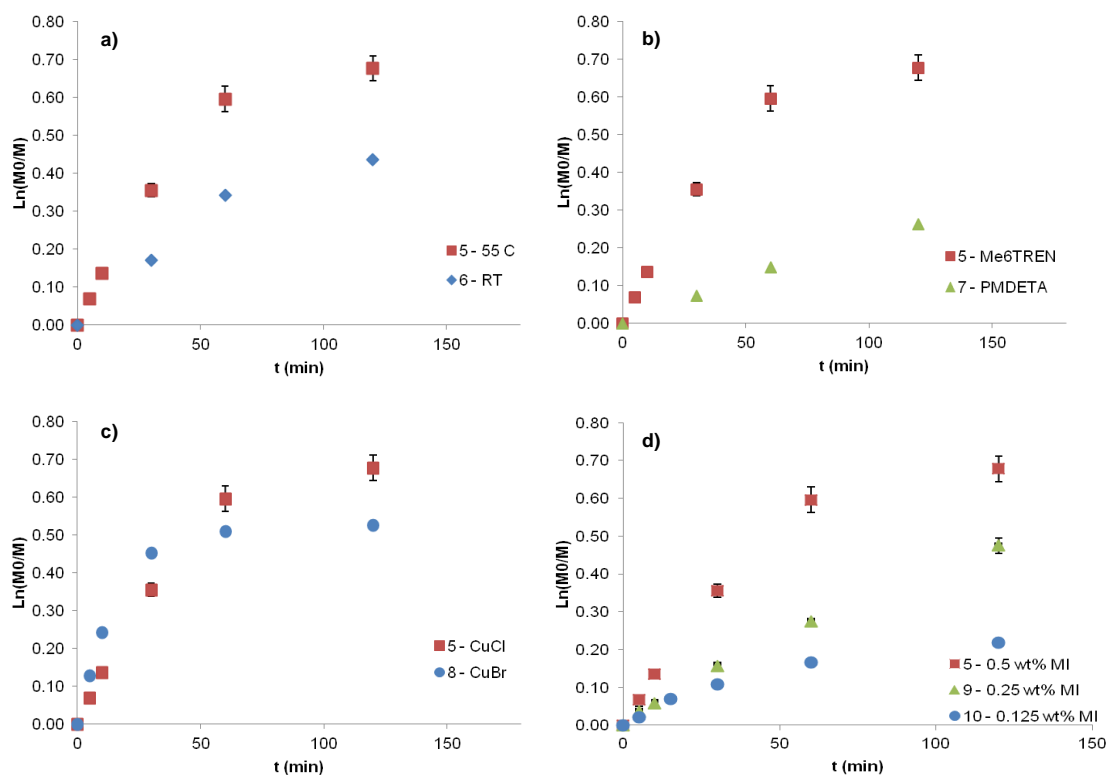


**Figure 3.3.9.** Semi-logarithmic plot of copolymerization of DEGMA and OEGMA, under different experimental conditions, from cellulose-based macroinitiator with high DS. (MI:(DEGMA:OEGMA):Lig:CuX - 1:100:1.2:1; DEGMA:OEGMA = 95:5; solvent: THF). **a)** Effect of Temperature: Exp # 5: 55°C, Exp # 6: RT; **b)** Effect of Ligand: Exp # 5: Me<sub>6</sub>TREN; Exp # 7: PMDETA; **c)** Effect of Halogen: Exp # 5: CuCl, Exp # 8: CuBr; **d)** [MI] wt%: Exp # 5: 0.5, Exp # 9: 0.25, Exp # 10: 0.125.

Note: Exps # 5 and 9 were done in duplicate.

The effect of gel formation on reaction kinetics and conversion was studied by running reactions at 55 °C (Exp # 5) and RT (Exp # 6) (**Figure 3.3.9 a)**). The objective was to decrease the rate of polymerization and avoid gelation, hence lowering the activation constant while increasing the deactivation constant. As expected, lowering the temperature avoided gel

formation, however, monomer conversion decreased from 45 to 29%. Likewise, changing the ligand to PMDETA (Exp # 7), known for its lower activation constant, and hence lower  $K_{\text{ATRP}}$ <sup>170</sup>, also avoided gelation (**Figure 3.3.9 b**). Although the linear kinetic regime extended to more than 2 hours using PMDETA, the rate of polymerization decreased substantially and monomer conversion was only 23%. The effect of the halogen in the catalytic system was also tested; CuCl was replaced by CuBr (Exp # 8). As expected, the rate of polymerization with CuBr increased due to the higher reactivity of C-Br as compared to C-Cl (**Figure 3.3.9 c**). A linear kinetic regime was observed for only 30 min with a conversion of 36%, after which a plateau formed. The higher reactivity of the C-Br present in the propagating chain might have increased the rate of polymerization causing an increment in the radical species and therefore, termination and gel formation.

Dilution is also known as an alternative to decrease the rate of polymerization and therefore avoid termination reactions which might lead to radical coupling between growing polymer chains, and gel formation.<sup>170</sup> Therefore, the reaction mixture was diluted two times (Exp # 9) and 4 times (Exp # 10). As expected, dilution decreased the rate of polymerization. A two-fold dilution (Exp # 9) increased the linear kinetic regime to almost 2 hours with a conversion of 38% and no gel formation was observed (**Figure 3.3.9 d**). Further dilution, Exp # 10, decreased the rate of polymerization even further, but also decreased the linear kinetic regime to approximately 30 min and only 10% conversion (**Figure 3.3.9 d**). Diluting the system decreases the concentration of monomer, which causes the rate of polymerization to decrease. However, termination and other side reactions may still occur at the same rate,<sup>170</sup> thus explaining the low conversion and shorter linear kinetic regime. In this particular system there seems to be an optimal relationship between dilution and monomer concentration, and their impact on the overall conversion and polymerization kinetics.

The number of molar equivalents of monomer, with respect to molar equivalents of MI, was also varied from 100, 50, 25 and 10 equivalents. As illustrated in **Figure 3.3.10** the rate of polymerization ( $R_p$ ) increased as the concentration of monomer (DEGMA+OEGMA) increased. However, the increase was not proportional, as shown in **Equation 3.3.1**.<sup>170</sup>

$$R_p = K_p [M] [P^*]$$

**Equation 3.3.1**

$R_p$ -rate of polymerization;  $K_p$ -propagation constant;  $[M]$ -monomer concentration and  $[P^*]$ -propagating polymer chain

If the concentration of monomer is too high it will cause the  $R_p$  to increase, which manifests in the  $[P^*]$  also being too high. The higher concentration of radicals causes radical coupling reactions between the propagating species (termination), and therefore gelation, as seen in the case of Exp # 5. This might explain why the monomer concentration is not directly proportional to

$R_p$  in this particular case. At lower monomer concentrations, the rate of polymerization was lower and so was the conversion (**Figure 3.3.10** and **Table 3.3.5**).

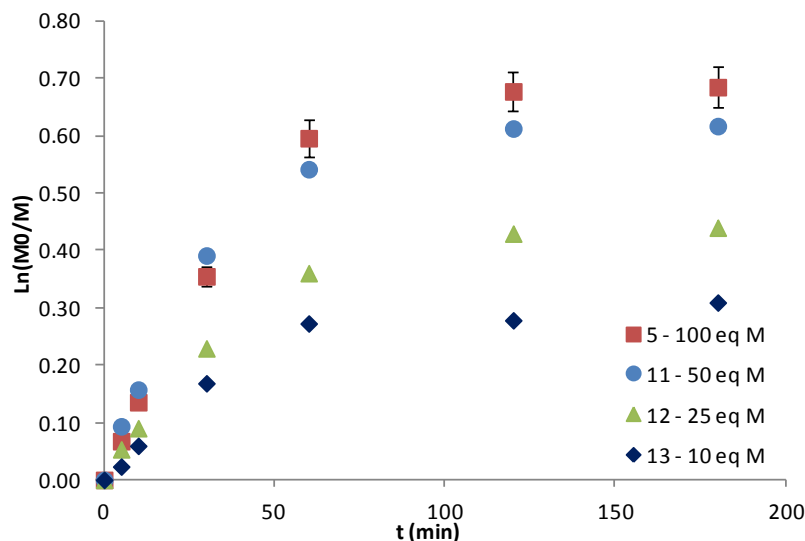


**Figure 3.3.10.** Semi-logarithmic plot of copolymerization of DEGMA and OEGMA from cellulose-based macroinitiator with high DS and with different monomer concentrations. MI:(DEGMA + OEGMA):Lig:CuX: Exp # **5** – 1:100:1.2:1; Exp # **11** - 1:50:1.2:1; Exp # **12** - 1:25:1.2:1; Exp # **13** - 1:10:1.2:1. Ratios were given in molar equivalents with respect to molar equivalents of MI. DEGMA:OEGMA = 95:5; solvent - THF. Exp # 5 was done in duplicate (error bars correspond to  $n = 2$ )

Overall, it was shown the conversion was not complete and the concentration of growing radicals was not constant throughout the chosen reaction time (3 h). Based on the information from the kinetic plots an optimal reaction time was determined in order to generate copolymers within the linear kinetic regime and with similar conversions. Therefore, Exps # 4 to 10 and 13 were run again and final products isolated, purified, as previously described in section 2.3.18 and analyzed by ATR-FTIR,  $^1\text{H}$ -,  $^{13}\text{C}$ -NMR, TGA, DSC, and GPC/MALS; according to their solubility (**Table 3.3.6**). The solubility of the copolymers was tested by preparing solutions with a concentration of 30 wt% copolymer. Common solvents such as, THF,  $\text{CHCl}_3$ , water, DMSO, DMA and DMF were tested however, only THF,  $\text{CHCl}_3$  and water were able to solubilise some of the synthesized copolymers.



**Table 3.3.6.** Set of selected experiments and respective time of reaction, conversion, DP and solubility in THF, CHCl<sub>3</sub> and H<sub>2</sub>O at 0.3 wt% copolymer.

Exp#	Time	Conv% <sup>(a)</sup>	DP <sup>(b)</sup>	THF <sup>(c)</sup>	CHCl <sub>3</sub> <sup>(c)</sup>	H <sub>2</sub> O <sup>(c)</sup>
4	25min	28%	31	yes	yes	no
5	25min	26%	26	no	no	no
6	45min	26%	25	no	no	no
7	2h	25%	26	yes	yes	yes
8	10min	21%	21	no	no	no
9	1h	26%	26	yes	yes	yes*
10	20min	7%	8	yes	yes	no
13	50min	23%	2	no	no	no

<sup>(a)</sup> Conv.% =  $\Delta[M] / [M]$  (calculated from kinetic plots); <sup>(b)</sup> DP =  $\Delta[M] / ([MI] * DS)$  (based on conversion obtained from kinetic plots); <sup>(c)</sup> ~ 90% of the copolymer was dissolved. See **Table 3.3.4** and **Table 3.3.5** for experimental conditions. <sup>(c)</sup> Solubility of the copolymers was tested at 0.3 wt% of the copolymer in respective solvents.

Note: To facilitate the discussion, the copolymers obtained from experiments 4-9, 10 and 13 will be called copolymers # 4-9, 10 and 13.

As previously mentioned, copolymers were collected in the linear kinetic regime at similar conversions. In Exp # 10 the copolymer was collected at 7% conversion of monomer due to the limited conversion of DEGMA and OEGMA into P(DEGMA-co-OEGMA). The reproducibility of this set of experiments was verified and all the results were found to fit the original kinetic plots previously presented, as shown in **APPENDIX-Selected kinetic graphs**. The solubility of the new cellulose-based copolymers was tested in THF, CHCl<sub>3</sub> and water at 0.3 wt% concentration (**Table 3.3.6**). Copolymers # 5, 6, 8 and 13 were not soluble in any of these solvents. On the other hand, copolymers # 4, 9 and 10 were found to be soluble in CHCl<sub>3</sub> and THF. Copolymers # 4 and 10 were not water soluble; however, copolymer # 9 was partially soluble in water (~ 90% in a 3 mg/mL aqueous solution). Finally, copolymer # 7 was soluble in CHCl<sub>3</sub>, THF and water. Similar solubility was observed between copolymers with different DP (copolymers # 9 and 10) and different solubility was observed between copolymers with the same DP (copolymers # 5 and 7). This means that no relation was found between solubility and DP.

To verify whether DEGMA and OEGMA polymerize by itself an ATRP polymerization was done in the absence of macroinitiator under the exact same conditions as Exp # 9. The reaction mixture was analyzed by <sup>1</sup>H-NMR which showed exclusively unreacted DEGMA and OEGMA, the spectrum can be found in **APPENDIX-Selected NMR spectra**.

The materials were characterized by ATR-FTIR (**Figure 3.3.11**),  $^1\text{H}$ - and  $^{13}\text{C}$ -NMR (**Figure 3.3.12** and **Figure 3.3.13**, respectively). The spectra obtained from the different samples were similar and therefore here are shown representative spectra.

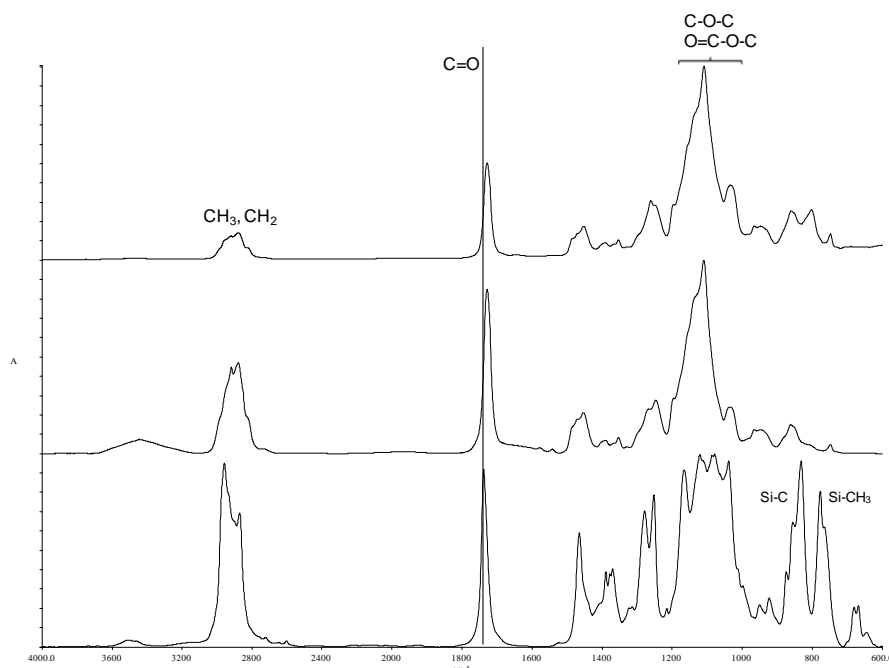


**Figure 3.3.11.** Comparison of ATR-FTIR spectra of cellulose-based macroinitiator with high (DS = 1) DS (bottom), P(DEGMA<sub>90</sub>-co-OEGMA<sub>10</sub>) (middle) and the synthesized 3-O-(3-O-(2-bromoisobutryl)-hydroxypropyl)-2,6-O-TDMS cellulose-g-P(DEGMA<sub>95</sub>-co-OEGMA<sub>5</sub>) (top).

The ATR-FTIR spectrum of the macroinitiator showed typical C=O stretching peak ( $\nu_{\text{C=O}}$ ) at  $1735\text{ cm}^{-1}$  from the initiator 2-bromoisobutryl moiety. However, when grafting the copolymer (DEGMA<sub>5</sub>-co-OEGMA<sub>95</sub>) from the cellulose-based macroinitiator the appearance of a new C=O stretching peak ( $\nu_{\text{C=O}}$ ) at  $1726\text{ cm}^{-1}$  was observed and corresponds to the ester bond of the grafted copolymer, as described in the literature.<sup>10,221</sup> This observation was supported by the FTIR of poly(DEGMA<sub>90</sub>-co-OEGMA<sub>10</sub>), previously synthesized for reference purposes (**Figure 3.3.11 middle**).

The successful grafting of P(DEGMA<sub>95</sub>-co-OEGMA<sub>5</sub>) from the regioselectively substituted cellulose-based macroinitiator through ATRP was evaluated by  $^1\text{H}$ - and  $^{13}\text{C}$ -NMR (**Figure 3.3.12** and **Figure 3.3.13**). Considering that the methylene groups and the methoxy group of the ethylene glycol fraction of P(DEGMA<sub>95</sub>-co-OEGMA<sub>5</sub>) overlap with the AGU protons of the cellulose macroinitiator, it was not expected to see those peaks in the  $^1\text{H}$ -NMR spectra.<sup>221</sup> The

partial hydrolysis of the grafted  $P(\text{DEGMA}_{95}\text{-co-OEGMA}_5)$  would have been ideal to detect the latter's protons as well as the AGU protons, however the attempts made to hydrolyze the copolymer grafts were unsuccessful. Therefore, to confirm the successful grafting, the peaks from the functional groups of the cellulose-based macroinitiator, TDMS and propyl, were used. This approach has been used for other cellulose derivatives where the AGU protons were not visible and the functional groups from the cellulose-based macroinitiator, such as methyl<sup>13</sup> and ethyl<sup>10,161</sup> were used to verify the successful graft copolymerization. The ratio of DEGMA:OEGMA present in the synthesized copolymers was calculated from the  $^1\text{H-NMR}$ , as described elsewhere.<sup>221</sup> The ratios of DEGMA:OEGMA were found to be 90:10 for  $P(\text{DEGMA-co-OEGMA})$  and 95:5 for the cellulose-based copolymers soluble in  $\text{CHCl}_3$ .

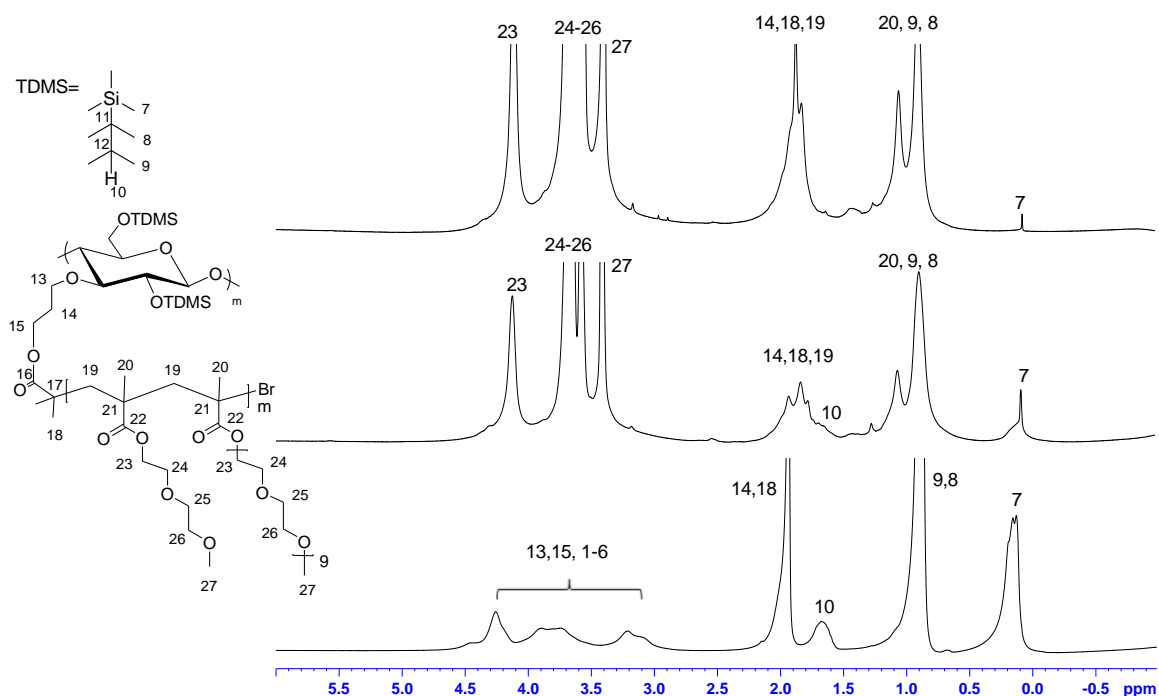


**Figure 3.3.12.** Comparison of  $^1\text{H-NMR}$  spectra of cellulose-based macroinitiator with high DS (bottom) and the synthesized 3-O-(3-O-(2-bromoisobutyryl)-hydroxypropyl)-2,6-O-TDMS cellulose-*g*-( $P(\text{DEGMA}_{95}\text{-co-OEGMA}_5)$ ) with lower (middle) and higher (top) DP of  $P(\text{DEGMA}_{95}\text{-co-OEGMA}_5)$ , see **Scheme 3.3.3**.

The  $^1\text{H-NMR}$  spectrum obtained from the cellulose-based copolymer with a higher DP (**Figure 3.3.12 top**) exhibited peaks mainly from the grafted copolymer ( $P(\text{DEGMA}_{95}\text{-co-OEGMA}_5)$ ). Peaks 19 and 20 correspond to the methylene and methyl protons in the backbone of the methyl ether methacrylate, respectively, while peak 27 is due to methyl protons in the

ethylene glycol chain, peak 23 the methylene protons linked to the ester group of the ethylene glycol chain, and finally peaks 24 to 26 are associated with the methylene groups from the same chain. The only signals from the macroinitiator are peaks 7, 9 and 8 however, peak 7 has a very low intensity and peaks 9 and 8 overlap with peak 20. On the other hand, the  $^1\text{H}$ -NMR spectrum of the cellulose-based copolymer with a lower DP (**Figure 3.3.12 middle**) clearly shows peak 7 as well as peaks 9 and 8. As mentioned above the protons from the AGU were not detected because they overlap with the protons from P(DEGMA<sub>95</sub>-co-OEGMA<sub>5</sub>). The DP could not be calculated from the  $^1\text{H}$ -NMR spectra because the peaks from the macroinitiator and the grafted copolymer overlap. The graft copolymers 3-O-(3-O-(2-bromoisobutryl)-hydroxypropyl)-2,6-O-TDMS-cellulose-*g*-(P(DEGMA<sub>95</sub>-co-OEGMA<sub>5</sub>)) with higher and lower DP of P(DEGMA<sub>95</sub>-co-OEGMA<sub>5</sub>) were also analyzed by  $^{13}\text{C}$ -NMR, **Figure 3.3.13**.

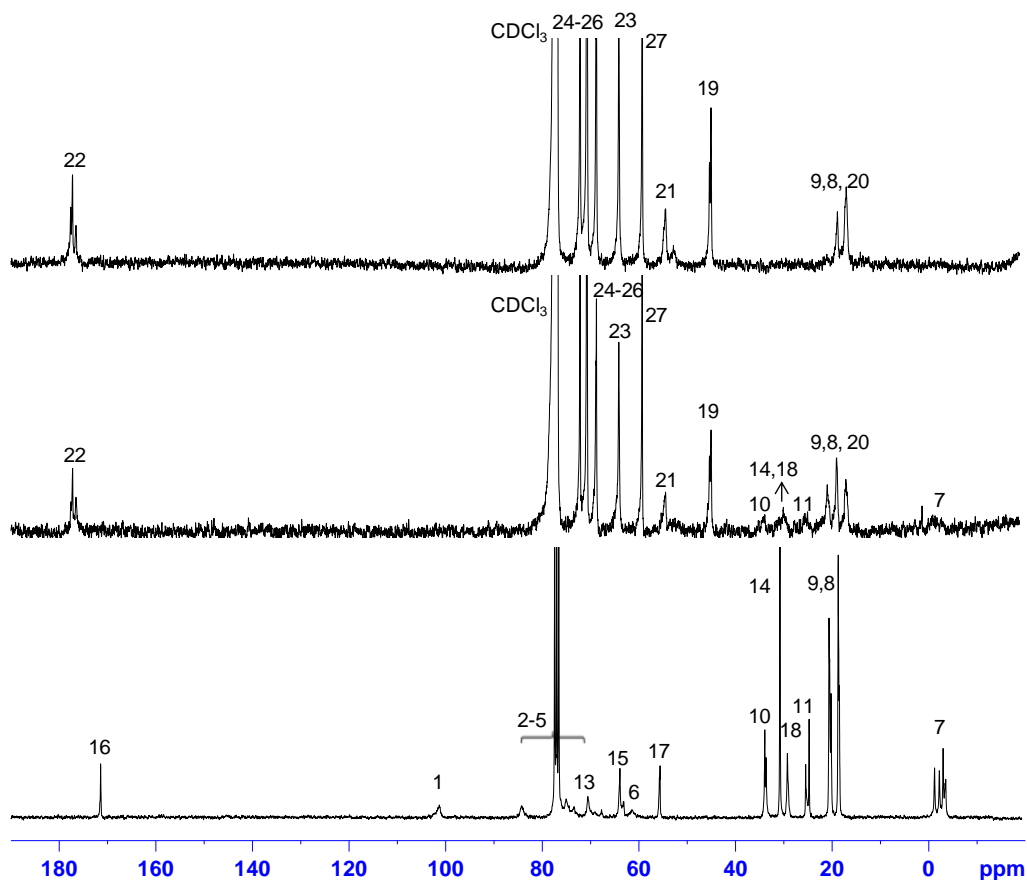


**Figure 3.3.13.** Comparison of  $^{13}\text{C}$ -NMR spectra of cellulose-based macroinitiator with high DS (bottom) and the synthesized 3-O-(3-O-(2-bromoisobutryl)-hydroxypropyl)-2,6-O-TDMS cellulose-*g*-(P(DEGMA<sub>95</sub>-co-OEGMA<sub>5</sub>)) with a lower (middle) and higher (top) DP of P(DEGMA<sub>95</sub>-co-OEGMA<sub>5</sub>). See **Scheme 3.3.3** and **Figure 3.3.12** for the identification of the peaks.

The  $^{13}\text{C}$ -NMR of the cellulose-based copolymer in **Figure 3.3.13 top**, clearly shows the peaks associated with the  $\text{P}(\text{DEGMA}_{95}\text{-co-OEGMA}_5)$ ; the methylene (peak 19) and methyl (peak 20) carbons from the methacrylate backbone, as well as those from the ethylene glycol side chains (peaks 21, 23, 24-27), including the  $\text{C=O}$  group (peak 22). However, no peaks from the cellulose-based macroinitiator were detected, to the exception of TDMS peaks 8 and 9 which overlap with peak 20. On the other hand, the  $^{13}\text{C}$ -NMR of 3-O-(3-O-(2-bromoisobutyryl)-hydroxypropyl)-2,6-O-TDMS-cellulose-*g*-( $\text{P}(\text{DEGMA}_{95}\text{-co-OEGMA}_5)$ ) with a lower DP, **Figure 3.3.13 middle**, clearly shows carbon peaks from TDMS (7, 8, 9, 10 and 11) and propyl (14), both functional groups of the cellulose-based macroinitiator. Therefore, the successful grafting of  $\text{P}(\text{DEGMA}_{95}\text{-co-OEGMA}_5)$  from 3-O-(3-O-(2-bromoisobutyryl)-hydroxypropyl)-2,6-O-TDMS cellulose was confirmed through the detection of the cellulose-based macroinitiator functional groups TDMS and propyl through  $^1\text{H}$ - and  $^{13}\text{C}$ -NMR analyses.

The cellulose-based copolymers were also subjected to thermal analysis by TGA and DSC to determine the decomposition temperature ( $T_d$ ) and glass transition temperature ( $T_g$ ), respectively. The objective was to correlate thermal properties with DP and solubility.

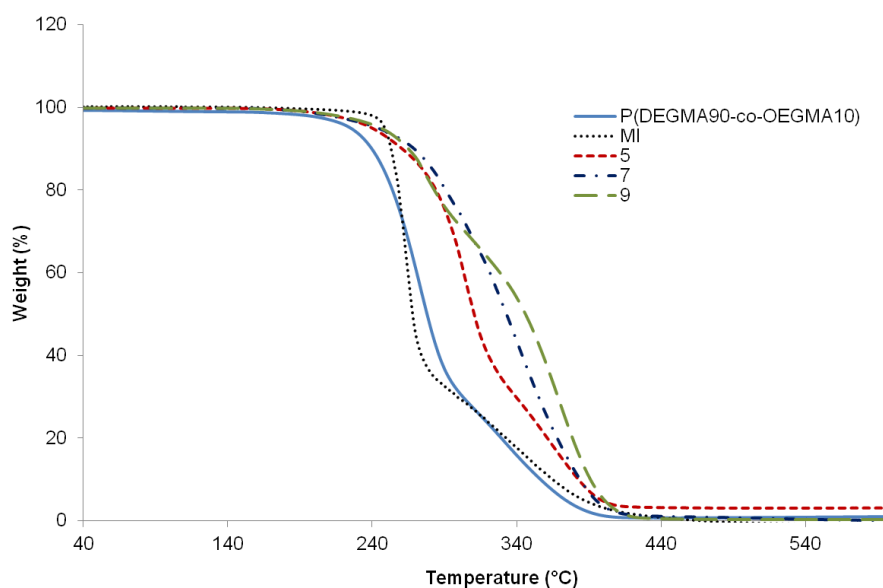


**Figure 3.3.14.** Comparison of TGA thermograms of  $\text{P}(\text{DEGMA}_{90}\text{-co-OEGMA}_{10})$ , MI (macroinitiator) and copolymers # 5, 7 and 9.

**Figure 3.3.14** shows the weight loss curves obtained from copolymers # 5, 9 and 7 along with that of the macroinitiator (MI) and P(DEGMA<sub>90</sub>-co-OEGMA<sub>10</sub>). The cellulose-based copolymers were selected based on solubility; copolymer # 5 was not soluble in water, THF or CHCl<sub>3</sub>, copolymer # 9 was partially soluble in water (~ 90% in a 3 mg/mL aqueous solution) and soluble in CHCl<sub>3</sub> and THF, and copolymer # 7 was soluble in CHCl<sub>3</sub>, THF and water (**Table 3.3.6**). The TGA measurements were done in duplicate and respective RPDs% were calculated as per **Equation 3.1.1** and found not to exceed 3%. A table with the values of the duplicates and respective RPDs% can be found in **APPENDIX-Duplicates and respective RPDs%**. The primary decomposition temperatures were determined based on the first derivative of the weight loss curve and weight losses below 5% were not considered, see **APPENDIX-Selected first derivative of TGA thermograms** and **Table 3.3.7**. Thermograms showed that the macroinitiator and P(DEGMA<sub>90</sub>-co-OEGMA<sub>10</sub>) had similar decomposition profiles (**Figure 3.3.14** and **Table 3.3.7**). The macroinitiator had two Tds at 271 °C and 349 °C as did the synthesized copolymer, P(DEGMA<sub>90</sub>-co-OEGMA<sub>10</sub>), at 269 °C and 333 °C. Although P(DEGMA<sub>90</sub>-co-OEGMA<sub>10</sub>) did not have the same ratio as the grafted copolymer (P(DEGMA<sub>95</sub>-co-OEGMA<sub>5</sub>)), the components were the same. Therefore, in this study P(DEGMA<sub>90</sub>-co-OEGMA<sub>10</sub>) was used as a reference.

**Table 3.3.7.** Decomposition temperature of macroinitiator, P(DEGMA<sub>90</sub>-co-OEGMA<sub>10</sub>) and cellulose-based graft copolymers and complementing information concerning DP.

Copolymer	DP <sup>(a)</sup>	Td <sub>1</sub> (°C)	Td <sub>2</sub> (°C)	Td <sub>3</sub> (°C)	Td <sub>4</sub> (°C)
Macroinitiator	N/A	271	349	-	-
P(DEGMA <sub>90</sub> -co-OEGMA <sub>10</sub> )	81	269	333	-	-
4	31	288	301	-	-
9	26	277	370	-	-
10	8	290	374	-	-
13	2	319	368		-
5	26	245	303	363	-
8	21	234	274	368	
6	25	300	316	357	-
7	26	290	310	326	340

<sup>(a)</sup> DP =  $\Delta[M] / ([MI] * DS)$  (based on conversion obtained from kinetic plots). See **Table 3.3.4** and **Table 3.3.5** for experimental conditions. The copolymer numbers refer to the experiment numbers as described in **Table 3.3.4** and **Table 3.3.5**.

Note: The Td analyses were done in duplicate and RPDs% found to be not higher than 3%. A table with duplicate values and respective RPDs% can be found in **APPENDIX-Duplicates and respective RPDs%**.

Td values of the macroinitiator and P(DEGMA<sub>90</sub>-co-OEGMA<sub>10</sub>) were within the range of Tds found for the cellulose-based copolymers (234-374 °C), **Table 3.3.7**. The different cellulose-based copolymers showed different numbers of Tds. For that reason they were grouped accordingly: copolymers # 4, 9, 10 and 13 exhibited two Tds; copolymers # 5, 6 and 8 three Tds and copolymer # 7 four Tds (**Table 3.3.7**). We tried to establish a correlation between the number of Tds and solubility. Copolymers with two Tds (# 4, 9, 10 and 13) were soluble in THF and CHCl<sub>3</sub> with the exception of copolymer # 13 which was insoluble in water, THF and CHCl<sub>3</sub>, the same behaviour found for copolymers # 5, 6 and 8. Copolymer # 7, which had four Tds, was soluble in water, THF and CHCl<sub>3</sub>. Unfortunately, no correlation was established between the Td values within the three groups. Likewise, no clear correlation was established between Tds and DPs.

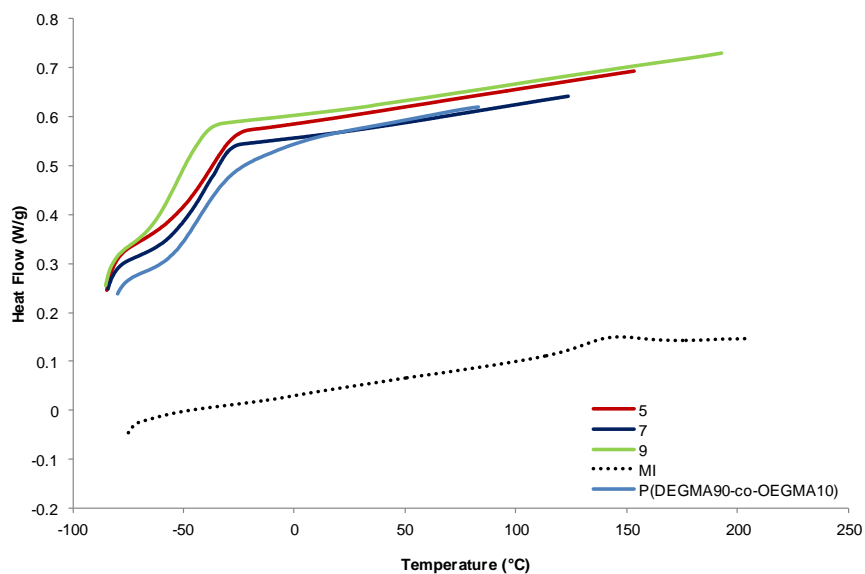


**Figure 3.3.15.** Comparison of DSC thermograms of P(DEGMA<sub>90</sub>-co-OEGMA<sub>10</sub>), MI (macroinitiator) and copolymers # 5, 7 and 9.

**Table 3.3.8.** Glass transition temperature of macroinitiator, P(DEGMA<sub>90</sub>-co-OEGMA<sub>10</sub>) and cellulose-based graft copolymers and complementing information concerning DP and solubility.

Copolymer	DP <sup>(a)</sup>	THF	CHCl <sub>3</sub>	H <sub>2</sub> O	T <sub>g</sub> (°C)
MI	N/A	yes	yes	no	129
P(DEGMA <sub>90</sub> -co-OEGMA <sub>10</sub> )	81	no	yes	no	-43
4	31	yes	yes	no	-40
5	26	no	no	no	-39
6	25	no	no	no	-36
7	26	yes	yes	yes	-40
8	21	no	no	no	-39
9	26	yes	yes	yes*	-51
10	8	yes	yes	no	-35
13	2	no	no	no	-25

<sup>(a)</sup> DP =  $\Delta[M] / ([MI] \cdot DS)$  (based on conversion calculated from kinetic plots); <sup>(\*)</sup> ~ 90% soluble in a 3 mg/mL aqueous solution. See **Table 3.3.4** and **Table 3.3.5** for experimental conditions. DSC measurements were done in duplicate and the respective RPDs% were calculated as per **Equation 3.1.1** and did not exceed 2%, **APPENDIX-Duplicates and respective RPDs%**.

**Figure 3.3.15** shows representative DSC thermograms of the isolated cellulose-based copolymers and respective T<sub>g</sub>s in **Table 3.3.8**. The DSC thermograms of the residual cellulose-based copolymers, as well as the duplicate values and respective RPDs% can be found in **APPENDIX-Selected DSC thermograms and Duplicates and respective RPDs**. The T<sub>g</sub> of P(DEGMA<sub>90</sub>-co-OEGMA<sub>10</sub>) was determined to be - 43 °C, which is very close to the – 45 °C value reported in the literature for the same copolymer.<sup>348</sup> Thus, the T<sub>g</sub> of copolymer P(DEGMA<sub>95</sub>-co-OEGMA<sub>5</sub>) is expected to be slightly higher, because of the higher fraction of DEGMA, which decreases the mobility of the methacrylate backbone as a result of the shorter side chains.<sup>348</sup> The T<sub>g</sub> of the cellulose-based macroinitiator was determined to be 129 °C, substantially higher than the one found for P(DEGMA<sub>90</sub>-co-OEGMA<sub>10</sub>). This difference would be attributed to the rigidity of the backbone of the macroinitiator compared to the more flexible P(DEGMA<sub>90</sub>-co-OEGMA<sub>10</sub>). Therefore, the T<sub>g</sub> values for the newly synthesized cellulose-based copolymers are expected to be between the T<sub>g</sub>s of the two components. Copolymers # 4 to 8 (DP = 31-21) exhibited T<sub>g</sub>s between - 40 and - 36 °C. These values are higher than the T<sub>g</sub> of P(DEGMA<sub>90</sub>-co-OEGMA<sub>10</sub>) (- 43 °C) and might be due to the cellulose-based macroinitiator component. However, the T<sub>g</sub> of copolymer # 9 (DP = 26) was - 51 °C, lower than anticipated. Copolymer # 10, which had a DP of 8 had a T<sub>g</sub> of - 35 °C and copolymer # 13 (DP = 2) had a T<sub>g</sub> of - 25 °C. With the exception of copolymer # 9, there appears to be a trend in which T<sub>g</sub> increases with decreasing P(DEGMA<sub>95</sub>-



co-OEGMA<sub>5</sub>) DP as shown in **Figure 3.3.16**. The odd behaviour of copolymer # 9 could be explained by an increment in chain mobility which would cause the lower T<sub>g</sub>. As mentioned in the literature, this could be achieved with an increment of OEGMA component in the P(DEGMA<sub>x</sub>-co-OEGMA<sub>y</sub>) as compared to P(DEGMA<sub>95</sub>-co-OEGMA<sub>5</sub>).<sup>348</sup> Further studies are necessary in order to fully understand this behaviour.

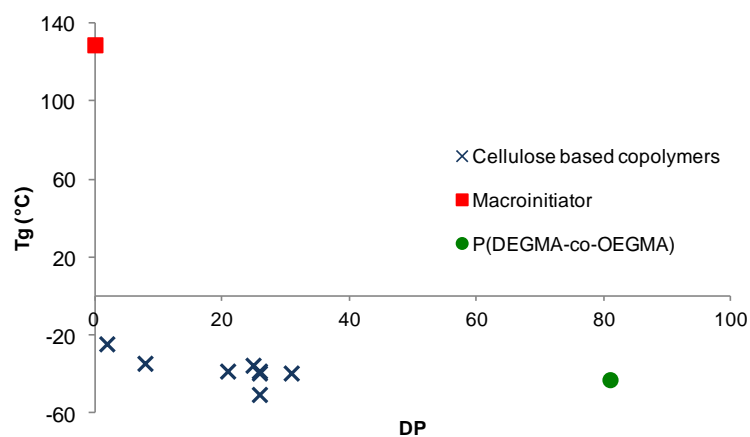


**Figure 3.3.16.** Chart illustrating relation between T<sub>g</sub> (°C) and DP of P(DEGMA<sub>90</sub>-co-OEGMA<sub>10</sub>), macroinitiator and cellulose-based graft copolymers

**Table 3.3.9.** DP,  $Mn_{(th)}$ ,  $Mn_{(GPC-MALS)}$  and PDI of macroinitiator and respective cellulose-based graft copolymers.

Exp#	DP <sup>(a)</sup>	$Mn_{(th)}$ <sup>(b)</sup> (g/mol)	$Mn_{(GPC/MALS)}$ (g/mol)	PDI <sub>(GPC/MALS)</sub>
MI <sup>(c)</sup>			$4.4 \cdot 10^4$	1.5
4	31	$4.3 \cdot 10^5$	$1.3 \cdot 10^6$	4.2
7	26	$4.0 \cdot 10^5$	$6.1 \cdot 10^5$	4.3
9	26	$4.0 \cdot 10^5$	$8.6 \cdot 10^6$	1.8
10 <sup>(d)</sup>	8	$1.5 \cdot 10^5$	$2.3 \cdot 10^5$	2.4

<sup>(a)</sup>  $DP = \Delta[M] / ([MI] \cdot DS)$  (based on conversion calculated from kinetic plots); <sup>(b)</sup>  $Mn_{(th)} = Mn_{(MI)} + [(0.95 \cdot MM_{DEGMA} + 0.05 \cdot MM_{OEGMA}) \cdot DP \cdot I.S.]$ ; MI = macroinitiator, MM = molar mass, DP = degree of polymerization; Initiating sites(I.S.) =  $Mn_{(MI)} / MM_{(Repeating\ unit)} \cdot DS$ ; <sup>(c)</sup> C3 macroinitiator with DS = 1; <sup>(d)</sup> bimodal. See **Table 3.3.4** and **Table 3.3.5** for experimental conditions. The GPC-MALS analysis were done in duplicate and the different RPDs% were calculated as per **Equation 3.1.1**, and found to be below 9%.

Cellulose-based copolymers soluble in THF were analyzed in duplicate by GPC-MALS to determine the Mn and PDI. A table with the duplicate values and respective RPDs% can be found in **APPENDIX-Duplicates and respective RPDs%**. Overall, the Mn theoretical values of the cellulose-based copolymers were considerably lower than the Mn determined by GPC-MALS, which might be due to radical coupling reactions between the growing polymer chains. Furthermore, the high values of the PDIs (1.8 to 4.3) revealed polydisperse copolymers (**Table 3.3.9**). These results are indicative of a lack of control during ATRP and may explain the unexpected solubility/insolubility of these copolymers. In Exp # 4, Cu(II) was used and the resulting copolymer (copolymer # 4) was found to be polydisperse (PDI = 4.2). This behaviour might be due to the higher temperature (55 °C) used in this reaction which caused an increment in the rate of polymerization when compared to the same reaction at room temperature (Exp # 3 vs. Exp # 4, **Figure 3.3.8 c**). In Exp # 7 PMDETA, a lower activity ligand, was used at 55 °C. Although the rate of polymerization decreased (**Figure 3.3.9 b**) the obtained PDI was also higher than desired. When diluting the system two times (Exp # 9, **Figure 3.3.9 d**) the PDI decreased substantially due to a potential decrease in termination reactions. However, when the dilution was increased by a factor of four the PDI increased from 1.8 to 2.4.

The chromatograms obtained from light scattering and RID were found to be dramatically different, **Figure 3.3.17**.

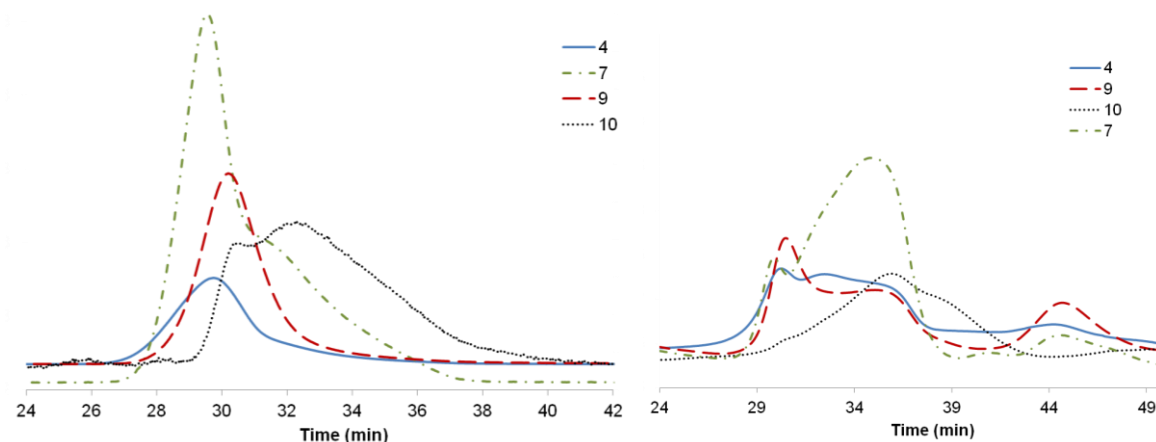


**Figure 3.3.17.** MALS (left) and RID (right) chromatograms of cellulose-based graft copolymers.

Light scattering chromatograms in **Figure 3.3.17** showed a bimodal peak for copolymer # 10 and a peak with a shoulder for copolymer # 7. On the other hand, copolymers from exps # 4 and 9 appear to be more homogeneous. However, when analysing the RID signal of the chromatograms, all the copolymers had a multi-modal molecular weight distribution. The intensity of these peaks was low and it might be reflective of sample loss during the processing. This was confirmed by calculating the percentage of mass recovery: 33, 33, 51 and 48% for copolymers # 4, 9, 10 and 7, respectively. Sample loss might have occurred while filtering the solution prior to analysis or a fraction of the sample was retained on the GPC column. Therefore, the values obtained through light scattering and RID were not representative of the entire material. Furthermore, it was not possible to calculate the  $dn/dc$  of the cellulose-based copolymers because the unfiltered samples displayed a high signal to noise ratio compromising the final results. Therefore, the  $dn/dc$  was calculated based on the  $dn/dc$  of the individual components and their weight fraction ( $W_x$ ) according to **Equation 3.3.2**.<sup>349</sup>

$$\frac{dn}{dc} = \frac{dn}{dc}_{MI} W_{MI} + \left[ \left( \frac{dn}{dc}_{DEGMA} W_{DEGMA} \right) + \left( \frac{dn}{dc}_{OEGMA} W_{OEGMA} \right) \right] \quad \text{Equation 3.3.2}$$

The cellulose-based copolymers are composed of the macroinitiator (dn/dc was previously calculated and found to be 0.0873 mL/g), POEGMA<sub>475</sub> with a dn/dc of 0.1146 mL/g<sup>350</sup> in THF and PDEGMA. The dn/dc of PDEGMA was not found in the literature, however, the dn/dc of poly(methoxyethyl methacrylate) in THF has been reported to be 0.077 mL/g.<sup>349</sup> The only difference between these two copolymers is the number of ethylene oxide groups, DEGMA has 2 and methoxyethyl methacrylate has one. Therefore, the dn/dc for PDEGMA was approximated at 0.077 mL/g. The weight composition of the DEGMA and OEGMA components of the P(DEGMA-co-OEGMA) was calculated based on the <sup>1</sup>H-NMR of the cellulose-based copolymers as described elsewhere.<sup>221</sup> The dn/dc of P(DEGMA<sub>95</sub>-co-OEGMA<sub>5</sub>) was first determined as described above, and found to be ~ 0.079 mL/g. The weight fraction of the cellulose macroinitiator was calculated based on the integration peak of TDMS at 0.08 ppm (12 protons) and the peak at 4.1 ppm which corresponds to P(DEGMA-co-OEGMA) (2 protons), **Figure 3.3.12**. Considering the low intensity of the TDMS peak these dn/dc values should be considered an approximation (**Table 3.3.10**).

**Table 3.3.10.** dn/dc values of the different cellulose-based graft copolymers

AXV	dn/dc (mL/g)
4	0.079
7	0.079
9	0.079
10	0.080

In light of the discussion above, the Mn determined by GPC-MALS is not representative of the entire sample. Furthermore, in work developed elsewhere<sup>351–353</sup> it was found that the determination of the molecular weight of copolymers through GPC-MALS is very challenging. The heterogeneity in chemical composition of the copolymer, means the dn/dc will often vary along the chromatogram and introduce errors in the calculation of the molecular weight. Another alternative would be to hydrolyze the grafted copolymer chains. However, this was not possible due to the presence of multiple ester linkages in the grafted copolymer. Although, completely hydrolyzed from the cellulose backbone P(DEGMA<sub>95</sub>-co-OEGMA<sub>5</sub>) grafts would also be fragmented generating a variety of small fragments and a very complex GPC profile. Despite this multiple attempts were made to hydrolyze the grafted P(DEGMA<sub>95</sub>-co-OEGMA<sub>5</sub>) but unfortunately were not successful; producing many insoluble fragments making GPC analysis impossible. The thermoresponsive behaviour of the cellulose-based copolymers was also assessed. Water

soluble copolymers # 7 and 9 had their lower critical solution temperatures (LCSTs) determined. Aqueous solutions (3 mg/mL) were prepared and the increment in turbidity with temperature was measured by UV-Vis spectroscopy and expressed as absorbance curves. The temperature was controlled through an immersed probe on top of the solutions. The LCST of P(DEGMA<sub>95</sub>-co-OEGMA<sub>5</sub>) is expected to be 32 °C,<sup>286</sup> however, with the introduction of a hydrophobic component and a decrease in the mobility of the copolymer grafts, a decrease in LCST was anticipated.<sup>10,221</sup> The LCST in water was measured based on the highest peak of the first derivative of the absorbance curve, see **APPENDIX-Selected first derivative of the absorbance curves from UV-Vis spectra/LCST**. The analyses were done in duplicate and a RPD% (**Equation 3.1.1**) of less than 3% was obtained. A table with the duplicate values and respective RPDs% is available in **APPENDIX-Duplicates and respective RPDs%**.

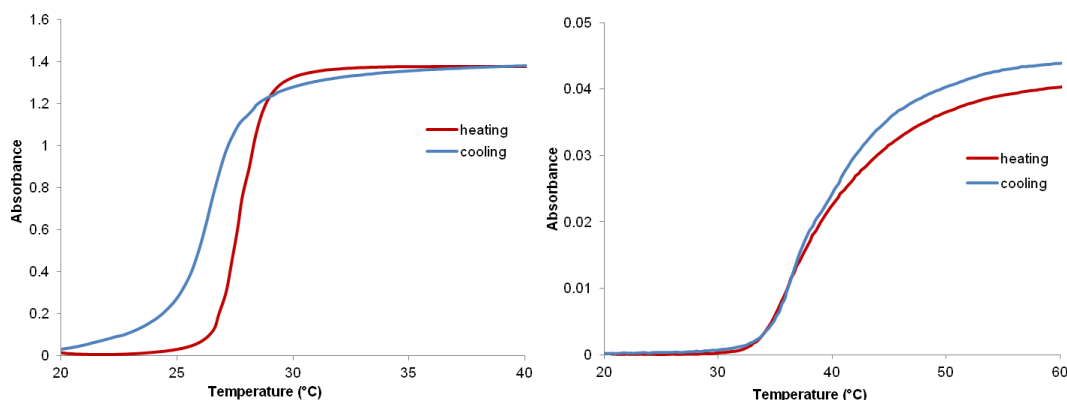


**Figure 3.3.18.** Absorbance vs. temperature plot illustrating the LCST of cellulose-based graft copolymers # 7 (left) and 9 (right) at a wavelength of 670 nm.

The LCST of copolymer # 7 (**Figure 3.3.18 (left)**) was determined to be 28 °C in the heating cycle and 26 °C in the cooling cycle. The transition observed in the heating cycle was sharp. However, a broad hysteresis was observed in the cooling cycle. This behaviour might have been caused by slow rehydration, formation of H-bonded network or crystallization during the phase separation.<sup>354</sup> On the other hand, the absence of a stirring system did not allow a homogeneous distribution of the temperature throughout the solution. As mentioned above, a LCST below 32 °C was anticipated due to the presence of the hydrophobic cellulose-based macroinitiator. Copolymer # 9 had a LCST at 36 °C in the heating cycle and 37 °C in the cooling cycle and in comparison to copolymer # 7, it exhibited a more uniform thermal profile. The LCST of 36 / 37 °C was higher than anticipated. This might be due to the presence of a higher amount of OEGMA in the P(DEGMA<sub>x</sub>-co-OEGMA<sub>y</sub>) component of copolymer # 9 as compared to P(DEGMA<sub>5</sub>-co-

OEGMA<sub>95</sub>).<sup>286</sup> This observation is in accordance to the lower T<sub>g</sub> previously determined for copolymer # 9 (**Table 3.3.8**).

The remaining cellulose-based copolymers were not water soluble and therefore their LCST could not be determined by turbidity measurements. As described elsewhere, DSC would have been a good alternative,<sup>13</sup> however, we were not able to detect any transition for our cellulose-based copolymers by DSC. Thus the thermoresponsive behaviour of the water insoluble copolymers was visually observed using 3 mg/mL aqueous suspensions that were heated to 60 °C (**Figure 3.3.19** and **Figure 3.3.20**). Although the copolymers were not water-soluble it was possible to visually observe whether or not an alteration in the appearance occurred for the different materials.

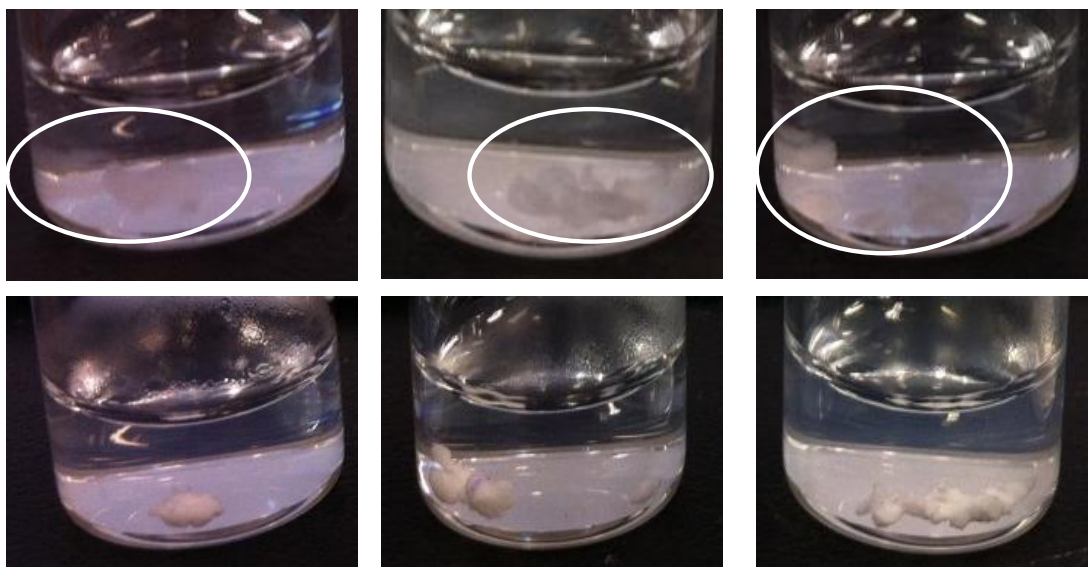


**Figure 3.3.19.** Thermoresponsive behaviour of cellulose-based graft copolymers. From left to right, copolymers # 4, 5, 6, at RT (top) and at 60 °C (bottom).

The insoluble copolymers # 4, 5 and 6 (**Figure 3.3.19 top**, from left to right) were translucent in water at room temperature. However, when the temperature increased to 60 °C the materials became opaque demonstrating the thermoresponsive behaviour (**Figure 3.3.19 bottom**).

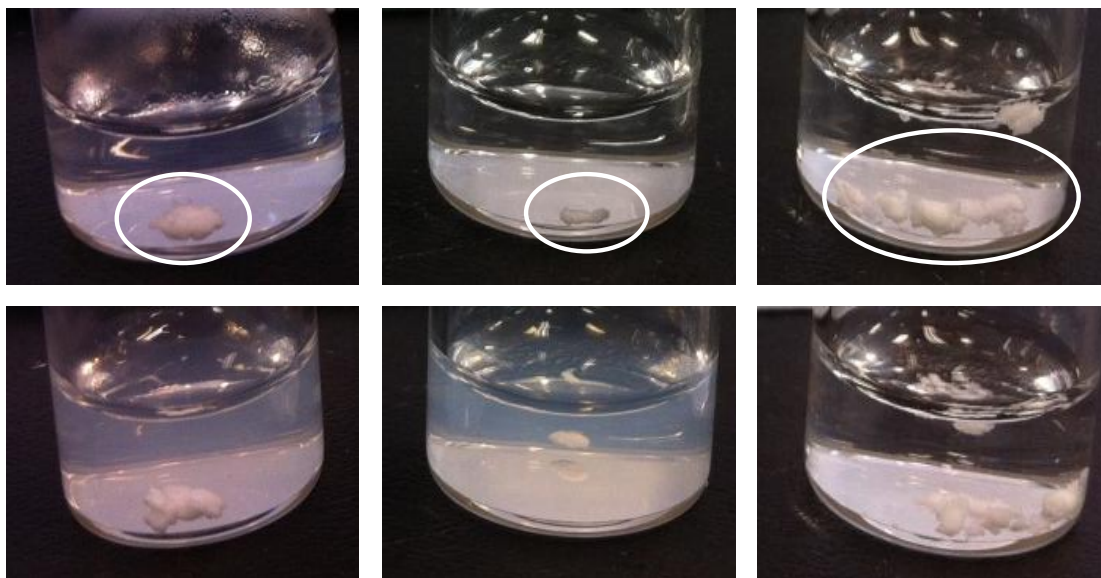


**Figure 3.3.20.** Thermoresponsive behaviour of cellulose-based graft copolymers. From left to right, copolymers # 8, 10 and 13 at RT (top) and at 60 °C (bottom).

The same procedure was followed for copolymers # 8, 10 and 13 (left to right in **Figure 3.3.20**). The three materials were opaque at RT (**Figure 3.3.20 top**) and no visual alteration was observed when the temperature was increased to 60 °C (**Figure 3.3.20 bottom**). This does not mean that the materials are not thermoresponsive; it may be that their DPs are not high enough to yield a visual response to temperature.

After fully characterizing the cellulose-based copolymers it was decided to choose copolymer # 9 to study the evolution of  $M_n$  with conversion. This decision was based on the PDI, the lowest obtained for these cellulose-based copolymers ( $PDI = 1.8$ ). This value is considered high for ATRP but expected, taking into account the high molecular weight of copolymer # 9, the polydisperse nature of the macroinitiator, and the difficulty in the analysis by GPC-MALS. In **Figure 3.3.21** the respective kinetic plot is presented as well as the fractions collected at different reaction times, 5, 15 min and 1 hour.

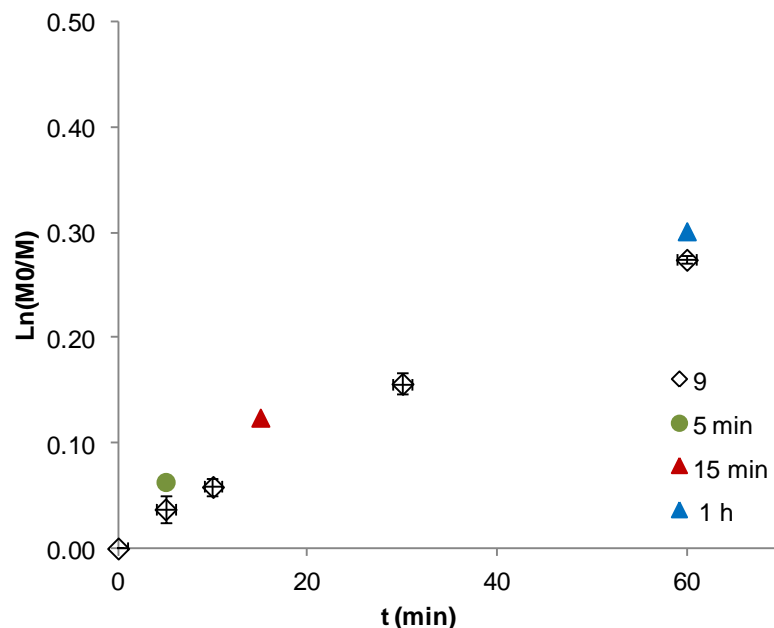


**Figure 3.3.21.** Semi-logarithmic plot of copolymerization of DEGMA and OEGMA from cellulose-based macroinitiator (Exp # 9) and respective data collected at different reaction times. MI:(DEGMA:OEGMA):Lig:CuX - 1:100:1.2:1; DEGMA:OEGMA = 95:5; solvent: THF, room temperature. Experiment # 9 (diamond) was done in duplicate.

The individual kinetic points collected at 5, 15 min and 1 hour fit the original curve obtained for Exp # 9. The collected copolymers were then characterized by GPC-MALS to determine their respective Mn and PDI values (**Table 3.3.11**). The duplicate values of each Mn and respective RPDs% can be found in **APPENDIX-Duplicates and respective RPDs%**.



**Table 3.3.11.** Characterization of cellulose-based graft copolymers at different reaction times.

Exp#	Time <sup>(a)</sup>	Conv(%) <sup>(b)</sup>	DP <sup>(c)</sup>	Mn <sub>(th)</sub> <sup>(d)</sup>	Mn <sub>(GPC/MALS)</sub>	PDI <sub>(GPC/MALS)</sub>
9-5min	5 min	6	7	1.3*10 <sup>5</sup>	8.4*10 <sup>5</sup>	2.4
9-15min	15 min	10	10	1.8*10 <sup>5</sup>	2.7*10 <sup>6</sup>	2.1
9-1h	1h	26	26	4.0*10 <sup>5</sup>	8.6*10 <sup>6</sup>	1.8

<sup>(a)</sup> Time within linear kinetic regime was observed <sup>(b)</sup>  $\Delta[M]/[M]$ ; <sup>(c)</sup>  $DP = \Delta[M]/([MI]*DS)$  (based on conversion obtained from kinetic plots); <sup>(d)</sup>  $Mn_{(th)} = Mn_{(MI)} + [(0.95*MM_{DEGMA} + 0.05*MM_{OEGMA}) * DP * I.S]$  MI = macroinitiator, MM = molar mass, DP = degree of polymerization =  $\Delta[M] / ([MI]*DS)$ , I.S. = initiating sites =  $Mn_{(MI)} / MM_{(Repeating\ unit)} * DS$ . The GPC-MALS analyses were done in duplicate and the different RPDs% were calculated as per **Equation 3.1.1** and found to be below 6%.

There was significant discrepancy between the theoretical values for Mn and those obtained from GPC-MALS. Once again, this could be due to radical coupling between growing chains, sample loss during filtration of the solution prior to analysis, column adsorption or due to inaccurate dn/dc values. This means that the Mn values obtained by GPC-MALS may not be representative of the entire sample. Therefore, the Mn and PDI vs. conversion graphs were not here presented.

The solubility of the synthesized cellulose-based copolymers is a complex matter as we have a graft-copolymer which is a random copolymer (P(DEGMA-co-OEGMA)). As suggested by Mark<sup>355</sup> the solubility of block and graft copolymers results in the overlapping of solubilities of both homopolymers. The solubility parameters seem to play an important role; hence if this difference is small the copolymer will show an intermediate solubility similar to that of the random copolymers. On the other hand, if the difference is large, the graft copolymer will show the solubility of both homopolymers and may also have insoluble domains if the molecular weights of each homopolymers are large enough.<sup>356</sup> The latter scenario was observed for copolymers # 7 and 9, which were soluble in chloroform and water. However, this was not observed for the remaining products; some were soluble in chloroform and others were insoluble in common organic solvents. The insolubility might be due to the establishment of cross-linking reactions between growing chains of DEGMA and OEGMA or to the formation of very large molecular weight copolymer (DEGMA-co-OEGMA).

In order to obtain a representative analysis of the samples, ATR-FTIR was used to analyze the solid materials. ATR-FTIR spectra of cellulose-based copolymers isolated after 5 and 15 min and 1 hour are shown in **Figure 3.3.22**. The objective was to confirm the increase in the C=O peak through time. The peaks from the grafted copolymer overlaid with most of the peaks from the cellulose-based macroinitiator, with exception of the C-Si peak from the TDMS group at 833

$\text{cm}^{-1}$ . The latter was visible in the spectrum of the sample taken at 5 min. However, that peak overlapped with another one associated with the copolymer, and became less visible as the DP increased, appearing as a shoulder in the samples taken at 15 and 60 min, as shown in the inset of **Figure 3.3.22**. Therefore, it was not possible to normalize the spectra. Nonetheless, the ATR-FTIR spectra confirmed the presence of  $\text{P}(\text{DEGMA}_{95}\text{-co-OEGMA}_5)$  in the cellulose-based copolymer. The lack of solubility of some of our products and the broad distribution of molecular weights obtained from the GPC-MALS may be demonstrating that the regioselective allocation of the ATRP initiator in the cellulose backbone was not enough to avoid radical coupling reactions between growing chains. Therefore, to minimize these reactions the use of a cellulose-based macroinitiator with a lower initiator density might be essential to obtain a controlled ATRP.

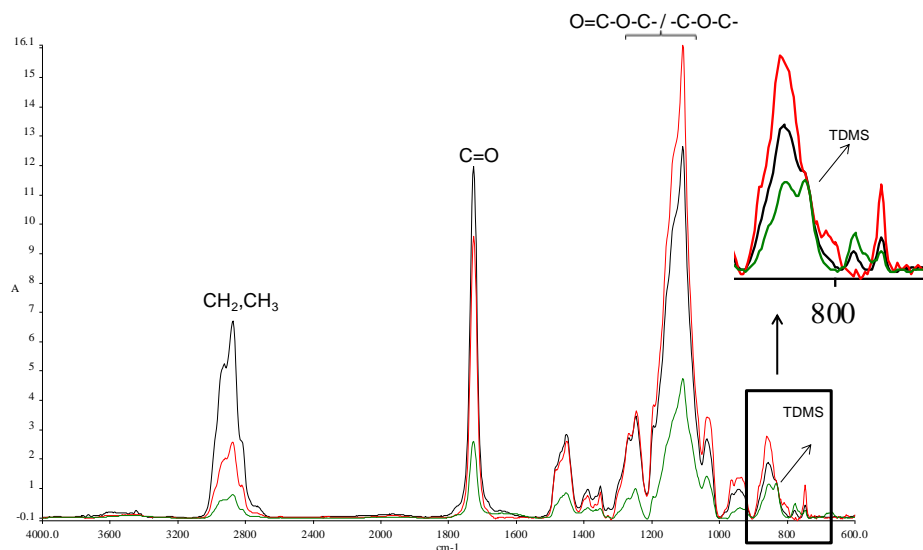


**Figure 3.3.22.** Comparison of ATR-FTIR spectra of copolymers # 9 at 5min (green), 15min (red) and 60min (black).

### 3.3.4 Effect of the degree of substitution on the homogeneous ATRP of DEGMA and OEGMA from 3-O-(3-O-(2-bromoisobutryl)-hydroxypropyl)-2,6-O-TDMS cellulose

As previously mentioned (sections 1.4.1.2 and 1.5), the high degree of substitution of 2-bromoisobutryl groups increases the number of initiating sites. This may contribute to higher concentrations of radicals that could increase the probability of radical coupling, i.e., termination reactions. The effect of different degree of substitution (DS) in non-regioselectively substituted cellulose-based macroinitiators was briefly discussed in section 1.4.1.2. In general, macroinitiators with lower DS produced copolymers with lower conversions.<sup>120,161</sup> However, similar conversions were also reported for macroinitiators with high and low DS.<sup>10,218</sup> Furthermore, an increment in DP<sup>218</sup> and slower rate of polymerization<sup>10</sup> were also observed when using macroinitiators with low DS.

In the present work 3-O-(3-O-(2-bromoisobutryl)-hydroxypropyl)-2,6-O-TDMS cellulose with medium (0.6) and low (0.2) initiator (2-bromoisobutryl) DS were synthesized and “grafted-from” P(DEGMA<sub>95</sub>-co-OEGMA<sub>5</sub>) with the aim of studying the effect of lower initiator density on the controlled character of the polymerization. **Table 3.3.12** outlines the conditions used and corresponding monomer conversions.

**Table 3.3.12.** Experimental conditions used in the ATRP of P(DEGMA<sub>95</sub>-co-OEGMA<sub>5</sub>) from 3-O-(3-O-(2-bromoisobutryl)-hydroxypropyl)-2,6-O-TDMS cellulose with different DS of 2-bromoisobutryl and respective conversions.

Exp#	DS	MI	“M” <sup>(a)</sup>	Time <sup>(b)</sup>	Conv <sup>(c)</sup>
Molar equivalents relative to MI initiating sites					%
5 <sup>(d)</sup>	1 (High DS)	0.5	100	1h	45
14	0.6 (Medium DS)	0.5	100	30min	19
15	0.2 (Low DS)	0.5	100	30min	13

Experimental conditions: MI/(OEGMA+DMEQ<sub>2</sub>MA)/Ligand/CuCl = (1:x:1.2:1); solvent=THF; Temperature = 55 °C; [MI] = 0.5 wt%; olig = oligomers; DEGMA/OEGMA = 95:5; <sup>(a)</sup> “M” – DEGMA (95%) and OEGMA (5%)  
<sup>(b)</sup> Time within linear kinetic regime was observed; <sup>(c)</sup> Conv.% =  $\Delta[M] / [M]$ , maximum monomer conversion attained within linear kinetic regime, calculated from kinetic plots; <sup>(d)</sup> gel formation was observed. For further information see section 2.3.18.

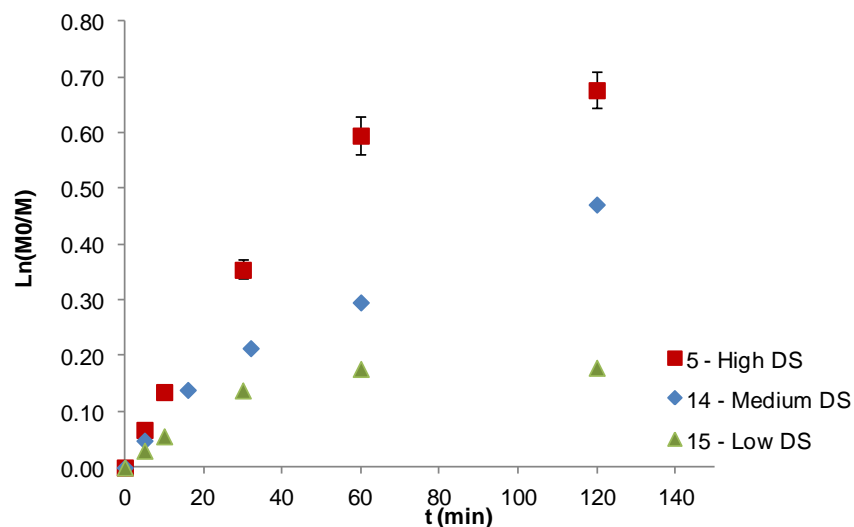


**Figure 3.3.23.** Semi-logarithmic plot of copolymerization of DEGMA and OEGMA from cellulose-based macroinitiator with different DS. Experiment # 5 (square) was done in duplicate.

The kinetic plots of the copolymerization from macroinitiators with high, medium and low DS are presented in **Figure 3.3.23**. It is evident that there is a considerably lower rate of polymerization for macroinitiators with medium and low DS (Exps # 14 and 15). The linear kinetic regime observed for these two copolymerizations was also shorter, 30 min vs. 1 hour for the macroinitiator with high DS (Exp # 5). As a result, the conversions for Exps # 14 and 15 were only 19 and 13%, respectively. These values were substantially lower than the 45%, conversion for Exp # 5. This might be related to the existence of a higher amount of free hydroxyl groups in the C3 position of the AGU. Kondo<sup>60</sup> found that intramolecular hydrogen bonds affect the ability of methylated cellulose derivatives to form or not a crystalline pattern. Based on these findings, the free hydroxyl groups may cause a change in the conformation of the cellulose backbone. The latter, may potentially bring the growing chains into closer contact enabling radical coupling, thus termination. On the other hand, a macroinitiator with higher initiator density (higher DS<sub>2-bromoisobutryl</sub>) might allow the cellulose backbone to adopt a more flexible conformation, which may minimize the interactions between growing chains. In order to confirm this hypothesis, further investigation is necessary.

Similarly to what was done in section 3.3.3, Exp # 15 was repeated in order to generate a copolymer within the linear kinetic regime. The reproducibility of this experiment was confirmed and found to fit the original kinetic plot, as shown in **APPENDIX-Selected kinetic graphs**. The final product (copolymer # 15) was isolated as previously described in section 2.3.18 and compared with copolymer # 5. The latter was previously produced and characterized from the macroinitiator with high DS (Exp # 5, **Table 3.3.6**). **Table 3.3.13** summarizes the properties of the

two copolymers. As anticipated the DP of copolymer # 15 (DP = 78) was substantially higher than copolymer # 5. The solubility of these two copolymers was also very different; copolymer # 5 was not soluble in any of the attempted solvents, while copolymer # 15 was soluble in THF and CHCl<sub>3</sub> but not in water.

**Table 3.3.13.** Cellulose-based graft copolymers with high and low initiator density and respective conversion, DP and solubility in THF, CHCl<sub>3</sub> and H<sub>2</sub>O.

Copolymer	Time	Conv <sup>(a)</sup>	DP <sup>(b)</sup>	THF	CHCl <sub>3</sub>	H <sub>2</sub> O
5 <sup>(c)</sup>	25 min	26%	26	no	no	no
15 <sup>(d)</sup>	40 min	15%	78	yes	yes	no

<sup>(a)</sup> Conv.% =  $\Delta[M] / [M]$ , (calculated from kinetic plots); <sup>(b)</sup> DP =  $\Delta[M] / ([MI] * DS)$  (calculated from kinetic plots); <sup>(c)</sup> Macroinitiator with DS = 1; <sup>(d)</sup> Macroinitiator with DS = 0.2. Solubility was tested by preparing solutions in THF, CHCl<sub>3</sub> and water with a concentration of 0.3 wt% of copolymer. Experimental conditions as described in **Table 3.3.12**. The copolymers numbers correspond to the respective experiment number as described in **Table 3.3.12**.

**Note:** To facilitate the discussion, the copolymers obtained from experiments 5, 14 and 15 will be called copolymers # 5, 14 and 15.

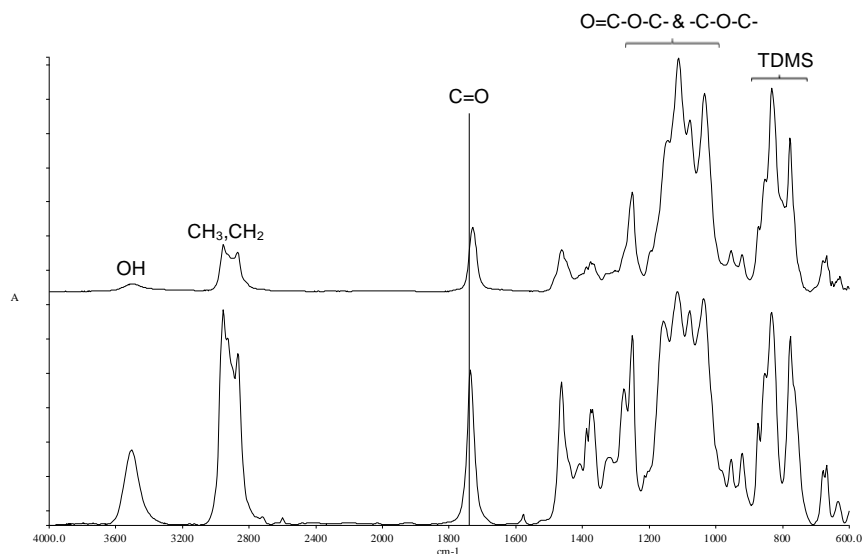


**Figure 3.3.24.** Comparison of ATR-FTIR spectra of cellulose-based macroinitiator with low DS (bottom) and the synthesized 3-O-(3-O-(2-bromoisobutyryl)-hydroxypropyl)-2,6-O-TDMS cellulose-g-P(DEGMA<sub>95</sub>-co-OEGMA<sub>5</sub>) (top).

The ATR-FTIR spectrum (**Figure 3.3.24**) of the newly synthesized cellulose-based copolymer clearly shows peaks from the grafted P(DEGMA<sub>95</sub>-co-OEGMA<sub>5</sub>) copolymer. Again there is the shift in the C=O stretching band from 1737 to 1729 cm<sup>-1</sup> associated with the grafting, as well as a change in the shape of bands associated with CH<sub>3</sub>, CH<sub>2</sub> moieties and the various C-O stretching bands of the ether and ester bonds. Unlike the high DS macroinitiator-based copolymers, the Si-C stretching bands associated with the TDMS groups of the cellulose-based macroinitiator remained quite well resolved. The <sup>1</sup>H- and <sup>13</sup>C-NMR spectra further substantiate the successful grafting of P(DEGMA<sub>95</sub>-co-OEGMA<sub>5</sub>), **Figure 3.3.25** and **Figure 3.3.26** confirming the success of the grafting.

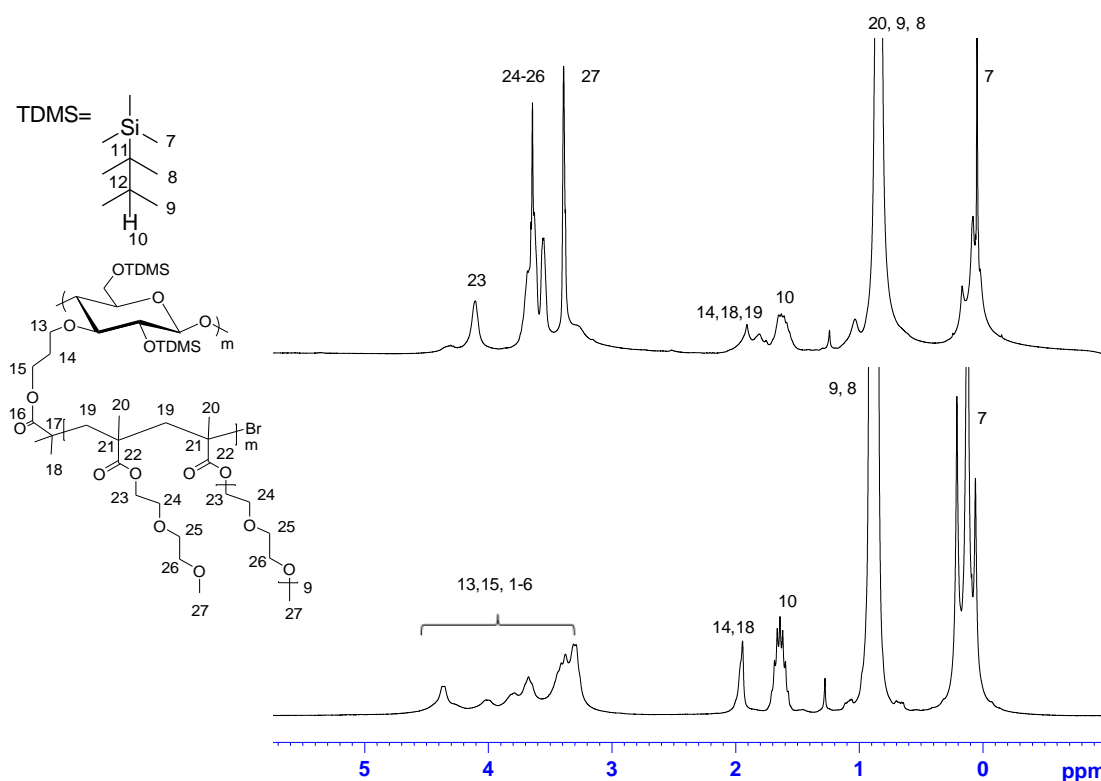


**Figure 3.3.25.** Comparison of <sup>1</sup>H-NMR spectra of cellulose-based macroinitiator with low DS (bottom) and the synthesized 3-O-(3-O-(2-bromoisobutyryl)-hydroxypropyl)-2,6-O-TDMS cellulose -g-(P(DEGMA<sub>95</sub>-co-OEGMA<sub>5</sub>)) (top).

The <sup>1</sup>H-NMR spectrum (**Figure 3.3.25**) of copolymer # 15 clearly shows peaks associated with the cellulose-based macroinitiator in particular, the TDMS group (peaks 7 to 10) and the initiator, 2-bromoisobutyryl, (peak 18). The grafting of P(DEGMA<sub>95</sub>-co-OEGMA<sub>5</sub>) was confirmed by the presence of peak 20, which overlapped with the methyl groups of the TDMS group, as well

as peaks 23 - 27, which overlapped with the peaks (1 - 6) of the cellulose backbone (AGU). The DP of the copolymer was not calculated due to the overlapping peaks between the AGU protons and the grafted P(DEGMA-*co*-OEGMA).

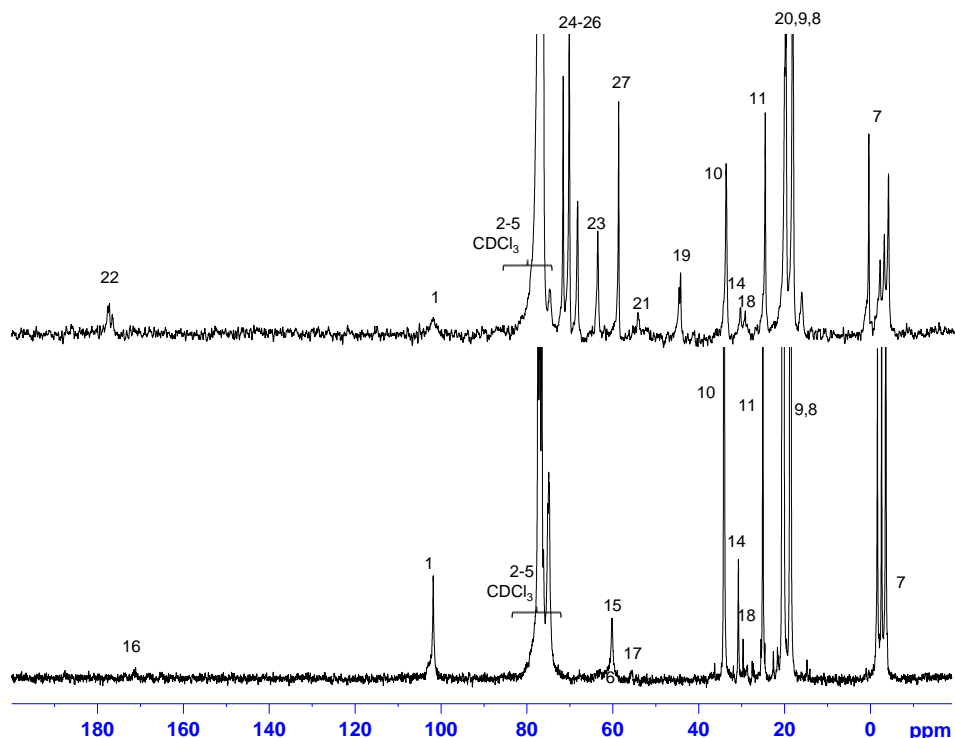


**Figure 3.3.26.** Comparison of  $^{13}\text{C}$ -NMR spectra of cellulose-based macroinitiator with low DS (bottom) and the synthesized 3-*O*-(3-*O*-(2-bromoisobutyryl)-hydroxypropyl)-2,6-*O*-TDMS cellulose-*g*-(P(DEGMA<sub>95</sub>-*co*-OEGMA<sub>5</sub>)) (top). See **Figure 3.3.25** for peak number assignments.

Similar results were obtained from the  $^{13}\text{C}$ -NMR spectrum. Once again, the peaks from both components are present in the cellulose-based graft copolymer in particular the peaks from the TDMS groups (peaks 7 to 11) as well as peak 1 corresponding to C1 from the AGU of the cellulosic backbone. Therefore, successful grafting was confirmed by ATR-FTIR,  $^1\text{H}$ - and  $^{13}\text{C}$ -NMR.

The thermal properties of the new material (low density grafted cellulose-based copolymer) were determined by TGA and DSC and compared against the densely grafted cellulose-based copolymer (copolymer # 5). The primary decomposition temperatures were determined based on the first derivative of the weight loss curve and weight losses below 5% were not considered, see **APPENDIX-Selected first derivative of TGA thermograms**. The TGA measurements were done in duplicate and respective RPDs% were calculated as per **Equation 3.1.1** and found not to

exceed 2%. A table with the values of the duplicates and respective RPDs% can be found in **APPENDIX-Duplicates and respective RPDs%**.

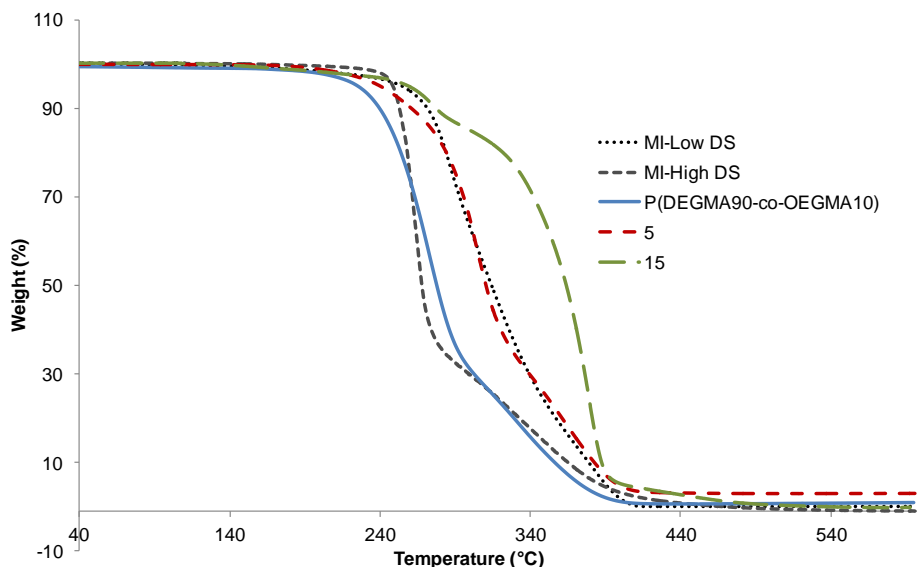


**Figure 3.3.27.** Comparison of TGA thermograms of P(DEGMA<sub>90</sub>-co-OEGMA<sub>10</sub>), MI (macroinitiator) and copolymers 5, and 15.

As compared to its higher DS counterpart, low DS macroinitiator (MI-Low DS) showed 3 Tds at 293 °C, 324 °C and 370 °C (the high DS macroinitiator Tds were 271 °C and 349 °C). The higher decomposition temperatures of the macroinitiator with low DS were due to the milder experimental conditions used in this synthesis. Furthermore, the potential establishment of intramolecular hydrogen bonds by the free OH groups in the C3 position might have also contributed to the higher Td. Copolymer # 5 displayed 3 Tds at 245 °C, 303 °C and 363 °C, whereas copolymer # 15 exhibited only two at 275 °C and 380 °C. The latter Tds were both higher than the Tds of copolymer # 5, but within the range found for the Tds of the residual copolymers listed in **Table 3.3.7**. In both cases, the grafting of P(DEGMA<sub>95</sub>-co-OEGMA<sub>5</sub>) from both macroinitiators caused an increment of the respective Tds (**Figure 3.3.27**).



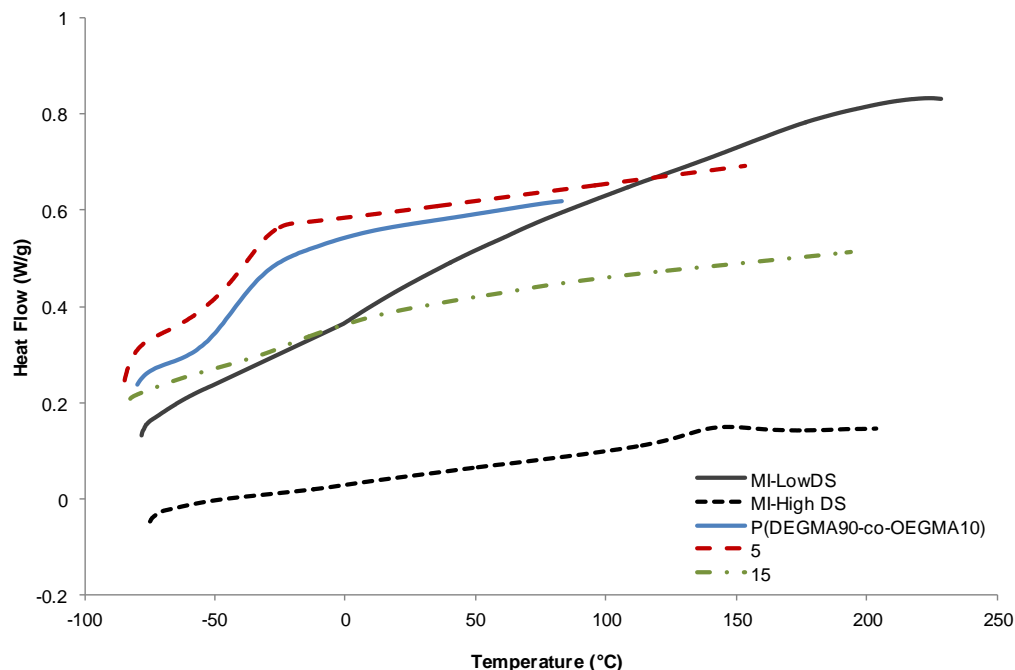


**Figure 3.3.28.** Comparison of DSC thermograms of P(DEGMA<sub>90</sub>-co-OEGMA<sub>10</sub>), MI (macroinitiator) and copolymers 5, and 15.

DSC thermograms of copolymer # 15 (low initiator density cellulose-based macroinitiator) and copolymer # 5 (high initiator density cellulose-based macroinitiator) are presented in **Figure 3.3.28**. The DSC measurements were done in duplicate and respective RPDs% were calculated as per **Equation 3.1.1** and found not to exceed 5%. A table with the values of the duplicates and respective RPDs% can be found in **APPENDIX**. The DSC thermogram of the cellulose-based macroinitiator with low DS did not show a clear T<sub>g</sub>. Copolymer # 15 had a T<sub>g</sub> higher than the T<sub>g</sub> of copolymer # 5, - 23 vs. - 38 °C, respectively. One possible explanation might be related to the existence of a higher fraction of cellulose-based macroinitiator in copolymer # 15 considering the high intensity of the TDMS peak in the <sup>1</sup>H-NMR spectrum (**Figure 3.3.25**).

The molecular weight and PDI of copolymer # 15 were determined by GPC-MALS (**Table 3.3.14**). However, no comparison against the high initiator density cellulose-based copolymer (copolymer # 5) was conducted due to its insolubility in THF. The GPC-MALS measurements were done in duplicate and respective RPDs% were calculated as per **Equation 3.1.1** and found not to exceed 4%. A table with the values of the duplicates and respective RPDs% can be found in **APPENDIX-Duplicates and respective RPDs%**.

**Table 3.3.14.** DP,  $Mn_{(th)}$ ,  $Mn_{(GPC-MALS)}$ , PDI of macroinitiator and respective cellulose-based graft copolymers.

Exp#	DP <sup>(a)</sup>	$Mn_{(th)}$ <sup>(b)</sup> g/mol	$Mn_{(GPC/MALS)}$ g/mol	DP <sub>(GPC-MALS)</sub> <sup>(c)</sup>	PDI <sub>(GPC-MALS)</sub>
MI-Low DS <sup>(a)</sup>			4.3*10 <sup>4</sup>		1.3
15-40min	78	3.2*10 <sup>5</sup>	6.1*10 <sup>4</sup>	8	1.8

<sup>(a)</sup>  $DP = \Delta[M] / ([MI] * DS)$  (calculated from kinetic plots); <sup>(b)</sup>  $Mn_{(th)} = Mn_{(MI)} + [(0.95 * MM_{DEGMA} + 0.05 * MM_{OEGMA}) * DP * I.S]$  MI = macroinitiator, MM = molar mass, DP = degree of polymerization =  $\Delta[M] / ([MI] * DS)$ , I.S. = initiating sites =  $Mn_{(MI)} / MM_{(Repeating\ unit)} * DS$ ; <sup>(c)</sup>  $DP = Mn_{(GPC-MALS)} - Mn_{(MI)} / [(0.95 * MM_{DEGMA} + 0.05 * MM_{OEGMA}) * DP * I.S]$  MI = macroinitiator, MM = molar mass, I.S. = initiating sites =  $Mn_{(MI)} / MM_{(Repeating\ unit)} * DS$ , DS = 0.2; The GPC-MALS analyses were done in duplicate and the different RPDs% were calculated (**Equation 3.1.1**) and found to be below 4%.

The molecular weight of the copolymer was determined by GPC-MALS and based on  $dn/dc$ , determined as previously described and calculated to be 0.082 mL/g (**Equation 3.3.2**). The chromatograms obtained from RID and MALS detectors are presented in **Figure 3.3.29**.

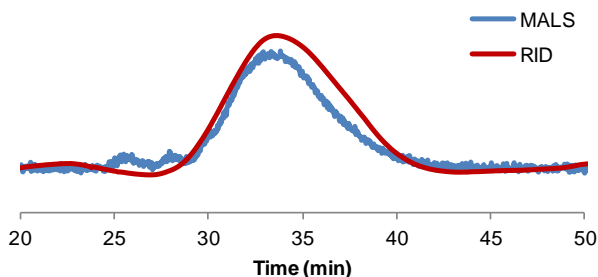


**Figure 3.3.29.** MALS and RID chromatograms of copolymer # 15.

Copolymer # 15 showed high solubility in THF as confirmed by a 93% mass recovery. Therefore, the value obtained from this analysis should be representative of the entire sample. The  $Mn_{(GPC-MALS)}$  ( $6.1 \times 10^4$  g/mol) was substantially lower than the  $Mn_{(th)}$  ( $3.2 \times 10^5$  g/mol). Therefore, the DP calculated from the GPC-MALS (DP = 8) is also dramatically different from the DP calculated from the kinetic plots (DP = 78). This dramatic difference in  $Mn$  and DP might be indicative of low initiation efficiency, 20% (initiation efficiency =  $Mn_{(th)}/Mn_{(GPC-MALS)}$ ) and chain transfer.

The LCST of copolymer # 15 could not be determined by DSC and due to the lack of solubility in water, turbidity measurements could not be done. The dissolution of the copolymer in a minimal amount of THF was done, but when water was added the solution turned cloudy. An attempt to visualize the thermoresponsive behaviour was made by preparing aqueous solutions with a concentration of 3 mg/mL and heating to 60 °C. A thermoresponsive behaviour was not observed however, this does not prove that the co-polymer is not thermoresponsive. The low DP of P(DEGMA<sub>95</sub>-co-OEGMA<sub>5</sub>) could be the cause for the lack of a visual phase transition.

### 3.3.5 Conclusions

A regioselectively substituted ATRP macroinitiator, 3-O-(3-O-(2-bromoisobutryl)-hydroxypropyl)-2,6-O-TDMS cellulose was synthesized with different degrees of substitution (DS of 0.2, 0.6, 1.0) of 2-bromoisobutryl initiator groups, through the introduction of a hydroxypropyl spacer at the C3 position of the AGU. The structure, DS and regiochemistry were confirmed by FTIR,  $^1\text{H}$ - and  $^{13}\text{C}$ -NMR spectroscopy. Thermoresponsive polymers, PNIPAM and P(DEGMA<sub>95</sub>-co-OEGMA<sub>5</sub>) were “grafting-from” the newly synthesized macroinitiators by ATRP and the resulting copolymers analyzed by FTIR,  $^1\text{H}$ -NMR and GPC-MALS. The effect of various reaction parameters on reaction kinetics was studied in order to extend the linear kinetic regime and obtain maximum conversions. In the reactions involving NIPAM and the high DS macroinitiator, decreasing the macroinitiator concentration (MI/solvent wt%) from 0.1 wt% to 0.05 wt% or increasing reaction temperature to 55 °C did not affect the linear kinetic regime or conversion, which remained at 30 min and ~ 7%, respectively. Increasing the amount of Cu(II) extended the linear kinetic regime from 30 min to 1 hour, and increased monomer conversion to 19%. ATRP-ARGET was also tested, but despite the linear kinetic regime being extended to more than 90 min, the rate of polymerization decreased substantially and only 4% conversion was obtained. Decreasing the initiator density (low DS (0.2) macroinitiator) did not impact the linear kinetic regime or conversion; remaining at 60 min and 25%, respectively after 3 hours. However, as expected the low initiator density copolymer had a substantially higher DP of 130 as compared to 28 for the high initiator density copolymer.

Copolymers # I, II and III had their  $\text{Mn}_{(\text{GPC-MALS})}$  close to their respective  $\text{Mn}_{(\text{th})}$  and PDIs were low, outside of the linear kinetic regime. This was attributed to a potential loss of catalytic sites before termination reactions became predominant, as frequently observed in the ATRP of (meth)acrylamides. Copolymer # IV presented a  $\text{Mn}_{(\text{th})}$  higher than the respective  $\text{Mn}_{(\text{GPC-MALS})}$  but the its PDI was low. The difference observed between  $\text{Mn}_{(\text{th})}$  and  $\text{Mn}_{(\text{GPC-MALS})}$  might be related to the increase in the rate of polymerization which caused the loss of active catalytic sites at an earlier stage of the ATRP. The use of a macroinitiator with a lower initiator density did not show any improvement in achieving a controlled ATRP with higher conversions. Furthermore, the chromatogram obtained from GPC-MALS showed two distinct peaks, suggesting a non-controlled ATRP.

In the reactions involving the homogeneous copolymerization of DEGMA and OEGMA from the cellulose-based macroinitiator with high and low DS of 2-bromoisobutryl it was found that removing MeOH from the solvent system (THF) increased the conversion from 13% to 26%. Unlike in the PNIPAM experiments changing the ratio Cu(I)/Cu(II) did not impact the kinetic plots or conversion. However, increasing temperature did result in an increase in conversion from 26 to

44%. The elimination of Cu(II) from the reaction mixture caused the system to gel, but the conversion remained the same (45%). Gel formation could be avoided by using lower temperature, a lower activity ligand (PMDETA) or dilution of the reaction mixture, but the conversion decreased substantially. Decreasing the initiator site density (low DS (0.2) macroinitiator) decreased the rate of polymerization and linear kinetic regime to 30 min and lowered the conversion to 13%, vs. 45% for the high DS (1.0) macroinitiator. Copolymers obtained within the linear kinetic regime were found to have different solubilities depending on the reaction conditions used. However, chemical (ATR-FTIR,  $^1\text{H}$ - and  $^{13}\text{C}$ -NMR spectroscopy) and thermal analysis (TGA and DSC) did not indicate any major differences between the copolymers, thus no correlation could be made between chemical structure, physical properties or solubilities. This may be due to the inaccuracy of the NMR analyses caused by an incomplete solubilisation of the copolymers in the NMR solvent. Water soluble copolymers showed thermoresponsive properties with LCSTs of 27 and 37 °C, respectively. It was not possible to measure the LCST of water-insoluble co-polymers.

## 4 CONCLUSIONS

The overall objective of the present work was to prepare well-defined thermoresponsive materials from regioselectively substituted cellulose. Ordered porous materials such as honeycomb films are of great interest due to its wide range of applications<sup>14–16,289–292</sup>, as described in section 1.6. The use of randomly and regioselectively substituted cellulose derivatives in the preparation of such films has been the subject of scientific articles.<sup>4,318,319,323–326,329</sup> To the best of our knowledge, the use of SI-ATRP to graft polymers from the surface of honeycomb films made from cellulose derivatives regioselectively substituted in position C6, has not been reported. The present work (section 3.1) was initiated with the preparation of homogeneous honeycomb films from regioselectively substituted 6-O-(2-bromoisobutryl)-TMS-O-cellulose, an ATRP macroinitiator. The surface of this film was then modified by grafting thermoresponsive polymer, PNIPAM via SI-ATRP. After ATRP, the homogeneous porous structure was kept and the properties of the surface altered due to the grafting of PNIPAM, as confirmed by ATR-FTIR, contact angle and AFM/QNM analysis. Unfortunately, the absence of adequate instrumentation did not allow observing the thermoresponsive behaviour of this grafted surface. In section 3.2, another cellulose-based ATRP macroinitiator, regioselectively substituted was synthesized as 3-O-(2-bromoisobutryl)-2,6-O-TDMS cellulose. Unexpectedly, this derivative did not form homogeneous honeycomb films but its non-regioselectively substituted counter-part (2,3-O-(2-bromoisobutryl)-2,6-O-TDMS cellulose) did form an ordered porous film. Interestingly, after surface grafting the film lost its homogeneous distribution of honeycomb pores. The preparation of homogeneous honeycomb films from cellulose based ATRP macroinitiators is a contribution for the advancement in the research of well-defined ATRP active surfaces. Polymers with specific properties can be grafted from these surfaces via SI-ATRP providing honeycomb films with tailored properties.

The homogeneous ATRP from cellulose derivatives as macroinitiators has been reported in the literature.<sup>11,13,120,122,123,161,217–221</sup> However, when using high initiator density macroinitiators termination reactions and gelation may occur and consequently cause the loss of the controlled character of the polymerization.<sup>120,221</sup> In order to overcome this drawback it was hypothesized that the ordered distribution of initiators throughout the cellulose backbone may minimize termination reactions between growing chains. In section 3.3, 3-O-(3-O-(2-bromoisobutryl)-hydroxypropyl)-2,6-O-TDMS cellulose, a regioselectively substituted cellulose derivative with a higher initiator density was synthesized and used as the macroinitiator. The grafting of PNIPAM from the cellulose based macroinitiator yielded copolymers with low PDI and the  $M_{n, GPC/MALS}$  close to their respective  $M_{n, th}$ . However, the linear kinetic regime was short and conversions were relatively

low. To extend the linear kinetic regime and increase the conversion, the same macroinitiator with a lower initiator density was used but with no significant improvement. It was decided to proceed in this study with P(DEGMA<sub>95</sub>-co-OEGMA<sub>5</sub>), a biocompatible and thermoresponsive copolymer with the same LCST as PNIPAM. Longer linear kinetic regimes and slightly higher conversions were obtained in some of the experiments. However, due to the low solubility and in some cases, insolubility of the cellulose based copolymers it was not possible to fully characterize the ATRP copolymerizations. Unfortunately, no correlation was found between this behaviour and the experimental conditions or the TGA and DSC results. To minimize potential termination reactions between growing chains, 3-O-(3-O-(2-bromoisobutyryl)-hydroxypropyl)-2,6-O-TDMS cellulose with a lower initiator density was used. The final copolymer was soluble, the  $M_{n, GPC-MALS}$  was closer to  $M_{n, th}$  and the respective PDI improved; however, the linear kinetic regime was not extended and the conversion decreased. Based on the results obtained in this last section a controlled copolymerization of DEGMA and OEGMA from 3-O-(3-O-(2-bromoisobutyryl)-hydroxypropyl)-2,6-O-TDMS cellulose was not achieved, probably due to undesirable termination reactions between the growing chains which may have been the cause for the high  $M_n$ . On the other hand, the polymerization of NIPAM from the same cellulose-based macroinitiator was more promising. Nonetheless, further studies are required in order to claim a controlled polymerization.

Graft copolymerization from macromolecules such as cellulose derivatives by ATRP is still a major challenge. It is essential to understand the role of each experimental parameter and is crucial to choose the most favourable combination of the cellulose ATRP macroinitiator, the monomer to be grafted and the solvent used. Once these questions have been addressed adequately, it will be possible to prepare well-defined cellulosic copolymers consistently.

## 5 FUTURE WORK

### *Synthesis of non-regioselectively substituted (2-bromoisobutyryl) TMS-O-cellulose DS ~ 1*

A significant difference was observed in the pore size of honeycomb films derived from regioselectively substituted 6-O-(2-bromoisobutyryl) TMS cellulose and non-regioselectively substituted (2-bromoisobutyryl) TMS-O-cellulose. This behaviour could be due to the regioselective character of the derivative, the DS or the use of a different solvent system (toluene vs.  $\text{CHCl}_3$ :toluene). Therefore, as future work, it is proposed to synthesize a non-regioselectively substituted 2-bromoisobutyryl TMS-O-cellulose, with a DS closer to 1 and soluble in toluene. This experiment would allow a better understanding of the effect of DS and regioselectivity in the formation of honeycomb films from these derivatives.

### *Preparation of honeycomb films from 6-O-(2-bromoisobutyryl)-TMS-O-cellulose*

It was demonstrated that 6-O-(2-bromoisobutyryl)-TMS-O-cellulose has the ability to form homogeneous honeycomb films. In order to find the optimal experimental conditions and to clarify the influence of each parameter in the film formation, it is proposed to statistically design an experiment with the objective to obtain the optimal honeycomb film with a homogeneous pore size distribution.

### *Test the thermoresponsiveness of substituted honeycomb patterned films*

The thermoresponsive behaviour in these honeycomb films is expected to change the hydrophilicity of the surface above/below the LCST. A contact angle instrument equipped with a heating plate would permit determining the thermoresponsiveness of the ensuing films. On the other hand, pore morphology would be expected to change above/below the LCST and could be monitored by AFM equipped with a fluid cell (water) and temperature controller.

### *Preliminary study to test the viability of using the honeycomb patterned film from 6-O-(2-bromoisobutyryl) TMS cellulose for cell tissue growth*

Recent studies on the use of honeycomb films for tissue growth have shown that the adhesion and proliferation of the cells are not affected.<sup>14,16,333,334</sup> Fukuhira et al.<sup>14</sup> and Tanaka et al.<sup>334</sup> also found that the architecture of honeycomb films provides cells with spherical shape, necessary for use in tissue engineering, and not flat like the ones formed on flat films. Therefore, the ordered porosity of our films may allow cell tissue growth. Furthermore, these surfaces might also be modified through surface initiated ATRP. For example, the grafting of PNIPAM from the honeycomb films may allow the preparation of switchable thermoresponsive surfaces for tissue



growth. The hydrophilic and hydrophobic properties of PNIPAM, below and above the LCST, might be very effective for reversing cell attachment and detachment without cell damage.<sup>357</sup>

In order to initiate a preliminary study about the use of the honeycomb films prepared in this work for cell tissue growth it would be necessary to execute preliminary studies which include: 1) test the thermoresponsiveness of these films; 2) verify the biocompatibility of the modified honeycomb surfaces, 3) optimize the preparation of larger honeycomb films and 4) test viability of cell tissue growth.

*Homogeneous polymerization of PNIPAM from 3-O-(3-O-(2-bromoisobutyryl)-hydroxypropyl)-2,6-O-TDMS cellulose*

The results obtained for this polymerization are promising considering the low PDIs obtained, in particular Exp # III, which has a  $Mn_{(th)}$  close to  $Mn_{(GPC-MALS)}$ , low PDI and DP that is not too low. Future work would include establishing Mn vs. conversion graphs and verifying if a linear relation is established or not. It would also be interesting to study the role of regioselectivity in this polymerization. Thus, we propose the synthesis of 2,3-O-(3-O-(2-bromoisobutyryl)-hydroxypropyl)-2,6-O-TDMS cellulose, based on the synthesis of 2,6-O-TDMS cellulose with a DS of approximately 1.3 (as described in section 3.2.2) and 3-O-(3-O-(2-bromoisobutyryl)-hydroxypropyl)-2,6-O-TDMS cellulose (as described in section 3.3.1), and then running a homogeneous polymerization of PNIPAM from 2,3-O-(3-O-(2-bromoisobutyryl)-hydroxypropyl)-2,6-O-TDMS cellulose.

*Homogeneous copolymerization of P(DEGMA<sub>95</sub>-co-OEGMA<sub>5</sub>) from 3-O-(3-O-(2-bromoisobutyryl)-hydroxypropyl)-2,6-O-TDMS cellulose*

This copolymerization requires further study. The insolubility of the synthesized copolymers may be caused by radical coupling reactions between growing chains, resulting in termination and potentially causing crosslinking. Therefore, experimental conditions need to be further optimized. In order to minimize these reactions, the use of a less reactive ligand like PMDETA in the presence of Cu(II) might be beneficial. Another possibility would include decreasing the initiator density, which can be done by using a low DS 3-O-(3-O-(2-bromoisobutyryl)-hydroxypropyl)-2,6-O-TDMS cellulose in combination with a lower activity ligand like PMDETA in the presence or absence of Cu(II).

Similarly to what was proposed for the future work in the homogeneous polymerization of PNIPAM, the role of regioselectivity in this reaction should be further studied. Thus, as future work we propose to run a homogeneous copolymerization of P(DEGMA<sub>95</sub>-co-OEGMA<sub>5</sub>) from 2,3-O-(3-O-(2-bromoisobutyryl)-hydroxypropyl)-2,6-O-TDMS cellulose.

## REFERENCES

- (1) Gomez, J. A. C.; Erler, U. K.; Klemm, D. *Macromol. Chem. Phys.* **1996**, 197, 953.
- (2) Koschella, A.; Heinze, T.; Klemm, D. *Macromol. Biosci.* **2001**, 1, 49.
- (3) Koschella, A.; Fenn, D.; Illy, N.; Heinze, T. *Macromol. Symp.* **2006**, 244, 59.
- (4) Kadla, J. F.; Asfour, F. H.; Bar-Nir, B. *Biomacromolecules* **2007**, 8, 161.
- (5) Ifuku, S.; Kamitakahara, H.; Takano, T.; Tanaka, F.; Nakatsubo, F. *Org. Biomol. Chem.* **2**, 402.
- (6) Sakakibara, K.; Ogawa, Y.; Nakatsubo, F. *Macromol. Rapid Commun.* **2007**, 28, 1270.
- (7) Klemm, D.; Heinze, T.; Philipp, B.; Wagenknecht, W. *Acta Polym.* **1997**, 48, 277.
- (8) Wang, J.; Matyjaszewski, K. *J. Am. Chem. Soc.* **1995**, 117, 5614.
- (9) Kato, M.; Kamigaito, M.; Sawamoto, M.; Higashimura, T. *Macromolecules* **1995**, 28, 1721.
- (10) Li, Y.; Liu, R.; Liu, W.; Kang, H.; Wu, M. I. N.; Huang, Y. *J. Polym. Sci. Part A Polym. Chem.* **2008**, 46, 6907.
- (11) Yan, L.; Tao, W. *J. Biomed. Sci. Eng.* **2008**, 1, 37.
- (12) Ma, L.; Liu, R.; Tan, J.; Wang, D.; Jin, X.; Kang, H.; Wu, M.; Huang, Y. *Langmuir* **2010**, 26, 8697.
- (13) Ifuku, S.; Kadla, J. F. *Biomacromolecules* **2008**, 9, 3308.
- (14) Fukuhira, Y.; Kaneko, H.; Yamaga, M.; Tanaka, M.; Yamamoto, S.; Shimomura, M. *Colloids Surfaces A Physicochem. Eng. Asp.* **2008**, 313-314, 520.
- (15) Mandal, K.; Balland, M.; Bureau, L. *arXiv1111.2510v1 [cond-matt]* 10 Nov **2011**, 1.
- (16) Chaudhuri, J. B.; Davidson, M. G.; Ellis, M. J.; Jones, M. D.; Wu, X. *Macromol. Symp.* **2008**, 272, 52.
- (17) Yabu, H.; Shimomura, M. *Langmuir* **2005**, 21, 1709.
- (18) Yabu, H.; Takebayashi, M.; Tanaka, M.; Shimomura, M. *Langmuir* **2005**, 21, 3235.
- (19) Tsai, H.; Xu, Z.; Pai, R. K.; Wang, L.; Dattelbaum, A. M.; Shreve, A. P.; Wang, H.-L.; Cotlet, M. *Chem. Mater.* **2011**, 23, 759.
- (20) Marx-Figini, M. *J. Polym. Sci. C Polym. Symp.* **2007**, 28, 57.

- (21) Smook, G. A. *Handbook for Pulp & Paper Technologists*; Angus Wilde Publications: Vancouver, 1992; p. Chapter 2.
- (22) Revol, J.-F.; Goring, D. A. I. *J. Appl. Polym. Sci.* **1981**, 26, 1275.
- (23) Atalla, R. H.; Vanderhart, D. L. *Science (80-. )*. **1984**, 223, 283.
- (24) Yamamoto, H.; Horii, F.; Odani, H. *Macromolecules* **1989**, 22, 4132.
- (25) Gardner, K. H.; Blackwell, J. *Biopolymers* **1974**, 13, 1975.
- (26) Blackwell, J.; Kolpak, F. J.; Gardner, K. H. In *ACS Symposium Series No 48*; Arthur, J. C., Ed.; Washington, 1977; p. 42.
- (27) Sarko, A.; Muggli, R. *Macromol. Symp.* **1974**, 7, 486.
- (28) Kroonbatenburg, L.M.J.; Kroon J.; Northolt, M. G. *Polym. Commun.* **1986**, 27, 290.
- (29) Kroon-Batenburg, L. M.; Kroon, J. *Glycoconj. J.* **1997**, 14, 677.
- (30) Langan, P.; Nishiyama, Y.; Chanzy, H. *J. Am. Chem. Soc.* **1999**, 121, 9940.
- (31) Klemm, D.; Heublein, B.; Fink, H.-P.; Bohn, A. *Angew. Chem. Int. Ed. Engl.* **2005**, 44, 3358.
- (32) Thielking, H., Schmidt, M. . Cellulose Ethers. *Ullmann's Encyclopedia of Industrial Chemistry*,, 2006, 1–18.
- (33) Käuper, P.; Kulicke, W.-M. W.; Horner, S.; Saake, B.; Puls, J.; Kunze, J.; Fink, H.-P.; Heinze, U.; Heinze, T.; Kloth, E.-A.; Thielking, H.; Koch, W. *Die Angew. Makromol. Chemie* **1998**, 260, 53.
- (34) Hebeish, A.; Guthrie, J. T. *The Chemistry and Technology of Cellulosic Copolymers. Polymers/Properties and Applications*; Springer-Verlag: Berlin, 1981; Vol. 85, p. 1085.
- (35) Heinze, T.; Liebert, T. *Prog. Polym. Sci.* **2001**, 26, 1689.
- (36) Malm, C. J.; Tanghe, L. E. O. J. *Ind. and Eng. Chem.* **1955**, 47, 995.
- (37) Krässig, H. A. *Cellulose-Structure, Accessibility and Reactivity*; Gordon and Breach Science Publishers: Yverdon, 1993; p. 376.
- (38) Carraher, C. E. J. *Introduction to Polymer Chemistry*; Press, C., Ed.; 2007.
- (39) Miller-chou, B. A.; Koenig, J. L. *Prog. Polym. Sci.* **2003**, 28, 1223.
- (40) Archer, W. L. *Ind. Eng. Chem. Res.* **1991**, 30, 2292.
- (41) Hansen, C. M. *Hansen Solubility Parameters: a users handbook*; 2nd ed.; CRC Press: Boca Raton, FL, 2007.

- (42) Elidrissi, A.; El, S.; Amhamdi, H.; Maaroufi, A.; Hammouti, B. *J. Mater. Environ. Sci.* **2012**, 3, 270.
- (43) Sudharshan, S. R. A.; Reddy, R. K. S. *Polym. Bull.* **2013**, 70, 1303.
- (44) Sefain, M. Z.; Nada, A. M. .; El-kalyoubi, S. F. *Cellul. Chem. Technol.* **1980**, 14, 139.
- (45) Seoud, O. E. A. El; Heinze, T. *Adv. Polym. Sci.* **2005**, 186, 103.
- (46) Dupont, A.-L. *Polymer (Guildf)*. **2003**, 44, 4117.
- (47) McCormick, C. L.; Hutchinson, B. H. *Macromolecules* **1985**, 18, 2394.
- (48) Ekmanis, J. L. *Am. Lab. News* **1987**, 10.
- (49) Takahashi, S. C.; Fujimoto, T.; Miyamoto, T.; Inagaki, H. *J. Polym. Sci. Part A Polym. Chem.* **1987**, 25, 945.
- (50) Fox, S. C.; Li, B.; Xu, D.; Edgar, K. J. *Biomacromolecules* **2011**, 12, 1956.
- (51) Heinze, T.; Koschella, A. *Macromol. Symp.* **2005**, 223, 13.
- (52) Fengel, D.; Wegener, G. *Wood: Chemistry, Ultrastructure, Reactions*; W. de Gruyter, 1984; p. Chapter 17.
- (53) Klemm, D.; Philipp, B.; Heinze, T.; Heinze, U.; Wagenknecht, W. *Comprehensive Cellulose Chemistry*; Wiley-VCH Verlag GmbH & Co. KGaA: Weinheim, 1998; p. Chapter 4.5.
- (54) Edgar, K. J. K.; Buchanan, C. M. C.; Debenham, J. J. S.; Rundquist, P. A.; Seiler, B. D.; Shelton, M. C.; Tindall, D. *Prog. Polym. Sci.* **2001**, 26, 1605.
- (55) Eastman.  
[http://www.eastman.com/Brands/Eastman\\_Cellulose\\_Esters/Pages/Overview.aspx](http://www.eastman.com/Brands/Eastman_Cellulose_Esters/Pages/Overview.aspx).
- (56) McCormick, C. *Macromolecules* **1990**, 23, 3606.
- (57) McCormick, C. L.; Lichatowich, D. K. K. *J. Polym. Sci. Polym. Lett. Ed.* **1979**, 17, 479.
- (58) Balser, K.; Hoppe, L.; Eicher, T.; Wandel, M.; Astheimer, H.-J.; Steinmeier, H.; Allen, J. M. Cellulose Esters. *Ullmann's Encyclopedia of Industrial Chemistry*, 2004, 333–376.
- (59) Heinze, T. In *Polysaccharides: Structural Diversity and Functional Versatility*; Dumitriu, S., Ed.; CRC Press, 2004.
- (60) Kondo, T. *J. Polym. Sci. Part B Polym. Phys.* **1997**, 35, 717.
- (61) Itagaki, H.; Takahashi, I.; Natsume, M.; Kondo, T. *Polym. Bull.* **1994**, 32, 77.
- (62) Itagaki, H.; Tokai, M.; Kondo, T. *Polymer (Guildf)*. **1997**, 38, 4201.

- (63) Norin, T.; Danchi, K. *Polymer (Guildf)*. **1998**, 39, 1123.
- (64) Kondo, T.; Nojiri, M. *Chem. Lett*. **1994**, 1003.
- (65) Nojiri, M.; Kondo, T. *Macromolecules* **1996**, 29, 2392.
- (66) Kondo, T.; Gray, D. G. *Carbohydr. Res*. **1991**, 220, 173.
- (67) Kondo, T. *Carbohydr. Res*. **1993**, 238, 231.
- (68) Kondo, T.; Sawatari, C. *Polymer (Guildf)*. **1996**, 37, 393.
- (69) Kern, H.; Choi, S.; Wenz, G.; Heinrich, J.; Ehrhardt, L.; Mischnick, P.; Garidel, P.; Blume, A. *Carbohydr. Res*. **2000**, 326, 67.
- (70) Croon, I.; Lindberg, B. *Sven. Papperstidning* **1957**, 60, 843.
- (71) Croon, I.; Lindberg, B. *Sven. Papperstidning* **1958**, 61, 919.
- (72) Kondo, T. *J. Polym. Sci. Part B Polym. Phys*. **1994**, 32, 1229.
- (73) Takahashi, S.-I.; Fujimoto, T.; Barua, B. M.; Miyamoto, T.; Inagaki, H. *J. Polym. Sci. Part A Polym. Chem*. **1986**, 24, 2981.
- (74) Erdmenger, T.; Haensch, C. *Macromolecular* **2007**, 7, 440.
- (75) Granström, M.; Majoinen, J.; Kavakka, J.; Heikkilä, M.; Kemell, M.; Kilpeläinen, I. *Mater. Lett*. **2009**, 63, 473.
- (76) Klemm, D.; Einfeldt, L. *Macromol. Symp*. **2001**, 163, 35.
- (77) Xu, D.; Li, B.; Tate, C.; Edgar, K. J. *Cellulose* **2010**, 18, 405.
- (78) Honeyman, J. *J. Chem. Soc*. **1947**, 168.
- (79) Hall, D. M.; Horne, J. R. *J. Appl. Polym. Sci*. **1973**, 17, 2891.
- (80) Heinze, T.; Röttig, K.; Nehls, I. *Macromol. Rapid Commun*. **1994**, 15, 295.
- (81) Gomez, J. A. C.; Erler, W. U.; Klemm, D. O. *Macromol. Chem. Phys*. **1996**, 197, 953.
- (82) Philipp, B.; Klemm, D.; Stein, A. *Das Pap*. **1995**, 49, 102.
- (83) Harkness, B. R.; Gray, D. G. *Macromolecules* **1991**, 24, 1800.
- (84) Koschella, A.; Klemm, D. *Macromol. Symp*. **1997**, 120, 115.
- (85) Klemm, D.; Stein, A. *J. Macromol. Sci. Part A Pure Appl. Chem*. **1995**, 32, 899.
- (86) Yin, X.; Koschella, a.; Heinze, T. *React. Funct. Polym*. **2009**, 69, 341.

- (87) Koschella, A.; Fenn, D.; Heinze, T. *Polym. Bull.* **2006**, 57, 33.
- (88) Heinze, T.; Pfeifer, A.; Sarbova, V.; Koschella, A. *Polym. Bull.* **2010**, 66, 1219.
- (89) Petzold, K.; Klemm, D.; Heublein, B.; Burchard, W.; Savin, G. *Cellulose* **2004**, 11, 177.
- (90) Fenn, D.; Heinze, T. *Cellulose* **2009**, 16, 853.
- (91) Schumann, K.; Pfeifer, A.; Heinze, T. *Macromol. Symp.* **2009**, 280, 86.
- (92) Bar-Nir, B. B.-A.; Kadla, J. F. *Carbohydr. Polym.* **2009**, 76, 60.
- (93) Tsunashima, Y.; Hattori, K. *J. Colloid Interface Sci.* **2000**, 228, 279.
- (94) Tasaka, K.; Umeda, H.; Kuzuhara, N.; Yajima, T. Cellulose ester film, its manufacturing method, optical retardation film, optical compensation sheet, elliptic polarizing plate, and image display. 7,306,832 B2, 2007.
- (95) Iwata, T.; Azuma, J.; Okamura, K. *Carbohydr. Res.* **1992**, 224, 277.
- (96) Kamide, K.; Saito, M. *Macromol. Symp.* **1994**, 83, 233.
- (97) Iwata, T.; Okamura, K.; Azuma, J.; Tanaka, F. *Cellulose* **1996**, 3, 91.
- (98) Iwata, T.; Okamura, K.; Azuma, J.; Tanaka, F. *Cellulose* **1996**, 3, 107.
- (99) Hsieh, C.-W. C.; Kadla, J. F. *Cellulose* **2012**, 19, 1567.
- (100) Xu, D.; Edgar, K. J. *Biomacromolecules* **2012**, 13, 299.
- (101) Gupta, K. C.; Khandekar, K. *Biomacromolecules* **2003**, 4, 758.
- (102) McDowall, D. J.; Gupta, B. S.; Stannett, V. T. *Prog. Polym. Sci.* **1984**, 10, 1.
- (103) Waly, A.; Abdel-Mohdy, F. A.; Aly, A. S.; Hebeish, A. *J. Appl. Polym. Sci.* **1998**, 68, 2151.
- (104) El-Salmawi, K. M.; Zaid, M. M. A.; Ibraheim, S. M.; El-Naggar, A. M.; Zahran, A. H. *J. Appl. Polym. Sci.* **2001**, 82, 136.
- (105) Hebeish, A.; El-Hilw, Z. H. *J. Appl. Polym. Sci.* **1998**, 67, 739.
- (106) Ushakov, S. N. *Fiz.-Mat. Nauk* **1943**, 1, 35.
- (107) Borner, H. G.; Matyaszewski, K. *Macromol. Symp.* **2002**, 177, 1.
- (108) Odian, G. *Principles of Polymerization*; 4th ed.; John Wiley and Sons: Hoboken, 2004.
- (109) Moad, G.; Solomon, D. H. *The Chemistry of Radical Polymerization*; 2nd ed.; Elsevier Ltd.: Oxford, 2006.
- (110) Chaudhuri, D. K.; Hermans, J. J. *J. Polym. Sci.* **1961**, 51, 373.

- (111) El-Alfy, E.; Khalil, M. I.; Hebeish, A. *J. Polym. Sci. Part A Polym. Chem.* **1981**, 19, 137.
- (112) Ikeda, I.; Kurushima, Y.; Talkashima, H.; Suzuki, K. *Polym. J.* **1988**, 20, 243.
- (113) Cheradame, H.; Tadjang, A. U.; Gandini, A. *Makromol. Chemie- Rapid Commun.* **1988**, 9, 255.
- (114) John, G.; Pillai, C. K. S. *Polym. Bull.* **1989**, 22, 89.
- (115) Cohen, E.; Avny, Y.; Zilkha, A. *J. Polym. Sci. Part A Polym. Chem.* **1971**, 9, 1469.
- (116) O. Y. Mansour and A. H. Basta. *Nord. Pulp Pap. Res. J.* **1991**, 6, 184.
- (117) Narayan, R.; Shay, M. *Polym. Prepr. (American Chem. Soc. Div. Polym. Chem.)* **1986**, 27, 204.
- (118) Lönnberg, H.; Zhou, Q.; Brumer, H.; Teeri, T. T.; Malmström, E.; Hult, A. *Biomacromolecules* **2006**, 7, 2178.
- (119) Hafrén, J.; Córdova, A. *Macromol. Rapid Commun.* **2005**, 26, 82.
- (120) Östmark, E.; Harrisson, S.; Wooley, K. L.; Malmström, E. E. *Biomacromolecules* **2007**, 8, 1138.
- (121) Hansson, S.; Ostmark, E.; Carlmark, A.; Malmström, E. *ACS Appl. Mater. Interfaces* **2009**, 1, 2651.
- (122) Shen, D.; Yu, H.; Huang, Y. *J. Polym. Sci. Part A* **2005**, 43, 4099.
- (123) Shen, D.; Huang, Y. *Polymer (Guildf.)* **2004**, 45, 7091.
- (124) Gupta, K. C.; Khandekar, K. *Polym. Int.* **2006**, 55, 139.
- (125) Shukla, S. R.; Rao, G. V. G.; Athalye, A. R. *J. Appl. Polym. Sci.* **1992**, 2, 1341.
- (126) Fernandez, M. J.; Casinos, I.; Guzman, G. M. *J. Polym. Sci. Part A Polym. Chem.* **1990**, 28, 2275.
- (127) Suo, A. L.; Qian, J. M.; Yao, Y.; Zhang, W. G. *J. Appl. Polym. Sci.* **2007**, 103, 1382.
- (128) Roy, D.; Semsarilar, M.; Guthrie, J. T.; Perrier, S. *Chem. Soc. Rev.* **2009**, 38, 2046.
- (129) Faessinger, R. W.; Conte, J. S. Graft polymerization using ferrated thioated cellulose substrate, products thereof and intermediates. 3,330,787, 1963.
- (130) Toledano-Thompson, T.; Loria-Bastarrachea, M. I.; Aguilar-Vega, M. J. *Carbohydr. Polym.* **2005**, 62, 67.
- (131) Shukla, S. R.; Athalye, A. R. *J. Appl. Polym. Sci.* **1994**, 54, 279.

- (132) Stannett, V. T.; Hopfenberg, H. B. *Cellulose and Cellulose Derivatives*; Bikales, N. M.; Segal, L., Eds.; John Wiley and Sons: New York, 1971; pp. 907–936.
- (133) Jenkins, D.; Hudson, S. *Chem. Rev.* **2001**, *101*, 3245.
- (134) Pulat, M.; Isakoca, C. *J. Appl. Polym. Sci.* **2006**, *100* 2343–2, 2343.
- (135) Gurdag, G.; Guclu, S.; Ozgumus, S. *J. Appl. Polym. Sci.* **2001**, *80*, 2267.
- (136) Doba, T.; Rodehed, C.; Ranby, B. *Macromolecules* **1984**, *17*, 2512.
- (137) Kubota, H.; Kuwabara, S. *J. Appl. Polym. Sci.* **1997**, *64*, 2259.
- (138) Daly, W. H.; Evenson, T. S.; Iacono, S. T.; Jones, R. W. *Macromol. Symp.* **2001**, *163*, 155.
- (139) Richards, G. N. *J. Appl. Polym. Sci.* **1961**, *5*, 553.
- (140) Koenig, H. S.; Roberts, C. W. *J. Appl. Polym. Sci.* **1974**, *18*, 651.
- (141) Shukla, S. R.; Athalye, A. R. *J. Appl. Polym. Sci.* **1992**, *44*, 435.
- (142) Shukla, S. R.; Athalye, A. R. *J. Appl. Polym. Sci.* **1995**, *57*, 983.
- (143) Jun, L.; Min, Y.; Jiuqiang, L.; Hongfei, H. *J. Appl. Polym. Sci.* **2001**, *81*, 3578.
- (144) Kumar, V.; Bhardwaj, Y. K.; Jamdar, S. N.; Goel, N. K. *J. Appl. Polym. Sci.* **2006**, *102*, 5512.
- (145) Sakata, I.; Goring, D. A. I. *J. Appl. Polym. Sci.* **1976**, *20*, 573.
- (146) Garnett, J. L.; Ng, L.-T.; Viengkhou, V. *Radiat. Phys. Chem.* **1999**, *56*, 387.
- (147) Lawrence, K. D. N.; Verdin, D. *J. Appl. Polym. Sci.* **1973**, *17*, 2653.
- (148) Takácsa, E.; Wojnárovitsa, L.; Borsab, J.; Pappa, J.; Hargittaia, P.; Koreczc, L. *Nucl. Instruments Methods Phys. Res. Sect. B Beam Interact. with Mater. Atoms* **2005**, *236*, 259.
- (149) Kumar, V.; Bhardwaj, Y. K.; Rawat, K. P.; Sabharwal, S. *Radiat. Phys. Chem.* **2005**, *73*, 175.
- (150) Wellons, J. D.; Stannett, V. *J. Polym. Sci. Part A Polym. Chem. A* **1965**, *3*, 847.
- (151) Sakurada, I. *Chemtech* **1972**, 376.
- (152) Šebenik, A. *Prog. Polym. Sci.* **1998**, *23*, 875.
- (153) Stannett, V. In *ACS Symposium Series, Vol. 187*; 1982; pp. 3–20.
- (154) Carlmark, A.; Malmström, E. E. *Biomacromolecules* **2003**, *4*, 1740.



- (155) Mansson, P.; Westfelt, L. *J. Polym. Sci. Part A Polym. Chem.* **1981**, 19, 1509.
- (156) Biermann, C. J.; Chung, J. B.; Narayan, R. *Macromolecules* **1987**, 20, 954.
- (157) Tsubokawa, N.; Iida, T.; Takayama, T. *J. Appl. Polym. Sci.* **2000**, 75, 515.
- (158) Månsson, P.; Westfelt, L. *J. Polym. Sci. Part A Polym. Chem.* **1981**, 19, 1509.
- (159) Feit, B. A.; Bar-Nun, A.; Lahav, M.; Zilkha, A. *J. Appl. Polym. Sci.* **1964**, 8, 1869.
- (160) Feit, B.-A. A.; Bar-Nun, A.; Lahav, M.; Zilkha, A. *J. Appl. Polym. Sci.* **1964**, 8, 1869.
- (161) Shen, D.; Yu, H.; Huang, Y. *Cellulose* **2006**, 13, 235.
- (162) Szwarc, M. *Nature* **1956**, 178, 1168.
- (163) Szwarc, M.; Levy, M.; Milkovich, R. *J. Am. Chem. Soc.* **1956**, 78, 2656.
- (164) Szwarc, M. *J. Polym. Sci. Part A Polym. Chem. A* **1998**, 36, ix.
- (165) Matyjaszewski, K. In *ACS Symposium Series*, 768; Matyjaszewski, K., Ed.; 2000.
- (166) Webster, O. W. *Science (80-. )*. **1991**, 251, 887.
- (167) Moad, G.; Chiefari, J.; Chong, B. Y. K.; Krstina, J.; Mayadunne, R. T. A.; Postma, A.; Rizzardo, E.; Thang, S. H. *Polym. Int.* **2000**, 1001, 993.
- (168) Chiefari, J.; Chong, Y. K.; Ercole, F.; Krstina, J.; Jeffery, J.; Le, T. P. T.; Mayadunne, R. T.; Meijs, G. F.; Moad, C. L.; Moad, G.; Rizzardo, E.; Thang, S. H. *Macromolecules* **1998**, 31, 5559.
- (169) Patten, T. E.; Xia, J.; Abernathy, T.; Matyjaszewski, K. *Science (80-. )*. **1996**, 272, 866.
- (170) Matyjaszewski, K.; Xia, J. *Chem. Rev.* **2001**, 101, 2921.
- (171) Hawker, C. J.; Bosman, W.; Harth, E. *Chem. Rev.* **2001**, 101, 3661.
- (172) Benoit, D.; Chaplinski, V.; Braslau, R. *J. Am. Chem. Soc.* **1999**, 121, 3904.
- (173) Leibler, L. *Prog. Polym. Sci.* **2005**, 30, 898.
- (174) Studer, A. *Chem. Rec.* **2005**, 5, 27.
- (175) Rizzardo, E.; Chiefari, J.; Mayadunne, R.; Moad, G.; Thang, S. *Macromol. Symp.* **2001**, 174, 209.
- (176) Destarac, M.; Charmot, D.; Franck, X. *Macromol. Rapid Commun.* **2000**, 21, 1035.
- (177) Kamigaito, M.; Ando, T.; Sawamoto, M. *Chem. Rev.* **2001**, 101, 3689.
- (178) Odin, G. *Principles of Polymerization*; 2004; pp. 325–330.

- (179) Braunecker, W. a.; Matyjaszewski, K. *Prog. Polym. Sci.* **2007**, 32, 93.
- (180) Fischer, H. *J. Am. Chem. Soc.* **1986**, 108, 3925.
- (181) Tang, W.; Matyjaszewski, K. *Macromolecules* **2007**, 40, 1858.
- (182) Gillies, M. B.; Matyjaszewski, K.; Norrby, P.-O.; Pintauer, T.; Poli, R.; Richard, P. *Macromolecules* **2003**, 36, 8551.
- (183) Kabachii, Y. A.; Kochev, S. Y.; M, L. M. B.; Inna, B.; Valetsky, P. M. *Polym. Bull.* **2003**, 50, 271.
- (184) Maria, S.; Stoffelbach, F.; Mata, J.; Daran, J.-C.; Richard, P.; Poli, R. *J. Am. Chem. Soc.* **2005**, 127, 5946.
- (185) Kotani, Y.; Kamigaito, M.; Sawamoto, M. *Macromolecules* **1999**, 32, 2420.
- (186) Matyjaszewski, K.; Wei, M.; Xia, J.; McDermott, N. E.; Krzysztof Matyjaszewski, M. W. *Macromolecules* **1997**, 30, 8161.
- (187) Percec, V.; Barboiu, B.; Neumann, A.; Ronda, J. C.; Zhao, M. *Macromolecules* **1996**, 29, 3665.
- (188) Wang, B.; Zhuang, Y.; Luo, X.; Xu, S.; Zhou, X. *Macromolecules* **2003**, 36, 9684.
- (189) Granel, C.; Dubois, P.; Jérôme, R.; Teyssié, P. *Macromolecules* **1996**, 29, 8576.
- (190) Lecomte, P.; Drapier, I.; Dubois, P.; Teyssié, P.; Jérôme, R. *Macromolecules* **1997**, 30, 7631.
- (191) Kizhakkedathu, J. N.; Kumar, K. R.; Goodman, D.; Brooks, D. E. *Polymer (Guildf)*. **2004**, 45, 7471.
- (192) Kizhakkedathu, J. N.; Norris-Jones, R.; Brooks, D. E. *Macromolecules* **2004**, 37, 734.
- (193) Patten, T. E.; Matyjaszewski, K. *Adv. Mater.* **1998**, 10, 901.
- (194) Patten, T. E.; Matyjaszewski, K. *Acc. Chem. Res.* **1999**, 32, 895.
- (195) Xia, J.; Zhang, X.; Matyjaszewski, K. In *ACS Symposium Series*, 760; 2000; pp. 207–223.
- (196) Wang, J.-S.; Matyjaszewski, K. *Macromolecules* **1995**, 28, 7901.
- (197) Xia, J.; Matyjaszewski, K. *Macromolecules* **1997**, 30, 7697.
- (198) Xia, J.; Gaynor, S. G.; Matyjaszewski, K. *Macromolecules* **1998**, 31, 5958.
- (199) Koňák, Č.; Ganchev, B.; Teodorescu, M.; Krzysztof Matyjaszewski, P. K.; Kopeček, J. *Polymer (Guildf)*. **2002**, 43, 3735.
- (200) Xia, J.; Matyjaszewski, K.; Zhang, X. *Macromolecules* **1999**, 32, 2434.

- (201) Kickelbick, G.; Pintauer, T. *New J. Chem.* **2002**, 462.
- (202) Shen, Y.; Tang, H.; Ding, S. *Prog. Polym. Sci.* **2004**, 29, 1053.
- (203) Tsarevsky, N.; Matyjaszewski, K. *J. Polym. Sci. Part A Polym. Chem.* **2006**, 44, 5098.
- (204) Matyjaszewski, K. *Macromolecules* **2012**, 45, 4015.
- (205) Matyjaszewski, K.; Jakubowski, W.; Min, K.; Tang, W.; Huang, J.; Braunecker, W. a; Tsarevsky, N. V. *Proc. Natl. Acad. Sci. U. S. A.* **2006**, 103, 15309.
- (206) Mueller, L.; Jakubowski, W.; Tang, W.; Matyjaszewski, K. *Macromolecules* **2007**, 40, 6464.
- (207) Zhu, G.; Zhang, L.; Zhang, Z.; Zhu, J.; Tu, Y. *Macromolecules* **2011**, 44, 3233.
- (208) Queffelec, J.; Gaynor, S. G.; Matyjaszewski, K. *Macromolecules* **2000**, 33, 8629.
- (209) Jakubowski, W.; Matyjaszewski, K. *Angew. Chem. Int. Ed. Engl.* **2006**, 45, 4482.
- (210) Matyjaszewski, K.; Coca, S.; Gaynor, S. G.; Wei, M.; Woodworth, B. E. *Macromolecules* **1997**, 30, 7348.
- (211) Jakubowski, W.; Matyjaszewski, K. *Macromolecules* **2005**, 38, 4139.
- (212) Jakubowski, W.; Min, K.; Matyjaszewski, K. *Macromolecules* **2006**, 39, 39.
- (213) Min, K.; Gao, H.; Matyjaszewski, K. *Macromolecules* **2007**, 40, 1789.
- (214) De Vries, A.; Klumperman, B.; de Wet-Roos, D.; Sanderson, R. D. *Macromol. Chem. Phys.* **2001**, 202, 1645.
- (215) Pietrasik, J.; Dong, H.; Matyjaszewski, K. *Macromolecules* **2006**, 39, 6384.
- (216) Matyjaszewski, K. In *ACS Symp. Ser.*, 685; 1998; pp. 258–283.
- (217) Meng, T.; Gao, X.; Zhang, J.; Yuan, J.; Zhang, Y.; He, J. *Polymer (Guildf)*. **2009**, 50, 447.
- (218) Vlček, P.; Janata, M.; Látalová, P.; Kríž, J.; Čadová, E.; Toman, L. *Polymer (Guildf)*. **2006**, 47, 2587.
- (219) Kang, H.; Liu, W.; He, B.; Shen, D.; Ma, L.; Huang, Y. *Polymer (Guildf)*. **2006**, 47, 7927.
- (220) Tang, X.; Gao, L.; Fan, X. *J. Polym. Sci. Part A Polym. Chem.* **2007**, 45, 1653.
- (221) Porsch, C.; Hansson, S.; Nordgren, N.; Malmström, E. *Polym. Chem.* **2011**, 2, 1114.
- (222) Jayachandran, K. N.; Takacs-Cox, A.; Brooks, D. E. *Macromolecules* **2002**, 35, 4247.
- (223) Kim, J.; Bruening, M.; Baker, G. *J. Am. Chem. Soc.* **2000**, 122, 7616.

- (224) Von Werne, T.; Patten, T. E. *J. Am. Chem. Soc.* **2001**, *123*, 7497.
- (225) Shah, R. R.; Merreceyes, D.; Husemann, M.; Rees, I.; Abbott, N. L.; Hawker, C. J.; Hedrick, J. L. *Macromolecules* **2000**, *33*, 597.
- (226) Matyjaszewski, K.; Miller, P. J.; Shukla, N.; Immaraporn, B.; Gelman, A.; Luokala, B. B.; Siclovan, T. M.; Kickelbick, G.; Vallant, T.; Hoffmann, H.; Pakula, T. *Macromolecules* **1999**, *32*, 8716.
- (227) Ejaz, M.; Yamamoto, S.; Ohno, K.; Tsujii, Y.; Fukuda, T. *Macromolecules* **1998**, *31*, 5934.
- (228) Ohno, K.; Morinaga, T.; Koh, K.; Tsujii, Y.; Fukuda, T. *Macromolecules* **2005**, *38*, 2137.
- (229) Xu, C.; Wu, T.; Mei, Y.; Drain, C.; Batteas, J.; Beers, K. *Langmuir* **2005**, *21*, 11136.
- (230) Zou, Y.; Kizhakkedathu, J. N.; Brooks, D. E. *Macromolecules* **2009**, *42*, 3258.
- (231) Coskun, M.; Temüz, M. M. *Polym. Int.* **2005**, *54*, 342.
- (232) Glaied, O.; Dubé, M.; Chabot, B.; Daneault, C. *J. Colloid Interface Sci.* **2009**, *333*, 145.
- (233) Jones, B. D. M.; Huck, W. T. S. *Adv. Mater.* **2001**, *16*, 1256.
- (234) Lindqvist, J.; Nyström, D.; Ostmark, E.; Antoni, P.; Carlmark, A.; Johansson, M.; Hult, A.; Malmström, E. *Biomacromolecules* **2008**, *9*, 2139.
- (235) Twaites, B. R.; Alarcón, C. de las H.; Cunliffe, D.; Lavigne, M.; Pennadam, S.; Smith, J. R.; Górecki, D. C.; Alexander, C. *J. Control. Release* **2000**, *97*, 551.
- (236) Juodkasis, S.; Mukai, N.; Wakaki, R.; Yamaguchi, A.; Matsuo, S.; Misawa, H. *Nature* **2000**, *408*, 178.
- (237) Filipcsei, G.; Fehér, J.; Zrínyi, M. *J. Mol. Struct.* **2000**, *554*, 109.
- (238) Zrínyi, M. *Colloid Polym. Sci.* **2000**, *278*, 98.
- (239) Galaev, I. Y.; Gupta, M. N.; Mattiasson, B. *Chemtech* **1996**, *26*, 19.
- (240) Hoffman, A. S.; Afrassiabi, A.; Dong, L. C. *J. Control. Release* **1986**, *4*, 213.
- (241) Bae, Y. H.; Okano, T.; Hsu, R.; Kim, S. W. *Macromol. Rapid Commun.* **1987**, *8*, 481.
- (242) Ding, Z.; Chen, G.; Hoffman, A. S. *J. Biomed. Mater. Res.* **1998**, *39*, 498.
- (243) Galaev, I. Y.; Mattiasson, B. *Enzyme Microb. Technol.* **1993**, *15*, 354.
- (244) Taylor, L. D.; Cerankowski, L. D. *J. Polym. Sci. Part A Polym. Chem.* **1975**, *13*, 2551.
- (245) Sawamoto, M. *Prog. Polym. Sci.* **1991**, *16*, 111.
- (246) Heskins, M.; Guillet, J. E. *J. Macromol. Sci. Part A - Chem.* **1968**, *2*, 1441.

- (247) Schild, H. G. *Prog. Polym. Sci.* **1992**, 17, 163.
- (248) Teodorescu, M.; Matyjaszewski, K. *Macromol. Rapid Commun.* **2000**, 21, 190.
- (249) Suwa, K.; Morishita, K.; Kishida, A.; Akashi, M. *J. Polym. Sci. Part A Polym. Chem.* **1997**, 35, 3087.
- (250) Lu, X.; Hu, Z.; Gao, J. *Macromolecules* **2000**, 33, 8698.
- (251) Xia, X.; Tang, S.; Lu, X.; Hu, Z. *Macromolecules* **2003**, 36, 3695.
- (252) Heitfeld, K. A.; Guo, T.; Yang, G.; Schaefer, D. W. *Mater. Sci. Eng.* **2008**, 28, 374.
- (253) G. Wanka; Hoffmann, H.; Ulbricht, W. *Macromolecules* **1994**, 27, 4145.
- (254) Lutz, J.-F. *J. Polym. Sci. Part A Polym. Chem.* **2008**, 46, 3459.
- (255) Peppas, N. A.; Bures, P.; Leobandung, W.; Ichikawa, H. *Eur. J. Pharm. Biopharm.* **2000**, 50, 27.
- (256) Langer, R.; Peppas, N. a. *AIChE J.* **2003**, 49, 2990.
- (257) Hoffman, A. S. *Clin. Chem.* **2000**, 46, 1478.
- (258) Dong, L. C.; Hoffman, A. S.; Afrassiabi, A. *J. Control. Release* **1986**, 4, 223.
- (259) Chen, G.; Hoffman, A. S. *Bioconjug. Chem.* **1994**, 4, 509.
- (260) Takei, Y. G.; Aoki, T.; Sanui, K.; Ogata, N.; Okano, T.; Sakurai, Y. *Bioconjug. Chem.* **1993**, 4, 42.
- (261) Lin, S.-Y.; Chen, K.-S.; Liang, R.-C. *Polymer (Guildf)*. **1999**, 40, 2619.
- (262) Boutris, C.; Chatzi, E. G.; Kiparissides, C. *Polymer (Guildf)*. **1997**, 38, 2567.
- (263) Otake, K.; Inomata, H.; Konno, M.; Saito, S. *Macromolecules* **1990**, 23, 283.
- (264) Inomata, H.; Goto, S.; Saito, S. *Macromolecules* **1990**, 23, 4887.
- (265) Mittal, V.; Matsko, N. B.; Butté, a.; Morbidelli, M. *Eur. Polym. J.* **2007**, 43, 4868.
- (266) Teodorescu, M.; Matyjaszewski, K. *Macromolecules* **1999**, 32, 4826.
- (267) Higashi, F.; Cho, C. S.; Kakinoki, H. *J. Polym. Sci. Part A Polym. Chem.* **1977**, 15, 2303.
- (268) Kilic, S.; Baysal, B. M. *J. Macromol. Sci. Part C Polym. Rev.* **1986**, 26, 483.
- (269) Masci, G.; Giacomelli, L.; Crescenzi, V. *Macromol. Rapid Commun.* **2004**, 25, 559.
- (270) Xia, Y.; Yin, X.; Burke, N. A. D.; Stöver, H. D. H. *Macromolecules* **2005**, 38, 5937.

- (271) Kim, Y.-H.; Kwon, I. C.; Bae, Y. H.; Kim, S. W. *Macromolecules* **1995**, *28*, 939.
- (272) Durme, K. Van; Rahier, H.; Mele, B. van. *Macromolecules* **2005**, *38*, 10155.
- (273) Virtanen, J.; Baron, C.; Tenhu, H. *Macromolecules* **2000**, *33*, 336.
- (274) Lutz, J.-F.; Akdemir, O.; Hoth, A. *J. Am. Chem. Soc.* **2006**, *128*, 13046.
- (275) Hsiue, G.-H.; Hsu, S.; Yang, C.-C.; Lee, S.-H.; Yang, I.-K. *Biomaterials* **2002**, *23*, 457.
- (276) Hsiue, G.-H.; Chang, R.-W.; Wang, C.-H.; Lee, S.-H. *Biomaterials* **2003**, *24*, 2423.
- (277) Matsumaru, Y. ; Hyodo, A. ; Nose, T. ; Ito, S. ; Hirano, T. ; Ohashi, S. *J. Biomater. Sci. Polym. Ed.* **1996**, *7*, 795.
- (278) Vihola, H.; Laukkanen, A.; Valtola, L.; Tenhu, H.; Hirvonen, J. *Biomaterials* **2005**, *26*, 3055.
- (279) Pelton, R. *Adv. Colloid Interface Sci.* **2000**, *85*, 1.
- (280) David C. Harsh; Gehrke, S. H. *J. Control. Release* **1991**, *17*, 175.
- (281) Caliceti, P.; Veronese, F. M. *Adv. Drug Deliv. Rev.* **2003**, *55*, 1261.
- (282) Harris, J. M.; Chess, R. B. *Nat. Rev. Drug Discov.* **2003**, *2*, 214.
- (283) Ma, H.; Hyun, J.; Stiller, P.; Chilkoti, A. *Adv. Mater.* **2004**, *16*, 338.
- (284) Tao, L.; Mantovani, G.; Lecolley, F.; Haddleton, D. M. *J. Am. Chem. Soc.* **2004**, *126*, 13220.
- (285) Lele, B. S.; Murata, H.; Matyjaszewski, K.; Russell, A. J. *Biomacromolecules* **2005**, *6*, 3380.
- (286) Lutz, J.-F.; Hoth, A. *Macromolecules* **2006**, *39*, 893.
- (287) Kujawa, P.; Segui, F.; Shaban, S.; Diab, C.; Okada, Y.; Fumihiko Tanaka, F. M. W. *Macromolecules* **2006**, *39*, 341.
- (288) Vigo, T. L. *Polym. Adv. Technol.* **1998**, *9*, 539.
- (289) Shimomura, M. *Prog. Polym. Sci.* **1993**, *18*, 295.
- (290) Akozbek, N.; John, S. *Phys. Rev. E* **1998**, *57*, 2287.
- (291) Ramsay, G. *Nat. Biotechnology* **1998**, *16*, 40.
- (292) Yonemura, M.; Nojima, S.; Yasutake, A. Honeycomb-type methanol reforming catalyst for polymer electrolyte fuel cell. 2002126538, 2002.
- (293) Shimomura, M.; Sawadaishi, T. *Curr. Opin. Colloid Interface Sci.* **2001**, *6*, 11.

- (294) Chen, Y.; Pépin, A. *Electrophoresis* **2001**, 22, 187.
- (295) Xia, Y.; Rogers, J. A.; Paul, K. E.; Whitesides, G. M. *Chem. Rev.* **1999**, 99, 1823.
- (296) Aitken, J. *Nature* **1911**, 86, 516.
- (297) Aitken, J. *Proc. R. Soc. Edinburgh* 20, 94.
- (298) Rayleigh, L. *Nature* **1911**, 86, 416.
- (299) Rayleigh, L. *Nature* **1912**, 90, 436.
- (300) François, B.; Pitois, O.; François, J. *Adv. Mater.* **1995**, 7, 1041.
- (301) Hoa, M. L. K.; Lu, M.; Zhang, Y. *Adv. Colloid Interface Sci.* **2006**, 121, 9.
- (302) Knobler, C. M.; Beysens, D. *Europhys. Lett.* **1988**, 6, 707.
- (303) Widawski, G.; Rawiso, M.; François, B. *Nature* **1994**, 369, 387.
- (304) Pitois, O.; François, B. *Eur. Phys. Journal B Condens. Matter Complex Syst.* **1999**, 8, 225.
- (305) Pitois, O.; François, B. *Colloid Polym. Sci.* **1999**, 277, 574.
- (306) Srinivasarao, M.; Collings, D.; Philips, A.; Patel, S. *Science (80-. )*. **2001**, 292, 79.
- (307) Schatz, M. F.; Neitzel, G. P. *Annu. Rev. Fluid Mech.* **2001**, 93.
- (308) Peng, J.; Han, Y.; Yang, Y.; Binyao, L. *Polymer (Guildf)*. **2004**, 45, 447.
- (309) Francois, B.; Ederle, Y.; Mathis, C. *Synth. Met.* **1999**, 103, 2362.
- (310) Maruyama, N.; Koito, T.; Nishida, J.; Sawadaishi, T.; Cieren, X.; Ijiro, K.; Karthaus, O.; Shimomura, M. *Thin Solid Films* **1998**, 327-329, 854.
- (311) Bunz, U. H. F. *Adv. Mater.* **2006**, 18, 973.
- (312) Stenzel, M. H. *Aust. J. Chem.* **2002**, 55, 239.
- (313) Stenzel, M. H.; Davis, T. P.; Fane, A. G.; Chen, V. *Angew. Chemie* **2001**, 113, 3428.
- (314) Maruyama, N.; Karthaus, O.; Ijiro, K.; Shimomura, M.; Koito, T.; Nishimura, S.; Sawadaishi, T.; Nishi, N.; Tokura, S. *Supramol. Sci.* **1998**, 5, 331.
- (315) Xu, Y.; B.K., Z.; Zhu, Y. Y. *Polymer (Guildf)*. **2005**, 46, 713.
- (316) Wong, K. H.; Davis, T. P.; Barner-Kowollik, C.; Stenzel, M. H. *Polymer (Guildf)*. **2007**, 48, 4950.
- (317) Nygard, A.; Davis, T. P.; Barner-Kowollik, C.; Stenzel, M. H. *Aust. J. Chem.* **2005**, 58, 595.

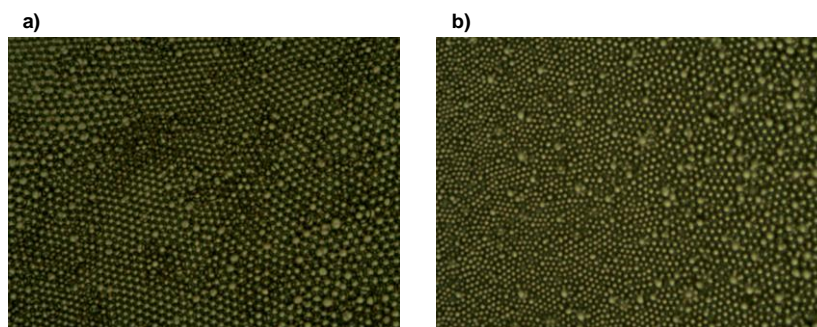
- (318) Xu, W. Z.; Kadla, J. F. *Langmuir* **2013**, 29, 727.
- (319) Xu, W. Z.; Zhang, X.; Kadla, J. F. *Biomacromolecules* **2012**, 13, 350.
- (320) Zhao, B.; Zhang, J.; Wang, X.; Li, C. *J. Mater. Chem.* **2006**, 16, 509.
- (321) Wong, K. H.; Hernández-Guerrero, M.; Granville, A. M.; Davis, T. P.; Barner-Kowollik, C.; Stenzel, M. H. *J. Porous Mater.* **2006**, 13, 213.
- (322) Nishikawa, T.; Nishida, J.; Ookura, R.; Nishimura, S.-I.; Wada, S.; Karino, T.; Shimomura, M. *Mater. Sci. Eng. C* **1999**, 8-9, 495.
- (323) Nemoto, J.; Uraki, Y.; Kishimoto, T.; Sano, Y.; Funada, R.; Obata, N.; Yabu, H.; Tanaka, M.; Shimomura, M. *Bioresour. Technol.* **2005**, 96, 1955.
- (324) Kasai, W.; Kondo, T. *Macromol. Biosci.* **2004**, 4, 17.
- (325) Stenzel, M. H.; Davis, T. P.; Fane, A. G. *J. Mater. Chem.* **2003**, 13, 2090.
- (326) Hernández-Guerrero, M.; Davis, T. P.; Barner-kowollik, C.; Stenzel, M. H. *Eur. Polym. J.* **2005**, 41, 2264.
- (327) Nishikawa, T.; Ookura, R.; Nishida, J.; Arai, K.; Hayashi, J.; Kurono, N.; Sawadaishi, T.; Hara, M.; Shimomura, M. *Langmuir* **2002**, 18, 5734.
- (328) Stenzel, M. H.; Barner-Kowollik, C.; Davis, T. P. *J. Polym. Sci. Part A Polym. Chem.* **2006**, 44, 2363.
- (329) Liu, W.; Liu, R.; Li, Y.; Wang, W.; Ma, L.; Wu, M.; Huang, Y. *Polymer (Guildf)*. **2009**, 50, 2716.
- (330) Karthaus, O.; Maruyama, N.; Cieren, X.; Shimomura, M.; Hasegawa, H.; Hashimoto, T. *Langmuir* **2000**, 16, 6071.
- (331) Stenzel, M. H.; Davis, T. P. *Aust. J. Chem.* **2003**, 56, 1035.
- (332) Hernández-Guerrero, M.; Min, E.; Barner-Kowollik, C.; Müller, A. H. E.; Stenzel, M. H. *J. Mater. Chem.* **2008**, 18, 4718.
- (333) Lee, C.-T.; Huang, C.-P.; Lee, Y.-D. *Biomacromolecules* **2006**, 7, 2200.
- (334) Tanaka, M.; Nishikawa, K.; Okubo, H.; Kamachi, H.; Kawai, T.; Matsushita, M.; Todo, S.; Shimomura, M. *Colloids Surfaces A Physicochem. Eng. Asp.* **2006**, 284-285, 464.
- (335) Keller, R. N.; Wrcoff, H. D.; Marchi, L. E. *Inorg. Synth.* **1946**, 2, 1.
- (336) Ciampolini, M.; Nardi, N. *Inorg. Chem.* **1966**, 5, 41.
- (337) Biswas, A.; Shogren, R. L.; Willett, J. L. *Biomacromolecules* **2005**, 6, 1843.
- (338) Liebert, T.; Hussain, M. a.; Heinze, T. *Macromol. Symp.* **2005**, 223, 79.



- (339) Förch, R.; Schönherr, H.; Tobias, A.; Jenkins, A. In *Surface Design: Applications in Bioscience and Nanotechnology*; Wiley-VCH, 2009; p. 471.
- (340) Kamitakahara, H.; Koschella, A.; Mikawa, Y.; Nakatsubo, F.; Heinze, T.; Klemm, D. *Macromol. Biosci.* **2008**, *8*, 690.
- (341) Carey, F. A.; Giuliano, R. M. *Organic Chemistry*; 8th ed.; McGraw-Hill; p. Chapter 8.
- (342) Tokaruk, W.; Molteno, T.; Morris, S. *Phys. Rev. Lett.* **2000**, *84*, 3590.
- (343) Xavier, A. F.; Kadla, J. F. In *ACS Symposium Series-Functional Materials from Renewable Sources*; ACS, Ed.; 2012; Vol. 1107, pp. 37–55.
- (344) Xia, Y.; Yin, X.; Burke, N. A. D.; Sto, H. D. H. **2005**, 5937.
- (345) Lutz, J.-F.; Weichenhan, K.; Akdemir, Ö.; Hoth, A. *Macromolecules* **2007**, *40*, 2503.
- (346) Maier, S.; Sunder, A.; Frey, H.; Mu, R.; Mülhaupt, R. *Macromol. Rapid Commun.* **2000**, *21*, 226.
- (347) Zhao, Y.; Chen, Y.; Chen, C.; Xi, F. *Polymer (Guildf)*. **2005**, *46*, 5808.
- (348) París, R.; Liras, M.; Quijada-Garrido, I. *Macromol. Chem. Phys.* **2011**, *212*, 1859.
- (349) Podzimek, S. *Light Scattering, Size Exclusion Chromatography and Asymmetric Flow Field Flow Fractionation*; 1st ed.; John Wiley & Sons: New Jersey, 2011; pp. 65–72.
- (350) Hussain, H.; Mya, K. Y.; He, C. *Langmuir* **2008**, *24*, 13279.
- (351) Radke, W.; Simon, F. W. P.; Müller, A. H. E. *Macromolecules* **1996**, *29*, 4926.
- (352) Se, K.; Sakakibara, T.; Ogawa, E. *Polymer (Guildf)*. **2002**, *43*, 5447.
- (353) Medrano, R.; Laguna, M. T. R.; Saiz, E.; Tarazona, M. P. *Phys. Chem. Chem. Phys.* **2003**, *5*, 151.
- (354) Longenecker, R.; Mu, T.; Hanna, M. *Macromolecules* **2011**, *44*, 8962.
- (355) Mark, H. *Angew. Chemie* **1955**, *67*, 53.
- (356) Molau, G. E. In *Characterization of Macromolecular Structure*; National Academy of Sciences: Washington, D.C., 1967; pp. 245–258.
- (357) Okano, T.; Yamada, N.; Sakai, H.; Sakurai, Y. *J. Biomed. Mater. Res.* **1993**, *27*, 1243.

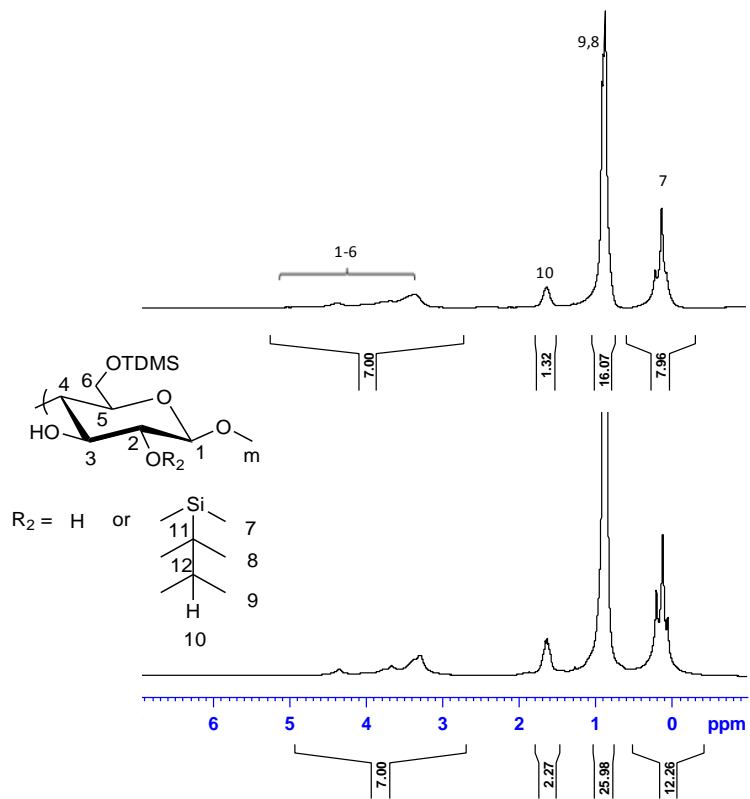
## APPENDIX

### Selected optical micrographs

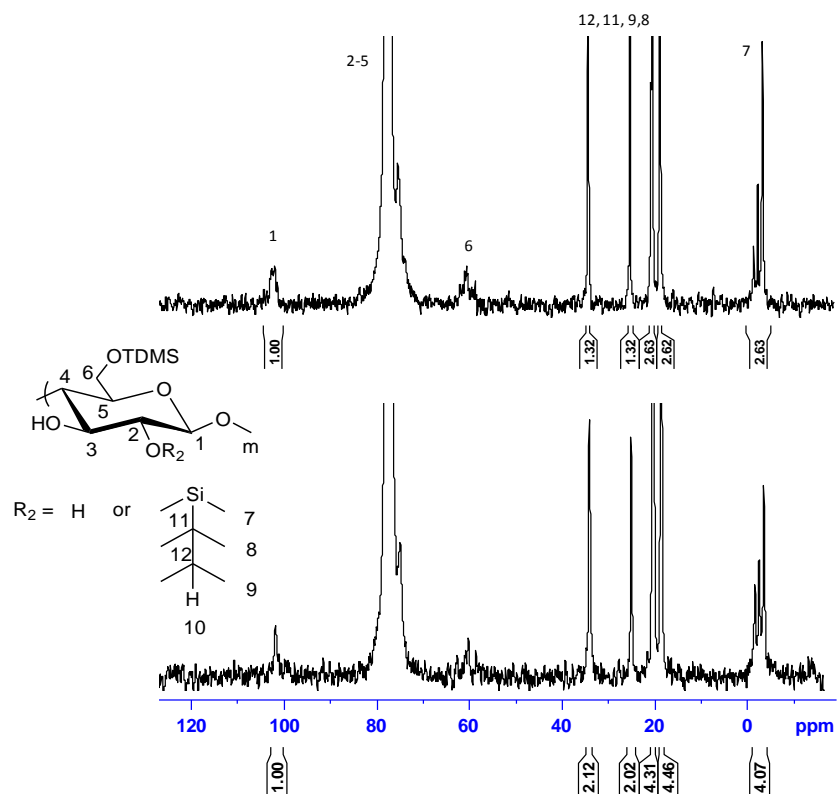


Optical micrographs, 500x magnification, of honeycomb films from 6-*O*-(2-bromoisobutryl) TMS-*O*-cellulose with low DS at different flow/humidity; a) 0.5 L/min and b) 0.7 L/min.

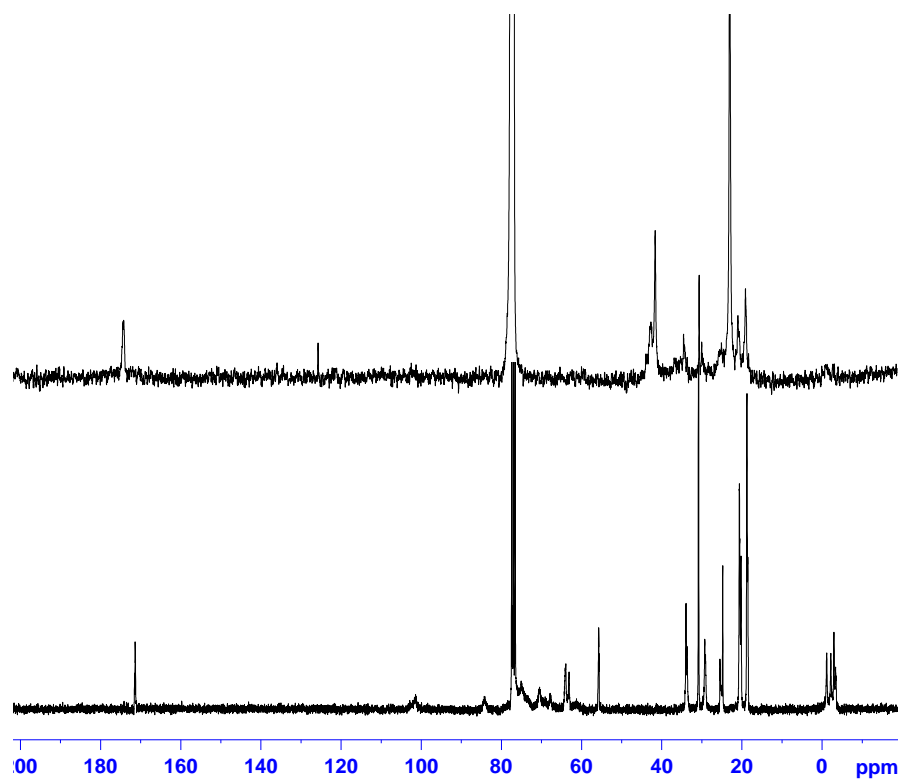
## Selected NMR spectra



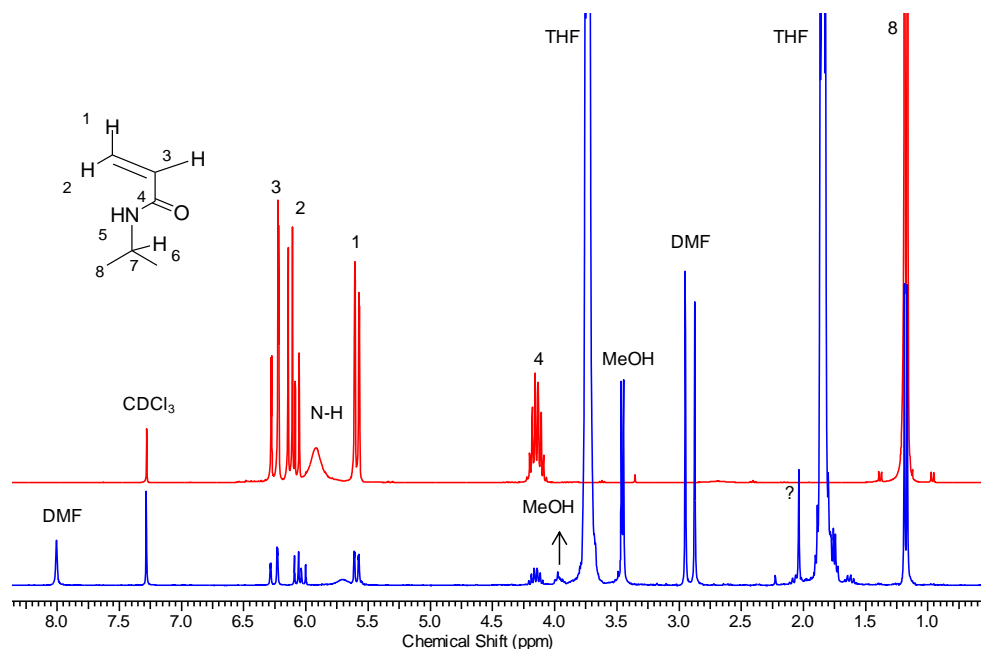
Comparison of  $^1\text{H}$ -NMR spectra of 2,6-O-TDMS cellulose with  $\text{DS}=1.3$  (top) and  $\text{DS}\sim 2.1$  (bottom).



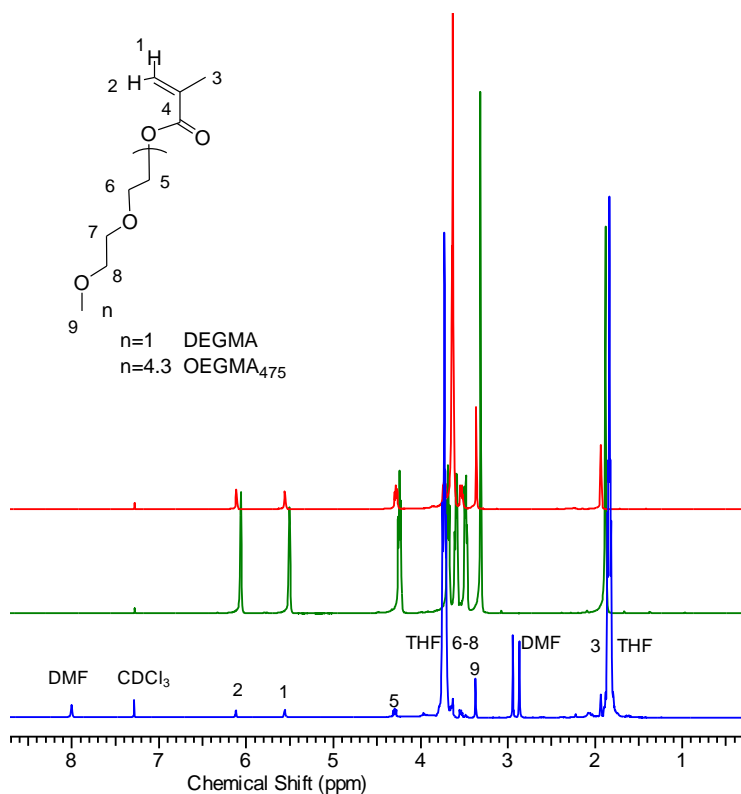
Comparison of  $^{13}\text{C}$ -NMR spectra of 2,6-O-TDMS cellulose with  $\text{DS}=1.3$  (top) and  $\text{DS}\sim 2.1$  (bottom).



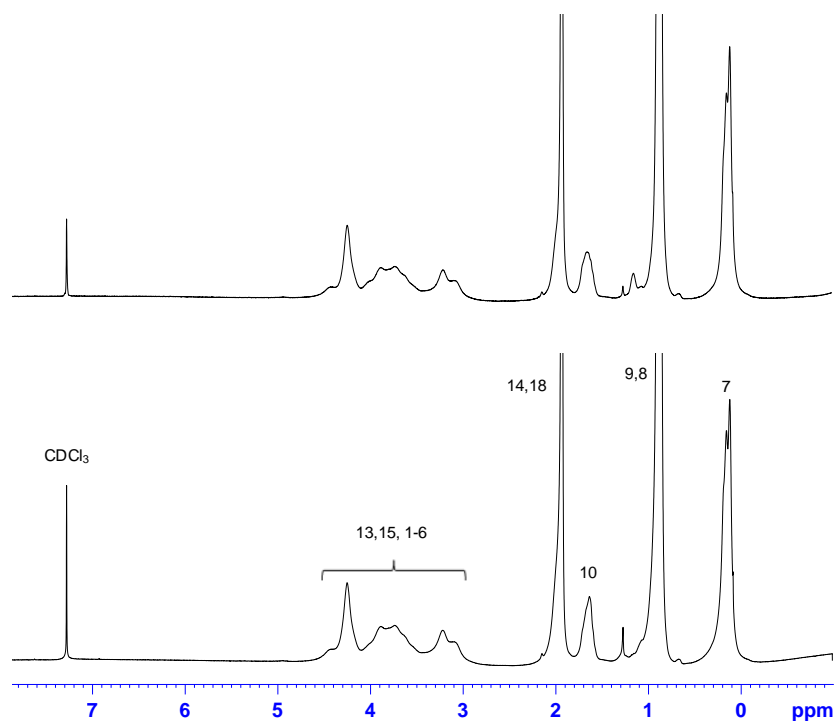
Comparison of  $^{13}\text{C}$ -NMR spectra of 3-O-(3-O-(2-bromoisobutyryl)-hydroxypropyl)-2,6-O-TDMS cellulose (bottom) and 3-O-(3-O-(2-bromoisobutyryl)-hydroxypropyl)-2,6-O-TDMS cellulose-g-PNIPAM (top).



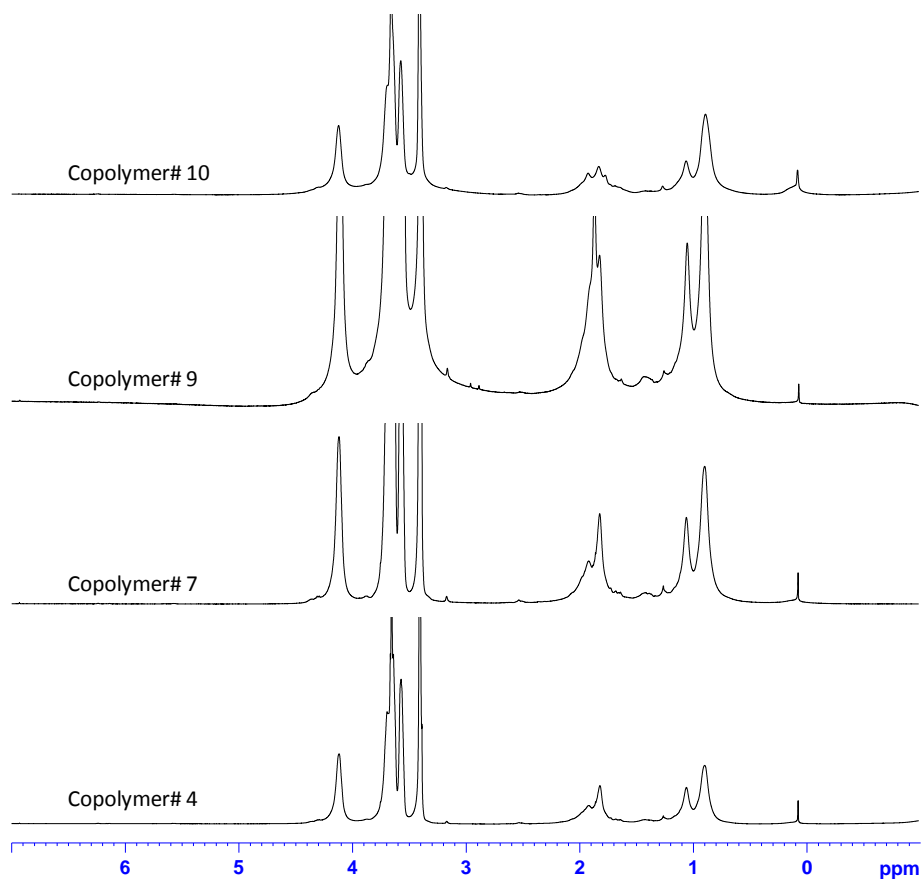
<sup>1</sup>H-NMR spectra of NIPAM (in red) and the reaction mixture of NIPAM homopolymerization in the absence of cellulose-based macroinitiator (in blue).



<sup>1</sup>H-NMR spectra of DEGMA (in red), OEGMA<sub>475</sub> (in green) and the reaction mixture of DEGMA and OEGMA copolymerization in the absence of cellulose-based macroinitiator (in blue).



$^1\text{H}$ -NMR spectra of 3-O-(3-O-(2-bromoisobutyryl)-hydroxypropyl)-2,6-O-TDMS cellulose (bottom) and the precipitate obtained after adding water to a solution in THF of 3-O-(3-O-(2-bromoisobutyryl)-hydroxypropyl)-2,6-O-TDMS cellulose and PNIPAM.



Comparison of  $^1\text{H}$ -NMR spectra of 3-O-(3-O-(2-bromoisobutyryl)-hydroxypropyl)-2,6-O-TDMS cellulose-*g*-P(DEGMA<sub>95</sub>-co-OEGMA<sub>5</sub>) copolymers.



## Duplicates and respective RPDs%

Duplicate values of DS of 2-bromoisobutyryl and Mn obtained from synthesized 6-O-(2-bromoisobutyryl) TMS-O-cellulose derivatives and respective RPDs%.

C6 derivative	DS <sub>2-bromoisobutyryl</sub>	RPD%	Mn (g/mol)	RPD%
L	0.24	4.3	$5.4 \times 10^4$	4.0
	0.23		$5.6 \times 10^4$	
M	0.50	0	$5.9 \times 10^4$	2.5
	0.5		$6.0 \times 10^4$	
H	0.80	0	$6.0 \times 10^4$	3.4
	0.8		$5.8 \times 10^4$	
Non-regioselective	2.2	0	$7.1 \times 10^4$	2.9
	2.2		$6.9 \times 10^4$	

Duplicate values of DS of 2-bromoisobutyryl and Mn obtained from the study of the synthesis of 3-O-(3-O-(2-bromoisobutyryl)-hydroxypropyl)-2,6-O-TDMS cellulose derivatives and respective RPDs%.

T (°C)	Time (h)	Base	Ratio	DS	RPD%	Mn (g/mol)	RPD%
2,6-O-TDMS cellulose						$3.9 \times 10^4$	2.0
						$4.0 \times 10^4$	
RT	19	Pyr	1:11:10:0	0.16	1.25	$3.3 \times 10^4$	5.9
				0.17		$3.5 \times 10^4$	
RT	19	Pyr	1:21:20:0	0.21	0.2	$3.1 \times 10^4$	3.6
				0.20		$3.0 \times 10^4$	
Refl	19	Pyr	1:11:10:0	0.22	0	$2.5 \times 10^4$	6.9
				0.22		$2.7 \times 10^4$	
RT	48	Pyr	1:11:10:0	0.28	0.28	$3.0 \times 10^4$	2.0
				0.27		$3.1 \times 10^4$	
RT	19	Im	1:11:10:0	<0.1		$3.2 \times 10^4$	5.3
						$3.0 \times 10^4$	
Refl	19	Pyr	1:20:20:0.05	0.26	2.7	N/A	
				0.27			

Duplicate values of DS of 2-bromoisobutryl and Mn obtained from the study of the effect of base in the synthesis of 2,3-O-(2-bromoisobutryl) 2,6-O-TDMS cellulose and respective RPDs%.

Exp#	DS	RPD%	Mn(g/mol)	RPD%
2,6 TDMS-O-cellulose			$5.5 \times 10^4$ $5.4 \times 10^4$	1.1
1	0.31	6.7	$4.8 \times 10^4$	5.2
	0.29		$4.5 \times 10^4$	
2	0.10	1	$5.5 \times 10^4$	4.1
	0.10		$5.2 \times 10^4$	
3	0.10	8.3	$4.7 \times 10^4$	4.6
	0.09		$4.5 \times 10^4$	
4	0.35	2.3	$5.2 \times 10^4$	3.2
	0.35		$5.4 \times 10^4$	

Duplicate values of DS of 2-bromoisobutryl and Mn obtained from the study of the effect of time and temperature in the synthesis of 2,3-O-(2-bromoisobutryl) 2,6-O-TDMS cellulose and respective RPDs%.

Exp#	DS	RPD%	Mn(g/mol)	RPD%
5	0.43		$3.0 \times 10^4$ $3.2 \times 10^4$	4.2
6	0.51	4.9	$2.7 \times 10^4$	4.4
	0.54		$2.8 \times 10^4$	
7	0.84	3.6	$2.1 \times 10^4$	5.2
	0.81		$2.2 \times 10^4$	
8	0.53	0.4	$2.7 \times 10^4$	0.7
	0.53		$2.7 \times 10^4$	

Duplicate values of DS of 2-bromoisobutyryl and Mn obtained from the study of the effect of the mole equivalents of 2-bromoisobutyryl bromide and anhydrous pyridine in the synthesis of 2,3-O-(2-bromoisobutyryl) 2,6-O-TDMS cellulose and respective RPDs%.

Exp#	DS	RPD%	Mn(g/mol)	RPD%
9	0.38	3.1	$5.4 \times 10^4$	1
	0.39		$5.4 \times 10^4$	
10	0.34	5.7	$5.3 \times 10^4$	2.2
	0.36		$5.4 \times 10^4$	
11	0.57	7.7	$5.0 \times 10^4$	5.8
	0.53		$5.3 \times 10^4$	
12	0.65	6.0	$4.1 \times 10^4$	7.1
	0.69		$4.4 \times 10^4$	
13	0.79	3.9	$3.7 \times 10^4$	3.8
	0.76		$3.6 \times 10^4$	

Duplicate values of DS of 2-bromoisobutyryl and Mn obtained from the study of the effect of the addition of a 2<sup>nd</sup> reaction cycle in the synthesis of 2,3-O-(2-bromoisobutyryl) 2,6-O-TDMS cellulose and respective RPDs%.

Exp#	DS	RPD%	Mn(g/mol)	RPD%
14	0.86	4.8	$2.3 \times 10^4$	8.3
	0.82		$2.5 \times 10^4$	
15	0.76	10	$2.4 \times 10^4$	3.4
	0.84		$2.3 \times 10^4$	

Duplicate values of DS of 2-bromoisobutyryl obtained from synthesized 3-O-(3-O-(2-bromoisobutyryl)-hydroxypropyl)-2,6-O-TDMS cellulose derivatives and respective RPDs%.

	DS <sub>2-bromoisobutyryl</sub>	RPD%
<b>Low DS</b>	0.21	9.1
	0.23	
<b>Medium DS</b>	0.63	3.2
	0.61	
<b>High DS</b>	1.0	0
	1.0	

Duplicate values of  $Mn_{(GPC-MALS)}$  obtained from synthesized 3-O-(3-O-(2-bromoisobutyryl)-hydroxypropyl)-2,6-O-TDMS cellulose (high and low DS) and cellulose-based graft PNIPAM copolymers and respective RPDs%.

Exp#	$Mn_{(GPC-MALS)} \cdot (g/mol)$	RPD%
MI-High DS	$4.6 \cdot 10^4$	9.1
	$4.2 \cdot 10^4$	
MI-Low DS	$4.2 \cdot 10^4$	4.7
	$4.4 \cdot 10^4$	
I	$1.3 \cdot 10^5$	6.5
	$1.2 \cdot 10^5$	
II	$1.7 \cdot 10^5$	9.2
	$1.5 \cdot 10^5$	
III	$1.3 \cdot 10^5$	1.6
	$1.3 \cdot 10^5$	
IV	$1.1 \cdot 10^5$	1.8
	$1.1 \cdot 10^5$	
V	N/A	
VI (1 <sup>st</sup> peak)	$1.8 \cdot 10^7$	9.9
	$1.6 \cdot 10^7$	
VI (2 <sup>nd</sup> peak)	$4.3 \cdot 10^4$	2.3
	$4.4 \cdot 10^4$	

Duplicate values and respective RPDs% of decomposition temperature of macroinitiator, P(DEGMA<sub>90</sub>-co-OEGMA<sub>10</sub>) and cellulose-based graft copolymers.

	Td <sub>1</sub> (°C)	RPD%	Td <sub>2</sub> (°C)	RPD%	Td <sub>3</sub> (°C)	RPD%	Td <sub>4</sub> (°C)	RPD%
Macroinitiator	262	3.4	353	1.1	-		-	
High DS	271		349					
Macroinitiator	292	0.7	320	1.9	369	1.9		
Low DS	294		326		373			
P(DEGMA <sub>90</sub> -co-OEGMA <sub>10</sub> )	274	0	332	0.2	-		-	
	274		332					
4	261	3.1	376	0.9	-		-	
	270		372					
9	277	0.3	368	0.4	-		-	
	278		366					
10	290	0.2	374	0.4	-		-	
	290		376					
13	292	0	366	1.0			-	
	292		362					
15	273	1.5	378	1.1				
	277		382					
5	247	0.9	302	0.5	358	1.4	-	
	245		303		363			
8	235	0.6	277	1.1	367	0.6		
	234		274		369			
6	300	0.5	316	3.4	357	0.2	-	
	298		326		358			
7	194	2.3	295	1.7	311	0.5	350	2.9
	190		290		310		399	

Duplicate values and respective RPDs% of glass transition temperature of macroinitiator, P(DEGMA<sub>90</sub>-co-OEGMA<sub>10</sub>) and cellulose-based graft copolymers.

Copolymer	Tg (°C)	RPD%
MI	128.6	0.5
High DS	129.3	
MI	N/A	
Low DS		
P(DEGMA <sub>90</sub> -co-OEGMA <sub>10</sub> )	-43.8	1.8
	-43.0	
4	-39.8	1.0
	-39.4	
5	-39.5	1.3
	-39.0	
6	-36	2.2
	-36.8	
7	-40.2	1.2
	-40.7	
8	-39.1	1.3
	-39.6	
9	-51.2	2.0
	-50.2	
10	-35.2	1.4
	-35.7	
13	-25.3	2.0
	-24.8	
15	-22.3	4.8
	-23.4	

Duplicate values of  $Mn_{(GPC-MALS)}$  obtained from synthesized 3-O-(3-O-(2-bromoisobutyryl)-hydroxypropyl)-2,6-O-TDMS cellulose (high and low DS) and cellulose-based graft P(DEGMA-co-OEGMA) copolymers and respective RPDs%.

Exp#	$Mn_{(GPC/MALS)}$ (g/mol)	RPD%
MI	$4.6 \times 10^4$	9.1
High DS	$4.2 \times 10^4$	
MI	$4.3 \times 10^4$	2.3
Low DS	$4.2 \times 10^4$	
4	$1.3 \times 10^6$	8
	$1.2 \times 10^6$	
7	$5.9 \times 10^5$	6.6
	$6.3 \times 10^5$	
9	$8.7 \times 10^6$	3.5
	$8.4 \times 10^6$	
	$1.3 \times 10^6$	
10	$2.4 \times 10^5$	8.7
	$2.2 \times 10^5$	
15	$6.2 \times 10^5$	4.1
	$5.9 \times 10^5$	

Duplicate values of LCST from copolymers # 7 and 9 and respective RPDs%.

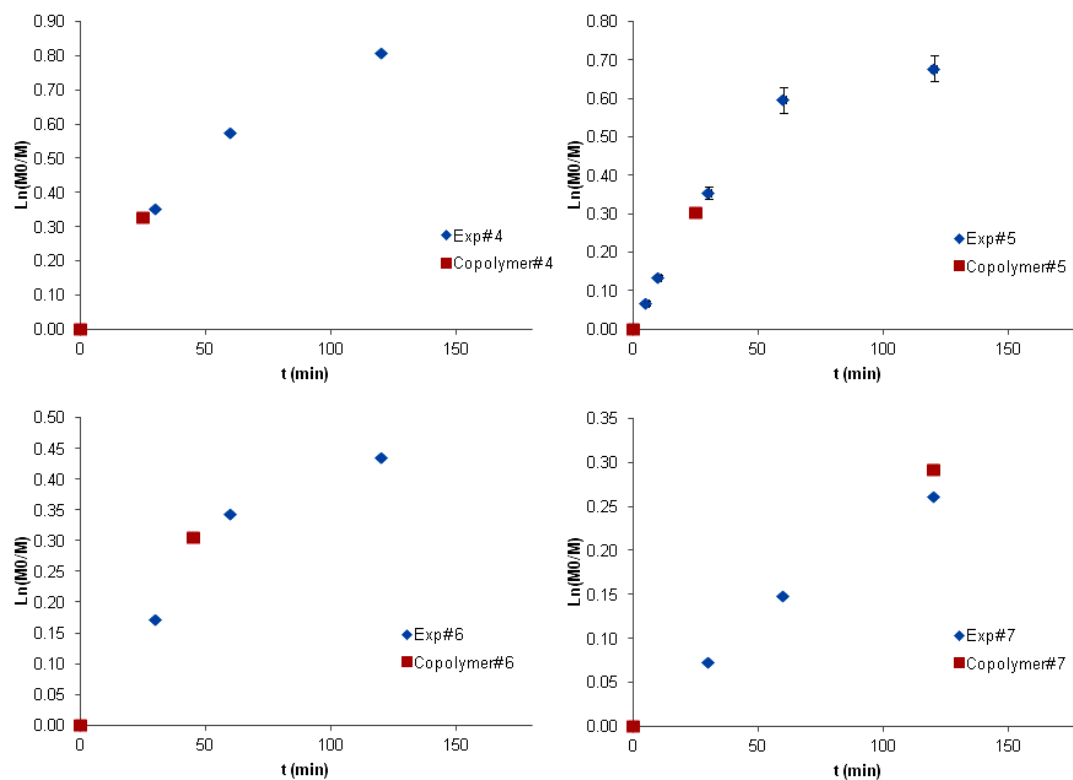
Copolymer	LCST(°C)	RPD%
# 7-cooling	25.9	0.4
	26.1	
# 7-heating	27.1	3.4
	28.0	
# 9-cooling	36.9	0.3
	36.8	
# 9-heating	36.0	0.4
	36.2	

Duplicate values of  $Mn_{(GPC-MALS)}$  obtained from cellulose-based graft P(DEGMA-co-OEGMA) copolymers and respective RPDs%.

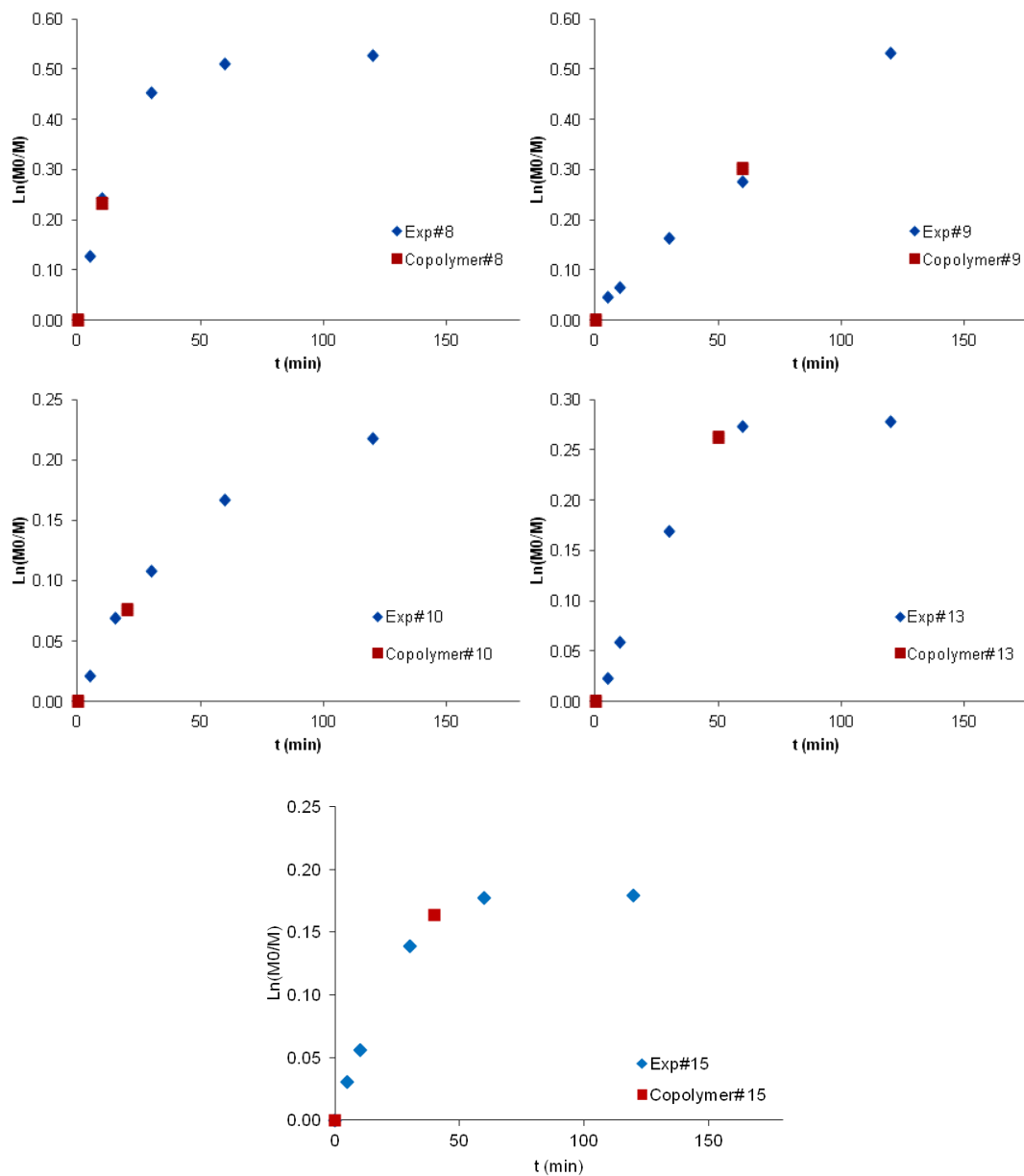
Exp#	$Mn_{(GPC/MALS)}$	RPDs%
9-5min	$8.2 \cdot 10^5$	4.8
	$8.6 \cdot 10^5$	
9-15min	$2.7 \cdot 10^6$	6.4
	$2.6 \cdot 10^6$	
9-1h	$8.7 \cdot 10^6$	3.5
	$8.4 \cdot 10^6$	



## Selected kinetic graphs

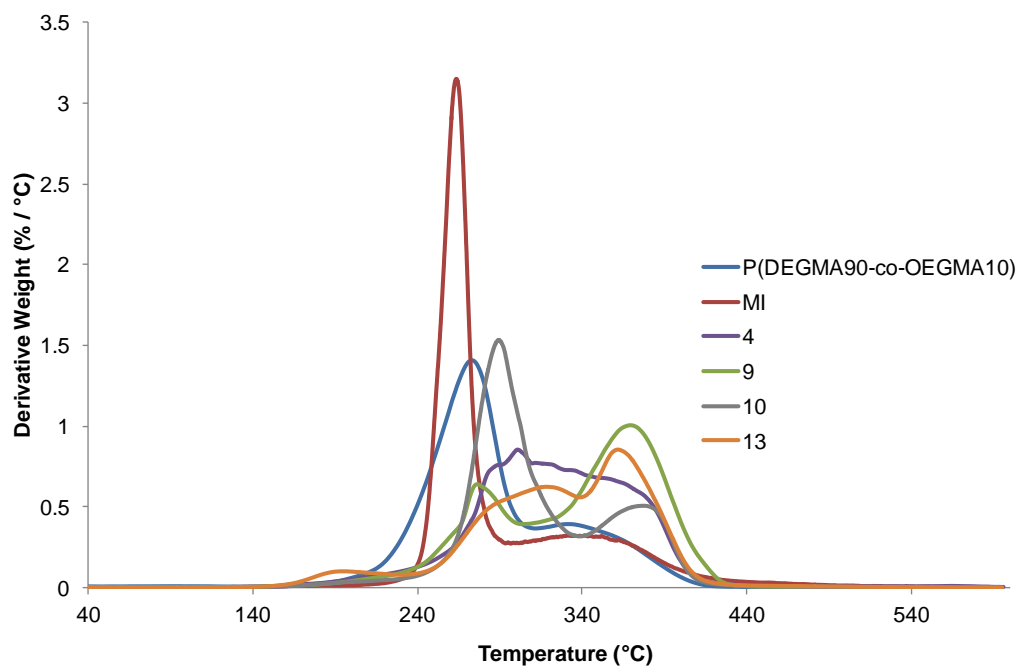


Fitting of single point collected for selected copolymers (red-square) in the respective kinetic plots of experiments (blue-diamond).

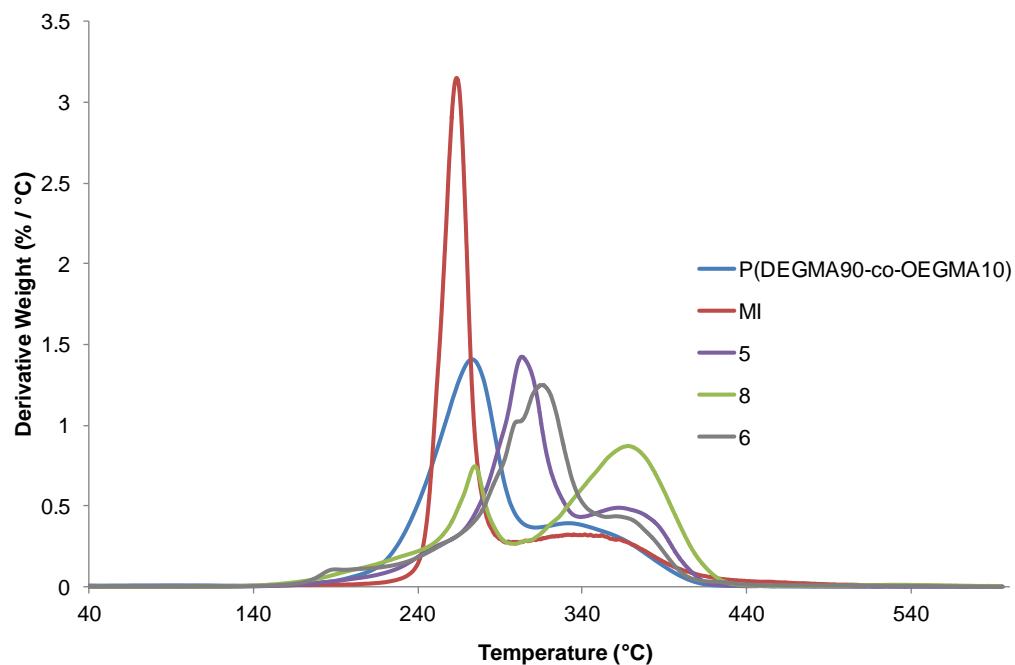


Fitting of single point collected for selected copolymers (red-square) in the respective kinetic plots of experiments (blue-diamond).

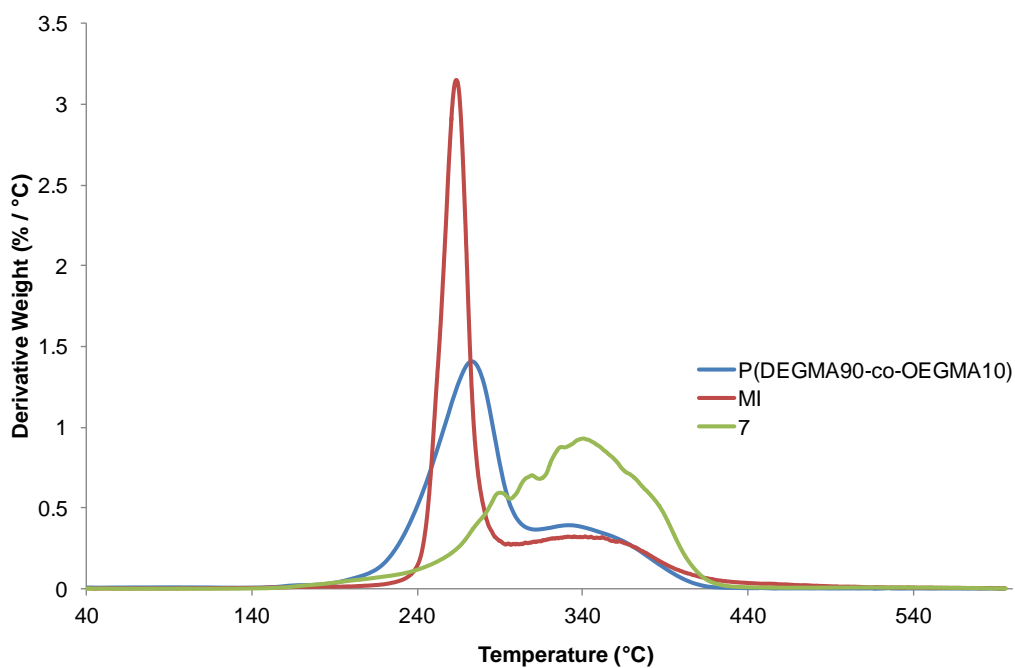
## Selected first derivative of TGA thermograms



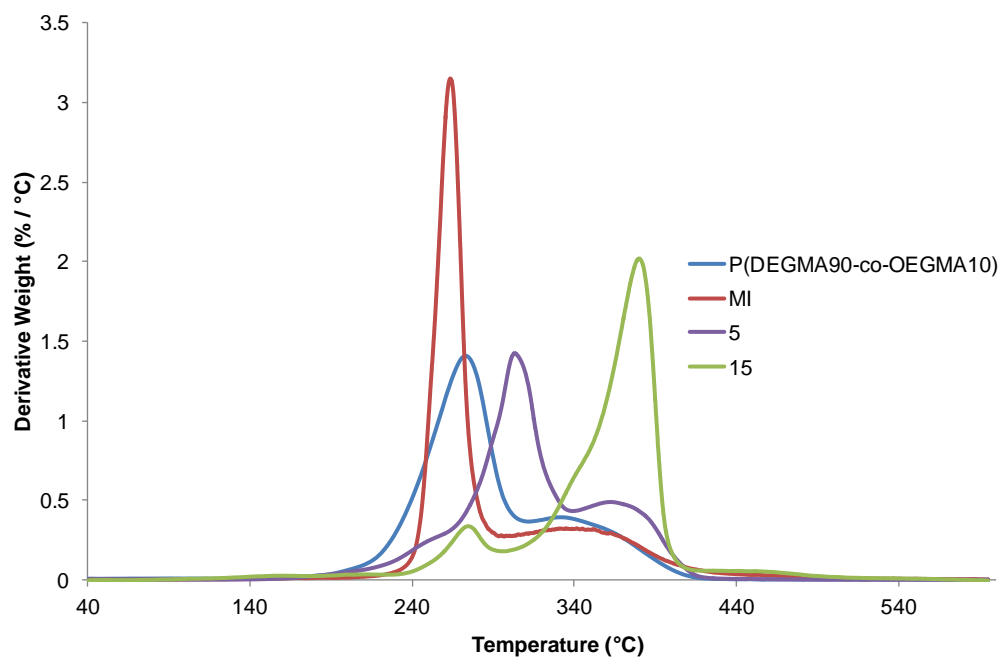
First derivative of TGA thermograms from copolymers # 4, 9, 10 and 13, respective macroinitiator and P(DEGMA<sub>90</sub>-co-OEGMA<sub>10</sub>).



First derivative of TGA thermograms from copolymers # 5, 8, and 6, respective macroinitiator and P(DEGMA<sub>90</sub>-co-OEGMA<sub>10</sub>).

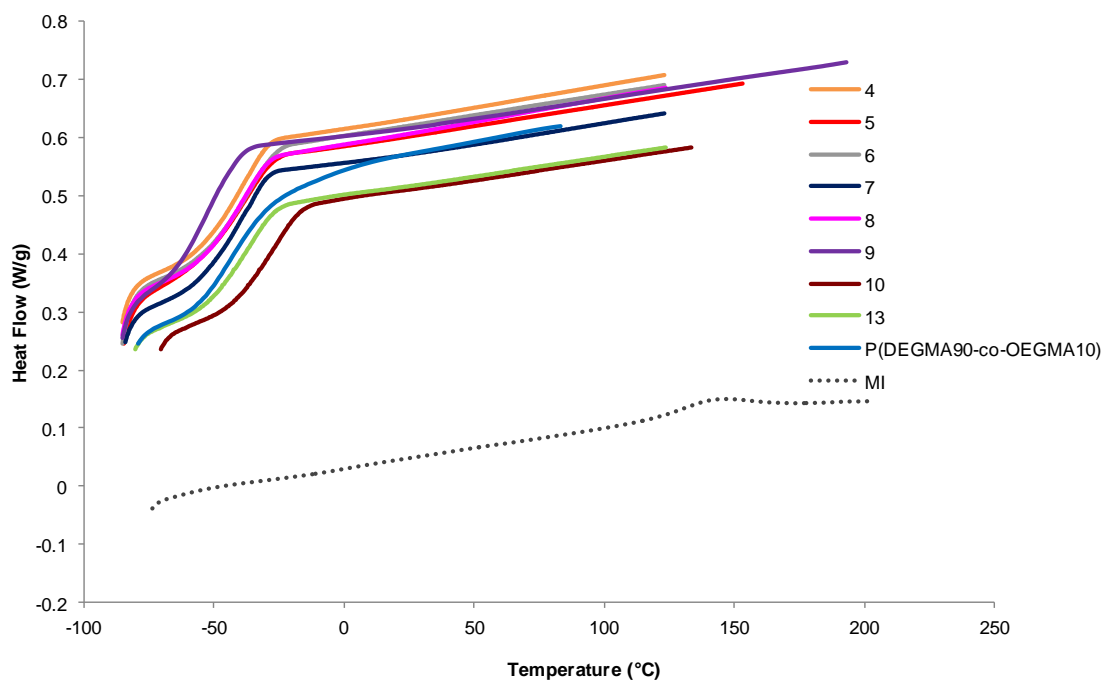


First derivative of TGA thermograms from copolymer # 7, respective macroinitiator and P(DEGMA<sub>90</sub>-co-OEGMA<sub>10</sub>).



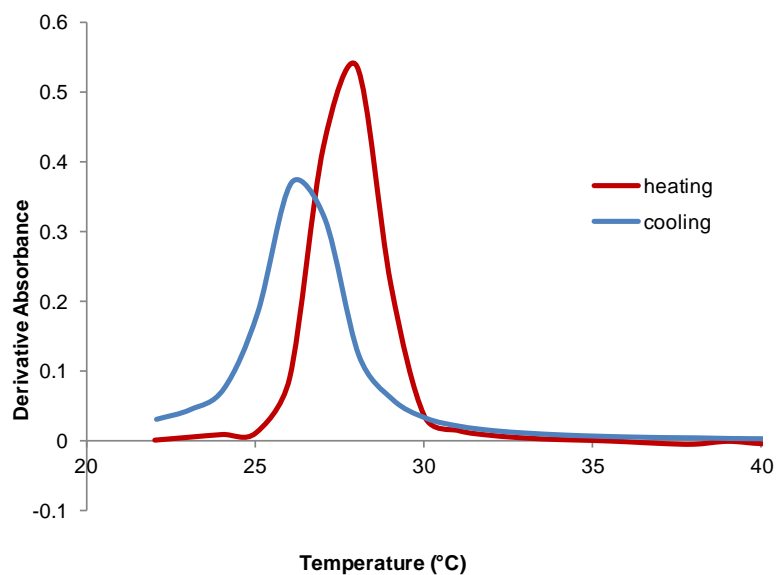
First derivative of TGA thermograms from copolymers # 5 and 15, respective macroinitiator and P(DEGMA<sub>90</sub>-co-OEGMA<sub>10</sub>).

## Selected DSC thermograms

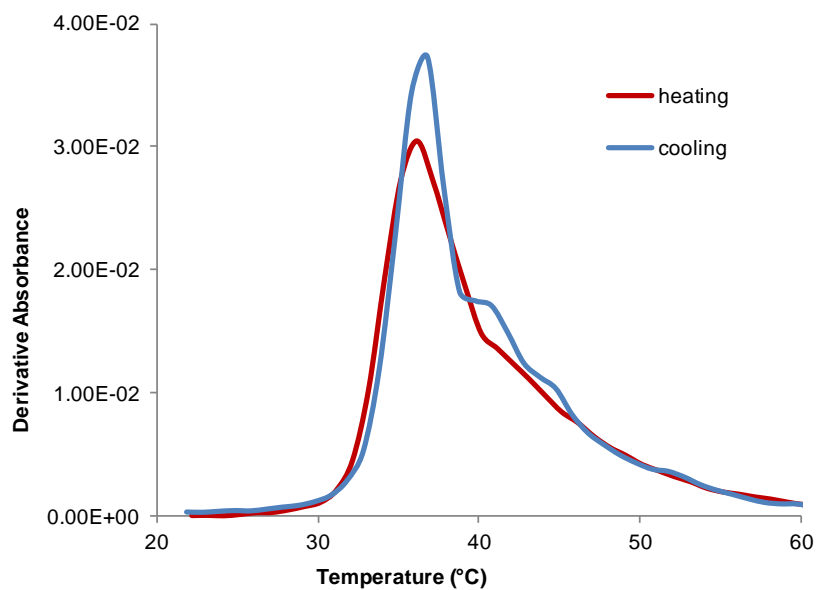


Comparison of DSC thermograms of copolymers # 4 to 10 and 13, respective macroinitiator and P(DEGMA<sub>90</sub>-co-OEGMA<sub>10</sub>).

## Selected first derivative of the absorbance curves from UV-Vis spectra/LCST



First derivative of absorbance vs. temperature plot illustrating the LCST of cellulose-based graft copolymer # 7 at 670nm.



First derivative of absorbance vs. temperature plot illustrating the LCST of cellulose-based graft copolymer # 9 at 670nm.